

24.8.78

THE UNIVERSITY OF ADELAIDE

Department of Mechanical Engineering

THE VIBRATIONAL ENERGY TRANSMISSION
THROUGH CONNECTED STRUCTURES

by

P.B. Swift, B.E.

Thesis for the degree of Doctor of Philosophy

May 1977.

SUMMARY

The methods of statistical energy analysis are used to predict vibrational energy distributions in connected structures. The limits of applicability of the prediction technique are investigated experimentally. The results of comparisons between measurement and prediction are used to investigate the [] theoretical limitations inherent in the analysis.

The analysis proceeds by considering the power flow between the parts of the structure and the nett energy balance in each part. Thus coupling loss factors, which describe the power flow between connected parts, and internal loss factors, which describe the nett loss of energy in the individual parts of a structure due to all forms of dissipation, play a central role in the analysis. The coupling loss factors are related to transmission coefficients. Expressions for the transmission coefficient are developed for the general case of four plates connected at a common join using wave transmission theory. For the range of plate thicknesses considered it has been sufficient to consider only bending waves and to neglect any energy loss due to wave transformation at the join. As the coupling between plates depends upon the angle of incidence of the initial exciting bending wave and in general all angles of incidence may be expected, it has been advantageous to calculate average transmission coefficients, hence average coupling loss factors. Alternatively an empirical equation is presented which allows considerable mathematical simplification in the calculation of the average transmission coefficients.

The neglect of longitudinal and transverse wave transmission and transformation at a four plate join is also investigated. Comparisons of average transmission coefficients calculated including longitudinal and transverse wave propagation along

with bending wave propagation, and average transmission coefficients calculated neglecting all but bending wave propagation, then show at what frequency and plate thickness combinations longitudinal and transverse waves can not be neglected. Empirically obtained charts are presented from which the high frequency thick plate average transmission coefficient may be estimated as a correction to the more easily calculated bending wave transmission coefficient. The effects of further wave transformation at subsequent joins are also discussed.

The internal loss factors of plates used in the experimental investigation were determined using a steady state measured power injection method. Loss factors thus determined were found to be consistently higher than those determined using the usual reverberation decay technique. However, the values determined by the steady state method were consistent with very short initially steeper decay rates that were frequently observed. Artificial damping was added to the various plates so that radiation losses could be neglected in comparison with internal losses. This insured that when the plates were subsequently joined together any effects on edge radiation would be quite immaterial to the investigation.

Energy level distributions over a number of single join multiplate structures were measured and compared with levels predicted using the methods of statistical energy analysis, calculated average coupling loss factors, and measured internal loss factors. These comparisons are then used to investigate the limits of applicability of the prediction technique. It is shown that the bounds, which are related to the number of resonant modes in the excitation band width at low frequencies and to the density of resonant modes and internal damping at high frequencies, are slightly different for the cases of two coupled

plates and three or four coupled plates at a single join.

Three multiplate, multijoin structures were investigated. Comparisons between measured and predicted plate energy levels were good over a mid frequency range consistent with that observed for the single join plates. The results outside of these bounds at low and high frequencies were also reasonably good. Thus methods and frequency range are established for the prediction of vibrational energy levels in multiplate, multijoin, structures to within ± 2 dB. An extended range has also been established over which the predicted and measured results are generally within ± 2 dB and, where the error is greater, the measured energy ratio is less than that predicted.

TABLE OF CONTENTS

	<u>Page</u>
Contents	i
Statement of originality	iv
Acknowledgements	v
List of figures	vi
List of tables	ix
Glossary of Symbols	x
1. INTRODUCTION	1
2. OBJECTIVES	6
3. POWER BALANCE EQUATIONS	8
3.1. Review of previous work.	8
3.2. Prediction of energy distribution in an N element connected structure	16
4. COUPLING LOSS FACTORS	20
4.1. Review of Previous Work.	20
4.2. Alternative Formulations in terms of wave transmission coefficients.	25
4.3. Bending Wave Solution - Any number of plates at a common join.	29
4.3.1. Wave Transmission Method	29
4.3.2. Energy Decay Method	32
4.3.3. Power Balance Method	37
4.3.4. Discussion of Theoretical Results	39
4.4. General Solution-Four Plates at a common join	50
4.4.1. Wave transmission method	50
4.4.2. Discussion of Theoretical Results	56
4.5. Experimental Methods	74
4.5.1. Apparent Loss Factor	74
4.5.2. Energy Decay Methods	76
4.5.3. Steady State Methods	77
4.5.4. The importance of the ratio of the coupling loss factor to the internal loss factor.	81
5. COMPARISON OF THEORETICALLY AND EXPERIMENTALLY DETERMINED ENERGY RATIOS IN COUPLED STRUCTURES.	90
5.1. Introduction	90
5.2. Single Join Structures	97

	<u>Page</u>
5.2.1. Two Plate Joins	97
5.2.2. Three and Four Plate Joins	107
5.3. Multijoin Structures	120
5.3.1. Two Plate Joins	120
5.3.2. Two, Three and Four Plate Joins	128
6. CONCLUSIONS	133
APPENDIX A. Energy Decay in a Two Dimensional Field	137
APPENDIX B. Solution of Simultaneous Equations to obtain Transmitted and Reflected Wave Amplitudes	141
B.1. Bending Wave Field Only	141
B.2. Bending, Longitudinal and Transverse Wave Fields	145
APPENDIX C. Computer Programmes	151
C.1. Computation of the Average Transmission Coefficient - Bending Wave Solution	151
C.2. Computation of the Average Transmission Coefficient - General Solution	162
C.3. Computation of the Vibrational Energy Ratios of a Connected Structure	172
APPENDIX D. Apparatus and Experimental Procedure	174
D.1. Introduction	174
D.2. Test Structure Support System	174
D.2.1. Requirements	174
D.2.2. Support Block	176
D.2.3. Point Contact Driver Support	176
D.3. Instrumentation and its Calibration	177
D.3.1. Acceleration measurement	179
D.3.2. Input Power measurement	179
D.3.3. Calibration	180
D.3.4. Mass Loading	181
D.4. Internal Loss Factor Measurement	182
D.4.1. Steady State Method	182
D.4.2. Decay Methods	183
D.5. Plate Energy Ratio Measurements	185
D.6. Accuracy of Experimental Results	185

	<u>Page</u>
APPENDIX E. Transducers and Instrumentation for Steady State Measurement of Loss Factor	188
E.1. Requirements	188
E.2. Transducer Construction and Theory	188
E.3. Instrumentation	193
E.4. Calibration Procedure	193
E.5. Transducer-Plate Impedance Matching	195
E.6. Transducer Testing	198
 References	 203

Statement of Originality

This thesis contains no material which has been accepted for the award of any other degree or diploma in any University. To the best of the author's knowledge and belief, this thesis contains no material previously published or written by another person, except where the reference is made in the text.

P.B. Swift
May, 1977

ACKNOWLEDGEMENTS

The work described in this thesis has been carried out in the Department of Mechanical Engineering of the University of Adelaide, under the aegis of Professor H.H. Davis initially, and finally, of Professor R.E. Luxton, to whom the author is indebted for the opportunity to conduct this research.

The author wishes to express his sincere appreciation to his supervisor, Dr. D.A. Bies, for the encouragement and assistance generously given throughout the duration of this research and for his constructive comments and guidance with the presentation of this thesis.

In addition, the author acknowledges the interest shown and helpful comments by a number of the academic staff of the Department.

The assistance of the workshop staff, under Mr. D. Kerr is gratefully acknowledged, in particular, the invaluable assistance provided by the electronic workshop team headed by Mr. H. Bode, in the development of the instrumentation used in this research.

The author wishes to express his appreciation to his wife and family for their continuing support over the duration of this research, and acknowledgement is made of the financial support provided by the Commonwealth Postgraduate Research Award, without which this work would not have been carried out.

LIST OF FIGURES

Figure No.	Title	Page No.
3-1	Power flow for two coupled elements	12
3-2	Four Element Structures	12
3-3	Three Element Structures	18
4-1	Travelling bending wave amplitudes and direction of propagation for an oblique bending wave incident on the junction of two edge coupled plates i and j.	23
4-2	Geometry and wave propagation directions for four plates at a common join.	28
4-3	Comparison of τ_{12} , $-\ln(1-\tau_{12})$ and TF_{12} for coupled plates at varying plate thickness ratios.	40
4-4	Variation of predicted energy ratio E_2/E_1 for 1dB variation in the loss factor ratio η_{21}/η_2 .	42
4-5	Comparison of computer evaluated and empirically determined values of T-for use in equation (4,40) to evaluate τ_{ij} .	45
4-6	Comparison of computer evaluated and empirically determined values of M-for use in equation (4,40) to evaluate τ_{ij} .	46
4-7	Nomenclature for two, three and four plate single join structures.	57
4-8	Bending to bending transmission coefficient from plate 1 to plate 3 for a 3 plate structure - variation with incident angle.	58
4-9	Variation of $(\tau_{BB}/\tau)_{1j}$ with F_{1j}^2 - single join structures.	61
4-10	Variation of $(\tau_{BB}/\tau)_{1j}$ with P_{ab} and Q_{ab} - single join structures.	63
4-11	Schematic diagram of the transmitted bending, longitudinal and transverse wavefields generated in connected plates from an incident bending wave.	65
4-12	Variation of $(\tau_{BL}/\tau_{BB})_{12}$ with P_{ab} and Q_{ab} - single join structures.	69
4-13	Multi-join structure comprising large thickness ratio 3 plate joins.	71

Figure No.	Title	Page No.
4-14	Comparison of point contact and non-contact excited measured plate energy ratios for 2 plate structures.	79
4-15	The experimentally determined coupling loss factor as a function of the measured apparent loss factor to internal loss factor ratio.	83
4-16	Modal energy ratio for two coupled elements as a function of the coupling loss factor to internal loss factor ratio.	84
4-17	Measured and Predicted energy ratios. Plates 1 and 2.	86
4-18	Coupling loss factors determined from measured energy ratios in 4-17.	87
5-1	Determination of the upper and lower bounds for two coupled plates.	103
5-2	Experimental and theoretical energy ratio level differences for two edge joined coupled plates - as a function of the number of modes in a frequency band.	104
5-3	Experimental and theoretical energy ratio level differences for two edge joined coupled plates - as a function of the modal overlap factor.	105
5-4	Determination of the upper and lower bounds for three and four plates at a common join.	115
5-5	Experimental and theoretical energy ratio level differences for three and four plates at a common join - as a function of the number of modes in a frequency band.	116
5-6	Experimental and theoretical energy ratio level differences for three and four plates at a common join - as a function of the modal overlap factor.	117
5-7	Experimental and theoretical energy ratios for the three element structures comprising plates 1, 2, 6A, plate 2 directly excited.	121
5-8	Experimental and theoretical energy ratios for the three element structures comprising plates 1, 2, 6A, plate 6 directly excited.	122
5-9	Experimental and theoretical energy ratios for the three element structures comprising plates 1, 2, 6A, plate 1 directly excited.	123

Figure No.	Title	Page No.
5-10	Experimental and theoretical energy ratios for the four element structure comprising plates 1, 2, 5A and 6A, plate 2 directly excited.	125
5-11	Experimental and theoretical energy ratios for the eight plate structure - plate 14 directly excited.	129
D-1	Steady State Measurement of the plate internal loss factor.	175
D-2	Decay method measurement of the plate internal loss factor.	175
D-3	Schematic Diagram - Instrumentation for the measurement of steady state internal loss factor.	178
D-4	Power flow transducer.	184
D-5	Three plate structure and support system.	184
D-6	Confidence limits for plate mean square acceleration levels - as a function of the number of measurement locations used.	187
E-1	Schematic Diagram - Instrumentation for the measurement of steady state internal loss factor.	189
E-2	Power flow transducer - construction.	190
E-3	Power flow transducer - mobility circuit.	190
E-4	Determination of equivalent mass M_2 of power flow transducer.	196
E-5	Damped plate internal loss factor - experimental results.	199
E-6	Damped plate internal loss factor - experimental results.	200

LIST OF TABLES

Table No.	Title	Page No.
4-1	Comparison of $(t_i/t_j)^{0.5}$ with typical values of τ_{ij}/τ_{ji} for various plate combinations.	48
5-1	List of Experimental Plates.	91
5-2	Plate Internal Loss Factors.	92
5-3	List of Coupled Elements.	93
5-4	Predicted and Measured Energy Ratios. Two Plate structure - Plate Nos. 1 & 2.	98
5-5	Predicted and Measured Energy Ratios. Two Plate structure - Plate Nos. 3 & 4.	99
5-6	Predicted and Measured Energy Ratios. Two Plate structure - Plate Nos. 5 & 6.	100
5-7	Predicted and Measured Energy Ratios. Two Plate structure - Plate Nos. 9 & 10.	101
5-8	Predicted and Measured Energy Ratios. Three Plates at a common join. Plate Nos. 7, 8 and 11. (a) Plate 7 directly excited. (b) Plate 8 directly excited. (c) Plate 11 directly excited.	108
5-9	Predicted and Measured Energy Ratios. Three Plates at a common join. Plate Nos. 9, 10 and 12. (a) Plate 9 directly excited. (b) Plate 10 directly excited. (c) Plate 12 directly excited.	111
5-10	Predicted and Measured Energy Ratios. Four Plates at a common join. Plate Nos. 9, 10, 12 and 13. Plate 10 directly excited.	114
E-1	Calibration Constants.	202

GLOSSARY OF SYMBOLS

a_i	propagating bending wave amplitude in plate i
a'_i	non propagating bending wave amplitude in plate i
$\langle a_i^2 \rangle$	mean square acceleration level of plate i : time and spatial average
A_i	area of plate i
b_i	amplitude of longitudinal wave in plate i
B_i	dimensionless factor - equation (4,19)
c_i	amplitude of transverse wave in plate i
C_{Li}	longitudinal wave speed in plate i
C_{Bi}	bending wave speed in plate i
D_i	bending stiffness of plate i
E_i	average bending wave vibrational energy level
E_i	modulus of elasticity - plate i. = $E_i^m / (1 - \sigma_i^2)$
E_i^m	modulus of elasticity of material of plate i
f	frequency
$f_c(t)$	instantaneous force
F_{ij}	dimensionless parameter - equation (4,54)
G_i	shear modulus of material of plate i
H_i	dimensionless factor - equation (B,30)
i	$\sqrt{-1}$
$i(\text{subscript})$	pertaining to plate i
$j(\text{subscript})$	pertaining to plate j
k_i	bending wave number in plate i
$k(\text{subscript})$	pertaining to plate k
L_{ij}	length of join between coupled plates i and j
m_i	mass of plate i
M	factor of empirical equation (4,40) - defined equation (4,39)
M_c	force transducer calibration mass

ML_i	accelerometer mass loading factor on plate i
$n(\text{subscript})$	pertaining to plate n
n_i	modal density of plate i (function of f)
N_i	number of resonant modes in excitation bandwidth in plate i
N_{\min}	Lesser of N_i and N_j for interaction of plates i and j
P_i	plate i longitudinal wavenumber
P_{ij}	power flow between coupled linear oscillators i and j
P_i	average power flow into element i
P_{ij}	nett average power flow from element i to element j
P_{ab}	Q_{ab} for steel, $C_L = 5170\text{m/s}$, - not dimensionless
q_i	plate i transverse wavenumber
Q_{ab}	dimensionless parameter - equation (4,57)
r	reflection coefficient = $1-\tau$ - Appendix A.
R_i	modal overlap factor for plate i
R_{\max}	larger of R_i and R_j for interaction of plates i and j
s	convenient form for $\sin\alpha_1$
t_i	thickness of plate i
T	factor for empirical equation (4,40) - defined equation (4,38)
$(TF)_{ij}$	transmission factor for coupled plates, i to j
u_i	displacement in x_i direction
v_i	displacement in y_i direction
w_i	displacement in z_i direction
x_i, y_i, z_i	3-D orthogonal spatial coordinates pertaining to plate i
α_i	propagation angle of bending wave in plate i
β_i	propagation angle of longitudinal wave in plate i
β_{ij}	coupling coefficient for power flow between two single oscillators
γ_i	propagation angle of transverse wave in plate i

∂	partial derivative
Δ	incremental
η_i	internal loss factor - plate i
$\eta_{i \text{ app}}$	apparent loss factor - plate i
η_{ij}	coupling loss factor from plate i to plate j
λ_{Bi}	bending wavelength in plate i
π	P_i
ρ_i	density of material of plate i
ρ_{si}	surface density of plate i
σ_i	Poisson ratio of material in plate i
Σ	summation
τ_{ij}	average transmission coefficient from plate i to plate j
$\tau_{ij} (s)$	oblique incidence transmission coefficient from plate i to plate j
$\tau_{ij} (o)$	normal incidence transmission coefficient from plate i to plate j
$\tau_{BB_{ij}}$	average bending to bending wave transmission coefficient - plate i to plate j
$\tau_{BL_{ij}}$	average bending to longitudinal wave transmission coefficient - plate i to plate j
$\tau_{BT_{ij}}$	average bending to transverse wave transmission coefficient - plate i to plate j
ϕ_i	average vibrational energy of simple oscillator i
χ_{ij}	dimensionless parameter - equation (4,17)
ψ_{ij}	dimensionless parameter - equation (4,17)
ω	radian frequency

SECTION 1. INTRODUCTION

Over the past few years, there has been increasing concern about the effect of pollutants on the quality of our environment and their effects on personal comfort and safety. Unwanted noise and vibration constitutes one form of pollution; concern comes not only from those who are professionally involved, but also from other members of society who are demanding their right to an environment free from irritating and harmful noise. Industry is being asked to reduce both in-plant and emitted noise levels while lower noise and vibration levels in air and surface transport are continually being sought. Current attitudes regarding noise pollution, resulting in existing and envisaged legislation, constitute a strong argument for continuing research into all aspects of noise and vibration control.

This thesis is concerned with the distribution of vibrational energy in an excited built up structure. Since all forms of air and surface craft, as well as many noise emitting, vibration inducing machines, can be thought of as built up structures consisting of collections of connected elements, it is felt that the work presented here will find practical application in the effort to control unwanted noise and vibration in our environment. It is worth noting that buildings too may be considered as built up structures and thus they too would be amenable to the analysis presented here. Thus the topic dealt with in this thesis should have very wide application.

With small structures, for example machines, one is generally concerned with radiated sound or vibration in critical areas around the structure. With larger structures, such as ships, aircraft, and buildings, we are generally concerned with noise and vibration within the confines of the structure. In

either case our ability to predict noise and vibration levels depends on a knowledge of the various energy inputs and their coupling to the structural elements, the resulting vibrational energy distribution throughout the structure and the acoustic coupling of the structural elements to the surrounding fluid, (usually air or water). The degree of coupling and the type of source from which the vibration comes, varies for different situations, hence research in this area is necessarily relevant only to that particular source type investigated, but prediction of the vibrational energy distribution in the structure is relevant to all structures, irrespective of the source, and is the subject of the research reported in this thesis.

When a structure is excited, vibrational energy is distributed throughout the structure in such a way that all the structural elements are excited to a level dependent on (a) the excitation frequencies, (b) structure geometry and (c) the physical characteristics of the structural elements.

Where the excitation is such that the lowest few modes of the structure dominate the response, existing classical modal response analysis techniques are satisfactory. These techniques are also theoretically valid for higher order modal response, but where the excitation is of a broad band nature, a large number of modes must be considered. In addition, the predicted higher order modal responses are more sensitive to variations in geometry and boundary conditions and it is often not possible to define these conditions accurately.

There are currently available computer programmes, based on classical techniques, useful for the prediction of structural response (Kayser and Bogdanoff, 1975)*, where computer memory

* See footnote on Page 3.

size and computing time are determined by the accuracy required. However, use of these programmes, when many modes must be considered, can be prohibitive in terms of computer time and finally memory size. Nonetheless a designer of a structure, be it ship or machine, often needs to predict vibrational energy distribution, for noise and vibration control purposes even though economic factors may preclude the use of extensive computing time.

A technique which has been developed over the last decade and which usually only requires a desk calculator for computation, is Statistical Energy Analysis, (SEA), which uses average parameters to predict average energy levels of the structural elements. These average parameters are independent of the boundary conditions of the elements. However, the method does require a basic minimum number of resonant modes in a measurement frequency band and this limits the method to broad band analysis, which is usually adequate for noise and vibration control engineering.

The technique has theoretical limitations on the extent of its use applying particularly to frequency range and bandwidth; these limitations are not, however, well defined. There are also some common structural configurations of interest where the coupling coefficients required for the analysis are not easily determined. For SEA to be of use to a designer of a general structure, these aspects need clarification and their clarification is the subject of this investigation.

Statistical energy analysis makes use of power balance equations which in turn depend upon an independent determination of loss and coupling loss factors, thus our investigation is

*Footnote: Two methods of referencing other works are used; for example -

(a)response (Kayser and Bogdanoff, 1975), where...
(b)where Lyon and Maidanik (1962) found...

naturally divided into two parts; the use of power balance equations to describe the energy distribution of an N element connected structure, and, the evaluation of the coupling loss factors required for use in the power balance equations. It is convenient to consider these separately and to present a separate relevant literature review for each. Thus while the objectives of this research are listed in Section 2, their justification comes later in Sections 3 and 4. In Section 3, the power balance equation for two coupled elements and the extension of the concepts to include N connected elements is traced in the review of previous work. However, the mathematics involved in deriving these equations from the original concept of power flow between two linearly coupled oscillators is not presented as it has been reviewed extensively by other authors, for example Fahy (1974) and Lyon (1975). Finally it is shown how the power balance equations for a general N element connected structure can be arranged as a matrix equation, in which the vibrational energy distribution in the structure is related to the internal and coupling loss factors for the various coupled elements.

The present methods of evaluating coupling loss factors for different coupled element arrangements are discussed in the literature review in section 4. It is shown that the coupling loss factor can be related to a wave transmission coefficient. The use of three different wave transmission coefficients is discussed.

The evaluation of average transmission coefficients for a junction of 4 plates, using wave transmission theory, is next presented and these considerations are the principal concern of Section 4. Two situations are presented: (a) a bending wave solution where bending waves only are considered, and (b) a general solution where wave transformations from bending to

longitudinal and transverse waves at the join are considered. An empirical equation which relates the average bending wave solution to the more easily calculated normal incidence bending wave solution is presented.

The predicted values of the average bending wave transmission coefficients to the average general solution transmission coefficients are compared in the discussion in Section 4.4. These indicate at what plate thickness and excitation frequency the effects of the longitudinal and transverse wave transformations can not be ignored.

In the remainder of Section 4, experimental methods used to measure coupling loss factors, and the problems involved, are discussed.

Transmission coefficients for a number of experimental model structures consisting of various combinations of joined plates are evaluated using the bending wave formulations previously derived. These transmission coefficients are used in conjunction with experimentally determined internal loss factors to predict energy distributions in the plate structures. Next, the structures are subjected to third octave broad band excitation and the energy distributions measured. In Section 5, comparisons between measured and predicted energy ratios are presented. Two plate single join structure results and three and four plate single join structure results are used to determine the restrictions within which the SEA technique gives reasonable agreement between measured and predicted energy distributions. Further results for larger multijoin structures are also presented.

The implications of the findings in Section 5 are discussed in Section 6 along with general conclusions and recommendations for further research in this field.

SECTION 2. OBJECTIVES

The frequency range over which the assumptions implicit in the formulation of statistical energy analysis are valid is limited for any particular structure, but the limits are ill defined. An objective of this research will be to give quantitative definition to the implied limits. Thus an objective will be to quantitatively define the lower bound, which is the minimum number of resonant modes required in an element in a measurement frequency band. Similarly another objective will be to determine an upper frequency bound which is related to a combination of the degree of damping of individual modes and their separation in frequency space. The latter concept is described as modal overlap. Thus an objective will be to quantitatively define the upper bound, which is the maximum permissible value of the modal overlap. For the purpose of defining upper and lower bounds, various models comprising two, three and four plates coupled at a common join will be considered. The proposed bounds will then be determined by comparing the predictions of SEA with measurements made on the various models.

Yet another objective will be to use SEA to predict the energy distribution for a multielement structure consisting of up to four inter-connected parts and compare the predictions with measurements taking due account for the previously determined upper and lower frequency bounds.

Many structures contain junctions of up to four plates at a common join and thus it will be an objective of this research to develop a general equation to predict the average coupling loss factor for a common welded join of up to four plates. Wave transformation can take place at a join, but it is not always important and its inclusion considerably complicates the required cal-

calculations. The cases when bending waves only need be considered and when wave transformation at a join can not be ignored will be investigated separately. Yet another objective of this research will be to quantitatively determine the bound between these cases. A final objective will be to develop a simplified procedure for estimating the more complicated average coupling loss factors from the simpler normal incident coupling loss factor expression, considering only bending waves.

SECTION 3. POWER BALANCE EQUATIONS

3.1. REVIEW OF PREVIOUS WORK

A structure can be considered as a number of interconnected elements comprised of plates, beams, shells and enclosed acoustic fields. For an excitation frequency bandwidth within the range of limits imposed by SEA, each element contains some similar resonant modes which can be considered to be ensembles of modes. Lyon (1975, (1)) showed that the modes of an element can be thought of as single oscillators. Lyon and Maidanik (1962) considered the modes of a structural element to be an ensemble of oscillators. Hence, a model of a resonant structure could be a group of resonant elements coupled together. Ungar and Scharon (1967) showed that any two coupled elements can be modelled as two ensembles of oscillators interacting and the nett power flow from one ensemble to the other is the sum of all the individual oscillator to oscillator power flows.

Lyon and Maidanik (1962) presented an equation relating the nett power flow between two linearly coupled oscillators excited by statistically independent random sources to the difference between the average vibrational energies of each oscillator.

This equation is

$$* \quad p_{12} = \beta_{12} (\Phi_1 - \Phi_2) \quad (3,1)$$

As the connected structure can be modelled as a collection of ensembles of oscillators interacting together, an equation predicting the power flow between these ensembles of oscillators is required. No exact relationship has been developed for the prediction of power flow for more than two coupled oscillators

* The symbols used are listed in the glossary at the beginning of this thesis.

of arbitrary coupling strength. However, with the assumption of weak coupling Lyon and Maidanik (1962) and Newland (1966) have shown that a relationship analogous to equation (3.1), relates the nett power flow to the average modal energy difference between the two ensembles of oscillators.

$$P_{ij} = \eta_{ij} \omega n_i (E_i/n_i - E_j/n_j) \quad \dots (3,2)$$

To obtain equation (3,2), a number of restrictions have been imposed on the two ensembles of oscillators or groups of resonant modes of the coupled elements contained within the excitation frequency band. Fahy (1974) extensively discusses these restrictions in a very good critical review of SEA. The steps involved in obtaining (3,2) from (3,1) will not be presented. However, for the convenience of the reader, the major assumptions and their implications are repeated here.

One of the restrictions is that the two elements should be weakly coupled. Fahy states that there are few cases where weak coupling criteria for specific systems have been published. Examples of the two cases considered are those of coupling between a structure and a fluid such as the acoustic coupling of a shell mode to an acoustic mode of a fluid volume. Reasonably good results also have been obtained using SEA to predict the power flow from panels to surrounding acoustic fluids (Lyon and Maidanik, 1962) (Crocker and Price, 1969). It is much more difficult to consider, however, two coupled structural elements as being weakly coupled. Fahy gives an example of weak coupling between beams as two beams connected by a weak rotational spring, as investigated by Crandall and Lotz (1971). Lotz and Crandall

(1973) measured power flow directly to show that power flow between two plates coupled by a light spring was proportional to the modal energy difference between the two plates. However, Lyon (1975) states that the weak coupling assumption is unnecessary if the uncoupled systems are defined as the blocked systems. Scharton and Lyon (1968) also considered two beams coupled by a stiff spring to be 'lightly' coupled in the sense that the angular movement at the junction was small. The coupling in a real welded structure is closer to this concept than to the others discussed.

In the work presented here, no attempt has been made to define the strength of the coupling, as part of this work is to show if and where SEA can be applied to general welded plate structures. Fahy points out in his review that investigations by Chintsun Hwang (1973) into coupling between a plate and a welded complete cylindrical shell led to the conclusion that the coupling was too strong for the methods of SEA to be applicable. However, Chintsun Hwang also investigated a structure composed of two edge connected flat plates where comparatively good results were obtained.

Another assumption is that the wave fields in each element are reverberant, which implies that there are a sufficient number of modes present in the bandwidth to constitute a reverberant field. Also there must be a sufficient number of modes that the coupling loss factor represents a good average value for all the individual coupling coefficients between the individual modes. However, no values for the minimum number of modes required for SEA to be usefully applied have been suggested in the published literature. It is one of the objectives of this research to determine experimentally the minimum number of modes required for acceptable comparisons of measurement with the

predictions of SEA.

Lyon and Maidanik (1962) also assumed that the modes should be lightly damped and be well separated. Lightly damped is often assumed to imply that the internal loss factor of the element $\eta_i \ll 1$ (Crandall and Lotz, 1971). The concept of well separated modes allows the power flows from each mode of one set to different modes of the second set to be summed without the need for considering the interaction between the modes of the one set. The assumption stated formally is that the average frequency difference between modes, which is $1/n_i$, the reciprocal of the modal density, is greater than the half power frequency bandwidth $(\Delta f)_{\frac{1}{2}}$ of the modal response. This can be written as an inequality, and if both sides are divided by the frequency f , then this and the light damping requirement can be expressed as

$$\eta_i \ll 1 \quad (3,3(a))$$

$$\eta_i < (n_i f)^{-1} \quad (3,3(b))$$

(3,3(b)) in effect suggests that there is an upper frequency limit, the determination of which is also an objective of this research.

Consideration of the power flow between two coupled elements which are excited by statistically independent broad band sources, (see Fig. 3-1), leads to the power balance equations for two coupled elements in steady state.

$$P_1 = \omega \eta_1 E_1 + \omega \eta_{12} n_1 (E_1/n_1 - E_2/n_2) \quad (3,4)$$

$$P_2 = \omega \eta_2 E_2 + \omega \eta_{21} n_2 (E_2/n_2 - E_1/n_1) \quad (3,5)$$

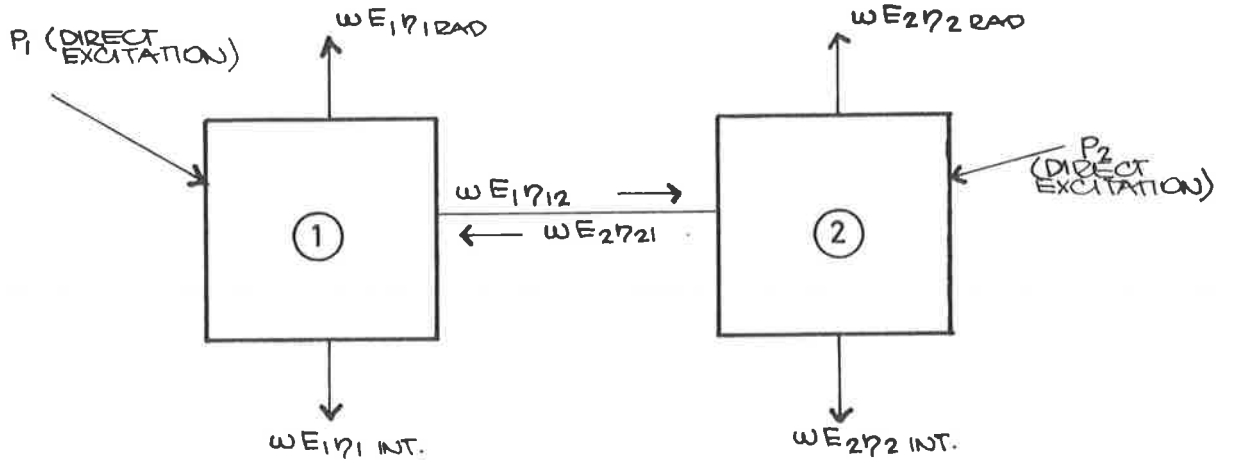
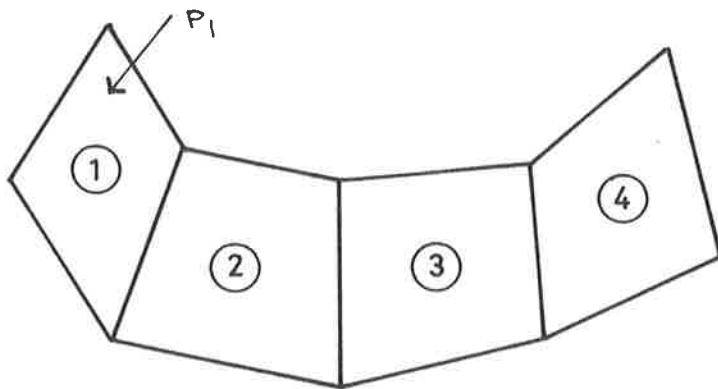
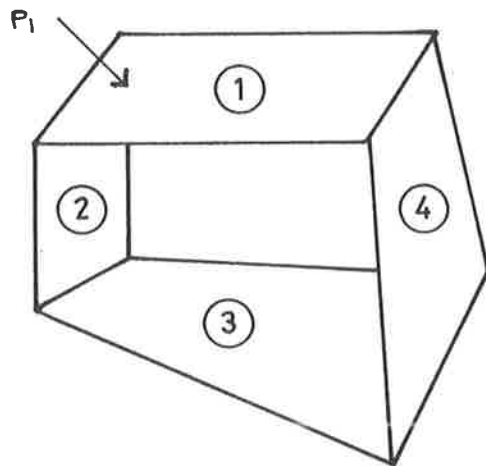


FIG. 3.1. POWER FLOW FOR TWO COUPLED ELEMENTS



(a) IN LINE STRUCTURE



(b) CLOSED STRUCTURE

FIG. 3.2. FOUR ELEMENT STRUCTURE

In these equations, the internal loss factor of an element is considered to be the sum of the radiation loss factor plus the plate internal loss factor

$$\eta_i = \eta_i \text{ int} + \eta_i \text{ rad}$$

A useful reciprocity relation follows from the observation that the power flow from element one to two must certainly equal the negative of the power flow from two to one. Equation (3,6) follows immediately

$$\eta_{12} n_1 = \eta_{21} n_2 \quad (3,6)$$

For $P_2 = 0$ in equation (3,5), the energy ratio E_2/E_1 can be expressed as

$$\begin{aligned} E_2/E_1 &= \eta_{12}/(\eta_2 + \eta_{21}) \\ &= (n_2/n_1) \eta_{21}/(\eta_2 + \eta_{21}) \end{aligned} \quad (3,7)$$

The derivations and implications of equations (3,4) to (3,7) are all presented and discussed by Fahy (1974) in his critical review.

Thus far, we have considered only two coupled element structures, whereas most structures contain many elements. In his review, Fahy stated that the weak coupling assumption allowed the vital simplification that the power flow from a mode of one element to a mode of the coupled element could be determined without including the interaction of any other mode. This

allowed the form of the power flow equation between coupled elements to be of the same form as the power flow equation between coupled oscillators, with the average coupling loss factor replacing the coupling coefficient. If we consider an element to be similar to an oscillator, with average characteristics replacing the characteristics of an oscillator, the weak coupling concept can be extended to allow the power flow from one element to a coupled element to be determined without including the interaction of any other coupled element. This was assumed by Eichler (1965) and led to an expression for the power balance equation for an element coupled to any number of other elements.

$$P_i = \omega E_i \eta_i + \omega E_i \sum_{\substack{j=1 \\ j \neq i}}^n \eta_{ij} - \omega \sum_{\substack{j=1 \\ j \neq i}}^n E_j \eta_{ji} \quad (3,8)$$

Equation (3,8) was used for $n = 3$ in three different investigations; the power flow from one acoustic field to another inside a box structure (Eichler, 1965); the transmission loss of a panel separating two acoustic fields (Crocker and Price, 1969); and the energy transmission from one flat plate to another via a connecting flat beam (Lyon and Scharton, 1965). All three are examples of elements coupled in tandem. The application of equation (3,8) to structures of three or more interconnected elements with various transmission paths is the subject of this investigation.

Postscript:

A report on the investigation into sound transmission in building structures was read just prior to submitting this work. The research (Gibbs and Gilford, 1976) investigates the power flow in building structures taking account of some wave transformations. They conclude that for simple (single join) structures, wave transformations are not important, but where more than one junction is involved, their results indicate that all structure borne waves should be considered.

3.2. PREDICTION OF ENERGY DISTRIBUTION IN AN N-ELEMENT CONNECTED STRUCTURE.

We consider any general N-element connected structure and apply the general power balance equation (3,8) to each of the N elements. These can be arranged to form a matrix relationship of the form $AX = B$ where A is a square matrix of coupling loss factors and X is a column matrix which gives the energy level distribution. We take the energy level of element N as a reference level, then the general form is

$$\begin{bmatrix}
 \eta_{11} & -\eta_{21} & -\eta_{31} & \dots & \dots & -\eta_{N-1,1} \\
 -\eta_{12} & \eta_{22} & -\eta_{32} & \dots & \dots & \vdots \\
 -\eta_{13} & \dots & \dots & \dots & \dots & \vdots \\
 \vdots & & & & & \vdots \\
 \vdots & & & & & \vdots \\
 -\eta_{1, N-1} & & & & -\eta_{N-1, N-2} & \eta_{N-1, N-1}
 \end{bmatrix}
 \begin{bmatrix}
 E_1/E_N \\
 E_2/E_N \\
 \vdots \\
 \vdots \\
 E_{N-1}/E_N
 \end{bmatrix}
 =
 \begin{bmatrix}
 P_1/\omega E_N + \eta_{N1} \\
 P_2/\omega E_N + \eta_{N2} \\
 \vdots \\
 \vdots \\
 P_{N-1}/\omega E_N + \eta_{N, N-1}
 \end{bmatrix}
 \quad (3,9)$$

$$\text{where } \eta_{ii} = \eta_i + \sum_{\substack{r=1 \\ r \neq i}}^n \eta_{ir}$$

The Nth equation which is required to predict absolute energy levels is

$$P_N/\omega E_N - \eta_{NN} = -\eta_{1N} E_1/E_N - \eta_{2N} E_2/E_N - \dots - \eta_{N-L, N} E_{N-1}/E_N$$

(3,10)

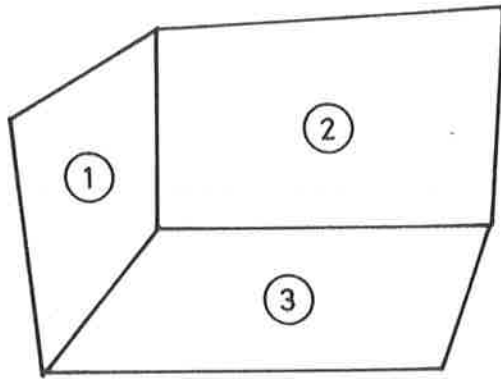
Where element N is the only element directly excited by an external source, the input power terms of B become zero leaving a column vector of the N-1 coupling loss factors from the directly excited element N to the other coupled elements.

The configuration of the connected structure determines which coupling loss factors will be zero, as where two elements i and j are not directly coupled, the coupling loss factors η_{ij} and η_{ji} are zero. For example, consider the two four plate structures in fig. (3-2) with element 1 directly excited in each case. For the box type structure, the matrix equation (3,9) becomes

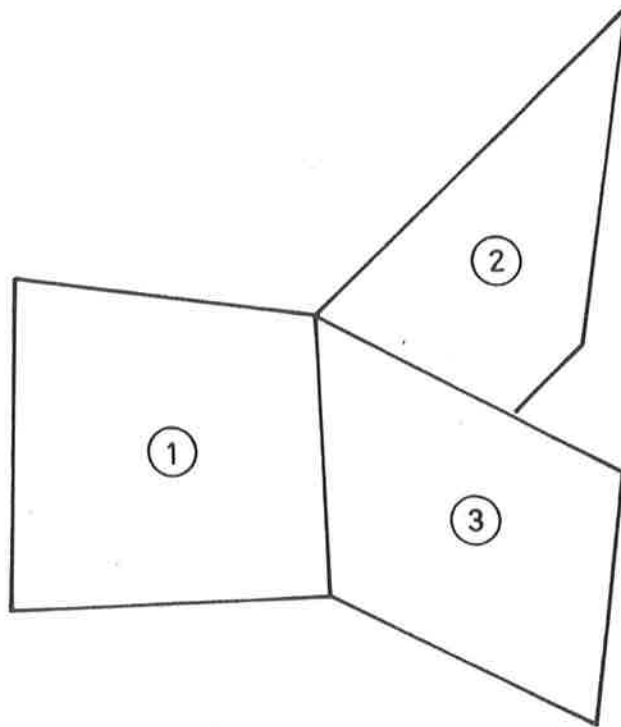
$$\begin{bmatrix} \eta_{22} & -\eta_{32} & 0 \\ -\eta_{23} & \eta_{33} & -\eta_{43} \\ 0 & -\eta_{34} & \eta_{44} \end{bmatrix} \begin{bmatrix} E_2/E_1 \\ E_3/E_1 \\ E_4/E_1 \end{bmatrix} = \begin{bmatrix} \eta_{12} \\ 0 \\ \eta_{14} \end{bmatrix} \quad (3,11)$$

Equation (3,11) also describes the in-line structure where $\eta_{14} = \eta_{41} = 0$. (Note that η_{41} is contained in the term η_{44}).

It should also be noted that two different structural configurations may be described by the same general matrix equations. For example, when equation (3,9) is used to describe the two structures shown in fig. (3-3) for the case where $P_2 = P_3 = 0$ the following equation results for both.



(a)



(b)

FIG. 3.3. THREE ELEMENT STRUCTURES

ENERGY RATIO EQUATION (3,12) IS APPLICABLE
TO BOTH STRUCTURES (a) & (b)

$$\begin{bmatrix} \eta_{22} & -\eta_{32} \\ -\eta_{23} & \eta_{33} \end{bmatrix} \begin{bmatrix} E_2/E_1 \\ E_3/E_1 \end{bmatrix} = \begin{bmatrix} \eta_{12} \\ \eta_{13} \end{bmatrix} \quad (3,12)$$

Although the plates and the coupling lengths may be the same for each case, the coupling loss factors will be different.

In a recent paper, Wöhle and Elmallawany (1975) presented a general solution for the prediction of energy distribution in complicated structures. Their solution is similar to equation (3,9). Acoustic fields within the structure were considered as elements. No discussion of the evaluation of structure to structure coupling loss factors was included. The authors referred to previously published works which contain only evaluation procedures for structure to acoustic field coupling loss factors.

SECTION 4. COUPLING LOSS FACTORS

4.1. REVIEW OF PREVIOUS WORK

It is clear from Section 3 that the important parameters required to determine the energy distribution in a structure are the respective coupling loss factors and internal loss factors. Internal loss factors of elements must be either measured or typical values used, taking into account the type of material and various other losses which contribute to the apparent internal loss. However at present, no general expression can be given for the coupling loss factors; each join must be considered as a special case.

The most common joins encountered in a connected structure are beam to beam, beam to plate, acoustic field to plate and plate to plate. Investigations have been carried out and expressions are available for evaluating coupling loss factors for beam to beam (Scharton and Lyon, 1968), (Crandall and Lotz, 1971); cantilevered beam to plate, (Lyon and Eichler, 1964); beam to plate edge, (Lyon and Scharton, 1965); and acoustic field to plate, (Crocker and Price, 1969).

It is interesting to note that Scharton and Lyon (1968), in developing an expression for the coupling loss factor between two coupled beams, assumed light damping in the following sense (Crandall and Lotz, 1971),

$$\eta_i \ll (n_i f)^{-1} \ll 1$$

which is in agreement with the inequalities (3,3(a) and (b)) with the added restriction $(n_i f)^{-1} \ll 1$. Lyon (1975(2)) has presented a general equation relating coupling loss factor η_{ij} to a transmission coefficient τ_{ij} for coupled plates,

$$\eta_{ij} = \frac{2}{\pi} \frac{L}{k_i A_i} \tau_{ij} \quad (4,1)$$

The transmission coefficient τ_{ij} is defined as the ratio of the energy transmitted across the join to the energy incident at the join. Equation (4,1) was first presented by Lyon and Eichler (1964) and was derived from an earlier expression by Heckl (1962), based on a 2 dimensional analogy to Sabine's reverberant room decay equations.

Lyon and Eichler used equation (4,1) to investigate the coupling loss factor for a cantilevered plate connected to an infinite support plate. Wave transmission analysis was used to obtain an expression for the average transmission coefficient of this T type join, which they considered as a 2 plate join.*

The expression for τ_{ij} was an integral equation too complicated to be of general use. Lyon and Eichler suggested that $\tau_{12} = 8/27$ for $k_1 = k_2$ and $\tau_{12} = D_1/D_2$ when $k_1 \gg k_2$. The use of these two values of τ_{12} to evaluate η_{12} restricts its application to only cantilevered plate junctions where either, the thicknesses of the two plates are equal, or where the support plate is much stiffer than the cantilevered plate.

Lyon (1975(2)) also presents an equation for τ applicable to the transmission of energy from one plate via a reinforcing beam to a second plate.

Other than the two examples quoted, there does not appear to be any other formulae readily available for calculating

*In the presentation of this thesis, the T type join is considered as a junction of three plates with $t_1 = t_3$ and t_2 the thickness of the cantilevered plate.

coupling loss factors for plate to plate joins. Fahy (1974) referred to investigations into two edge joined (L-type) coupled plate by Chintsun Hwang (1973), but attempts to obtain a copy of this report have been unsuccessful.

Lyon (1975(2)), in considering transmission through plate junctions states that background information required to make calculations for other systems may be found in his references. It appears that it would be most useful to use the latter background information to develop general equations for the evaluation of the average transmission coefficients for a general 4 plate join. This would then allow coupling loss factors for such a structure to be evaluated and as stated previously in Section 2. This problem will be considered in the following sections.

The most convenient method to determine the transmission coefficient for an energy flow from one plate to another is to use the travelling wave method. Consider the two plate junction in Fig. 4-1, where a travelling bending wave of unit amplitude displacement in plate i is incident on the join at angle α_i . Some of the energy is transmitted to form a bending wave of amplitude a_j propagating at angle α_j in plate j and the remainder is reflected in plate i . The transmitted energy and incident energy can be expressed in terms of the plate characteristics and travelling wave amplitudes and propagating angles, hence the average value for the transmission coefficient from plates i to j is

$$\tau_{ij} = \int_{-\frac{\pi}{2}}^{\frac{\pi}{2}} \frac{\rho_{sj}}{k_j} |a_j|^2 \cos \alpha_j d\alpha_j \bigg/ \int_{-\frac{\pi}{2}}^{\frac{\pi}{2}} \frac{\rho_{si}}{k_i} \cos \alpha_i d\alpha_i \quad (4,2)$$

Note that the general expression for energy flow is $\rho_s c_g |v|^2$ where c_g , the group velocity, is numerically proportional to phase velocity ω/k for bending waves in plates.

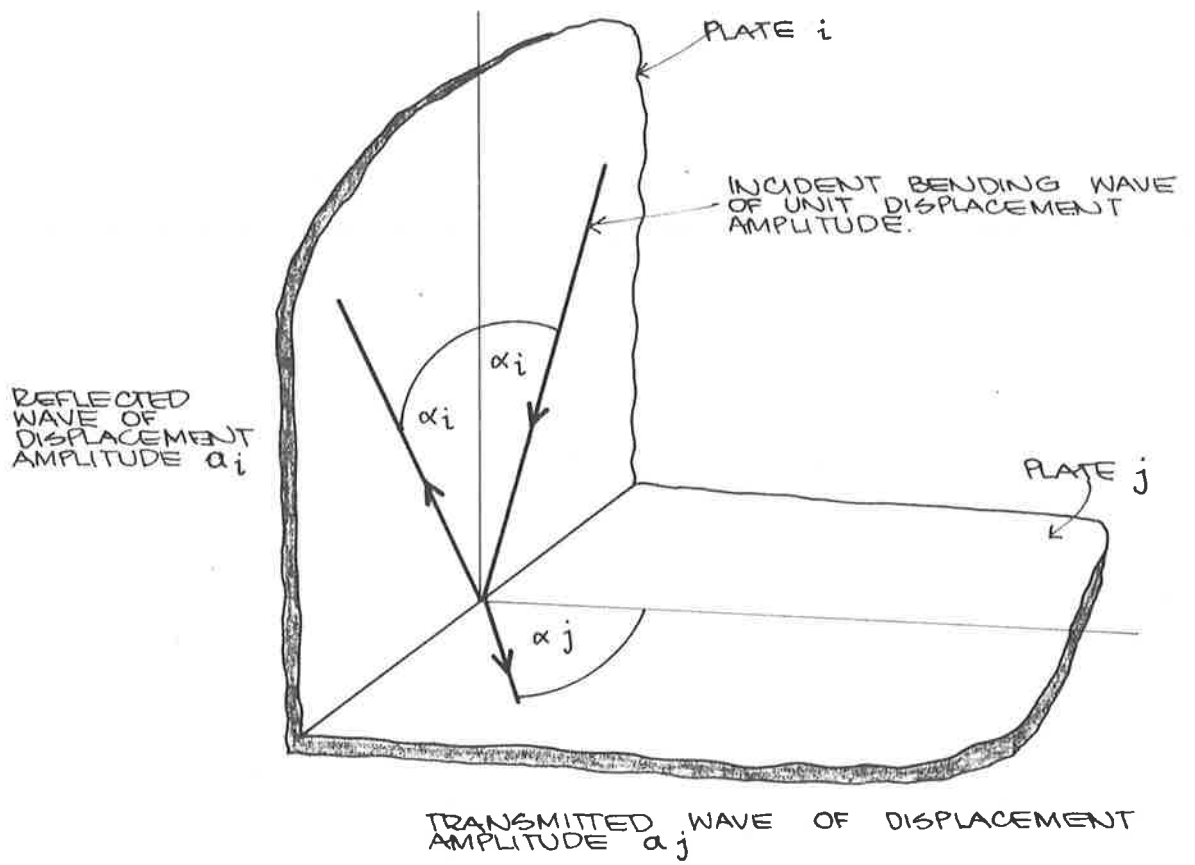


FIG. 4.1. TRAVELLING BENDING WAVE AMPLITUDES AND DIRECTION OF PROPAGATION FOR AN OBLIQUE BENDING INCIDENT ON THE JUNCTION OF TWO EDGE COUPLED PLATES i & j

Equation (4,2) was used by Lyon and Eichler (1964) but included a factor of 2 in the numerator to account for the two equal plates receiving transmitted energy. $|a_j|$ can be determined by considering the boundary conditions at the join.

The wave transmission approach for two L-joined plates is fully discussed by Cremer (Cremer, Heckl and Ungar, 1973 (1)&(2)) where it is used to develop equations for the normal incidence and average transmission coefficients. These coefficients were used to determine the transmission loss (TL) at the join where

$$TL = 10 \log (1/\tau) \quad (4,3)$$

However, no attempt was made to apply these results to SEA.

Cremer also derived expressions for τ_{ij} for special cases of 3 or 4 plate joins for normal incidence only. The special cases were either, all plates equal or at least opposite plates equal.

With thicker structures or higher frequencies, the longitudinal and transverse waves must be considered as well as bending waves. This problem was first considered for 4 plates at a join by Budrin and Nikiforov (1964), for normal incidence only. Wave transmission through concrete structure joins of 4 elements was investigated by Kihlman (1970). He used average transmission coefficients to predict mean square vibration levels in a thick structure. Comparisons between measured and predicted levels showed that longitudinal and transverse waves had to be considered in evaluating the average transmission coefficient. The method of evaluating the coefficients was not presented, but references were made to an earlier paper (Kihlman, 1967). Attempts to obtain this earlier paper have been unsuccessful.

In the previous discussion the joints were considered in isolation. In a real structure there are many joints and the longitudinal and transverse waves can carry vibrational energy to a second or third junction where wave transformations can cause bending waves to be produced, forced by the longitudinal and transverse waves. Bhattacharya, Mulholland and Crocker (1971) investigated the wave transformations in a two joint structure and concluded that for some structures predictions of energy distribution based on joints considered in isolation, may be in error. By comparing predicted average transmission coefficients, evaluated using a bending wave solution and a general solution, the conditions when wave transformations, and hence the multi-joint effects, can not be ignored, will be investigated, as was stated in Section 2.

4.2. ALTERNATIVE FORMULATIONS IN TERMS OF WAVE TRANSMISSION COEFFICIENTS.

Equation (4,1) was derived from consideration of the energy density decay in a vibrating plate; this approach is analogous to the three dimensional room acoustics theory and in particular is analogous to the sabine reverberation time formulation theory. (Beranek 1971(1).) Millington and Sette have formulated an alternative theory for room decay. The two dimensional analog of this theory leads to a similar equation to (4,1) but with $-\ln(1 - \tau_{ij})$ replacing τ_{ij} . The derivation is presented in Appendix A and leads to

$$\eta_{ij} = \frac{2}{\pi} \frac{L}{k_i A_i} \left[-\ln(1 - \tau_{ij}) \right] \quad (4,4)$$

There is conjecture which room decay model more closely fits the real case. In room acoustics, the different theories can lead to different values of the absorption coefficient for highly absorbent materials. However, in this work, it is shown in 4.3.4 that for the range of values of τ_{ij} for connected structures, there is little difference between the values of the two coefficients.

A third relationship between the coupling loss factor and a transmission coefficient is developed by expressing the steady state power flow and energy levels of the power flow equation (3,2) in terms of the travelling waves in Fig. 4-1. Equation (3,2) then becomes

$$\int_{-\frac{\pi}{2}}^{\frac{\pi}{2}} LD_j k_j \omega |a_j|^2 \cos \alpha_j d\alpha_i \quad (4,5)$$

$$= \frac{\eta_{ij} n_i \omega}{2} \int_{-\frac{\pi}{2}}^{\frac{\pi}{2}} \left[\frac{m_i \omega^2}{n_i} (1 + |a_i|^2) - \frac{m_j \omega^2}{n_j} |a_j|^2 \right] d\alpha_i$$

If the modal density equation for flat plates (Beranek 1971 (2))

$$n_i(f) = A_i \sqrt{3/c} / L_i t_i \quad (4,6)$$

and the wave number equation (Lyon and Eichler 1964) for flat plates

$$k_i^4 = \omega^2 \rho_{si} / D_i \quad (4,7)$$

are substituted into (4,5), the average coupling loss factor can be expressed as

$$\eta_{ij} = \frac{2 L}{\pi A_i k_i} \left[(\text{TF})_{ij} \right] \quad (4,8)$$

where

$$(\text{TF})_{ij} = \pi \frac{k_i \int_{-\frac{\pi}{2}}^{\frac{\pi}{2}} |a_j|^2 \cos \alpha_j d\alpha_j}{k_j \int_{-\frac{\pi}{2}}^{\frac{\pi}{2}} \left(\frac{t_i}{t_j} (1 + |a_i|^2) - \frac{t_j}{t_i} |a_j|^2 \right) d\alpha_i} \quad (4,9)$$

We have named $(\text{TF})_{ij}$ the transmission factor from i to j .

Equations (4,1), (4,4) and (4,8) are all of the same form, hence a comparison between the coupling loss factors is a comparison between the different transmission coefficients, τ_{ij} , $-\ln(1-\tau_{ij})$ and $(\text{TF})_{ij}$.

The equations (4,2) and (4,9) remain in the same form when applied to three or four plates at a common join. The energy transmitted from plate i to plate j and the energy levels of plates i and j are the required parameters. The other plate or plates connected at the join affect the transmitted and reflected wave amplitudes a_i and a_j . Hence the wave transmission coefficients are affected numerically, but the assumptions used leading to the form of equations (4,2) and (4,9) remain unchanged.

When expressions for the three wave transmission coefficients have been determined for the four plate single join structure, the differences between the three different forms for the wave transmission coefficient will be shown to be quite small.

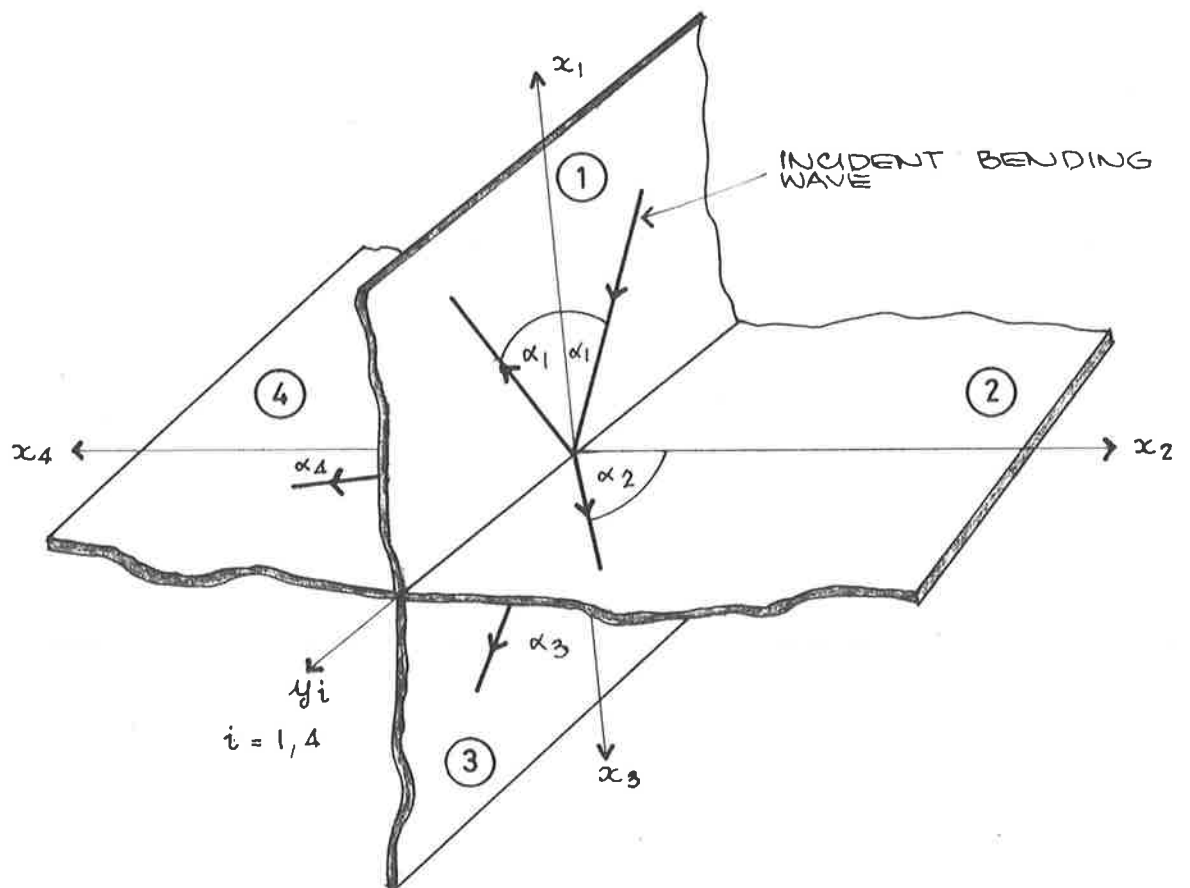


FIG. 4.2. GEOMETRY AND WAVE PROPAGATION DIRECTIONS FOR FOUR PLATES AT A COMMON JOIN.

4.3. BENDING WAVE SOLUTION - ANY NUMBER OF PLATES AT A COMMON JOIN.

4.3.1. Wave Transmission Method.

To begin, we consider four plates connected at a common join with coordinates as shown in Fig. 4-2. A bending wave of unit amplitude displacement in plate 1 is incident at the common join at angle α_1 to the normal. There is a reflected wave in plate 1 of amplitude a_1 travelling away from the join at reflected angle α_1 , and transmitted waves a_2 , a_3 and a_4 travelling at refracted angles α_2 , α_3 and α_4 respectively. With each transmitted and reflected wave there is also a non propagating component with a maximum amplitude of a_i' . As only bending waves are considered, the energy is transmitted from one plate to another only by bending moments at the join. Note that the plates do not need to be at right angles to each other for this analysis. Hence the analysis is applicable to any number of plates at a common join, although four plates are shown and discussed in the formulation. However, as there would be few structures containing joins at which there were more than four plates, it is sufficient to consider the four plate case.

For mathematical convenience, each plate has its own coordinate system. The join is the y axis assumed positive out of the page; each plate is in its own x-y plane with positive x increasing away from the y axis, and positive z direction is taken in the clockwise direction when viewed from the positive y direction, forming a series of right handed coordinate systems. Displacement in the z_i direction is w_i .

The boundary conditions are

- (a) no displacement in any direction along the y axis, i.e. $w_i = 0$ at $x_i = 0$ for all i,
- (b) the join is assumed stiff in comparison with the plate bending stiffnesses, hence the relative angle

between any two plates remains constant, i.e. $\frac{\partial w_i}{\partial x_i}$ is the same for all i , at $x_i = 0$

- (c) the sum of the bending moments about the join is zero, assuming that the join has zero moment of inertia.

$$\sum_{i=1}^4 D_i \frac{\partial^2 w_i}{\partial x_i^2} = 0 \text{ at } x_i = 0$$

The displacement equation for plate 1 is

$$\begin{aligned} w_1(x_1, y_1, t) = & \left[\exp(i k_1 x_1 \cos \alpha_1 - i k_1 y_1 \sin \alpha_1) + \right. \\ & a_1 \exp(-i k_1 x_1 \cos \alpha_1 - i k_1 y_1 \sin \alpha_1) + \\ & \left. a_1' \exp(-k_1 x_1 \sqrt{1 + \sin^2 \alpha_1} - i k_1 y_1 \sin \alpha_1) \right] \\ & \exp(i \omega t) \end{aligned} \quad (4,10)$$

The displacement equations for the remaining plates are

$$\begin{aligned} w_n(x_n, y_n, t) = & \left[a_n \exp(-i k_n x_n \cos \alpha_n - i k_n y_n \sin \alpha_n) \right. \\ & \left. + a_n' \exp(-k_n x_n \sqrt{1 + \sin^2 \alpha_n} - i k_n y_n \sin \alpha_n) \right] \exp(i \omega t) \end{aligned} \quad (4,11)$$

where the plates are identified by the subscript n

for $n = 2, 3$ and 4 respectively.

The trace wave lengths along the y axis are equal for each plate, hence

$$k_1 \sin \alpha_1 = k_2 \sin \alpha_2 = k_3 \sin \alpha_3 = k_4 \sin \alpha_4 \quad (4,12)$$

The factors in (4,12) and $\exp(i \omega t)$ are common to all four equations and can be omitted from the displacement equations

when the boundary conditions are considered. The omitted terms must be considered if any derivatives with respect to time or position y are required. The reduced equations (4,10) and (4,11) become

$$w_1(x_1) = \exp(i k_1 x_1 \cos \alpha_1) + a_1 \exp(-i k_1 x_1 \cos \alpha_1) + a_1' \exp(-k_1 x_1 \sqrt{1 + \sin^2 \alpha_1}) \quad (4,13)$$

$$w_n(x_n) = a_n \exp(-i k_n \cos \alpha_n) + a_n' \exp(-k_n x_n (1 + \sin^2 \alpha_n)^{0.5}) \quad (4,14)$$

Use of the boundary conditions (a), (b) and (c) leads to the following expressions for the constants a_1 as shown in Appendix B.

$$a_1(\alpha_1) = - \frac{1+B_1^* \sum_{j=2}^4 \frac{\psi_{1j}}{\chi_{1j}} \left(\frac{1}{B_j}\right)}{B_1 \sum_{j=1}^4 \frac{\psi_{1j}}{\chi_{1j}} \left(\frac{1}{B_j}\right)} \quad (4,15)$$

$$a_n(\alpha_1) = \frac{2i}{B_1 B_n \sum_{j=1}^4 \frac{\psi_{1j}}{\chi_{1j}} \left(\frac{1}{B_j}\right)} \frac{\cos \alpha_1}{\chi_{1n}} \quad (4,16)$$

where the following relationships are used

$$\chi_{mn} = k_n / k_m \quad (4,17)$$

$$\psi_{mn} = D_n k_n^2 / D_m k_m^2$$

$$\begin{aligned} B_n(\alpha_1) &= \sqrt{1 + \sin^2 \alpha_n} - i \cos \alpha_n \\ &= (1 + \sin^2 \alpha_1 / \chi_{1n}^2)^{0.5} - i (1 - \sin^2 \alpha_1 / \chi_{1n}^2)^{0.5} \end{aligned} \quad (4,19)$$

for $|\sin \alpha_1| < \chi_{1n}$

B_n^* is the complex conjugate of B_n

There are structures where $\sin\alpha_1 > \chi_{1n}$. This occurs when the wave number in plate 1 is greater than the wave number in plate n. In this case, the first term of the displacement equation (4,14) for w_n becomes

$$a_n \exp \left[-k_n x_n \left(\frac{\sin^2 \alpha_1}{\chi_{1n}^2} - 1 \right)^{0.5} \right]$$

The sign of the square root is chosen on the basis that the displacement decreases exponentially with increasing x_n . Hence where $\sin\alpha_1 > \chi_{1n}$, equation (4,19) becomes

$$B_n(\alpha_1) = (1 + \sin^2 \alpha_1 / \chi_{1n}^2)^{0.5} - \left(\frac{\sin^2 \alpha_1}{\chi_{1n}^2} - 1 \right)^{0.5} \quad (4,20)$$

which is real.

A general expression for $|a_n|^2$ would be complicated by attempting to allow for the different conditions, $|\sin\alpha_1| < \chi_{1n}$ and $\sin\alpha_1 > \chi_{1n}$, hence equation (4,16) is not reduced further.

The expressions for $a_1(\alpha_1)$ and $a_n(\alpha_1)$ can be used to obtain the $|a_1|^2$ and $|a_n|^2$ terms in the transmission coefficient equations (4,2) and (4,9).

4.3.2. Energy Decay Method

The equations for predicting coupling loss factors based on energy decay theory are (4,1) and (4,4). These equations require the average transmission coefficient τ_{ij} . Using the wave number equation (4,7), the ratio of surface densities ρ_{si}/ρ_{sj} can be related to the plate parameters χ_{ij} and ψ_{ij} ,

$$\frac{\rho_{si}}{\rho_{sj}} = \frac{D_j}{D_i} \left(\frac{k_j}{k_i} \right)^3 = \psi_{ij} \chi_{ij} \quad (4,21)$$

Both of the integral expressions in equation (4,2) are symmetrical about $\alpha_1 = 0$, hence using equation (4,21), (4,2) becomes

$$\begin{aligned} \tau_{ij} &= \chi_{ij} \psi_{ij} \int_0^{\pi/2} |a_j|^2 \cos \alpha_j d\alpha_i / \int_0^{\pi/2} \cos \alpha_i d\alpha_i \\ &= \chi_{ij} \psi_{ij} \int_0^{\pi/2} |a_j|^2 \cos \alpha_j d\alpha_i \end{aligned} \quad (4,22)$$

It is mathematically convenient to integrate with respect to $\sin \alpha_1 = s$ rather than to α_1 . This is achieved by multiplying (4,22) by $\cos \alpha_i / \cos \alpha_i$, setting $i = 1$ and $j = n$, to become

$$\begin{aligned} \tau_{1n} &= \chi_{1n} \psi_{1n} \int_0^1 |a_n|^2 (\cos \alpha_n / \cos \alpha_1) ds \\ &= \int_0^1 \tau_{1n}(s) ds \end{aligned} \quad (4,23)$$

$\tau_{1n}(s)$ is the transmission coefficient for a wave in plate 1 incident at angle α_1 and partially transmitted to plate n.

$$\tau_{1n}(s) = \chi_{1n} \psi_{1n} \frac{\cos \alpha_n}{\cos \alpha_1} |a_n|^2 \quad (4,24)$$

in which both $\cos \alpha_n$ and $|a_n|^2$ are functions of s .

Equation (4,16) can be written as

$$a_n(s) = A_n(s) \cos \alpha_1 / \chi_{1n} \quad (4,25)$$

where

$$A_n(s) = \frac{2i}{B_1(s) B_n(s) \sum_{j=1}^4 \frac{\psi_{1j}}{\chi_{1j}} (1/B_j(s))} \quad (4,26)$$

$|a_n|^2(s)$ can be determined for any incident angle and plate parameters

$$|a_n|^2(s) = |A_n|^2(s) \cos^2 \alpha_1 / \chi_{1n}^2 \quad (4,27)$$

Substituting (4,27) into (4,24) and expressing the $\cos \alpha$ terms as functions of s gives

$$\tau_{1n}(s) = (\psi_{1n} / \chi_{1n}) |A_n|^2(s) (1-s^2 / \chi_{1n}^2)^{0.5} (1-s^2)^{0.5} \quad (4,28)$$

The average transmission coefficient is obtained from (4,23) where the upper integration limit of 1 can be replaced by χ_{1n} when $\chi_{1n} < 1.0$ since no additional energy is transmitted

to plate n at an incident angle greater than the critical angle $\alpha_{1c} = \arcsin \chi_{1n}$, or $s = \chi_{1n}$.

When two plates only are considered $t_3 = t_4 = 0$ and (4,26) reduces to

$$A_2(s) = \frac{2i}{B_2 + \frac{\psi_{12}}{\chi_{12}} B_1} \quad (4,29)$$

When equation (4,29) is substituted into equation (4,28), the transmission coefficient for two coupled plates for a travelling wave incident on the join at angle $\arcsin(s)$ is

$$\tau_{12}(s) = \frac{2\psi_{12}(\chi_{12}^2 - s^2)^{0.5}(1-s^2)^{0.5}}{\chi_{12}^2 + \psi_{12}^2 + \psi_{12}(\chi_{12}^2 + s^2)^{0.5}(1+s^2)^{0.5} + \psi_{12}(\chi_{12}^2 - s^2)^{0.5}(1-s^2)^{0.5}} \quad (4,30)$$

which is equivalent to the expression for oblique incidence transmission coefficient for two coupled plates derived by Cremer (Cremer, Heckl & Ungar, 1973(2)).

For the special 3 plate case with $t_2 = t_3$ and $t_4 = 0$, the two plate equation can be used with ψ_{12} replaced by $2\psi_{12}$ (Cremer, Heckl & Ungar 1973). In this case (4,29) and (4,30) reduce to the same equation as Lyon and Eichler (1964) obtained for the cantilevered plate coupled to a support plate. The parameter 'r' used by Lyon and Eichler is equivalent to $\chi_{12}/2\psi_{12}$.

Although it is not productive to reduce the general equation for $\tau_{1n}(s)$ further, the normal incidence transmission coefficient $\tau_{1n}(0)$ can be expressed in a relatively simple form. For $s = 0$

$$B_1 = B_n = 1-i$$

$$A_n(0) = -(1-i) / \left(\sum_{n=1}^4 \psi_{1n} / \chi_{1n} \right)$$

$$|A_n|^2(0) = 2 / \left(\sum_{n=1}^4 \psi_{1n} / \chi_{1n} \right)^2$$

and

$$\tau_{1n}(0) = \frac{2(\psi_{1n} / \chi_{1n})}{\left[\sum_{n=1}^x (\psi_{1n} / \chi_{1n}) \right]^2} \quad (4,31)$$

where the summation for 4 plates has been replaced by a summation for x plates.

For two coupled plates, (4,31) becomes

$$\begin{aligned} \tau_{12}(0) &= 2(\psi_{12} / \chi_{12}) / \left[1 + (\psi_{12} / \chi_{12}) \right]^2 \\ &= 2 / \left[(\chi_{12} / \psi_{12})^{0.5} + (\psi_{12} / \chi_{12})^{0.5} \right]^2 \end{aligned}$$

which is in agreement with the 2 coupled plate normal incidence transmission coefficient equation obtained by Cremer, Heckl & Ungar (1973(1)).

4.3.3. Power Balance Method

The power balance equation led to the definition of $(TF)_{ij}$ in equation (4,9). Changing the variable to $s = \sin \alpha_1$ and setting $i = 1$ and $j = n$ gives

$$(TF)_{1n} = \frac{\left(\frac{\pi}{\psi_{1n}}\right) \int_0^u \frac{\psi_{1n}}{\chi_{1n}} |A_n|^2(s) (1-s^2/\chi_{1n}^2)^{0.5} (1-s^2)^{0.5} ds}{\frac{\pi}{2} \chi_{1n}^4 + \int_0^1 \chi_{1n}^4 \frac{|a_1|^2(s)}{(1-s^2)^{0.5}} ds - \int_0^u \frac{|A_n|^2(s) (1-s^2)^{0.5}}{\chi_{1n}^2} ds} \quad (4,32)$$

where the upper limit of integration, u , is set equal to the lesser of χ_{1n} and 1.

Although an expression for $|a_1|^2(s)$ could be derived from (4,15), it is more convenient to use the relationship that the sum of all the transmission coefficients and the reflection coefficient must be unity. For convenience, τ_{11} has been used to denote the reflection coefficient

$$\begin{aligned} \tau_{11}(s) &= |a_1|^2(s) \\ &= 1 - \sum_{n=2}^4 \tau_{1n}(s) \end{aligned} \quad (4,33)$$

For any incidence angle, α_1 ,

$$|a_1|^2(s) = 1 - \left(1-s^2\right)^{0.5} \sum_{m=2}^4 |A_m|^2(s) (1-s^2/\chi_{1m}^2)^{0.5} \quad (4,34)$$

where

$$(1-s^2/\chi_{1m}^2)^{0.5} = 0 \text{ for } s > \chi_{1m}$$

By using this expression for $|a_1|^2(s)$, the denominator of (4,32) becomes, for x plates connected to plate 1

$$\text{DENOM} = \pi \chi_{1n}^4 - \int_0^1 \chi_{1n}^4 \sum_{m=2}^x \frac{\psi_{1m} |A_m|^2(s) (1-s^2/\chi_{1m}^2)^{0.5}}{\chi_{1m}} ds - \int_0^u \frac{|A_n|^2(s) (1-s^2)^{0.5} ds}{\chi_{1n}^2} \quad (4,35)$$

The integrand in the numerator of (4,32) is the same as the transmission coefficient equation (4,28).

The analysis to this point has been applicable to any material or mixture of materials. For the purpose of this research, test plates of the same material have been used. This allows the equations (4,17) and (4,18) to reduce to expressions involving the ratio of plate thicknesses. Note that the absolute plate thickness is not important, provided that the classical bending wave theory restrictions are observed, i.e. $t_n < \lambda_{Bn}/6$

As the bending stiffness of a plate is proportional to t^3 ,

$$D_n/D_m = (t_n/t_m)^3$$

From the wave number equation for plates (4,7), $k_1^4 \propto (t_1/D_1)$, hence

$$\begin{aligned} \chi_{mn} &= k_n/k_m \\ &= \left[\frac{t_n/D_n}{t_m/D_m} \right]^{0.25} \end{aligned}$$

$$= (t_m/t_n)^{0.5} \quad (4,36)$$

and

$$\begin{aligned} \psi_{mn} &= (D_n/D_m) \chi_{mn}^2 \\ &= (t_n/t_m)^2 \end{aligned} \quad (4,37)$$

A computer programme was used to compute the value of $\tau_{ln}(s)$ for a specific set of plates and value of s . A Simpson's Rule subroutine was used to determine the integral value, hence average transmission coefficient. The two integral equations in equation (4,35) were written into the same programme. This allowed $(TF)_{ln}$ to be evaluated from equation (4,32). With these integrals numerically calculated, the average values of τ_{ij} , $-\ln(1-\tau_{ij})$ and $(TF)_{ij}$ were evaluated for any set of 2, 3 or 4 flat plates at a common join.

4.3.4. Discussion of Theoretical Results

The greatest difference between the average values of τ_{ij} , $-\ln(1-\tau_{ij})$ and $(TF)_{ij}$ occurs at the largest numerical values of the transmission coefficient. This occurs for the two plate junction. The variation of the three coefficients with plate thickness ratio for two coupled plates is shown in Fig. 4-3. It can be seen that the greatest difference between $(TF)_{12}$ and τ_{12} occurs when the plates are of equal thickness and the values are $(TF)_{12} = 0.44$ and $\tau_{12} = 0.33$. The ratio of $(TF)_{12}/\tau_{12}$, 1.33, is also a maximum for the equal plate thickness case. This ratio is reduced to 1.05 for a thickness

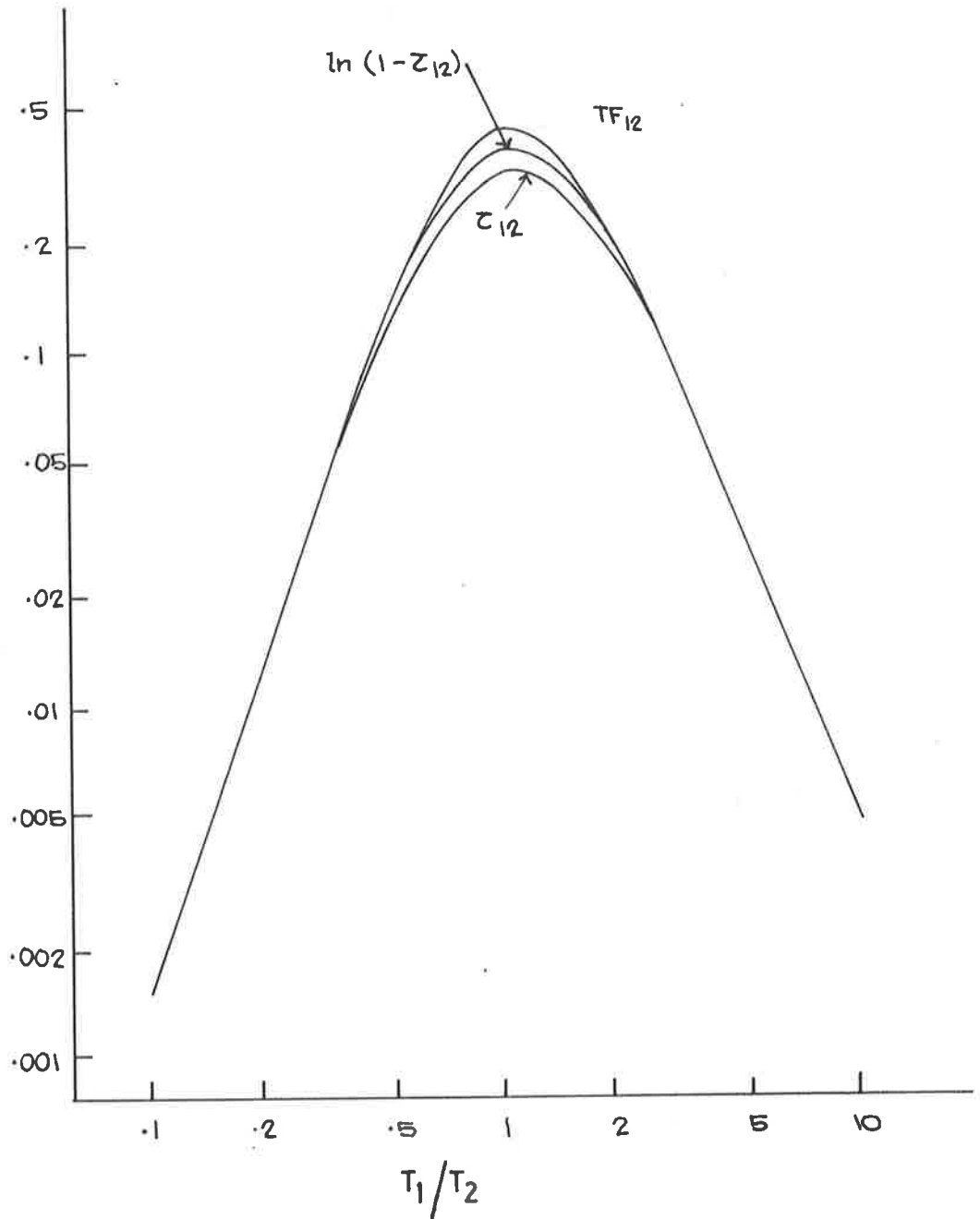


FIG. 4.3. COMPARISON OF z_{12} , $-\ln(1-z_{12})$ AND TF_{12} FOR TWO COUPLED PLATES AT VARYING PLATE THICKNESS RATIOS

ratio of 0.5. The value of $-\ln(1-\tau_{ij})$ falls between the other two coefficients for all plate thickness ratios.

We now consider how important, or unimportant, these differences are. The transmission coefficients are required to evaluate the coupling loss factors which in turn are required to predict the energy distribution in a coupled structure. Equation (4,1) shows that for a given plate and frequency, the coupling loss factor is proportional to the transmission coefficient. Let us consider the energy ratio between two coupled elements, equation (3,7) for $i = 1$ and $j = 2$. Inspection of (3,7) shows that for very large coupling loss factors compared with the internal loss factor, the energy ratio becomes insensitive to the value of the coupling loss factor. As the coupling loss to internal loss factor ratio reduces, the sensitivity increases. Fig. 4-4 shows the variation in the predicted energy ratio E_2/E_1 for a change in value of the coupling loss factor to internal loss factor ratio of 1dB, i.e. for the same internal loss factor, if η_{21} increased to η_{21}^1 , then $10\log \eta_{21}^1/\eta_{21} = 1\text{dB}$, and the change in energy ratio is shown. Fig. 4-4 shows that the variation in energy ratio approaches 1dB if η_{21}/η_2 is very small. However, for a two plate junction, a typical coupling loss factor is at least equal to and generally greater than the internal loss factor, resulting in reduced sensitivity of the predicted energy ratio to a variation in the coupling loss factor value.

For a four plate junction, the transmission coefficients, hence coupling loss factor to internal loss factor ratio, is smaller but the ratio of the two coefficients $(TF)_{ij}/\tau_{ij}$ for the worst case of all plates of equal thickness is only 1.15 or 0.6dB.

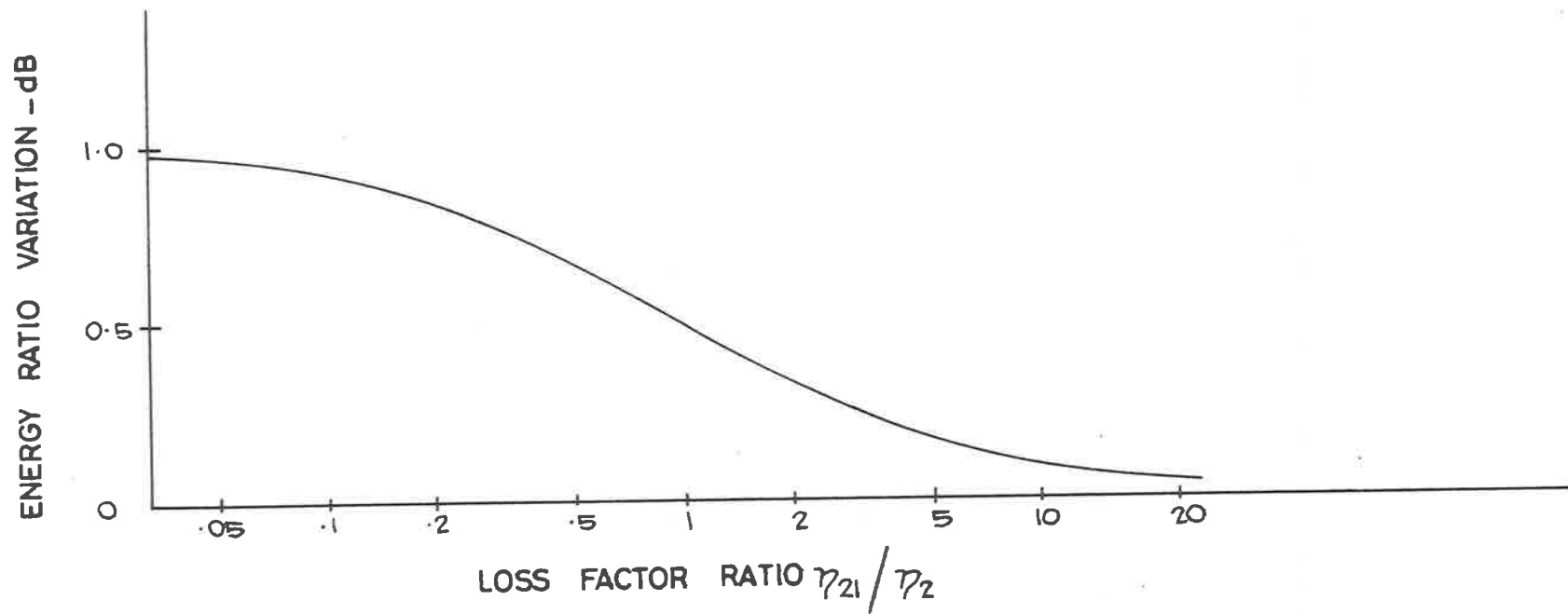


FIG. 4.4. VARIATION OF PREDICTED ENERGY RATIO E_2/E_1 FOR +1dB VARIATION IN THE LOSS FACTOR RATIO η_{21}/τ_2

Thus it is apparent that the differences between the three transmission coefficients are of little importance when considering their application to SEA.

For the remainder of this work, τ_{ij} has been used, as the computation only requires one integral to be evaluated and the computation time is less.

Although the average transmission coefficient can be evaluated for any number of plates at a join, it is a process which relies on a computer to evaluate the integral equation (4,23). Such an exercise must then be repeated for the next join with another set of plate thickness ratios. Such involved computation is not satisfactory for general use and a simpler approach to the problem of computation will be found.

The normal incidence transmission coefficient, equation (4,31), is relatively easy to evaluate and it will be useful for our purpose. When $\tau_{ij}/\tau_{ij}(0)$ is plotted against t_1/t_2 for two coupled plates, the computer evaluated ratios lie along a reasonably smooth curve. This curve can be approximated by the empirical equation.

$$(\tau_{ij}/\tau_{ij}(0))_{2\text{Plates}} = T = \frac{0.85x}{1+x} \quad (4,38)$$

$$\text{for } x = 3.24 t_i/t_j$$

The $\tau_{ij}/\tau_{ij}(0)$ values for 3 and 4 plates at a join lie off the curve by varying amounts depending on the thickness ratios of the plates at the join. By comparing τ_{ij} for 3 and 4 plate joins with τ_{ij} for 2 plate joins for the same t_i/t_j ratios, a further approximate relationship was found which is

$$M = 1 - 0.7 (t_m/t_c - 1.2) \text{ for } t_m/t_c \geq 1.2 \quad (4,39)$$

$$M = 1 \quad \text{for } t_m/t_c < 1.2$$

where t_m is the thickness of the thickest plate at the join and t_c is the greater of t_i and t_j .

Hence the average transmission coefficients τ_{ij} can be evaluated empirically by the following equation

$$\tau_{ij} = MT\tau_{ij}(o) \quad (4,40)$$

where T and M are defined by equations (4,38) and (4,39).

The factors T and M are plotted along with some computed results in figures 4-5 and 4-6. It can be seen that the average transmission coefficient can be determined from the normal incidence transmission coefficient by equation (4,40) within 0.25dB of the computer evaluated result for thickness ratios t_i/t_j from 0.2 to 5. The equations can be used outside of this range with a decrease in accuracy.

Inspection of Fig. 4-5 shows that for two coupled plates, if $\tau_{ij}(o)$ is used instead of τ_{ij} , as long as $\tau_{ij}(o)$ is always evaluated for $t_i \geq t_j$, the error involved is a maximum of 1.8dB at $t_i = t_j$. The coupling loss factor for j to i can then be determined from the reciprocity equation (3,6).

Let us examine the reciprocity relationships for n plates at a join. In the steady state condition, the power flow from plate 1 to all of the (n-1) connected plates must be

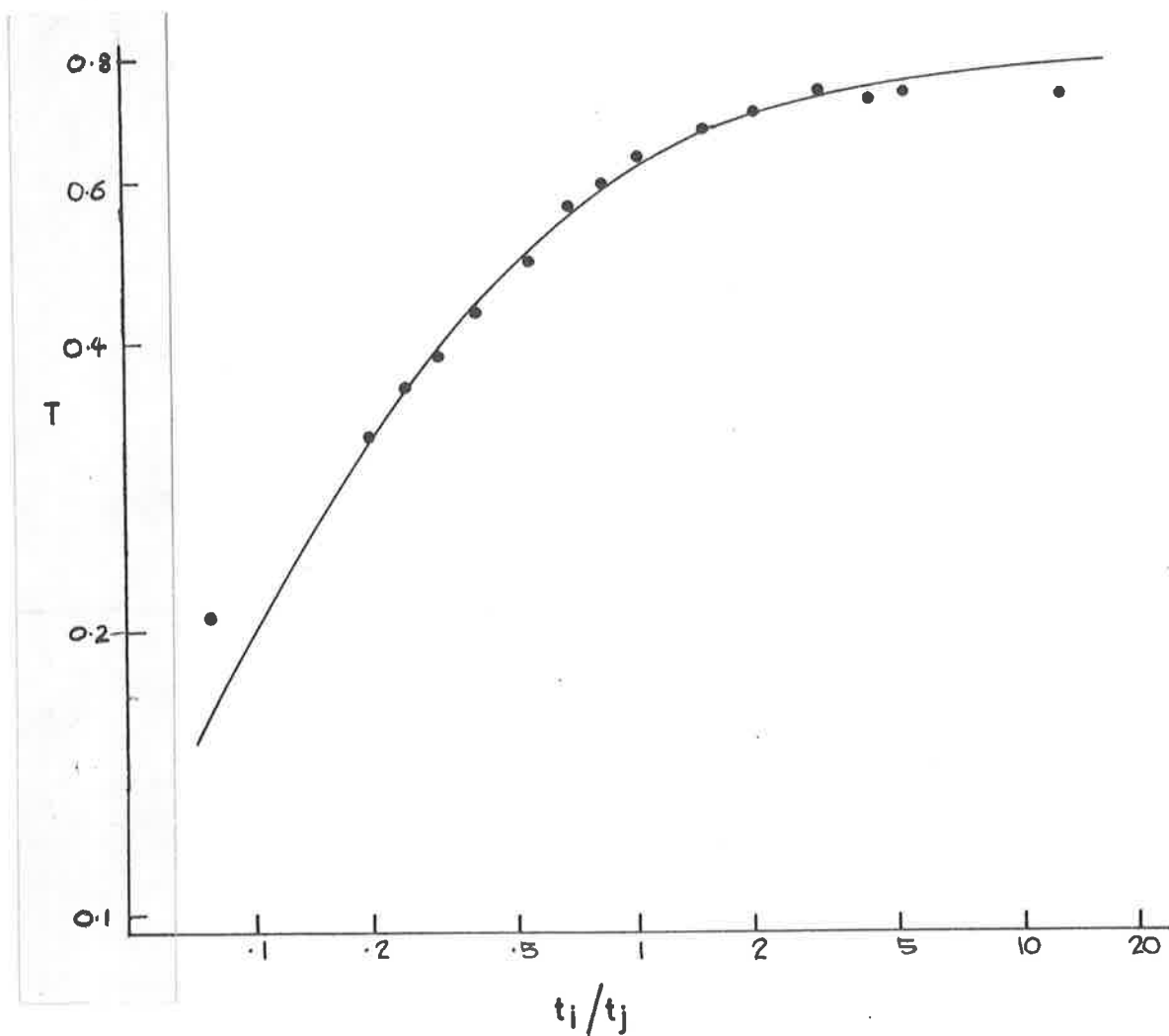


FIG. 4.5. COMPARISON OF COMPUTER EVALUATED AND EMPIRICALLY DETERMINED VALUES OF T FOR USE IN EQUATION (4,40) TO EVALUATE τ_{ij}

—, EMPIRICAL; •, COMPUTED.

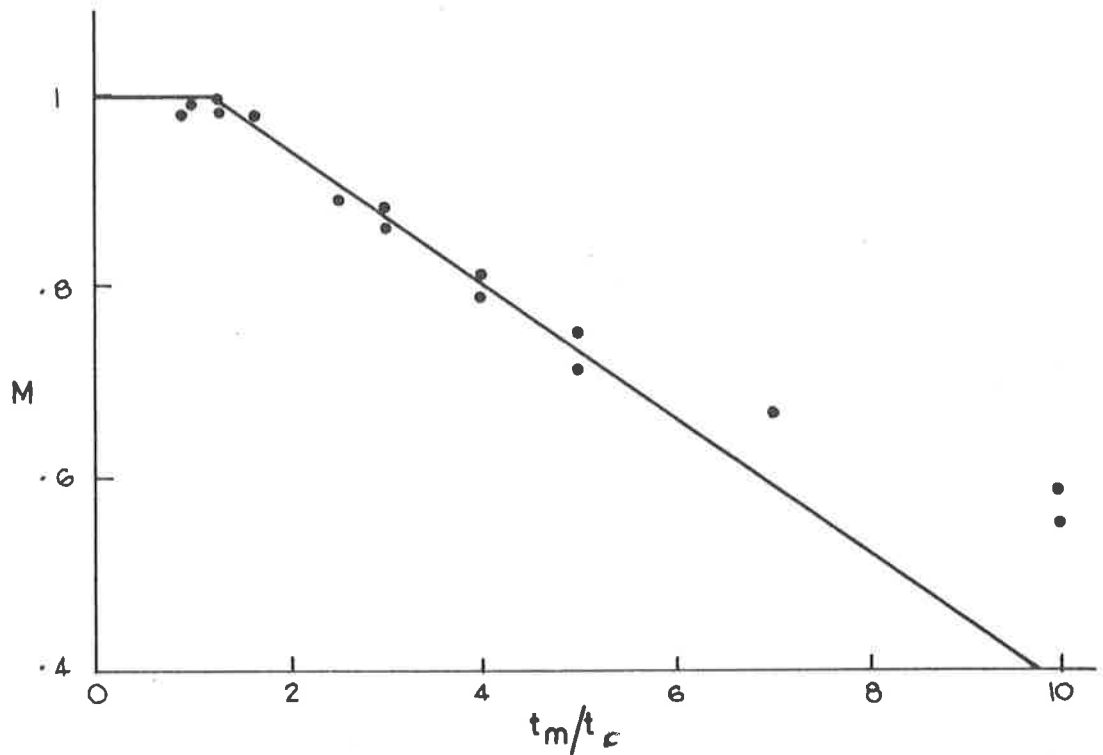


FIG. 4.6. COMPARISON OF COMPUTER EVALUATED AND EMPIRICALLY DETERMINED VALUES OF M FOR USE IN EQUATION (4,40) TO EVALUATE τ_{ij} (t_c GREATER OF t_i AND t_j) (t_m THICKEST PLATE THICKNESS)

—, EMPIRICAL: • COMPUTED.

equal to the nett power flows returning from the (n-1) plates back into plate 1. This leads to the expression

$$\sum_{j=2}^n n_1 \eta_{1j} = \sum_{j=2}^n n_j \eta_{j1} \quad (4,41)$$

However, if it is also assumed that for any two plates i and j at the n plate join, the power flow from i to j is equal to the power flow back from j to i. We have the same reciprocity relationship as (3,6) for plates i and j.

$$\eta_{ij}/\eta_{ji} = n_j/n_i \quad (4,42)$$

However, if (4,42) is true, then the ratio of transmission coefficients τ_{ij}/τ_{ji} can be related to the plate thickness ratio in the following way. When

$$k_i = 2\pi f^{0.5} / (1.814 C_L t_i)^{0.5}$$

is substituted into equation (4,1), it becomes

$$\eta_{ij} = \frac{L}{A_i} \left[\frac{t_i}{f} \right]^{0.5} \frac{\tau_{ij}}{\text{constant}}$$

and as $n_i \propto A_i/t_i$

$$\frac{A_j}{A_i} \left(\frac{t_i}{t_j} \right)^{0.5} \frac{\tau_{ij}}{\tau_{ji}} = \frac{A_j}{A_i} \frac{t_i}{t_j}$$

hence

$$\frac{\tau_{ij}}{\tau_{ji}} = \left(\frac{t_i}{t_j} \right)^{0.5}$$

TABLE 4-1.

Comparison of $(t_i/t_j)^{0.5}$ with typical values of τ_{ij}/τ_{ji} for various plate combinations.

$(t_i/t_j)^{0.5}$	τ_{ij}/τ_{ji}		
	No. of plates at a common join		
	2	3	4
0.2739			0.2738
0.3162	0.3162		
0.4472	0.4470	0.4470	0.4470
0.500		0.500	0.500
0.5477		0.5476	0.5477
0.5773		0.5773	0.5774
0.6124			0.6125
0.7071	0.7069	0.7071 0.7069	0.6978 0.7071 0.7071
0.7746	0.7745	0.7743	
0.7937		0.7936	0.7937
0.8165		0.8164	0.8163
0.8367		0.8366	0.8367 0.8367 0.8368
0.8660			0.8662
0.8944	0.8942	0.8943	0.8944
0.9129		0.9127	
0.9487	0.9487	0.9487	0.9483

The ratio τ_{ij}/τ_{ji} was evaluated for a number of different 2, 3 and 4 plate junctions. These ratios are compared with $(t_i/t_j)^{0.5}$ in Table 4-1 where it can be seen that the agreement is very good. Some 3 and 4 plate cases were investigated where t_i/t_j was held constant while the thickness of the other plates was varied and accounts for more than one value of τ_{ij}/τ_{ji} in the table for a given thickness ratio and number of plates. We conclude from the comparisons in Table 4-1 that the reciprocity relationship, equation (4,42), derived for two coupled plates is also valid for 3 and 4 coupled plates at a join, and thus we are led to believe that it is probably true for any number of plates at a join.

It is interesting to note that for structures of similar materials, $\tau_{ij}(o) = \tau_{ji}(o)$ for all thickness ratios. This can be shown by substituting $\psi_{ij}/\chi_{ji} = (t_j/t_i)^{2.5}$ into equation (4,31) and expanding for, say $x = 4$, and $n = 2$.

$$\begin{aligned} \tau_{12}(o) &= \frac{2(t_2/t_1)^{2.5}}{\left[1 + (t_2/t_1)^{2.5} + (t_3/t_1)^{2.5} + (t_4/t_1)^{2.5} \right]^2} \\ &= \frac{2}{\left[(t_1/t_2)^{1.25} + (t_2/t_1)^{1.25} + (t_3^2/t_1 t_2)^{1.25} + (t_4^2/t_1 t_2)^{1.25} \right]^2} \end{aligned} \quad (4,43)$$

The denominator of (4,43) is invariant to an interchange of indices 1 and 2, hence $\tau_{12}(o) = \tau_{21}(o)$ and therefore normal incidence transmission can not satisfy the reciprocity relationship.

The calculated average transmission coefficients have been used to evaluate the average coupling loss factors which

in turn have been used to predict the energy ratios of the experimental test structures reported in Section 5.

4.4. GENERAL SOLUTION: FOUR PLATES AT A COMMON JOIN

4.4.1. Wave Transmission Method

We shall now reconsider the problem of wave transmission at a four plate join. The boundary condition that $w_i = 0$ at $x_1 = 0$ is relaxed to allow the generation and propagation of longitudinal and transverse waves, as well as the previously considered bending waves.

The method which will be used is basically the same as used in Section 4.3 except that two more wave fields must be considered. Longitudinal and transverse waves produced in each plate propagate away from the join at angles determined by the trace wavelength and wave propagation speeds.

In Section 4-3, both τ_{ij} and $(TF)_{ij}$ were calculated but as it was shown that their values were very close, only τ_{ij} will be calculated in this section as the computation time required is much less than for $(TF)_{ij}$.

Four plates at right angles at a common join are considered with the same coordinate systems as used previously and shown in Figure 4-2. We consider an incident bending wave in plate 1 which subsequently generates bending, longitudinal and transverse waves at the join. The displacements in the x_i , y_i and z_i directions are u_i , v_i and w_i respectively. After the common time dependent term $\exp(i \omega t)$ and the trace wavelength terms, including $p_i \sin \beta_i = q_j \sin \gamma_j = k_1 \sin \alpha_1$, have been omitted, the displacement equations for the four are as follows:

Note that the longitudinal and transverse waves are considered as a means of transmitting energy at the join, forced by the incident wave. It is not assumed that the longitudinal and transverse waves necessarily form resonant wavefields.

$$u_j(x_j) = b_j \cos \beta_j \exp(-ip_j x_j \cos \beta_j) + c_j \sin \gamma_j \exp(-iq_j x_j \cos \gamma_j)$$

for $j = 1, 2, 3$ and 4 (4,44)

$$v_j(x_j) = b_j \sin \beta_j \exp(-ip_j x_j \cos \beta_j) - c_j \cos \gamma_j \exp(-iq_j x_j \cos \gamma_j)$$

for $j = 1, 2, 3$ and 4 (4,45)

$$w_j(x_j) = a_j \exp(-ik_j x_j \cos \alpha_j) + a_j \exp(-k_j x_j (1 + \sin^2 \alpha_j)^{0.5})$$

for $j = 2, 3$ and 4 (4,46)

$$w_1(x_1) = \exp(ik_1 x_1 \cos \alpha_1) + a_1 \exp(-ik_1 x_1 \cos \alpha_1)$$

$$+ a_1 \exp(-k_1 x_1 (1 + \sin^2 \alpha_1)^{0.5})$$

(4,47)

k_j , p_j and q_j are the bending, longitudinal and transverse wave numbers and α_j , β_j and γ_j are the respective wave propagating angles.

For this analysis we have assumed that the incident wave is a bending wave. There is no way that the incident bending wave can cause a nett displacement in the y direction. This means that $v_j = 0$ for all plates. Further more the join has no mass, thus the boundary conditions at $x_j = 0$ are;

(a) continuity of linear displacement

$$u_1 = -u_3$$

$$u_1 = -w_2$$

$$w_1 = u_2$$

(4,48a-j)

$$w_1 = -w_3$$

$$w_1 = -u_4$$

$$u_1 = w_4$$

$$v_j = 0 \text{ for } j = 1, 2, 3 \text{ and } 4.$$

(b) continuity of angular displacement

$$\frac{\partial w_1}{\partial x_1} = \frac{\partial w_j}{\partial x_j} \quad \text{for } j = 2, 3 \text{ and } 4 \quad (4,48k,1,m)$$

(c) the sum of bending moments is zero

$$\sum_{j=1}^4 D_j \frac{\partial^2 w_j}{\partial x_j^2} = 0 \quad (4,48n)$$

(d) the sum of forces in the x_1 and z_1 directions is zero. (There are no forces in the y direction since $v_j = 0$)

$$D_1 \frac{\partial^3 w_1}{\partial x_1^3} + E_2 t_2 \frac{\partial u_2}{\partial x_2} - D_3 \frac{\partial^3 w_3}{\partial x_3^3} - E_4 t_4 \frac{\partial u_4}{\partial x_4} = 0 \quad (4,48,o)$$

$$D_2 \frac{\partial^3 w_2}{\partial x_2^3} + E_3 t_3 \frac{\partial u_3}{\partial x_3} - D_4 \frac{\partial^3 w_4}{\partial x_4^3} - E_1 t_1 \frac{\partial u_1}{\partial x_1} = 0 \quad (4,48,p)$$

There are now three types of wave transmission coefficients to be considered. These are bending to bending, $\tau_{BB_{1n}}$, bending to longitudinal, $\tau_{BL_{1n}}$, and bending to transverse, $\tau_{BT_{1n}}$, where the definition of each is similar to that given previously, i.e. the ratio of the average energy transmitted into plate n (bending, longitudinal or transverse) to the average energy incident on the join (bending wave energy in this case).

The transmitted and reflected wave amplitudes a_j , b_j and c_j can be determined for a particular incident angle α_1 from the sixteen boundary condition equations. The squares of the moduli $|a_j|^2$, $|b_j|^2$ and $|c_j|^2$, also functions of α_1 , can

then be used to calculate the various oblique incidence transmission coefficients which can be integrated over all incident angles to give the average transmission coefficients. The oblique incidence transmission coefficients are obtained from consideration of power transmitted in each wave.

The incident bending wave energy in plate 1 is

$$D_1 \omega k_1^3 \cos \alpha_1$$

where the wave amplitude has been taken as unity. The longitudinal wave energy transmitted across the join per unit length is

$$\rho t C_L \omega^2 \frac{|b_j|^2}{2} \cos \beta_j$$

and the transverse wave energy transmitted across the join per unit length is

$$\rho t C_T \omega^2 \frac{|c_j|^2}{2} \cos \gamma_j$$

Hence,

$$\begin{aligned} \tau_{BL_{1j}}(\alpha_1) &= \rho_j t_j C_L^2 p_j |b_j|^2 \cos \beta_j / 2 D_1 k_1^3 \cos \alpha_1 \\ &= E_j t_j p_j |b_j|^2 \cos \beta_j / 2 D_1 k_1^3 \cos \alpha_1 \end{aligned} \quad (4,49)$$

$$\begin{aligned} \tau_{BT_{1j}}(\alpha_1) &= \rho_j t_j C_T^2 q_j |c_j|^2 \cos \gamma_j / 2 D_1 k_1^3 \cos \alpha_1 \\ &= \left(\frac{G}{E}\right) E_j t_j q_j |c_j|^2 \cos \gamma_j / 2 D_1 k_1^3 \cos \alpha_1 \end{aligned} \quad (4,50)$$

where

$$p_j = \omega / C_{Lj} \quad (4,51a)$$

and

$$q_j = \omega / C_{Tj} \quad (4,51b)$$

are the respective longitudinal and transverse wave numbers in plate j , and $|b_j|^2$, $|c_j|^2$, $\cos \beta_j$ and $\cos \gamma_j$ are all functions of α_1 .

After setting $s = \sin \alpha_1$, as in Section 4.3, the average transmission coefficients $\tau_{BL_{1n}}$ and $\tau_{BT_{1n}}$ are

$$\tau_{BL_{1n}} = F_{1n} \int_0^1 \frac{|b_n|^2}{2} \frac{\cos \beta_n}{\cos \alpha_1} ds \quad (4,52)$$

$$\tau_{BT_{1n}} = \left(\frac{G}{E}\right)_n \left(\frac{q}{p}\right)_n F_{1n} \int_0^1 \frac{|c_n|^2}{2} \frac{\cos \gamma_n}{\cos \alpha_1} ds \quad (4,53)$$

$$\text{where } F_{1n} = E_n t_n p_n / D_1 k_1^3$$

$$= C_{Ln} \rho_n t_n / C_{B1} \rho_1 t_1 \quad (4,54)$$

The expression for the average value of $\tau_{BB_{1n}}$ is the same as the expression of τ_{1n} , equation (4,22). If equation (4,54) is squared and the plate bending wave equation

$$C_B = (1.814 C_L f t)^{0.5}$$

is substituted

$$F_{1n}^2 = \left(\frac{C_{Ln}^2}{1.814 C_{L1}}\right) \left(\frac{t_n}{t_1}\right)^2 \frac{1}{f t_1} \quad (4,55)$$

A parameter which includes plate thickness and excitation frequency will be required for the comparison of the bending wave solution and general solution of the bending to bending transmission coefficients. F_{1n}^2 contains plate thicknesses and excitation frequency and will be discussed further in Section 4.4.2.

It would be possible to proceed further to obtain some complicated expressions for the wave amplitudes, as was done in Section 4.3, but the task is cumbersome since it involves the solution of sixteen simultaneous equations. An alternative approach is more attractive.

The solutions are obtained by processing the sixteen equations in a matrix form. This is set out in Appendix B.2. A 16x16 matrix may be reduced to a 12x12 matrix by eliminating c_j using equations (4,48g,h,i,j). The required computing time may still further be reduced. As shown in the Appendix, some simple relationships may be used to eliminate the b_j terms reducing the 12x12 matrix to an 8x8 matrix. This 8x8 matrix is solved for each specific value of s and a subroutine based on Simpson's rule is again used to evaluate the integrals of equations (4,51), (4,52) and (4,53). The average transmission coefficients are then evaluated. Energy conservation requires that

$$\sum_{n=1}^4 (\tau_{BB_{1n}} + \tau_{BL_{1n}} + \tau_{BT_{1n}}) = 1 \quad (4,56)$$

When $n = 1$, the terms are interpreted as the respective reflection coefficients. Equation (4,56) is used as a check on the computed values.

A listing of the programmes used are included in Appendix C.

4.4.2. Discussion of Theoretical Results

The evaluation of the various average transmission coefficients for a number of 2, 3 and 4 plate single joint structures was carried out using the general solution outlined in Section 4.4.1. The computations showed that the bending to bending wave average transmission coefficient, $\tau_{BB_{ij}}$, varies not only with plate thickness ratios, t_i/t_j , but also with absolute plate thicknesses and excitation frequency. Furthermore, the computed results showed that $\tau_{BB_{ij}}$ depended on whether plate j was orthogonal to plate i or in the same plane as plate i . By contrast, it was shown in Section 4.3 that the bending wave solution transmission coefficient, τ_{ij} , depended only upon the plate thickness ratios. We will now review these results.

It will be useful to compare the computed values of $\tau_{BB_{ij}}$ and τ_{ij} for the same set of plate thickness ratios to determine at what absolute plate thicknesses and excitation frequency the computed values differ substantially indicating when the more complicated general solution should be used. However, before proceeding further with this comparison, it will be of interest to discuss one unexpected result of these computations.

Initial comparisons of the ratio $(\tau_{BB}/\tau)_{ij}$ for different structures, plate thicknesses and excitation frequencies showed that for 3 and 4 plate structures, see Fig. 4-7(b) & (c), $(\tau_{BB}/\tau)_{13}$ became greater than unity for small values of F_{13}^2 , i.e. for high excitation frequency or thick plates. By contrast, in earlier work, Cremer and Heckl (Cremer, Heckl & Ungar, 1973(1)) showed that the bending to bending transmission coefficient reduced for increasing frequency and plate thicknesses. In their analysis, they investigated the junction of two plates of

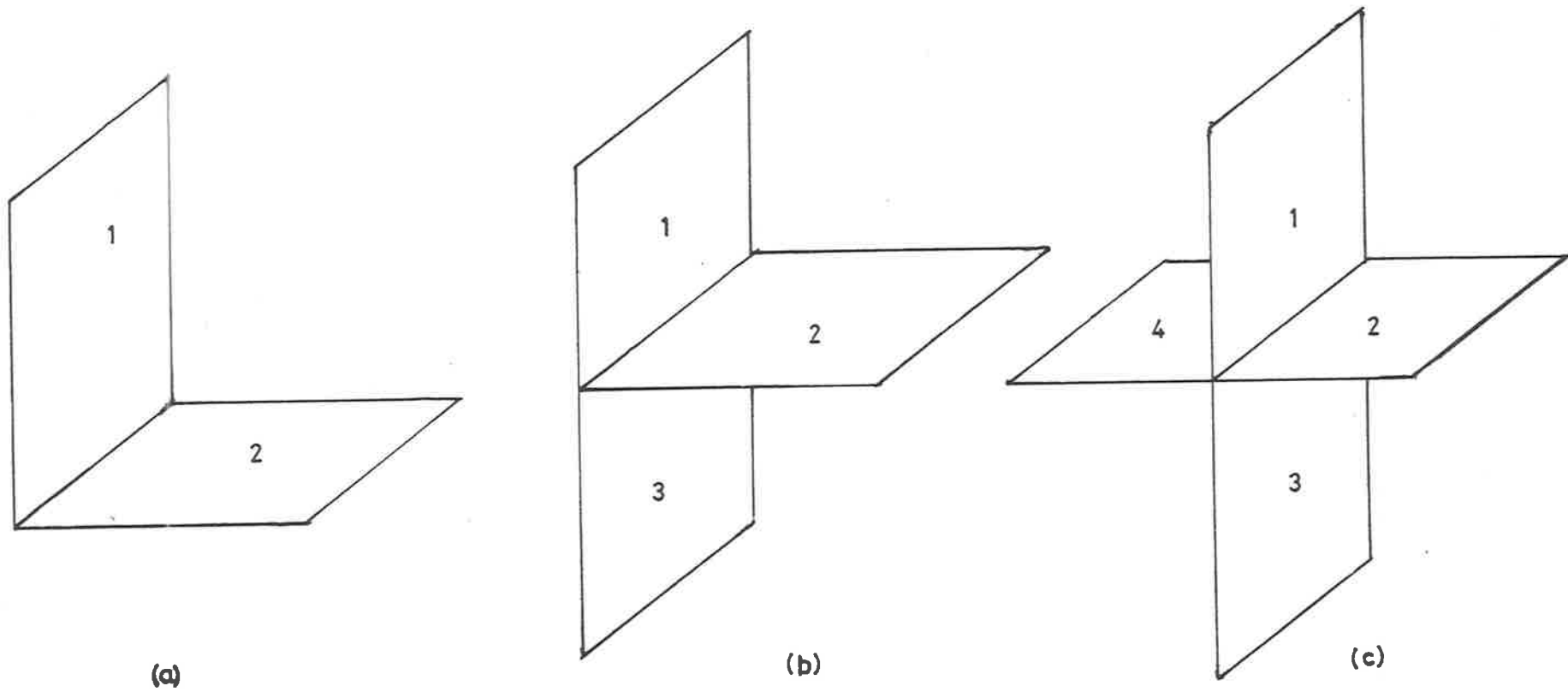


FIG. 4.7. NOMENCLATURE FOR TWO, THREE AND FOUR PLATE SINGLE JOIN STRUCTURE.

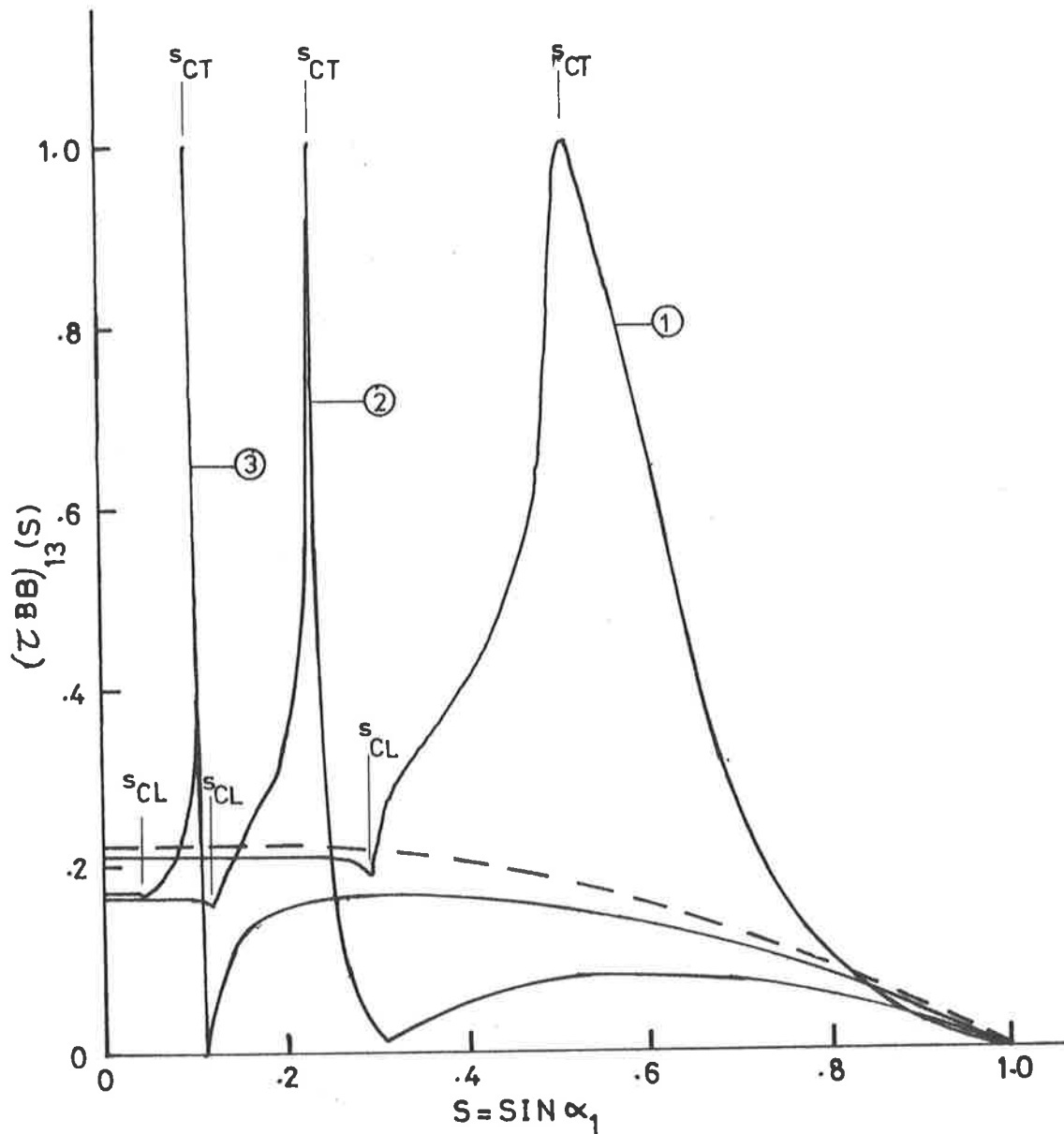


FIG. 4-8. BENDING TO BENDING TRANSMISSION COEFFICIENT FROM PLATE 1 TO PLATE 3 FOR THE THREE PLATE STRUCTURE (FIG. 4-7(b)), $t_1 = t_2 = t_3$ - VARIATION WITH INCIDENT ANGLE AND PARAMETER F^2 .

①, $F_{13}^2 = 12$; ②, $F_{13}^2 = 57$; ③, $F_{13}^2 = 287$; ---, BENDING WAVE SOLUTION.

equal thickness and for normal incidence when bending and longitudinal waves were considered. Their result could be explained on the basis that more energy was transmitted in other forms. It was thus surprising to find that in some cases, more bending wave energy was transmitted than predicted by the simple bending wave solution.

During the course of the investigation to verify this result, the oblique incidence bending to bending transmission coefficient, $\tau_{BB_{13}}(s)$ for a 3 plate structure (Fig. 4-7(b)) was evaluated at various values of s with interesting results. Fig. 4-8 shows some typical values of $\tau_{BB_{13}}(s)$ for such a 3 plate structure where all plates are of equal thickness, and of the same material, viz. steel with $C_L = 5170\text{m/s}$. In the figure, the simple bending wave solution is also shown for comparison. For each case the average transmission coefficient, $\tau_{BB_{13}}$, is proportional to the area contained under the curve. For this structure, at $F_{13}^2 = 12$, the plate thickness is equal to one sixth of the plate bending wavelength, the limit of classical bending wave theory. The critical values s_{CL} and s_{CT} , after which longitudinal and transverse waves do not propagate away from the join into plate 3, are marked on each curve. Note that for each value of F_{13}^2 there is an incident angle (equal to s_{CT}) where total transmission of bending wave energy occurs and another more oblique incident angle (designated s_0) at which no bending wave energy is transmitted. For the limiting curve, $F_{13}^2 = 12$, this occurs at approximately $s = 1$. As F_{13}^2 decreases (frequency and plate thickness increase), the difference $s_0 - s_{CL}$ increases and hence $\tau_{BB_{13}}$ becomes greater than τ_{13} , mainly because of the increased transmission at more oblique incident angles. For progressively larger values of F_{13}^2 , the $\tau_{BB_{13}}(s)$ curve approaches that of the bending wave solution curve with

a sharp deviation near s_{CT} .

We now return to the comparison of the general solution and bending wave solution of the transmission coefficients. We now consider 2, 3 and 4 plate structures as shown in Fig. 4-7. Cremer used the reciprocal of F_{1j}^2 when investigating the two plate junction mentioned previously. We shall investigate the usefulness of F_{1j}^2 for our purpose. For plates of the same material, equation (4,55) becomes

$$F_{1j}^2 = \left(\frac{C_L}{1.814} \right) \left(\frac{t_j}{t_1} \right)^2 \frac{1}{ft_1}$$

Graphs showing the variation of $(\tau_{BB}/\tau)_{1j}$ with F_{1j}^2 are shown in Fig. 4-9. Representative values of bending wave transmission from plate one to the other plates of 2, 3 and 4 plate joins have been plotted in the figure. The curves have been drawn through calculated points determined from the computed evaluations of $\tau_{BB_{1j}}$ and τ_{1j} for the respective structure thickness ratios and excitation frequencies.

The first thing Fig. 4-9 shows is that F_{1j}^2 is not a good choice for a parameter which could be used to give an indication where $\tau_{BB_{1j}}$ should be used instead of the more easily evaluated τ_{1j} . The second observation is that the variation with f and t_1 of $(\tau_{BB}/\tau)_{12}$ and $(\tau_{BB}/\tau)_{14}$ (see Fig. 4-7) for any particular structure is generally as expected; that is for progressively lower values of F_{1j}^2 less energy is transmitted as bending waves. The previously mentioned unexpected upward trend of $(\tau_{BB}/\tau)_{13}$ for decreasing F_{13}^2 (see Fig. 4-7(b) and (c)) is apparent.

A parameter which is reasonably simple and which collapses the $(\tau_{BB}/\tau)_{ij}$ values closer together is required if any

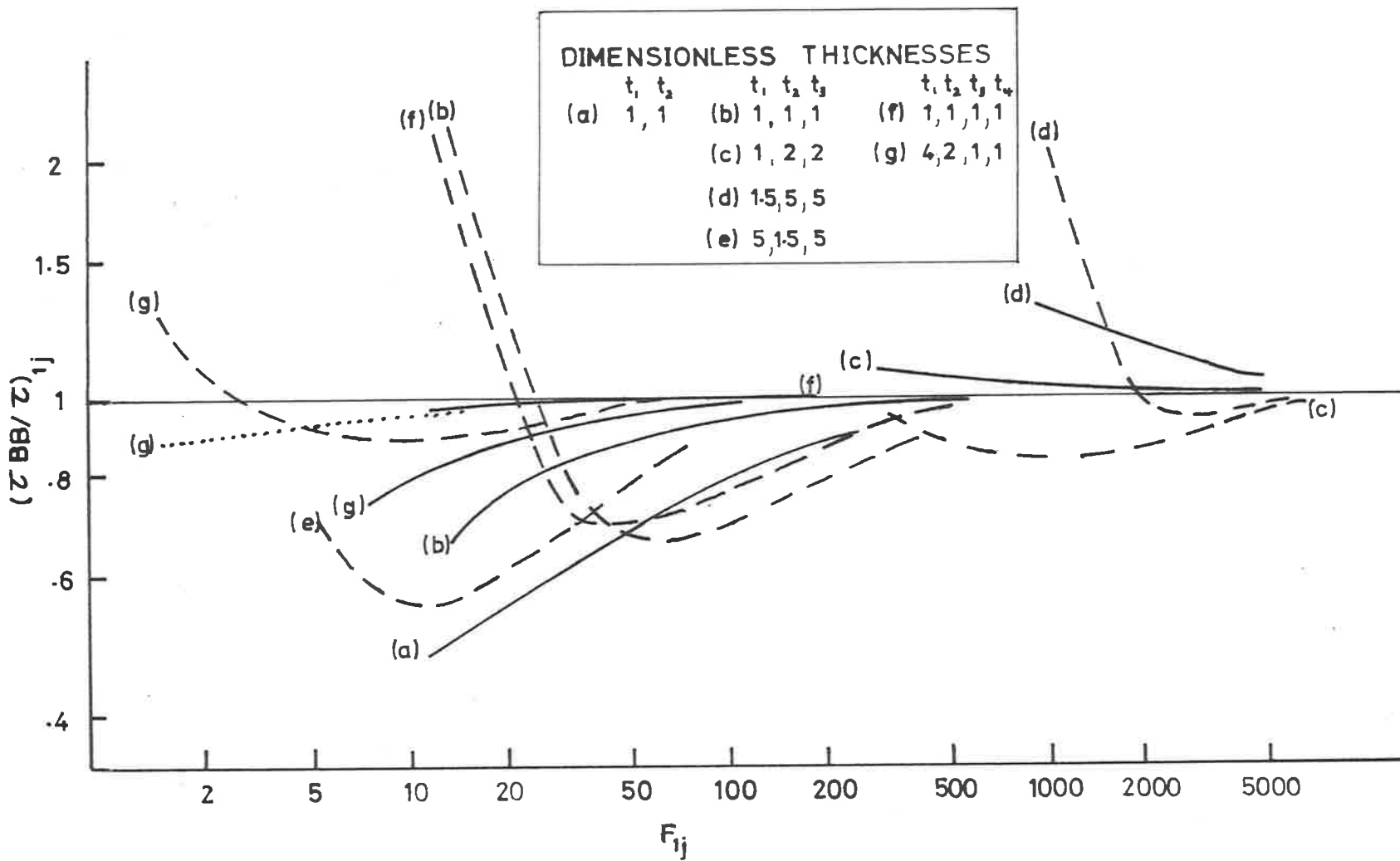


FIG. 4-9. VARIATION OF $(\tau_{BB}/\tau)_{1j}$ WITH F_{1j}^2 - SINGLE JOIN PLATE STRUCTURES: —, $j = 2$;
 ---, $j = 3$; , $j = 4$

general guidelines relating to the use of $\tau_{BB_{ij}}$ rather than τ_{ij} are to be presented.

A parameter which results in a reasonably satisfactory collapse of the $(\tau_{BB}/\tau)_{ij}$ curves is

$$\begin{aligned} Q_{ab} &= \frac{t_b}{t_a} \frac{1}{F_{ab}^2} \\ &= f \frac{t_a^2}{t_b} \frac{1.814}{C_L} \end{aligned} \quad (4,57)$$

where

$$\begin{aligned} t_a &= t_1 && \text{for } t_1 > t_j \\ t_b &= t_j \\ t_a &= t_j && \text{for } t_1 < t_j \\ t_b &= t_1 \end{aligned}$$

As steel is often used in structures, it is informative to present a related parameter P_{ab} where

$$P_{ab} = f t_a^2 / t_b \quad (4,58)$$

for t_a and t_b as defined above. Note that P_{ab} has the dimension of velocity.

The variation of $(\tau_{BB}/\tau)_{ij}$ with P_{ab} is shown in Figure 4-10. Corresponding values of the nondimensional parameter Q_{ab} are also shown on the figure. The parameter P_{ab} allows the reader to obtain an idea of the thickness and frequency

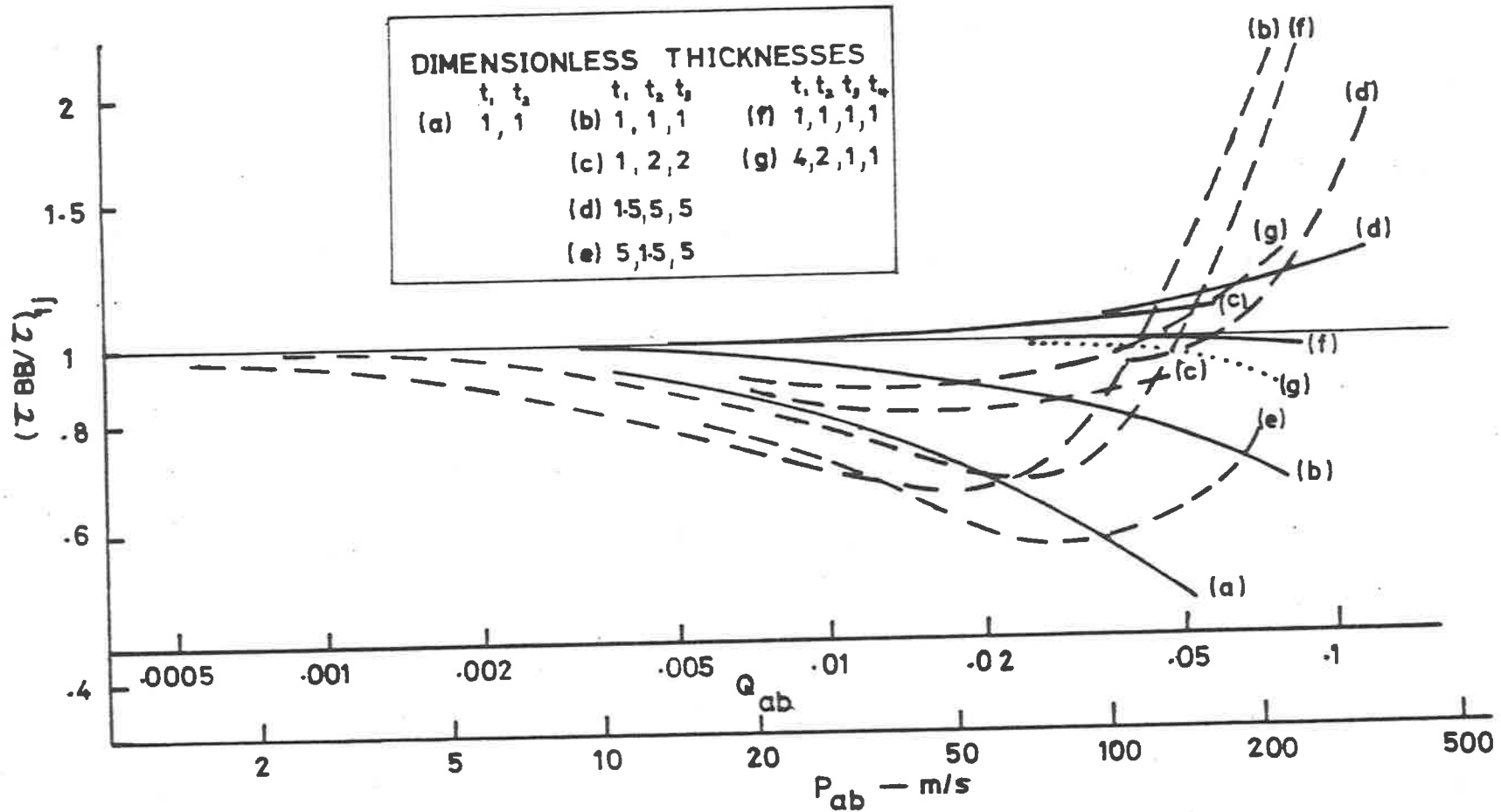


FIG. 4-10. COMPARISON OF $(\tau_{BB}/\tau)^{1/j}$ WITH P_{ab} AND Q_{ab} - SINGLE JOIN STRUCTURES: — ; $j = 2$;
 ----, $j = 3, \dots, j = 4.$

at which the bending wave solution for the transmission coefficient is substantially different from the general solution for steel plates.

For $P_{ab} < 50\text{m/sec.}$, $(\tau_{BB}/\tau)_{ij}$ lies between 1.0 and 0.6 and for most curves between 1.0 and 0.8. Large variations ($\pm 100\%$) do not occur unless $P_{ab} > 100\text{m/sec.}$ Thus a value of P_{ab} less than or equal to 50m/sec. implies that for two plates, 5mm thick, τ_{ij} can be used for frequencies up to 10kHz without more than a 2dB maximum error in τ_{ij} , and generally the error will be much less, but if a 5mm and a 1mm plate are considered,

$$P_{ab} = 50\text{m/sec. at } f = 2\text{kHz}$$

It can be seen from Figure 4-10 that for $(\tau_{BB}/\tau)_{12}$ and $(\tau_{BB}/\tau)_{14}$, except for the 2 coupled plate case, the (τ_{BB}/τ) curves remain near unity for $P_{ab} < 100\text{m/s.}$ Comparison of curves (a), (b) and (f) for $j = 2$ indicates that the variation of $(\tau_{BB}/\tau)_{12}$ is less for the 4 plate case, than for the 3 plate case which in turn is less than for the two plate case.

To this point we have considered only bending waves incident upon a single join in isolation and we have shown that besides transmitting bending waves, longitudinal and transverse waves are produced at the join and transmitted in the adjoining plates. Thus at subsequent joins, longitudinal and transverse waves as well as bending waves will be incident and must be considered. Furthermore the incident longitudinal and transverse waves will be partially transformed back into bending waves at subsequent joins and these transformations will have to be considered as well.

Let us consider the energy flow through a multi-join

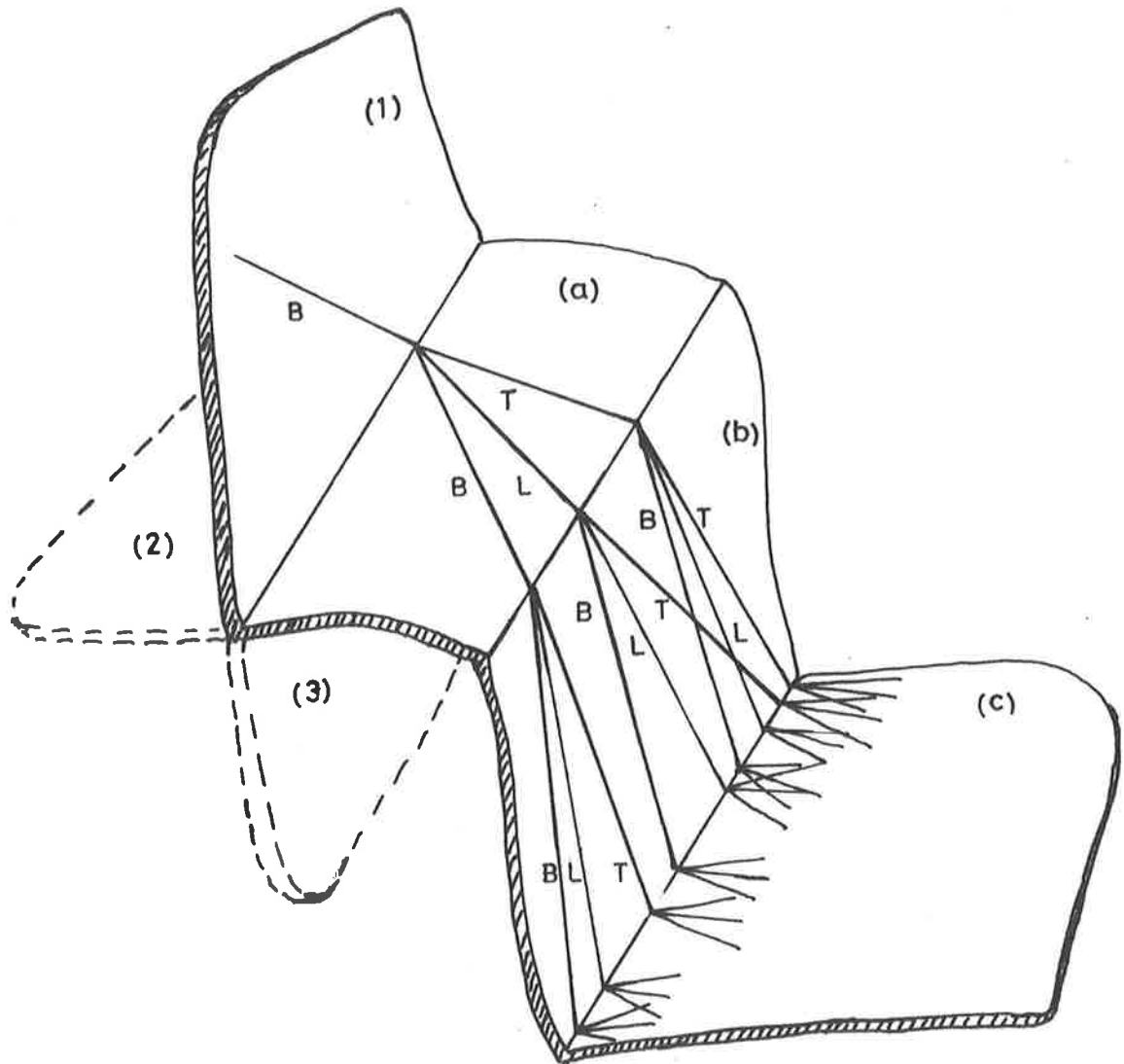


FIG. 4-11. SCHEMATIC DIAGRAM OF THE TRANSMITTED BENDING, LONGITUDINAL AND TRANSVERSE WAVEFIELD GENERATED IN CONNECTED PLATES FROM AN INCIDENT BENDING WAVE.

structure. A 4 plate structure comprising plates a, b, c and d, is shown in Fig. 4-11 in which we assume a bending wave of unit energy in plate 1 is incident upon the join. For the moment, assume plates 2 and 3 are removed. Bending, longitudinal and transverse wave energy is transmitted into plate b where this energy is incident on the second join. Each wave type acts on the join and bending, longitudinal and transverse wave energy is transmitted into plate c from each of the three incident wave fields. This cascade of energy flow is illustrated in Fig. 4-11.

We now consider multireflections in a two plate structure. Each time energy is transmitted from one plate to the other some transformation of energy from one field to another takes place. Thus we have exactly the same cascading effect as previously illustrated in Figure 4-11, but in this case each join of the figure represents an event at the single join of the two plate structure.

We consider the bending wave energy in each plate relative to the incident bending wave energy in the previous plate. Unit bending wave energy is assumed in plate 1 and hence, bending wave energy in plate b is $\tau_{BB_{1b}}$. In plate c, the transmitted bending wave energy is

$$(\tau_{BB})_{1b} (\tau_{BB})_{bc} + (\tau_{BL})_{1b} (\tau_{LB})_{bc} + (\tau_{BT})_{1b} (\tau_{TB})_{bc} \quad (4,59)$$

The incident bending wave energy in plate b at the join is just $\tau_{BB_{1b}}$. Hence the 'correct' transmission coefficient, $C_{\tau_{BB_{bc}}}$ for plate b to c is

$$C_{\tau_{BB_{bc}}} = \tau_{BB_{bc}} + (\tau_{BL})_{1b} (\tau_{LB})_{bc} / (\tau_{BB})_{1b} + (\tau_{BT})_{1b} (\tau_{TB})_{bc} / (\tau_{BB})_{1b}$$

Cremer (Cremer, Heckl & Ungar, 1973(1)) showed that there is a reciprocity relationship for wave transformation for two coupled plates when considering normal incidence. i.e. $\tau_{BL} = \tau_{LB}$, $\tau_{BT} = \tau_{TB}$. Hence the ratio of the 'correct' transmission coefficient to the single join general solution transmission coefficient for transmission from plate b to c may be written as

$$\frac{C\tau_{BB}}{\tau_{BB}_{bc}} = 1 + \left(\frac{\tau_{BL}}{\tau_{BB}_{bc}} \right) \left(\frac{\tau_{BL}}{\tau_{BB}_{lb}} \right) + \left(\frac{\tau_{BT}}{\tau_{BB}_{bc}} \right) \left(\frac{\tau_{BT}}{\tau_{BB}_{lb}} \right) \quad (4,61)$$

When we consider energy transmission at subsequent joins we see from the schematic diagram of Figure 4-11 that each group of three incident wave fields undergo transformations to create nine new fields. However the nine new fields add and reduce to three which are a bending, longitudinal and transverse field. Thus for any join between two plates b and c equation (4.61) holds, provided that there is only one other plate connected to plate b.

We now include plates 2 and 3 as shown in Figure 4-11 and follow the previous procedure. Now, the bending wave energy transmitted to plate b from plates 1, 2 and 3 is

$$\sum_{i=1}^3 \tau_{BB}_{ib}$$

and, as before, this is the bending wave energy incident on the join of plates b and c. When the previous procedure is followed through, we arrive at an equation for $(C\tau_{BB}/\tau_{BB})_{bc}$ similar to (4,61)

$$(C\tau_{BB}/\tau_{BB})_{bc} = 1 + \left(\frac{\tau_{BL}}{\tau_{BB}} \right)_{bc} \frac{\sum_{i=1}^3 (\tau_{BL})_{ib}}{\sum_{i=1}^3 (\tau_{BB})_{ib}} + \left(\frac{\tau_{BT}}{\tau_{BB}} \right)_{bc} \frac{\sum_{i=1}^3 (\tau_{BT})_{ib}}{\sum_{i=1}^3 (\tau_{BB})_{ib}} \quad (4,61(a))$$

Inspection of many computed results shows that generally τ_{BT}_{ij} is approximately equal to $0.7\tau_{BL}_{ij}$, but to be conservative, we assume $\tau_{BL}_{ij} = \tau_{BT}_{ij}$. Then equation (4,61(a)) becomes

$$\left(\frac{C\tau_{BB}}{\tau_{BB}} \right)_{jk} = 1 + 2 \left(\frac{\sum_i \tau_{BL}_{ij}}{\sum_i \tau_{BB}_{ij}} \right) \left(\frac{\tau_{BL}}{\tau_{BB}} \right)_{jk} \quad (4,62)$$

Equation (4,62) shows that when considering the transmission coefficient from any plate (j) in a structure, to another (k), due regard should be paid to the transmitted longitudinal (and transverse) waves from any other join on plate (j) including the energy flow back from (k) to (j).

We now consider the relationship of $(\tau_{BL}/\tau_{BB})_{ij}$ to excitation frequency, plate thicknesses and plate thickness ratios. The ratio $(\tau_{BL}/\tau_{BB})_{12}$ was computed for a number of two, three and four plate single join structures at various excitation frequencies. $(\tau_{BL}/\tau_{BB})_{13}$ ratios (see Fig. 4-7) are very much less than for orthogonal plates, hence only $(\tau_{BL}/\tau_{BB})_{12}$ are presented, plotted against P_{ab} in Fig. 4-12. The use of this parameter does not produce a collapse of the data onto a single line or even a small range. Various parameters were tried but none achieved an adequate collapse of the data to warrant the introduction of a more complicated parameter.

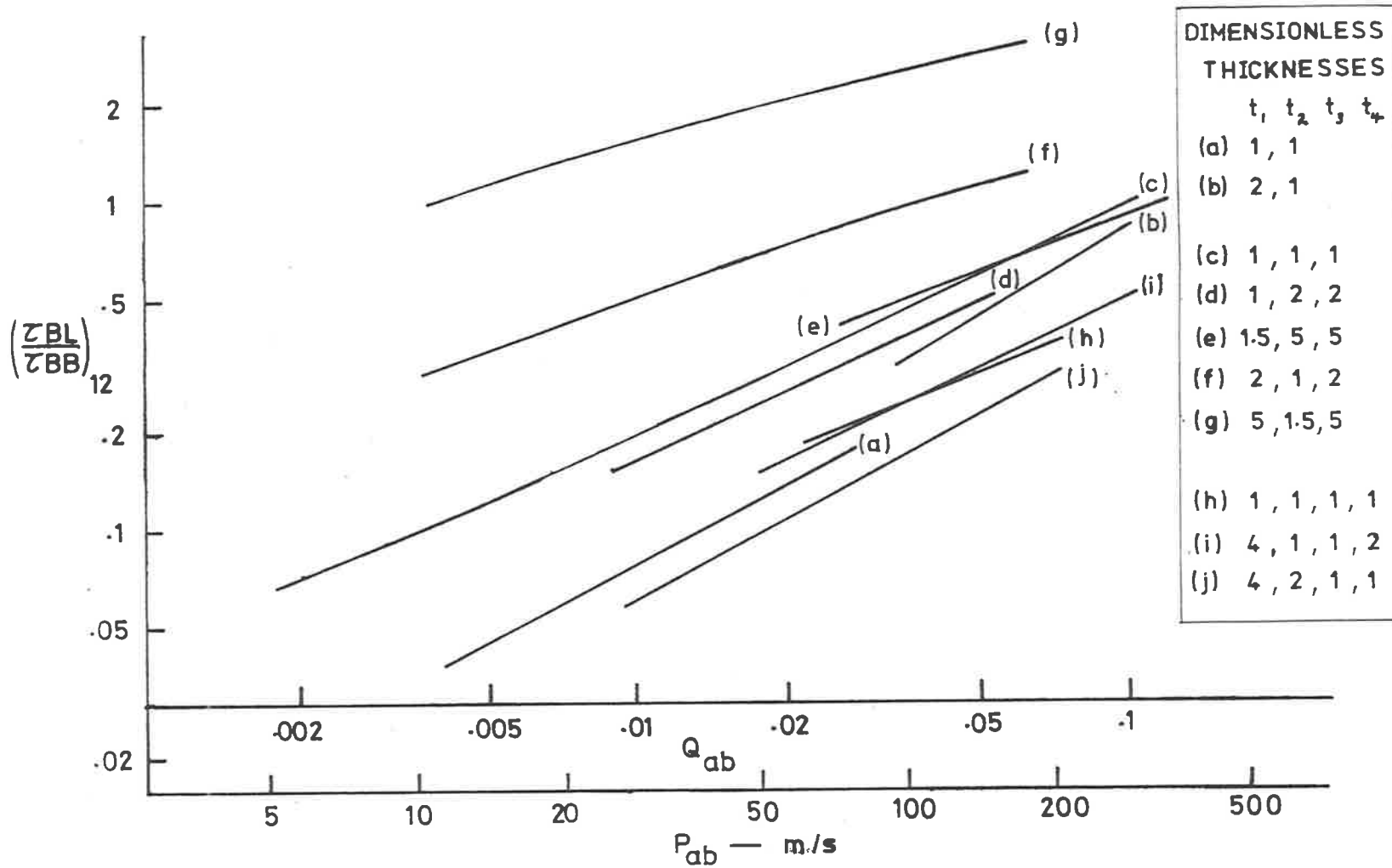


FIG. 4-12. VARIATIONS OF $(\tau_{BL}/\tau_{BB})_{12}$ WITH P_{ab} AND Q_{ab} - SINGLE JOINT PLATE STRUCTURES.

If the product $\left(\frac{\tau_{BL}}{\tau_{BB}}\right)_{jk} \left\{ \frac{\sum_i \tau_{BL}_{ij}}{\sum_i \tau_{BB}_{ij}} \right\}$ is equal to 0.3, then $(C\tau_{BB}/\tau_{BB})_{jk}$ is approximately 1.6 according to equation (4,62); approximately a 2dB error is incurred if τ_{BB}_{jk} is used alone without correction. If we consider only one of the τ_{BL}_{ij} and τ_{BB}_{ij} terms under the summation (say plate 1 and b in Fig. 4-11) and assume that the ratio $(\tau_{BL}/\tau_{BB})_{ij}$ associated with these two plates is larger than the ratio associated with any other plate interactions at this join (say plates 2 to b and 3 to b in Fig. 4-11), then $(\tau_{BL}/\tau_{BB})_{ij}$ is greater than $(\sum_i \tau_{BL}_{ij} / \sum_i \tau_{BB}_{ij})$. This being so, we inspect Fig. 4-12 to determine below what value of P_{ab} the product $(\tau_{BL}/\tau_{BB})_{ij} (\tau_{BL}/\tau_{BB})_{jk}$ is less than 0.3. For $(\tau_{BL}/\tau_{BB})_{ij}$ approximately equal to $(\tau_{BL}/\tau_{BB})_{jk}$, values of $P_{ab} < 100\text{m/s}$ appears to be a suitable criterion for $(\tau_{BL}/\tau_{BB})_{12} < 0.55$ if curves (f) and (g) are excluded. It is not unreasonable to exclude (f) and (g) as it is unlikely that a structure would contain plates where two consecutive joins, of three plates at each join had plate thickness ratios 5:1.5:5 at each join. This would imply that the thickness ratio of plate i to k, considering $(\tau_{BL}/\tau_{BB})_{ij} (\tau_{BL}/\tau_{BB})_{jk}$, would be 11:1. However, where larger thickness ratio structures are considered, more care is required, especially with three plate joins as shown in Fig. 4-7(b). Curves (f) and (g) in Fig. 4-12 show that large values of $(\tau_{BL}/\tau_{BB})_{12}$, and thus $(C\tau_{BB}/\tau_{BB})$ according to equation (4,62), occur for three plate joins with plate 2 (see Fig. 4-7(b)) much thinner than plates 1 and 3. A structure with this type of join is shown in Fig. 4-13 and consists of a number of sequential three plate joins. We assume that the plates 1, 3, 4, 5 and 7 are all 5mm thick while the plates 2 and 6 are each 1.5mm thick. As $(\tau_{BL}/\tau_{BB})_{12}$ is equal to $(\tau_{BL}/\tau_{BB})_{32}$, we can use equation (4,62) to write

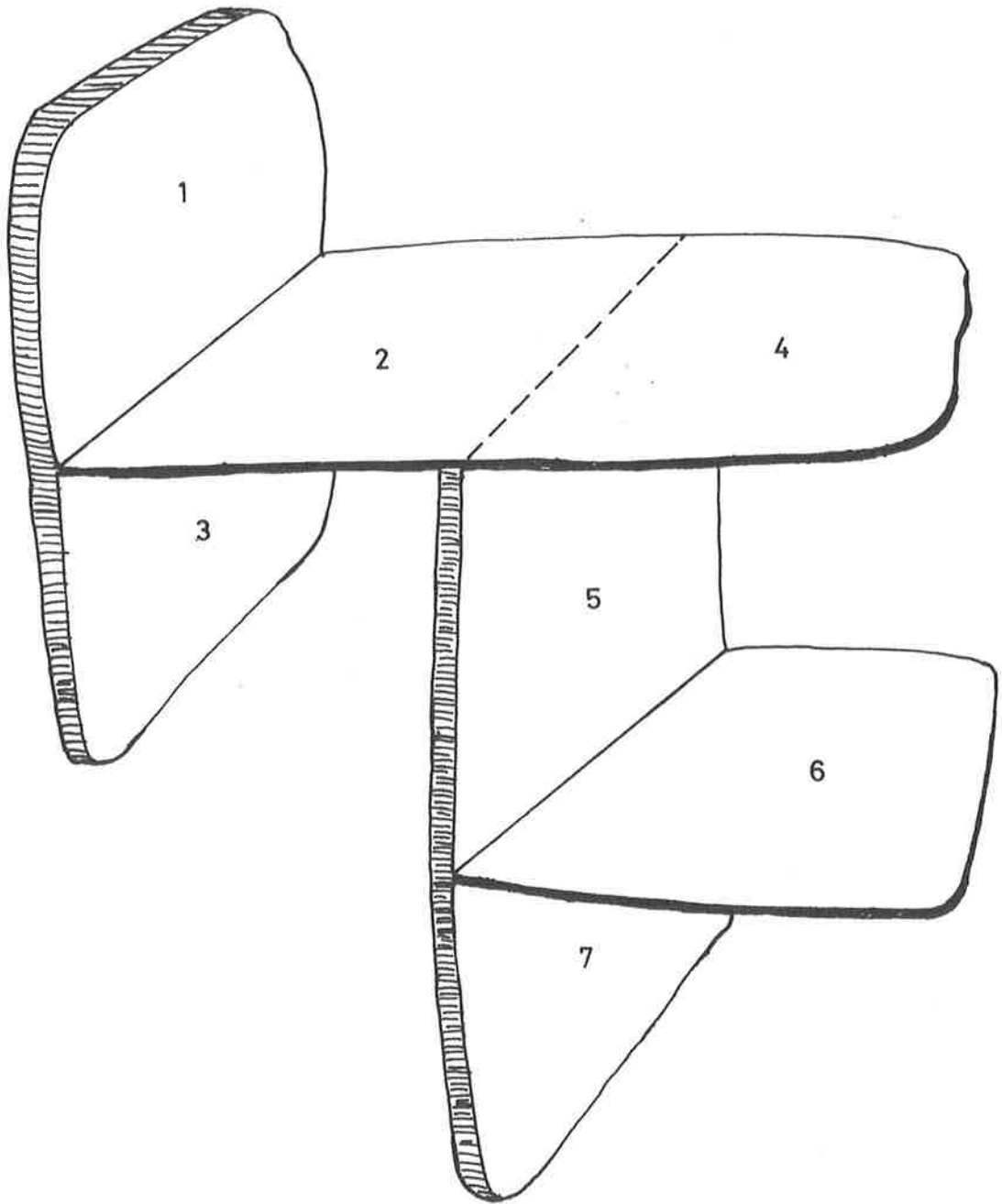


FIG. 4-13. MULTI-JOIN STRUCTURE WITH LARGE THICKNESS RATIO
THREE PLATE JOINS.

$$t_2 = t_6 = 1.5 \text{ mm.}$$

all other plate thicknesses = 5mm.

$$(C_{\tau BB}/\tau_{BB})_{25} = 1 + 2(\tau_{BL}/\tau_{BB})_{12} (\tau_{BL}/\tau_{BB})_{25}$$

At $P_{ab} = 100\text{m/s}$, curves (d) and (f) of Fig. 4-12 show (τ_{BL}/τ_{BB}) values which determine $(C_{\tau BB}/\tau_{BB})_{25}$ is 4, i.e. a 6dB error. For $P_{ab} = 50\text{m/s}$, $(C_{\tau BB}/\tau_{BB})_{25}$ is reduced to 2.2 or approximately a 3dB error. Similarly, as $(\tau_{BL}/\tau_{BB})_{25}$ is equal to $(\tau_{BL}/\tau_{BB})_{45}$ and using equation (4,62), we can write

$$(C_{\tau BB}/\tau_{BB})_{56} = 1 + 2(\tau_{BL}/\tau_{BB})_{25} (\tau_{BL}/\tau_{BB})_{56}$$

but as $(\tau_{BL}/\tau_{BB})_{56}$ is the same as $(\tau_{BL}/\tau_{BB})_{12}$, then $(C_{\tau BB}/\tau_{BB})_{56}$ is equal to $(C_{\tau BB}/\tau_{BB})_{25}$ for the same values of P_{ab} , i.e. at the same excitation frequency.

As the general solution is required to obtain τ_{BB} , and as it requires very little extra computation to obtain values of τ_{BL} and τ_{BT} , it is then a relatively easy task to use the correct bending to bending transmission coefficient, from equation (4,61(a)).

If the bending wave solution transmission coefficients are used, $(C_{\tau BB}/\tau)_{jk}$ will be less than the previously discussed ratio $(C_{\tau BB}/\tau_{BB})_{jk}$, since in nearly all cases for $P_{ab} < 100\text{m/s}$ $(\tau_{BB}/\tau)_{jk}$ is between 0.6 and 1.0.

From the discussion it can be seen that for $P_{ab} < 100\text{m/s}$ the bending wave solution for the transmission coefficient can be used for both single join and multi-join structures provided that the plate thickness ratios at consecutive joins are not too large or too small. If the structure is such that thickness ratios of approximately 3 to 1 at one join are followed by thickness ratios of approximately 1 to 3 at a consecutive join, then $P_{ab} < 50\text{m/s}$ should be the criterion for minimum errors in

the evaluated transmission coefficient of less than a factor of 2. For the structure shown in Fig. 4-12, $P_{ab} = 50\text{m/s}$ occurs at an excitation frequency of 3kHz.

4.5. EXPERIMENTAL METHODS.

4.5.1. Apparent Loss Factor

It is now appropriate to discuss methods of experimentally determining coupling loss factors. At present there is no way of measuring the coupling loss factor directly. What is measured is an apparent loss factor for an element from which the coupling loss factor can be determined provided that the other losses included in the apparent loss factor are known. This can be mathematically expressed in two equations; one considering the energy flow in and out of an element of a coupled structure,

$$P_i = \omega E_i \eta_{i \text{ app}} + dE_i/dt \quad (4,63)$$

and the other showing the composition of the apparent loss factor $\eta_{i \text{ app}}$.

$$\eta_{i \text{ app}} = \eta_{i \text{ int}} + \eta_{i \text{ rad}} + \eta_{\text{support loss}} + \eta_{\text{coupled structures}} \quad (4,64)$$

With careful design of the experimental apparatus the support losses can be made negligible and provided the internal (mechanical) loss of the element is large compared to the radiation loss factor, the apparent loss factor reduces to merely the sum of the internal loss and coupled loss. Equation (4,64) becomes

$$\eta_{i \text{ app}} = \eta_{i \text{ int}} + \eta_{\text{coupled structures}} \quad (4,65)$$

where η_i is as defined in Section 3.

The coupling loss factor is included in the η_{coupled} structure term. How η_{ij} is included depends on the structure to which the element is coupled.

The discussion now reduces to an examination of methods to determine the apparent loss factor. These fall into two categories; energy decay methods where P_i in equation (4,63) is set equal to zero and the energy decay rate is measured and, steady state methods where the energy level E_i and input power P_i are steady, hence the rate of change of energy is zero.

For the purpose of the discussion, we consider a two coupled element structure. If the element connected to element i is infinite or has a very large modal density compared with that of element i , then the power flow from the connected element back to element i can be neglected, hence

$$\eta_{i \text{ app}} = \eta_i + \eta_{ij} \quad (4,66)$$

Lyon and Eichler (1964) used Equation (4,66) when investigating two coupled plates neglecting power flow back from the second element. However, when the power flow back from the coupled element j can not be neglected

$$\eta_{i \text{ app}} = \frac{\eta_i + \eta_{ij} - \eta_{ji} \eta_{ij}}{\eta_{ji} + \eta_j} \quad (4,67)$$

The reciprocity relationship of (3,6) allows (4,67) to be rearranged to give

$$\eta_{ij} = \frac{(n_j/n_i) \eta_j (\eta_{i \text{ app}}^{-\eta_i})}{\eta_i + (n_j/n_i) \eta_j - \eta_{i \text{ app}}} \quad (4,68)$$

Much of the following discussion is concerned with the experimental measurement of both $\eta_{i \text{ app}}$ and η_i . The apparent loss factor is determined from tests on element i of the coupled structure; η_i is determined from tests on element i before it is coupled to any other element.

4.5.2. Energy Decay Methods

There are two commonly used methods of obtaining the average energy decay rate of an element excited by band limited noise. One is the pause method where a band limited random signal excites the element. The signal is cut off and the decay rate measured. This method has been in use for many years for measuring room absorption and it is tempting to consider its use for plates. However, its use for plates experiences difficulty because of the low modal density associated with plates. The modal density of plates remains constant independent of frequency unlike that of rooms which increases rapidly with increasing frequency. The problems associated with the low frequency excitation of rooms, for example, erratic decay curves and consequent large spread of decay rates, are associated with plate excitation at all frequencies. Thus large numbers of tests are required to obtain accurate average loss factors, for both $\eta_{i \text{ app}}$ and η_i measurements.

The second decay method is a newer technique developed by Schroeder (1965) and improved by Kuttroff and Jusofie (1967/8). This method produces an ensemble of all possible decay curves at once so that a single average decay rate is determined. The loss factor so determined is then equivalent to the average loss factor that would be determined from an infinite number of pause tests. However for plates, in contrast to rooms with single slopes, the curves often show clearly double slopes, triple

slopes and sometimes continuously varying slopes as well.

If a decay method is used, the question still arises which decay slope to use when more than one slope is obtained. Shall it be the average of the first 5, 7 or 10dB? As the loss factors are for use to determine steady state energy levels, it seems likely that the initial decay rate is the one which should be used, but inspection of many Schroeder-Kuttroff obtained decay curves show distinct initial slopes of only 1 or 2dB before a change of slope and these are very difficult to measure. Thus for accurate work an alternative must be found.

4.5.3. Steady State Methods

One way to determine an appropriate value of a loss factor for an element is to measure the loss factor while the element is at a steady excitation level. This is the case when dE_i/dt in (4,63) is zero.

In order to solve (4,63), P_i , the nett power flow from an external source into element i , as well as the mean energy level of the element, must be measured. If the element is not coupled to a structure, η_i is determined and if element i is coupled to another element, $\eta_{i \text{ app}}$ is measured, η_{ij} can then be determined from equation (4,68).

Although this power flow method is useful for determining the internal loss factor of individual elements and was used for this purpose in this research, as described in Appendix D.4., there is another consideration which may render the technique unsuitable for use on coupled structures. In order to measure P_i , we have used point excitation of the plate and Fahy (1970) raises doubts that SEA can be applied to a point excited coupled structure. Fahy points out that the theories of energy flow between randomly excited coupled oscillators have assumed that

the external sources of input power to the oscillators are statistically independent, but for a panel excited by a point force, the modal forces on the panel cannot be statistically independent. The doubts raised by Fahy do not affect the validity of the point excitation method to determine the uncoupled element internal loss factors η_i , or the coupled element apparent loss factors $\eta_{i \text{ app}}$. However, the relationship between $\eta_{i \text{ app}}$ and η_{ij} , equation (4,68), is based on SEA; it does assume that the external modal forces on the modes of the plates are statistically independent and hence its validity could be questioned.

In order to investigate this further, four different two coupled element structures were excited by exciting one of the two plates in each case by (a) point contact excitation and (b) non contact excitation. For a given coupled structure, the energy level ratio E_j/E_i should be the same, within the expected experimental range, for both point contact and non contact excitation if SEA is applicable for both forms of excitation. The mean energy level ratios for each structure for both forms of excitation were measured, as described in Appendix D.5 and D.6. The measured energy ratio level differences for the two excitation methods are presented in Fig. 4-14. The spread of results is larger than that predicted in Appendix D.6, Fig. D-6. Not only is the scatter larger than is reasonably expected, but it does not reduce for higher excitation frequency, as does the standard deviation of expected measured energy ratios, shown in Fig. D-6. These results do indicate that the energy ratios measured during point contact excitation are not necessarily the same as those measured during non contact excitation.

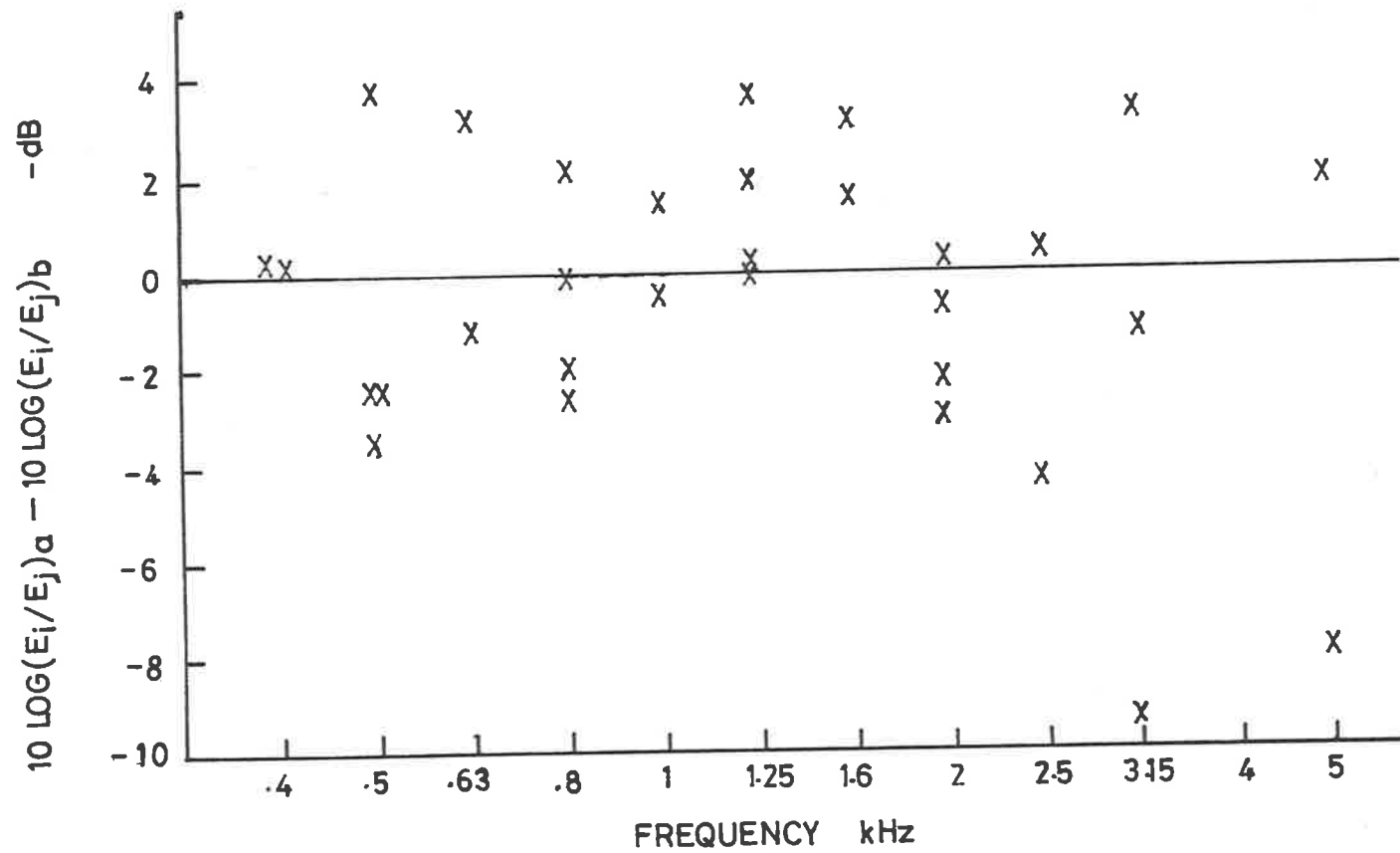


FIG. 4-14. COMPARISON OF MEASURED ENERGY RATIOS FOR TWO PLATE STRUCTURES; PLATE j DIRECTLY EXCITED

- (a) POINT CONTACT DRIVER
- (b) NON CONTACTING DRIVER

There is, however, another way of measuring coupling loss factors under steady state conditions without the requirement for measuring the input power P_i . This second steady state measurement technique is based on the power balance equations for coupled structures where the input power P_i is zero, i.e. when only one element of the structure is excited. For a two coupled element structure, with $P_2 = 0$ and element 1 directly excited, equation (3,7) results. The modal density ratio can be calculated from known formulae, (Hart and Shah, 1971) and the coupling loss factor η_{21} can be determined. An extension of this method can also be used to determine η_{21} and η_{12} without assuming the reciprocity relationship (3,6).

If a second test is carried out where element 2 is directly excited, the two power balance equations for the indirectly excited elements can be written in matrix form

$$\begin{bmatrix} (E_1)_1 & -(E_2)_1 \\ -(E_1)_2 & (E_2)_2 \end{bmatrix} \begin{bmatrix} \eta_{12} \\ \eta_{21} \end{bmatrix} = \begin{bmatrix} (E_2)_1 & \eta_2 \\ (E_1)_2 & \eta_1 \end{bmatrix} \quad (4,69)$$

where $(E_i)_j$ is the mean energy level of element i when element j is directly excited from an external (non contact) source.

The above method can be extended for three plates or four plates at a common join. Consider the three plate single join structure. There are six coupling loss factors, hence six simultaneous equations are required to determine the coupling loss factors.

In this case, three separate tests are carried out, with each of the three elements directly excited in turn. For each test, there are two power balance equations with $P_j = 0$ and

these give the required six power balance equations. The following matrix equation results.

$$\begin{bmatrix}
 -(E_1)_1 & 0 & (E_2)_1 & (E_2)_1 & 0 & -(E_3)_1 \\
 0 & -(E_1)_1 & -(E_2)_1 & 0 & (E_3)_1 & (E_3)_1 \\
 (E_1)_2 & (E_1)_2 & 0 & -(E_2)_2 & -(E_3)_2 & 0 \\
 0 & -(E_1)_2 & -(E_2)_2 & 0 & (E_3)_2 & (E_3)_2 \\
 (E_1)_3 & (E_1)_3 & 0 & -(E_2)_3 & -(E_3)_3 & 0 \\
 -(E_1)_3 & 0 & (E_2)_3 & (E_2)_3 & 0 & -(E_3)_3
 \end{bmatrix}
 \begin{bmatrix}
 \eta_{12} \\
 \eta_{13} \\
 \eta_{23} \\
 \eta_{21} \\
 \eta_{31} \\
 \eta_{32}
 \end{bmatrix}
 =
 \begin{bmatrix}
 -\eta_2 (E_2)_1 \\
 -\eta_3 (E_3)_1 \\
 -\eta_1 (E_1)_2 \\
 -\eta_3 (E_3)_2 \\
 -\eta_1 (E_1)_3 \\
 -\eta_2 (E_2)_3
 \end{bmatrix}
 \tag{4,70}$$

The four plate single joint configuration requiring four separate tests, leads to a set of 12 simultaneous equations to determine the 12 coupling loss factors.

It can be seen that the energy level measurement method to determine coupling loss factors does not require the assumption of reciprocity and a non contact source may be used. The only information required other than the measured energy levels are the experimentally determined internal loss factors of the individual elements.

4.5.4. The Importance of Coupling Loss Factor to internal loss factor ratio.

It is important to consider the sensitivity of the experimentally determined coupling loss factor to the variation in the directly measured quantities required. Consider the equation (4,68) relating η_1 app to η_{12} for the two coupled element situation. If $\eta_1 = \eta_2$, and as η_{12} must be positive,

then the following inequality must be true

$$1 < \eta_{1 \text{ app}}/\eta_1 < 1 + \eta_1/\eta_2 \quad (4,71)$$

(4,71) is applicable irrespective of whether energy decay methods or the steady state measurement of input power method is used.

Fig. 4-15 shows the relationship of η_{12}/η_1 to $\eta_{1 \text{ app}}/\eta_1$ based on equation (4,68) for $n_1 = n_2$ and $\eta_1 = \eta_2$. It can be seen that a small error in the measurement of $\eta_{1 \text{ app}}$ or η_1 can result in a large error in η_{12} if η_{12} is much greater or much less than η_1 . The best range to experiment in is for η_{12} approximately equal to η_1 .

Similar considerations are true for the energy ratio measurement method. If each side of equation (3,7) is divided by the modal density ratio the average modal energy ratio is

$$(E_2/n_2)/(E_1/n_1) = \eta_{21}/(\eta_{21} + \eta_2) \quad (4,72)$$

Equation (4,72) is shown in Fig. 4-16 where inspection shows that a small error in the measured energy ratio can cause a large error in η_{21}/η_2 if η_{21}/η_2 is much greater than 1. For this method however, as η_{21}/η_2 becomes less, the sensitivity to error in E_2/E_1 becomes less.

The last method which uses the simultaneous equations is also bound by this restriction. The determinant of the 2x2 matrix in (4,69) is

$$|\text{DET}| = \begin{bmatrix} 1 & - \left(\frac{E_2}{E_1} \right) \left(\frac{E_1}{E_2} \right) \\ \left(\frac{E_1}{E_2} \right)_1 & \left(\frac{E_2}{E_1} \right)_2 \end{bmatrix} \quad (4,73)$$

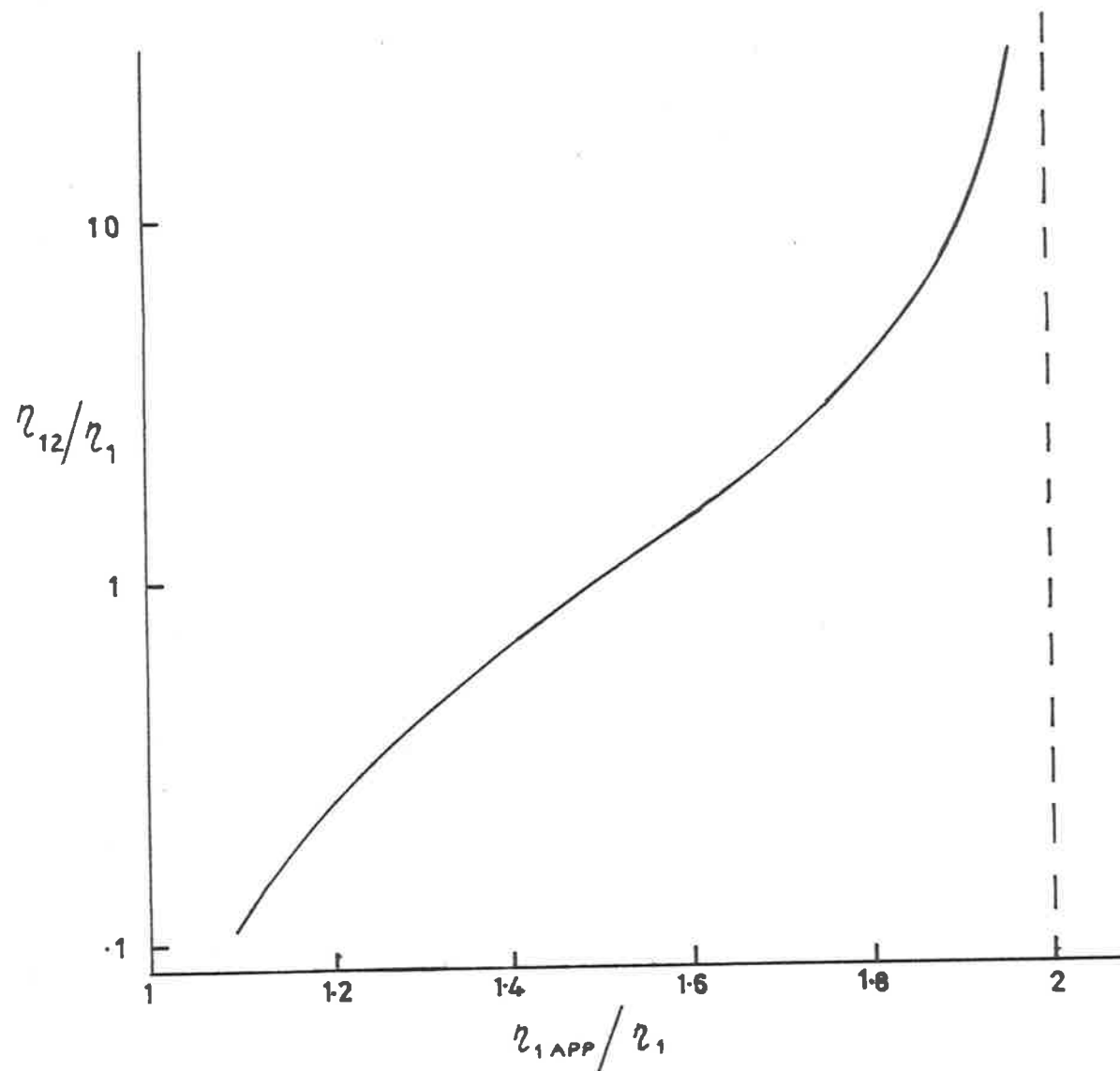


FIG. 4-15. THE EXPERIMENTALLY DETERMINED COUPLING LOSS FACTOR FROM PLATE 1 TO PLATE 2 AS A FUNCTION OF THE MEASURED APPARENT LOSS FACTOR (WHEN COUPLED) TO INTERNAL LOSS FACTOR RATIO. $n_1 = n_2$; $\eta_1 = \eta_2$

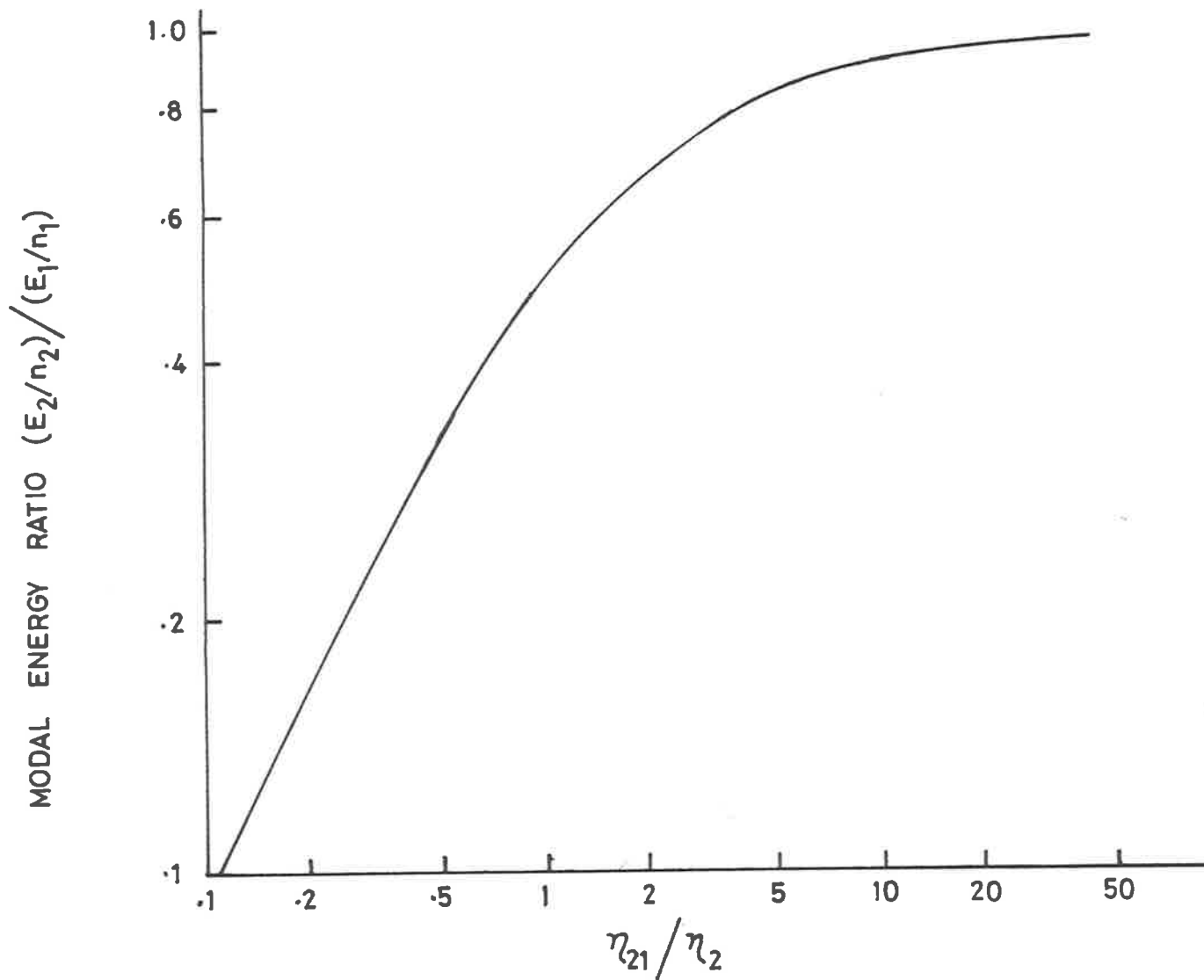


FIG. 4-16. MODAL ENERGY RATIO FOR TWO COUPLED ELEMENTS AS A FUNCTION OF THE COUPLING LOSS FACTOR TO INTERNAL LOSS FACTOR RATIO.

When the energy ratio expressions are substituted with the appropriate loss factor formulae, the expression in the square bracket becomes

$$1 - \frac{\eta_{12}\eta_{21}}{(\eta_{12}\eta_{21} + \eta_1\eta_{21} + \eta_2\eta_{12} + \eta_1\eta_2)} \quad (4,74)$$

If the internal loss factors are much less than the coupling loss factors, then the determinant is very small. Small variations in the measured energy ratios then have a magnified effect on the experimental value of the coupling loss factors.

It is apparent from this discussion that it would be preferable to increase the damping of the elements to reduce the coupling loss factor to internal loss factor ratio nearer to one, or less than one for steady state experimental methods. However, since the upper frequency bound discussed in Section 3 is proportional to the internal loss factor, an increase in the internal loss factor reduces the experimentally useful frequency range. This limits the amount of damping which can be added to the elements. For two coupled plate structures, the minimum coupling loss to internal loss factor ratios obtained were often still greater than one.

We have reviewed the difficulties involved in using experimentally measured energy levels to accurately determine the coupling loss factors of a structure. Although we have not discussed experimental results at this stage, it is useful to use some of the experimental results for a two element coupled structure to illustrate the sensitivity of the experimentally determined coupling loss factor to apparent slight errors in the

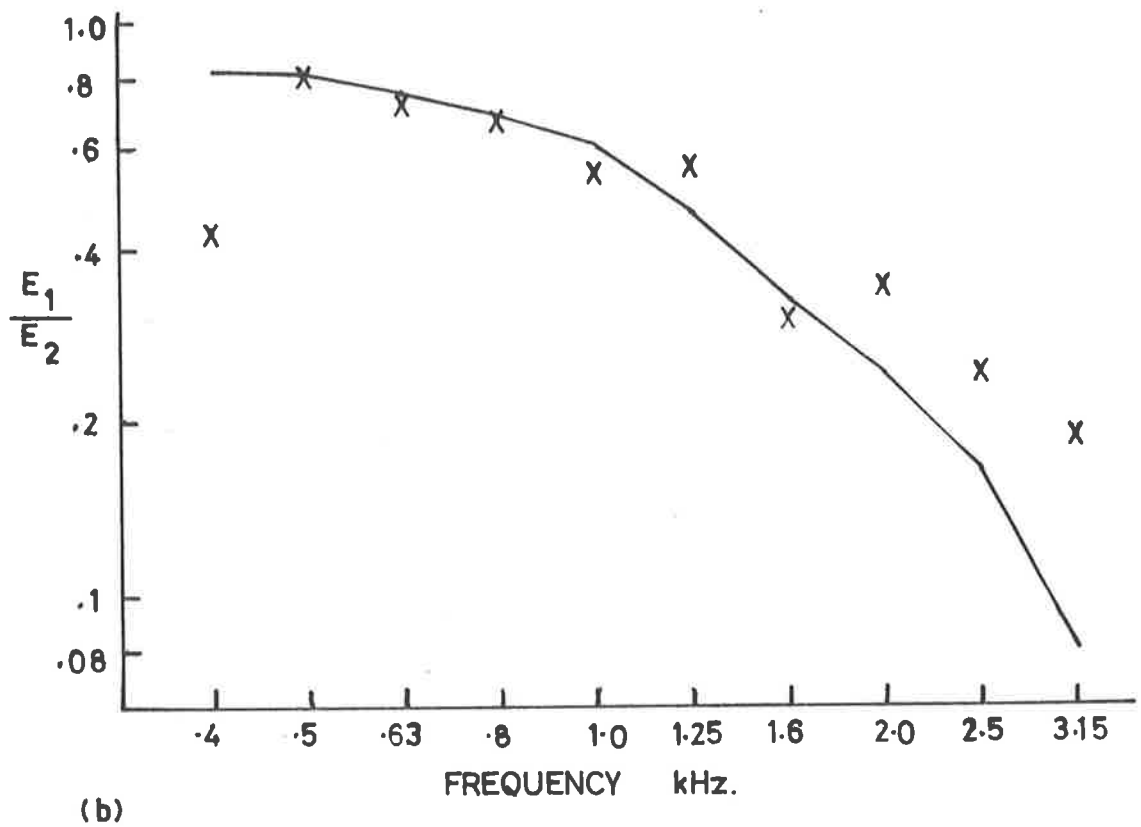
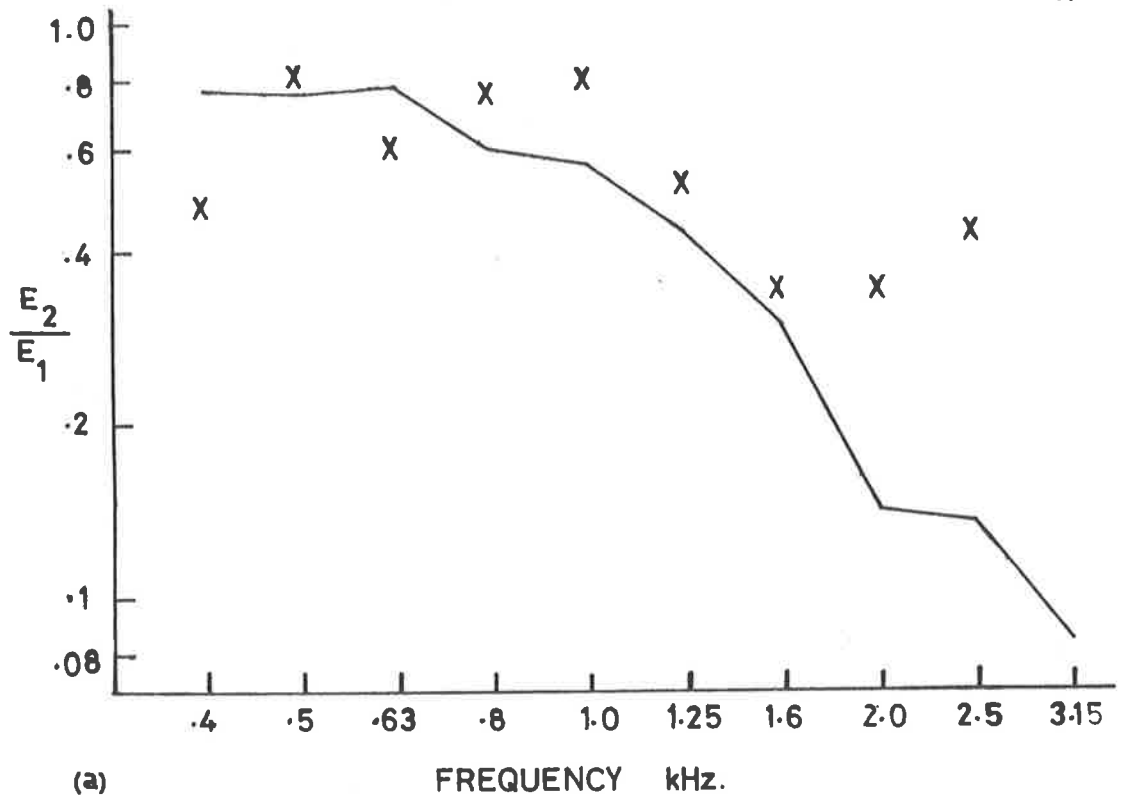


FIG. 4-17. MEASURED AND PREDICTED ENERGY RATIOS OF COUPLED PLATES 1 AND 2.

(a) PLATE 1 DIRECTLY EXCITED

(b) PLATE 2 DIRECTLY EXCITED.

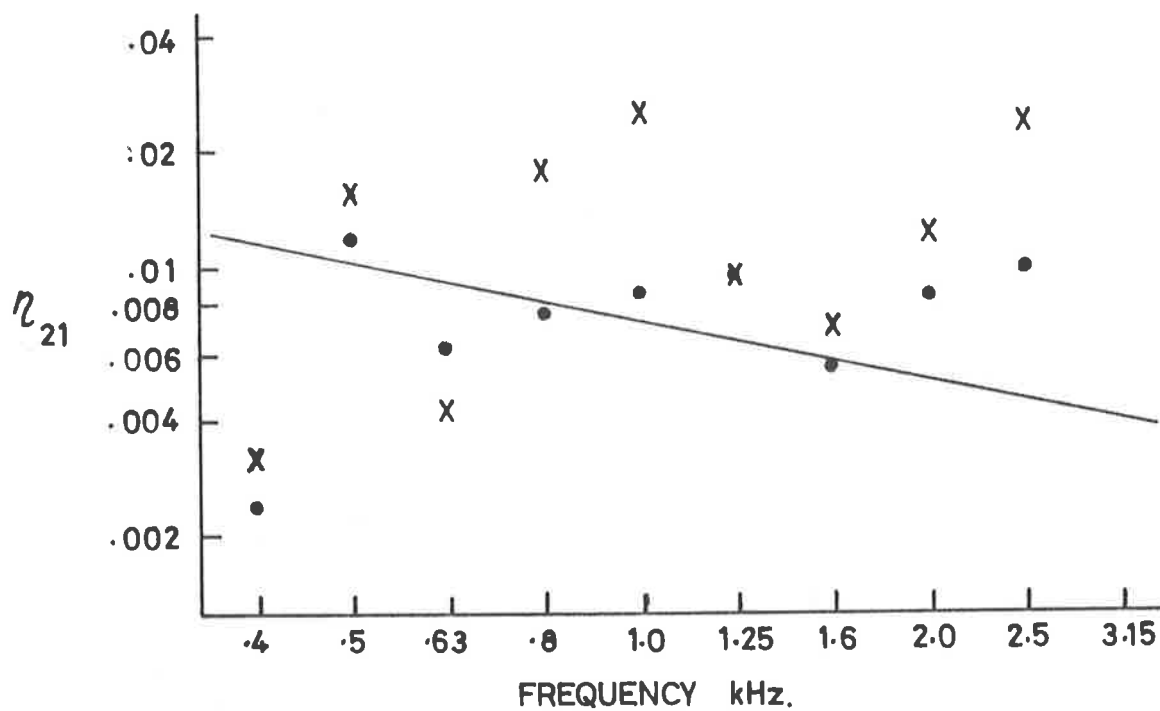
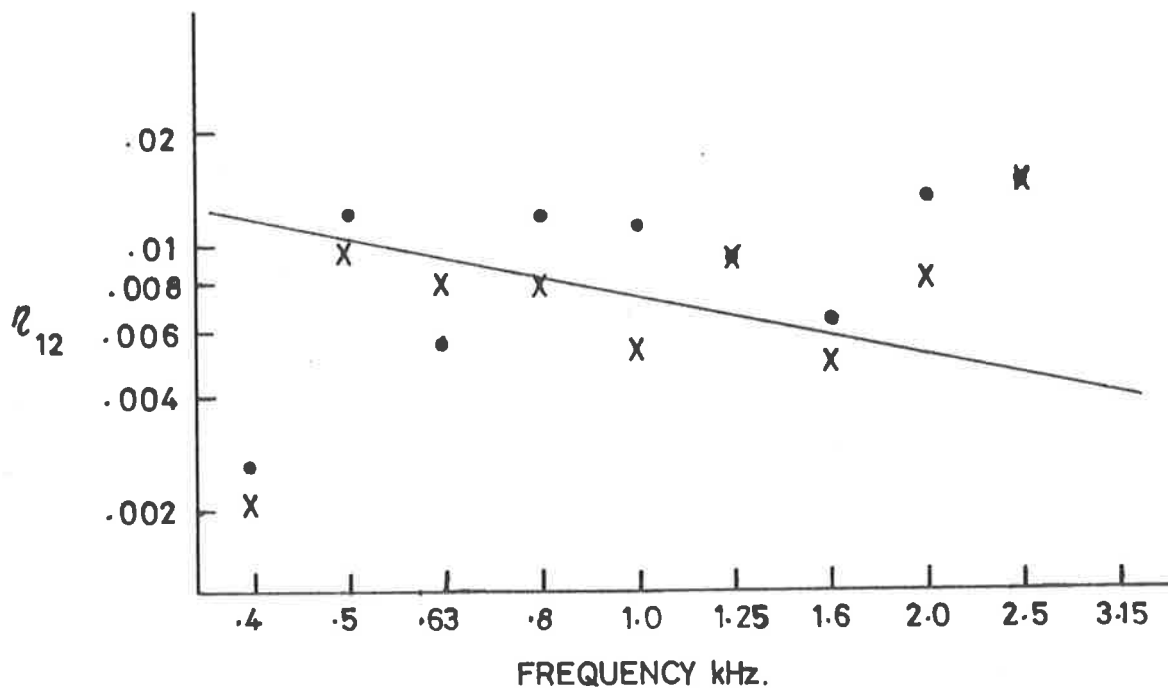


FIG. 4-18. COUPLING LOSS FACTORS DETERMINED FROM MEASURED ENERGY RATIOS IN FIG. 4-17: —, THEORETICAL, EQUATION (4,40); x, RECIPROCALITY ASSUMED; •, SIMULTANEOUS EQUATION.

measured element energy levels.

Fig. 4-17(a) and (b) shows the measured mean energy level ratios E_2/E_1 for element 1 directly excited and E_1/E_2 for element 2 directly excited. Also shown is the theoretical energy ratios calculated using SEA. The internal loss factors were experimentally measured and the coupling loss factors were evaluated using equation (4,40) and (4,1). The coupling loss factor to internal loss factor ratio varied from approximately 1.8 at 500Hz to approximately 0.7 at 1600Hz, and it can be seen that there is good agreement between theory and experiment in this range.

This data was then used to determine the coupling loss factors using two steady state methods; (a) assuming reciprocity as in equation (3,7) and (b) using simultaneous equations as in (4,69). These results and the theoretical bending wave coupling loss factors are shown in Fig. 4 - 18

The spread of the experimentally determined coupling loss factor results derived from an apparently experimentally good set of measured energy level results indicate that it is not very informative to present the results as a comparison of predicted and measured coupling loss factors.

The objective of this work is to indicate for what range of excitation frequencies for a given structure SEA can be used to predict the energy distribution in the connected structure. Thus it seems appropriate to present the results as a comparison between predicted and measured energy level ratios. The predicted ratios are determined using SEA techniques as presented in Section 3. The coupling loss factors required for the energy distribution equations are evaluated using equations (4,40) and (4,1) and hence agreement between predicted and experimentally measured energy ratios shows where equations (4,1),

(4,40) and (3,9) can be used to predict the energy distribution in a structure.

Before closing this discussion on experimental methods and accuracy of results, there is one other consideration to be discussed. We wish to ensure that the measured internal loss factor of each element, η_i , is unchanged when the element is incorporated in a structure. This assumes the optimum measuring method is used. As mentioned previously, the measured internal loss factor is due to the sum of the mechanical internal losses of the element plus the loss due to radiation to the surrounding fluid, assuming that the losses via the support system are negligible.

The losses due to radiation in an undamped metal plate are often more significant than the mechanical internal losses, especially near critical frequency. If this loss factor could be assumed to be constant for all plate configurations, there would be no problem. The plate is tested by itself to obtain η_i . When it is connected to another plate or combinations of plates, not only has the acoustic space into which it radiates been altered, but also the edge condition of the plate has been altered. Maidanik (1962) has shown that below critical frequency the radiation is from the plate corners and edges, hence it is most likely that the radiation loss factor for a coupled plate would be different from that of the uncoupled plate. If additional damping is provided, the added damping on the plates increases η_{int} and reduces the overall variation of η_i from the uncoupled to the coupled condition. The increased damping also reduces the influence of any losses due to the support system.

SECTION 5. COMPARISON OF THEORETICALLY AND EXPERIMENTALLY DETERMINED ENERGY RATIOS IN COUPLED STRUCTURES.

5.1. INTRODUCTION

In this section, the measured plate energy ratio levels of various steel plate structures are compared with the theoretical energy ratio levels, predicted using the matrix equation (3,9). The coupling loss factors required were evaluated using the bending wave solution empirical equation (4,40) to obtain τ_{ij} , which was substituted into the coupling loss factor equation (4,1). Bending wave solution average transmission coefficients were used for all the coupled structures investigated as the maximum value of P_{ab} in any structure at the highest excitation frequency used was much less than 50m/s. Additional damping was added to each plate and its internal loss factor was experimentally measured using the point contact excited steady state method discussed in Section 4.5.3. The apparatus and experimental procedure used to measure the loss factors are described in Appendix D.

The physical characteristics of all plates used are listed in Table 5-1. The measured internal loss factors of these plates are presented in Table 5-2.

Single join structures were investigated first. Four two-plate, two three-plate and one four-plate single join structures were tested. Other plates were then added to some of these single join structures, and structures were coupled together to form three multi-join structures, two of which contained only two-plate joins and one contained two, three and four plate joins. Table 5-3 shows a line sketch of each coupled structure, together with the lengths of join between the coupled elements. The coupling loss factors required, evaluated at 1000Hz, are also listed. The coupling loss factor at any

TABLE 5-1.

LIST OF EXPERIMENTAL PLATES

Plate No.	Area m ²	Thickness mm.	Mass kg.	Modal Density n(f)
1	0.140	0.99	1.168	47.4x10 ⁻³
2	0.171	1.24	1.654	46.0x10 ⁻³
3	0.118	1.27	1.290	31.3x10 ⁻³
4	0.195	0.79	1.214	82.9x10 ⁻³
4A	0.186	0.79	1.152	79.3x10 ⁻³
5	0.201	1.27	2.133	53.0x10 ⁻³
5A	0.179	1.27	1.872	47.3x10 ⁻³
6	0.185	1.27	1.957	48.7x10 ⁻³
6A	0.139	1.27	1.460	36.7x10 ⁻³
7	0.293	1.27	2.416	63.1x10 ⁻³
7A	0.178	1.27	1.800	47.1x10 ⁻³
8	0.124	1.27	1.265	32.7x10 ⁻³
9	0.388	1.27	3.865	102. x10 ⁻³
10	0.245	1.27	2.435	64.4x10 ⁻³
11	0.200	0.79	1.287	85.3x10 ⁻³
12	0.314	1.57	3.947	66.9x10 ⁻³
13	0.280	1.57	3.552	59.8x10 ⁻³
14	0.237	1.57	2.968	50.5x10 ⁻³

TABLE 5-2
PLATE INTERNAL LOSS FACTORS (x1000)

Hz	1	2	3	4,4A	5,5A,6,6A	7,7A,8	9,10	11	12	13
400	2.94	3.29	2.46	2.39	4.56	2.12	1.21	2.66	1.82	1.13
500	2.68	3.05	4.03	2.20	7.07	1.63	1.03	2.88	0.981	1.24
630	3.24	2.50	3.17	2.19	4.83	1.38	1.22	3.17	1.90	1.08
800	4.10	5.18	2.19	2.13	6.40	1.46	1.18	2.43	1.50	1.29
1000	4.80	5.70	2.28	2.14	5.90	1.60	1.04	2.56	1.05	1.10
1250	7.50	8.40	1.97	2.05	9.17	1.50	1.14	2.98	1.21	1.35
1600	12.2	13.1	2.30	4.53	18.4	1.72	1.66	2.64	1.64	1.64
2000	16.2	30.0	4.96	4.15	18.1	2.42	1.52	3.77	2.37	2.37
2500	23.4	30.3	3.98	4.86	31.9	3.27	2.49	4.18	2.93	2.61
3150	47.3	45.4	3.56	4.16	30.5		2.52		2.57	2.57
4000			4.01	5.42			3.59		3.44	3.44
5000			6.94	11.8			6.92		7.32	7.17

TABLE 5-3
LIST OF COUPLED ELEMENTS

Plates are shown in edge view except for those denoted 3 or 6A which are in plan view.

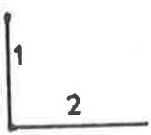

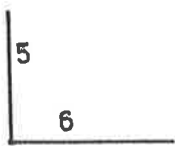
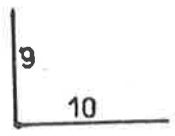
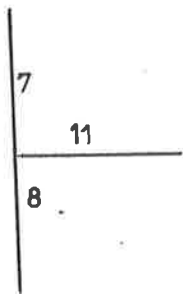
Element Nos. and Sketch	Coupling Lengths Metres	Coupling Loss Factors at 1kHz X1000
	$L_{12} = 0.356$	$\eta_{12} = 7.12$ $\eta_{21} = 7.31$
	$L_{34} = 0.223$	$\eta_{34} = 5.39$ $\eta_{43} = 2.03$
	$L_{56} = 0.13$	$\eta_{56} = 2.39$ $\eta_{65} = 2.60$
	$L_{910} = .561$	$\eta_{910} = 5.33$ $\eta_{109} = 8.48$
	$L_{711} = L_{811} = 0.421$	$\eta_{711} = 1.55$ $\eta_{117} = 1.19$ $\eta_{78} = 4.71$ $\eta_{87} = 9.45$ $\eta_{811} = 3.10$ $\eta_{118} = 1.19$

TABLE 5-3 (cont'd)

LIST OF COUPLED ELEMENTS

Element Nos. and Sketch	Coupling Lengths Metres	Coupling Loss Factors at 1kHz X1000
	$L_{9\ 10} = L_{10\ 12}$ $= L_{9\ 12} = 0.561$	$\eta_{9\ 10} = 1.56 \quad \eta_{10\ 9} = 2.47$ $\eta_{9\ 12} = 2.49 \quad \eta_{12\ 9} = 3.94$ $\eta_{10\ 12} = 3.81 \quad \eta_{12\ 10} = 3.81$
	<p>Common length</p> $L = 0.561$	$\eta_{9\ 10} = 0.731 \quad \eta_{10\ 9} = 1.16$ $\eta_{9\ 12} = 1.17 \quad \eta_{12\ 9} = 1.79$ $\eta_{9\ 13} = 1.17 \quad \eta_{13\ 9} = 2.00$ $\eta_{10\ 12} = 1.85 \quad \eta_{12\ 10} = 1.79$ $\eta_{10\ 13} = 1.85 \quad \eta_{13\ 10} = 2.00$ $\eta_{12\ 13} = 2.91 \quad \eta_{13\ 12} = 3.26$
	$L_{1\ 2} = .354$ $L_{1\ 6A} = .359$ $L_{2\ 6A} = .352$	$\eta_{1\ 2} = 7.12 \quad \eta_{2\ 1} = 7.31$ $\eta_{1\ 6A} = 7.04 \quad \eta_{6A\ 1} = 9.09$ $\eta_{2\ 6A} = 7.47 \quad \eta_{6A\ 2} = 9.40$
	$L_{1\ 2} = .354$ $L_{1\ 6A} = .359$ $L_{1\ 5A} = .305$ $L_{2\ 6A} = .352$ $L_{5A\ 6A} = .352$	<p>As for the previous structure</p> <p>plus</p> $\eta_{1\ 5A} = 6.10 \quad \eta_{5A\ 1} = 5.99$ $\eta_{5A\ 6A} = 7.25 \quad \eta_{6A\ 5A} = 9.35$

TABLE 5-3 (cont'd)

LIST OF COUPLED ELEMENTS

Element No. and Sketch	Coupling Lengths Metres	Coupling Loss Factors at 1kHz X1000
	common length	$\eta_{9\ 10} = 0.731$ $\eta_{10\ 9} = 1.16$
	$L_{9,10,12,13} = .561$	$\eta_{9\ 12} = 1.17$ $\eta_{12\ 9} = 1.79$
	$L_{3\ 4A} = .223$	$\eta_{9\ 13} = 1.17$ $\eta_{13\ 9} = 2.00$
	$L_{3\ 12} = .223$	$\eta_{10\ 12} = 1.85$ $\eta_{12\ 10} = 1.79$
	$L_{4A\ 12} = .416$	$\eta_{10\ 13} = 1.85$ $\eta_{13\ 10} = 2.00$
	$L_{4A\ 7A} = .360$	$\eta_{12\ 13} = 2.91$ $\eta_{13\ 12} = 3.26$
	$L_{7A\ 12} = .434$	$\eta_{3\ 4A} = 5.39$ $\eta_{4A\ 3} = 2.12$
	$L_{7A\ 14} = .394$	$\eta_{3\ 12} = 6.10$ $\eta_{12\ 3} = 2.84$
	$L_{13\ 14} = .425$	$\eta_{4A\ 12} = 1.36$ $\eta_{12\ 4A} = 1.61$
		$\eta_{4A\ 7A} = 0.644$ $\eta_{7A\ 4A} = 1.08$
	$\eta_{7A\ 12} = 6.60$ $\eta_{12\ 7A} = 4.70$	
	$\eta_{13\ 14} = 6.23$ $\eta_{14\ 13} = 7.38$	
	$\eta_{7A\ 14} = 7.13$ $\eta_{14\ 7A} = 6.65$	

other frequency can be evaluated from these values since η_{ij} is proportional to $(\omega)^{0.5}$.

In all experiments, only one element at any one time was directly excited by a non contacting external source and all the energy ratio levels presented in this section are relative to the directly excited element.

The experimental procedures and instrumentation used to measure the energy ratios of the coupled structures are discussed in Appendix D.

In Section 5.2., the single join structure results are presented and discussed, and in Section 5.3, the multi-join structure results are presented. In Section 5.2, the two plate single join structure results and the three and four plate single join structure results are presented separately.

The single join structure results are used to determine the bounds within which the agreement between predicted and measured energy ratio levels is satisfactory. In order to do this, parameters to define the bounds are required as well as a criterion for acceptability.

The lower bound is related to the number of resonant modes in the excitation frequency bandwidth N_i , where for each element

$$N_i = 0.23n_i f \quad (5,1)$$

as all tests were carried out using one third octave broad band noise. The possibility that an upper bound may exist was mentioned in the literature review of Section 3, as a consequence of the inequality (3,3(b)). If both sides of the inequality are multiplied by $(n_i f)$, then (3,3(b)) can be written as $R_i < 1$ where R_i , a modal overlap factor, is

$$R_i = \eta_i n_i f \quad (5,2)$$

There is an R_i and N_i value for each element at each excitation frequency. Hence, for four plates at a single join, there are four R_i and four N_i values which are applicable to that structure. Only one R and one N is required as a parameter. The parameters used in Section 5.2 to determine the lower and upper bounds are N_{\min} and R_{\max} where N_{\min} is the lesser of N_i and N_j and R_{\max} is the larger of R_i and R_j when the energy ratios between elements i and j are being considered, irrespective of the values of N and R of any other plates at the common join. A suitable criterion for satisfactory agreement between predicted and measured energy ratio levels is that the level difference be not greater than $\pm 2\text{dB}$.

In Section 5.2, the results are presented as a level difference in dB between measured and predicted plate energy ratios. In Section 5.3, the predicted and measured energy ratio are plotted against frequency for each individual multi-join structure. The results are discussed with reference to the upper and lower bounds determined from the single join structure results in 5.2.

5.2. SINGLE JOIN STRUCTURES

5.2.1. Two Plate Joins

The theoretical energy ratios of the four single join structures, shown in Table 5-3, were predicted as described in Section 5.1. The energy ratios, with one element directly excited in each case, were measured as described in Appendix D. The measured and predicted energy ratios of the four single join structures and the measured and predicted level differences

TABLE 5-4

PREDICTED AND MEASURED ENERGY RATIOSTwo plate coupled structure - Plate Nos. 1 & 2.

Frequency Hz	E_1/E_2		Level Diff. dB	E_2/E_1		Level Diff. dB
	Meas.	Pred.		Meas.	Pred.	
400	.432	.814	-2.75	.476	.758	-2.02
500	.805	.810	-0.02	.811	.753	0.32
630	.732	.754	-0.13	.613	.766	-0.97
800	.680	.677	0.02	.754	.596	1.02
1000	.543	.613	0.53	.793	.547	1.61
1250	.569	.471	0.82	.526	.426	0.91
1600	.301	.324	-0.31	.340	.298	0.57
2000	.347	.243	1.54	.339	.140	3.86
2500	.250	.166	1.79	.427	.129	5.20
3150	.188	.080	3.71	1.15	.081	11.51

TABLE 5-5

PREDICTED AND MEASURED ENERGY RATIOSTwo plate coupled structure - Plate Nos. 3 & 4.

Frequency Hz	E_3/E_4		Level Diff. dB	E_4/E_3		Level Diff. dB
	Meas.	Pred.		Meas.	Pred.	
400	.105	.292	-4.44	.260	1.524	-7.68
500	.085	.246	-4.64	.307	1.504	-6.90
630	.272	.257	0.25	.532	1.433	-4.31
800	.365	.276	1.21	1.14	1.373	-0.81
1000	.200	.264	-1.22	.732	1.293	-2.47
1250	.176	.267	-1.81	.861	1.250	-1.62
1600	.219	.244	-0.48	.735	.696	0.24
2000	.149	.164	-0.41	.680	.682	-0.01
2500	.255	.174	1.67	.449	.555	-0.92
3150	.218	.173	0.87	.692	.573	0.82
4000	.160	.151	0.24	.613	.419	1.65
5000	.163	.097	2.24	.296	.190	1.92

TABLE 5-6

PREDICTED AND MEASURED ENERGY RATIOSTwo plate coupled structure - Plate Nos. 5 & 6.

Frequency Hz	E_5/E_6		Level Diff. dB	E_6/E_5		Level Diff. dB
	Meas.	Pred.		Meas.	Pred.	
400	.372	.493	-1.23	.321	.435	-1.32
500	.164	.351	-3.30	.386	.314	0.89
630	.346	.418	-0.81	.343	.370	-0.33
800	1.029	.321	5.06	.237	.287	-0.82
1000	.450	.314	1.56	.203	.280	-1.40
1250	.165	.205	-0.96	.192	.185	0.15
1600	.242	.101	3.79	.179	.092	2.89
2000	.390	.093	6.22	.163	.085	2.82
2500	.121	.049	3.91	.092	.045	3.11

TABLE 5-7

PREDICTED AND MEASURED ENERGY RATIOSTwo plate coupled structure - Plate Nos. 9 & 10

Frequency Hz	E_9/E_{10}		Level Diff. dB	E_{10}/E_9		Level Diff. dB
	Meas.	Pred.		Meas.	Pred.	
400	.832	1.392	-2.23	.650	.576	0.53
500	.783	1.400	-2.52	.565	.579	-0.11
630	1.066	1.347	-1.02	.520	.564	-0.35
800	1.282	1.330	-0.16	.545	.559	-0.11
1000	1.032	1.332	-1.11	.600	.560	0.30
1250	1.488	1.284	0.64			
1600	.936	1.143	-0.87	.412	.503	-0.87
2000	.966	1.133	-0.69			
2500	1.109	.916	0.83	.472	.429	0.41
3150	.884	.866	0.09	.498	.411	0.83
4000	.903	.678	1.24	.460	.340	1.31
5000	.841	.407	3.15	.497	.222	3.50

in dB are presented in Tables 5-4, 5-5, 5-6 and 5-7.

The ± 2 dB criterion of acceptability is applied to each level difference result which has a particular value of R_{\max} and N_{\min} associated with it. Fig. 5-1 represents a plot of the corresponding values of R_{\max} and N_{\min} for all the two plate test results and shows which results met the ± 2 dB criterion. It is then used to determine the upper and lower bounds. The bounds indicated are such that 95% of the data points within those bounds meet the ± 2 dB criterion. Because of the possibility of experimental error and the statistical spread of results, it is unreasonable to place the bounds so that all the enclosed data points meet the ± 2 dB criterion. The data points are in groups of two because for each N_{\min} and R_{\max} coordinate, there are two results, the E_i/E_j level difference and the E_j/E_i level difference. A series of curves are formed by the data points because both N_{\min} and R_{\max} increase with frequency, and from equations (5.1) and (5.2), it can be seen that for each structure, the slope of the curve at any point is given by

$$R_{\max}/N_{\min} = (\eta)_{\max}/0.23n_{\min} \quad (5.3)$$

It is coincidental that 3 of the 4 sets of two coupled plates have similar values for this factor, and this accounts for the grouping of the data points. The lower bound is $N_{\min} = 6$, and the upper bound is $R_{\max} = 1.0$.

The presentation in Fig. 5-1 is used to determine the bounds but does not indicate how the level differences vary with N_{\min} and R_{\max} . The variation is shown in Fig. 5-2 and Fig. 5-3 respectively, where the level differences are presented as a mean value \pm one standard deviation. Individual data points are

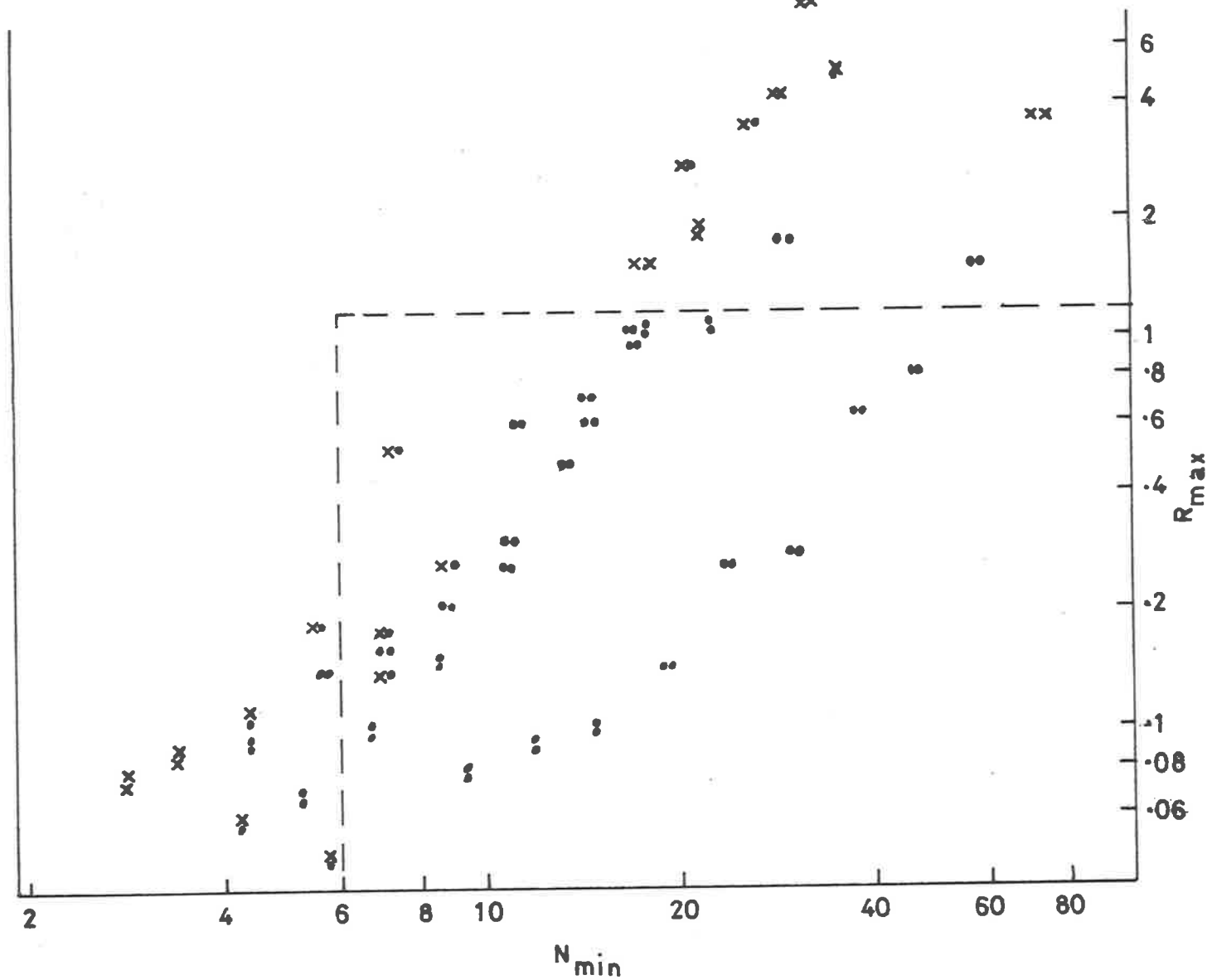


FIG. 5-1. DETERMINATION OF UPPER AND LOWER BOUNDS FOR TWO COUPLED PLATES; •, DATA MEETS $\pm 2\text{dB}$ CRITERION; x, DATA DOES NOT MEET $\pm 2\text{dB}$ CRITERION.

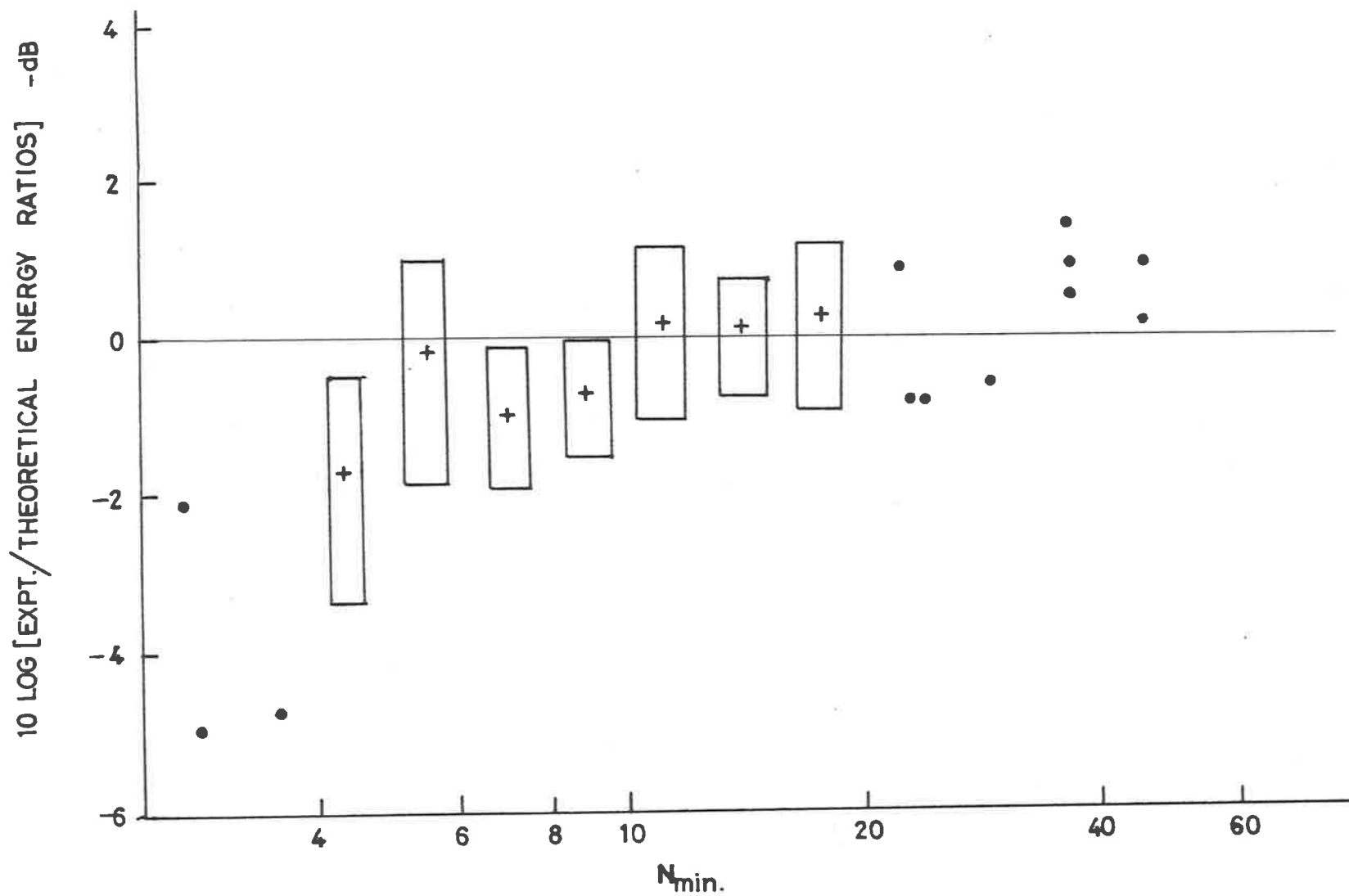


FIG. 5-2. EXPERIMENTAL AND THEORETICAL ENERGY RATIO LEVEL DIFFERENCES FOR TWO EDGE JOINED COUPLED PLATES - AS A FUNCTION OF THE NUMBER OF MODES IN A FREQUENCY BAND N_{min} .

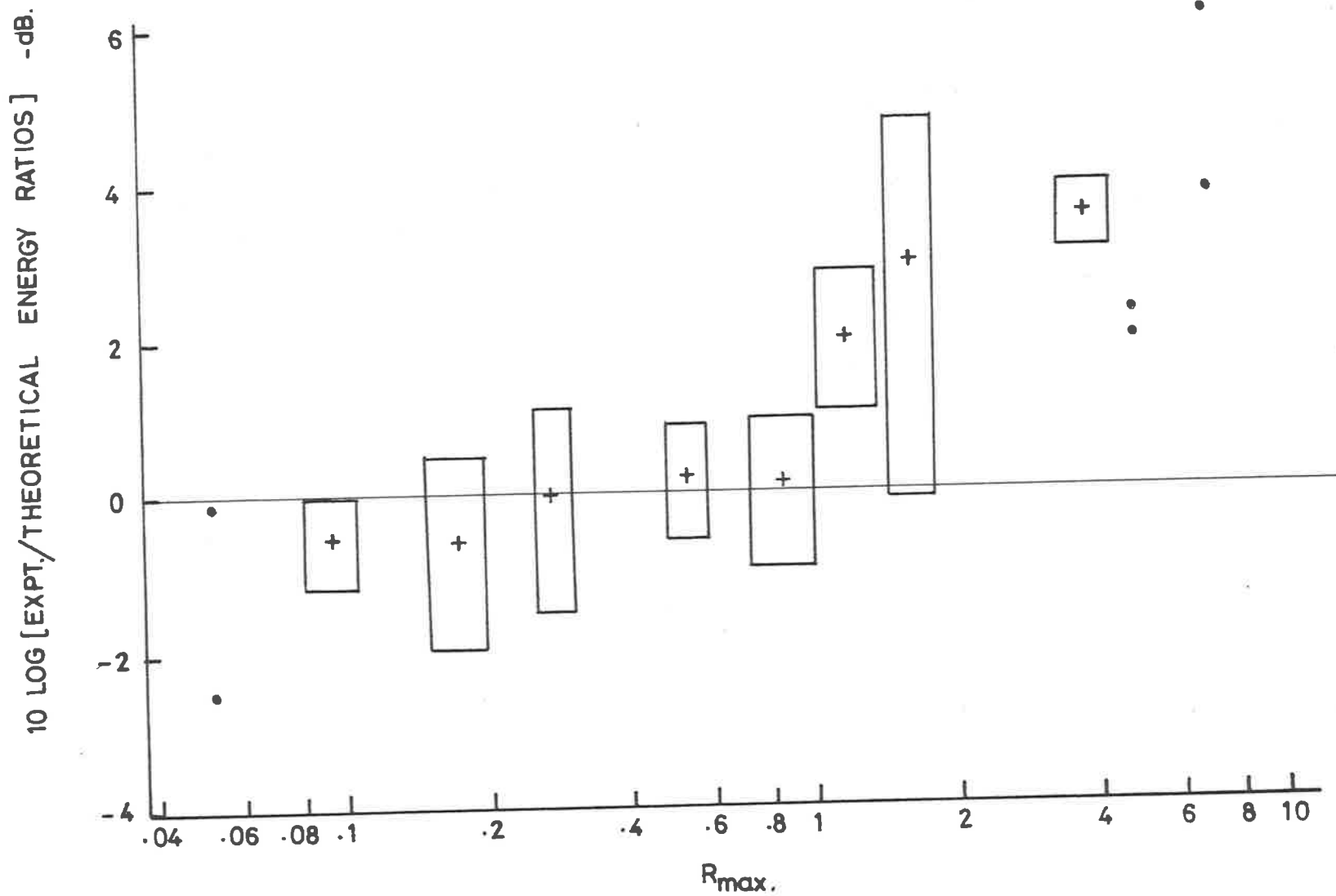


FIG. 5-3. EXPERIMENTAL AND THEORETICAL ENERGY RATIO LEVEL DIFFERENCES FOR TWO EDGE JOINED COUPLED PLATES - AS A FUNCTION OF THE MODAL OVERLAP FACTOR R_{max} .

shown where insufficient results are available to present a mean value and standard deviation. In Fig. 5-2, all data points where $R_{\max} > 1.0$ have been omitted to avoid masking the effect of N_{\min} on the level differences. Similarly, in Fig. 5-3, all data points where $N_{\min} < 6$ have been omitted.

Inspection of Fig. 5-2 shows that as N_{\min} decreases below 6 the spread of results increases and the measured energy ratio tends to be less than the predicted energy ratio.

The dependence of the level difference on the modal overlap factor R is much more distinct. Fig. 5-3 shows that as R_{\max} increases, the spread of results does not increase markedly (except at one particular value of R_{\max}), but there is a distinct change of slope of the general line of mean values at approximately $R_{\max} = 1.0$. The measured energy ratio is greater than the predicted energy ratio for $R_{\max} > 1$, but the results show that this upward trend can be approximately predicted by adding 2dB to the originally predicted energy ratio level for each doubling of R_{\max} above 1.

Both parameters R_{\max} and N_{\min} are proportional to frequency. Generally, if the internal loss factors of each plate are approximately of the same order, then

$$N_{\min} = 0.23n_{\min}f$$

and

$$R_{\max} = \eta_i n_{\max} f$$

The upper and lower limits $R_{\max} = 1$ and $N_{\min} = 6$ can be related to frequency and hence the frequency range in which the coupling loss factor prediction technique can be directly applied to a structure, assuming third octave band excitation, is given by

$$\frac{N_L}{0.23n_{\min}} \leq f \leq \frac{R_U}{\eta_i n_{\max}} \quad (5,4)$$

where N_L is the lower bound and R_U is the upper bound. It can be seen from (5.4) that for the two plates, there is a value of η_i at which the upper and lower frequency bounds coincide and there is no directly usable frequency range. For two coupled element structures,

$$\begin{aligned} \eta_i &= 0.23 \frac{R_U}{N_L} \frac{n_{\min}}{n_{\max}} \\ &= 0.038 n_{\min}/n_{\max} \end{aligned} \quad (5,5)$$

that is, the internal loss factors of two coupled element structures must be much less than 0.038 for there to be any usable frequency range. As previously discussed, the frequency range can be extended upwards to at least five times the upper limit by adding $10 \log \left(\frac{R_{\max}}{R_U} \right)^{2/3}$ to the predicted energy ratio level for $R_{\max} > 1$.

5.2.2. Three and Four Plate Join

The theoretical energy ratios for the two three plate and one four plate single join structures, described in Table 5-3, were evaluated as described in Section 5-1. The energy ratios of each structure were measured, as described in Appendix D. The measured and predicted energy ratios and the level difference between them, in dB, for all three and four plate single join structures are listed in Tables 5-8, 5-9 and 5-10.

The ± 2 dB criterion is again used to determine the upper and lower bounds in Fig. 5-4 and the mean and standard deviation of the level differences are plotted against N_{\min} and R_{\max} in

TABLE 5-8(a)

PREDICTED AND MEASURED ENERGY RATIOSThree plates at a common join - Plate Nos. 7, 8 and 11.Plate 7 directly excited

Frequency Hz	E_8/E_7		Level Diff. dB	E_{11}/E_7		Level Diff. dB
	Meas.	Pred.		Meas.	Pred.	
500	.345	.399	-0.64	.322	.631	-2.92
630	.266	.395	-1.72	.454	.567	0.97
800	.499	.392	1.04	.590	.608	-0.13
1000	.295	.380	-1.10	.382	.552	-1.59
1250	.325	.371	-0.58	.655	.473	1.41
1600	.305	.358	-0.70	.463	.465	-0.01
2000	.458	.320	1.56	.463	.330	1.47
2500	.191	.286	-1.74	.443	.271	2.14
3150	.344	.251	1.37	.568	.158	5.55

TABLE 5-8(b)

PREDICTED AND MEASURED ENERGY RATIOSThree Plates at a common join - Plate Nos. 7, 8 and 11.Plate 8 directly excited

Frequency Hz	E_7/E_8		Level Diff. dB	E_{11}/E_8		Level Diff. dB
	Meas.	Pred.		Meas.	Pred.	
800	0.610	1.430	-3.70	0.832	1.167	-1.47
1000	0.606	1.359	-3.51	.855	1.053	-0.90
1250	1.288	1.324	-0.12	1.248	.902	1.41
1600	1.033	1.243	-0.80	.817	.878	-0.31
2000	0.826	1.079	-1.16	.771	.630	0.87
2500	0.948	0.870	0.38	.716	.495	1.61
3150	1.43	0.737	2.88	1.101	.288	5.82
4000	1.06	0.596	2.50	.907	.226	6.03
5000	0.839	0.330	4.05	.471	.0911	7.13

TABLE 5-8(c)

PREDICTED AND MEASURED ENERGY RATIOSThree Plates at a common join - Plate Nos. 7, 8 and 11.Plate 11 directly excited

Frequency Hz	E_7/E_{11}		Level Diff. dB	E_8/E_{11}		Level Diff. dB
	Meas.	Pred.		Meas.	Pred.	
500	.262	.483	-2.66	.308	.254	0.84
630	.496	.493	0.03	.125	.258	-3.14
800	.400	.460	-0.61	.394	.243	2.10
1000	.326	.421	-1.11	.221	.225	-0.09
1250	.520	.413	1.00	.169	.221	-1.17
1600	.522	.362	1.59	.247	.197	0.98
2000	.500	.275	2.59	.372	.156	3.77
2500	.595	.204	4.64	.396	.122	5.11

TABLE 5-9(a)

PREDICTED AND MEASURED ENERGY RATIOSThree Plates at a common join - Plate Nos. 9, 10 and 12.Plate 9 directly excited

Frequency Hz	E_{10}/E_9		Level Diff. dB	E_{12}/E_9		Level Diff. dB
	Meas.	Pred.		Meas.	Pred.	
400	.247	.482	-2.92	.362	.501	-1.41
500	.447	.505	-0.53	.604	.539	0.49
630	.291	.452	-1.92	.407	.468	-0.61
800	.395	.451	-0.50	.317	.476	-1.77
1000	.463	.463	0.00	.689	.498	1.41
1250	.274	.434	-2.01	.352	.467	-1.24
1600	.207	.364	-2.44	.310	.405	-0.70
2000	.260	.336	-1.11	.349	.348	0.02
2500	.255	.255	0.00	.267	.285	-0.29
3150	.314	.242	1.14	.430	.283	1.82
4000	.563	.176	5.05	.469	.219	3.31
5000	.293	.0917	5.05	.425	.119	5.54

TABLE 5-9(b)

PREDICTED AND MEASURED ENERGY RATIOS

Three Plates at a common join - Plate Nos. 9, 10 and 12
Plate 10 directly excited

Frequency Hz	E_9/E_{10}		Level Diff. dB	E_{12}/E_{10}		Level Diff. dB
	Meas.	Pred.		Meas.	Pred.	
500	.909	1.178	-1.13	.754	.827	-0.40
630	.574	1.036	-3.13	.684	.715	-0.17
800	1.094	1.028	-0.27	.928	.726	1.07
1000	.657	1.055	-2.06	.741	.758	-0.10
1250	.680	.973	-1.55	.649	.710	-0.39
1600	.783	.779	0.02	.691	.607	-0.56
2000	.803	.720	0.48	.796	.523	1.82
2500	.504	.513	-0.07	.513	.426	0.80
3150	.623	.479	1.14	.571	.422	1.31
4000	1.153	.332	5.41	.994	.329	4.80
5000	.635	.162	5.93	.573	.181	4.98

TABLE 5-9(c)

PREDICTED AND MEASURED ENERGY RATIOS

Three Plates at a common join - Plate Nos. 9, 10 and 12.
Plate 12 directly excited

Frequency Hz	E_9/E_{12}		Level Diff. dB	E_{10}/E_{12}		Level Diff. dB
	Meas.	Pred.		Meas.	Pred.	
500	.515	1.210	-3.67	.382	.796	-3.19
630	1.826	1.131	2.08	.643	.754	-0.69
800	.697	1.106	-2.10	.613	.740	-0.82
1000	.718	1.111	-1.90	.678	.743	-0.40
1250	.975	1.044	-0.30	.458	.706	-1.88
1600	1.048	.863	0.84	.712	.605	0.70
2000	.693	.852	-0.90	.544	.599	-0.39
2500	.630	.619	0.08	.480	.460	0.18
3150	.655	.572	0.59	.644	.431	1.74
4000	.685	.411	2.22	.777	.327	3.76
5000	.914	.219	6.21	.741	.189	5.93

TABLE 5-10

PREDICTED AND MEASURED ENERGY RATIOS

Four Plates at a common join - Plate Nos. 9, 10, 12 and 13.

Plate 10 directly excited

Frequency Hz	E_9/E_{10}		Level Diff. dB	E_{12}/E_{10}		Level Diff. dB	E_{13}/E_{10}		Level Diff. dB
	Meas.	Pred.		Meas.	Pred.		Meas.	Pred.	
400	.412	.918	-3.47	.538	.640	-0.75	.471	.604	-1.08
500	.203	.958	-6.75	.224	.694	-4.92	.222	.617	-4.44
630	.344	.820	-3.92	.446	.578	-1.12	.276	.557	-3.06
800	.291	.791	-4.34	.235	.576	-3.90	.318	.532	-2.24
1000	.544	.818	-1.77	.507	.611	-0.81	.442	.552	-0.96
1250	.336	.720	-3.31	.255	.548	-3.32	.337	.492	-1.65
1600	.716	.535	1.26	.455	.444	0.11	.495	.406	0.86
2000	.510	.466	0.39	.417	.351	0.75	.489	.324	1.79
2500	.336	.312	0.31	.307	.277	0.43	.321	.267	0.81
3150	.256	.286	-0.47	.290	.273	0.27	.275	.253	0.35
4000	.375	.185	3.07	.313	.201	1.94	.306	.188	2.11
5000	.566	.0825	8.37	.390	.0989	5.96	.324	.0962	5.27

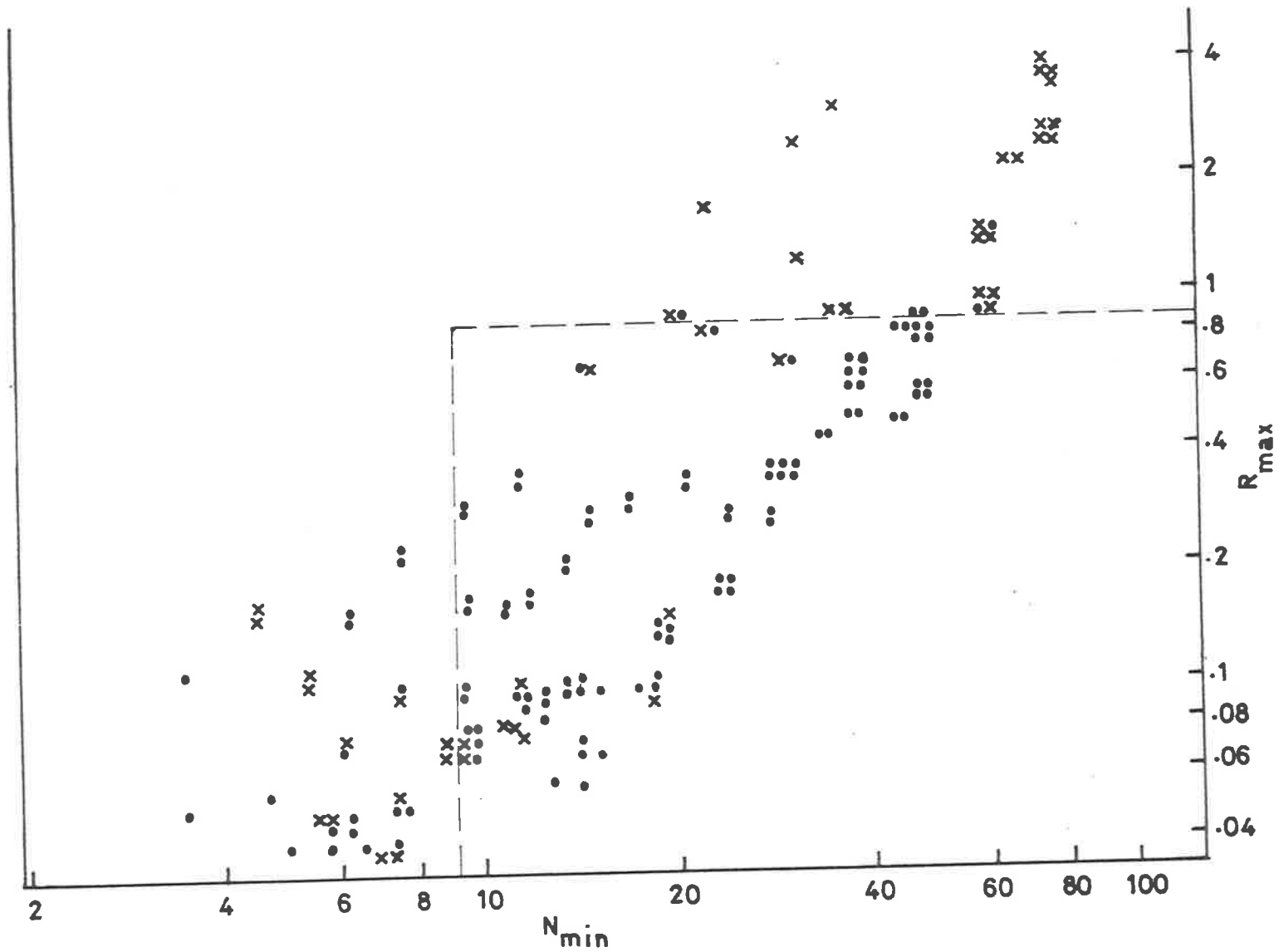


FIG. 5-4. DETERMINATION OF UPPER AND LOWER BOUNDS FOR THREE AND FOUR PLATES AT A COMMON JOIN;
 • , DATA MEETS $\pm 2\text{dB}$ CRITERION; x , DATA DOES NOT MEET $\pm 2\text{dB}$ CRITERION.

10 LOG. [EXPT./THEORETICAL ENERGY RATIOS] -dB.

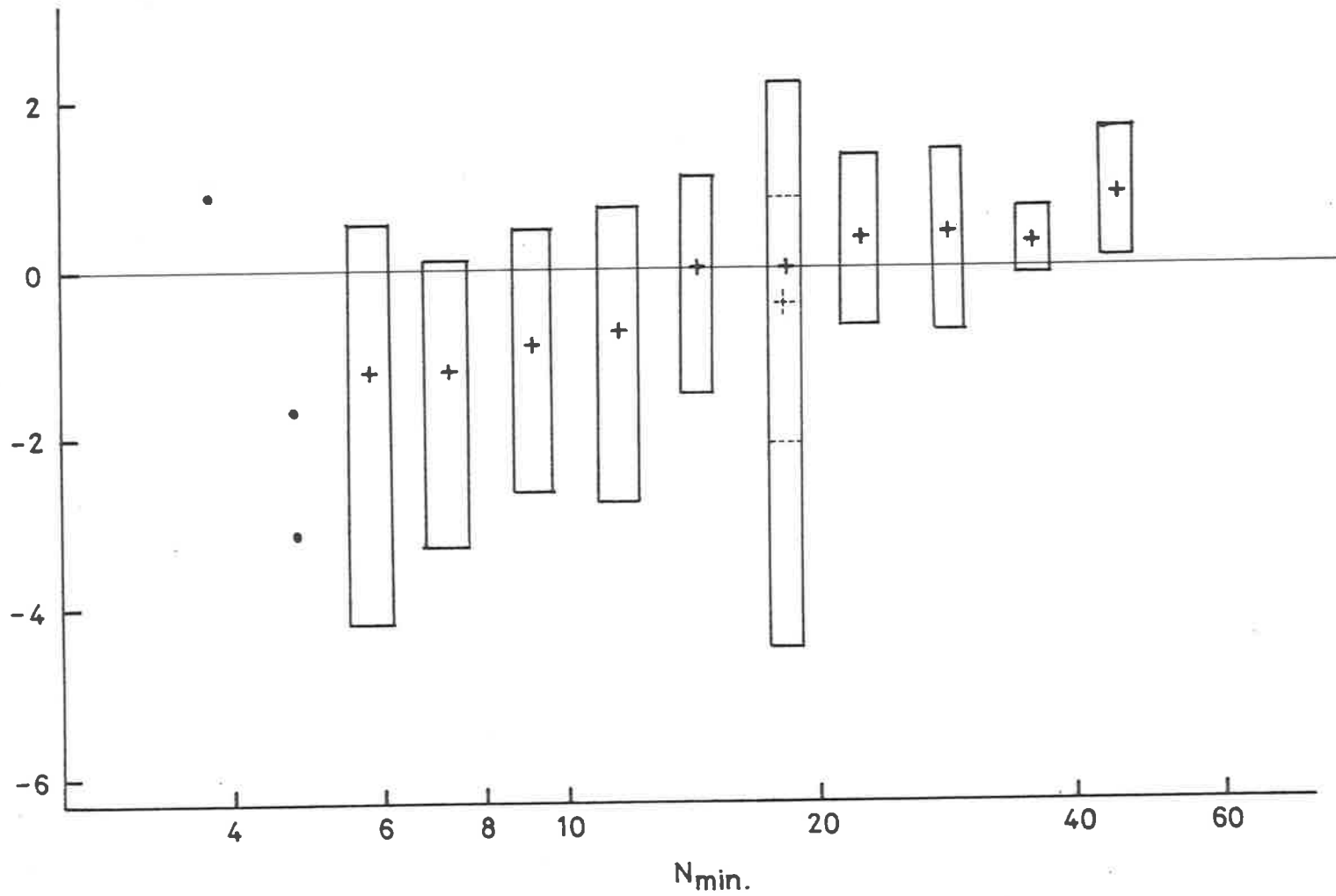


FIG. 5-5. EXPERIMENTAL AND THEORETICAL ENERGY RATIO LEVEL DIFFERENCES FOR THREE AND FOUR PLATES AT A COMMON JOIN - AS A FUNCTION OF THE NUMBER OF MODES IN A FREQUENCY BAND N_{min}

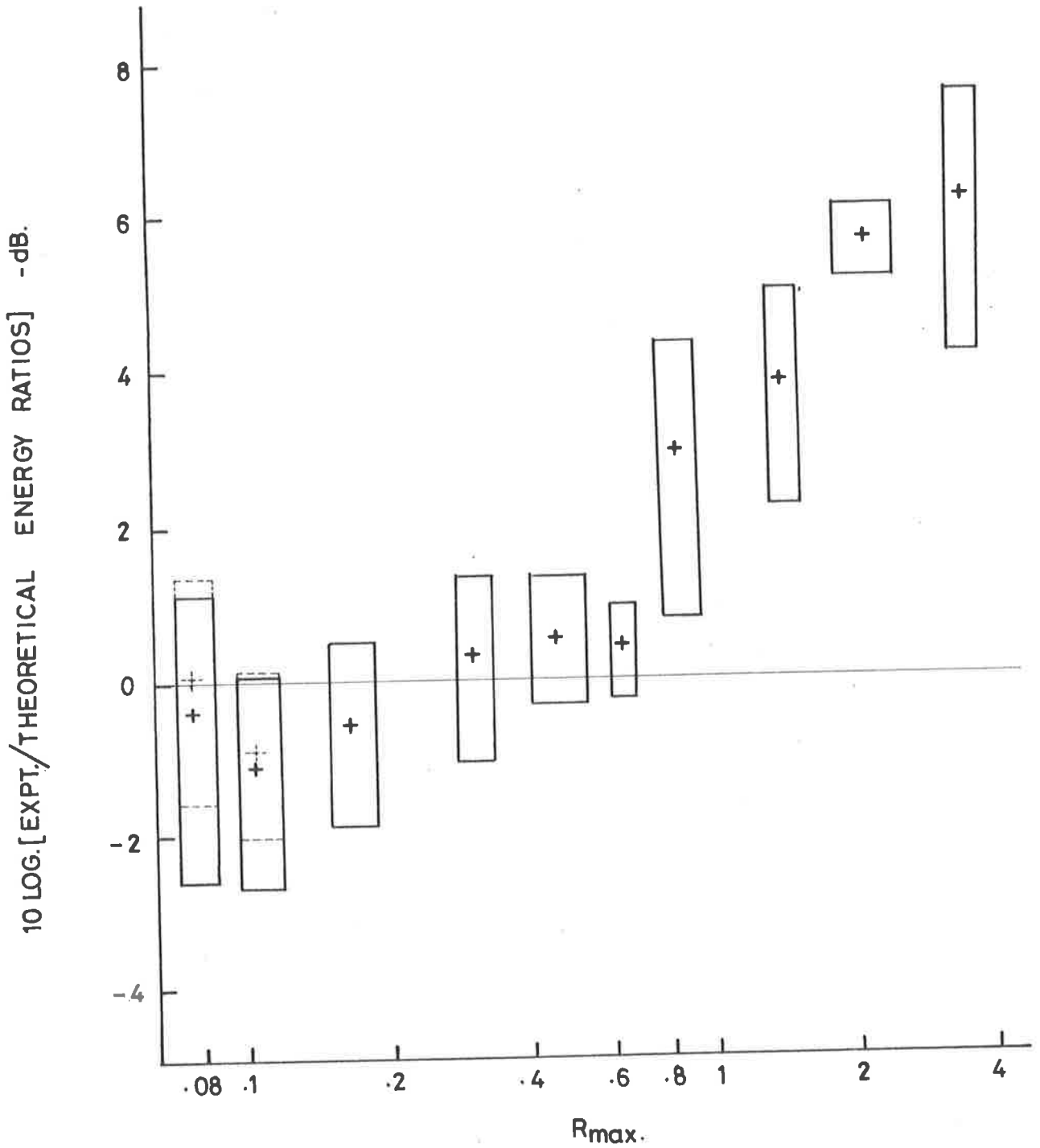


FIG. 5-6. EXPERIMENTAL AND THEORETICAL ENERGY RATIO LEVEL DIFFERENCES FOR THREE AND FOUR PLATES AT A COMMON JOIN - AS A FUNCTION OF THE MODAL OVERLAP FACTOR R_{max}

Fig. 5-5 and 5-6 in a similar manner to the presentation of the two coupled plate results in 5.2.1.

Again N_{\min} is the lesser of N_i and N_j and R_{\max} is the greater of R_i and R_j when considering the level differences of E_i/E_j and E_j/E_i irrespective of the values of N and R of the other plates at the join.

The bounds deduced from the data in Fig. 5-4 are $N_{\min} = 9$ and $R_{\max} = 0.8$. In this case, approximately 90% of the data points within these bounds meet the $\pm 2\text{dB}$ criterion. Half of the remaining 10% of data points within the bounds but not meeting the $\pm 2\text{dB}$ level difference criterion are from results involving a specific plate (plate number 10) excited at a specific $1/3$ octave band, (centre frequency 1250Hz). This indicates that either the experimentally measured internal loss factor of plate 10 in the 1250Hz band is in error, leading to an erroneous predicted energy ratio, or the number and/or spacing of resonant modes in that band is far from the assumed statistical average.

As in 5.2.1, the data points with $R_{\max} > 0.8$ have been omitted in Fig. 5-5, as have those data points with $N_{\min} < 9$ in Fig. 5-6. The standard deviations of the level differences are generally greater in both Fig. 5-5 and Fig. 5-6 than for the respective two coupled plate results. The mean energy levels of each plate were evaluated from mean square acceleration levels determined from measured acceleration levels at 8 locations on each plate. In the 2 plate experiments, 10 measurement locations were used on each plate. In Appendix D, in which the accuracy of measured results are discussed, Fig. D-5 shows that the 95% confidence limits of the experimentally measured plate mean square acceleration levels does not increase by more than 0.2dB for a reduction in the number of measurement locations from 10 to 8, hence it appears to be unlikely that the increase

in the standard deviation of the energy ratio level differences is due to the reduced number of measurement locations. It is probable that the increase spread of results for the 3 and 4 plate single joint structures compared with the two plate structure results is because the evaluation of the power flow in a 3 or 4 plate coupled structure is further removed from the original SEA extension to evaluating power flow between two lightly coupled elements from the basic concept of power flow between two coupled oscillators.

Inspection of Fig. 5-5 indicates that for $N_{\min} < 9$, the mean value decreases slowly with decreasing N_{\min} but the standard deviation increases. The standard deviation generally decreases with increasing N_{\min} with the exception at $N_{\min} = 18$. This large standard deviation is caused by some results involving plate 10 at 1250Hz 1/3 octave band excitation previously mentioned. When these results are omitted, the mean value and standard deviation are as shown by the dashed line.

It can be seen in Fig. 5-6 that the variation of R_{\max} does not appear to affect the standard deviation of the level differences but, as for the two coupled plate results, there is a distinct change of slope of the mean values of the level differences for $R_{\max} > 0.8$. Again, it appears that this upward trend can be approximately predicted by adding 2dB to the predicted energy ratio per doubling of R_{\max} above $R_{\max} = 0.8$. The effect of omitting the poor results involving plate 10 at 1250Hz excitation is not as pronounced as it is in Fig. 5-5, since the particular data points affect the mean value and standard deviation at two values of R_{\max} , 0.08 and 0.12. As in Fig. 5-4, the mean values and standard deviations with these data points omitted are shown dotted in Fig. 5-5.

The bounds determined from the two plate data presented in Fig. 5-1 are slightly different from those determined from Fig. 5-4 for the three and four plate single join structures. It seems likely that the bounds are impossible to define exactly, hence to avoid unnecessary complications when considering multi-join structures, we have assigned a lower and an upper bound for all single join structures. These bounds $N_{\min} = 6$ and $R_{\max} = 1.0$ will be used when discussing the results in Section 5.3.

5.3. MULTI-JOIN STRUCTURES

5.3.1. Two Plate Joins

(a) The measured and predicted energy ratios of a coupled structure comprising plates 1, 2 and 6A, connected as shown in Table 5-3, are presented in Figs. 5-7, 5-8 and 5-9 where the directly excited plates are 2, 6A and 1 respectively. The frequency at which $N_{\min} = 6$ is noted in each figure, i.e. the frequency at which the lower of N_i or N_j is equal to 6 when considering the energy ratio E_i/E_j . Above $R_{\max} = 1$, the adjusted predicted energy ratio is also shown.

As there are three interconnecting plates, there is a second energy flow path through the third plate which affects the energy ratio E_i/E_j . This being so, then it seems probable that the N_k and R_k values of the third plate k , should be considered in determining N_{\min} and R_{\max} for the structure. If the inclusion of the N_k and R_k values of the third plate restrict the frequency range determined by N_{\min} and R_{\max} from elements i and j only, then the frequency at which $N_k = 6$ is noted and the predicted energy is adjusted above $R_k = 1$. As the upper bound frequencies approximately coincide only one adjusted predicted average ratio is shown in each of the graphs.

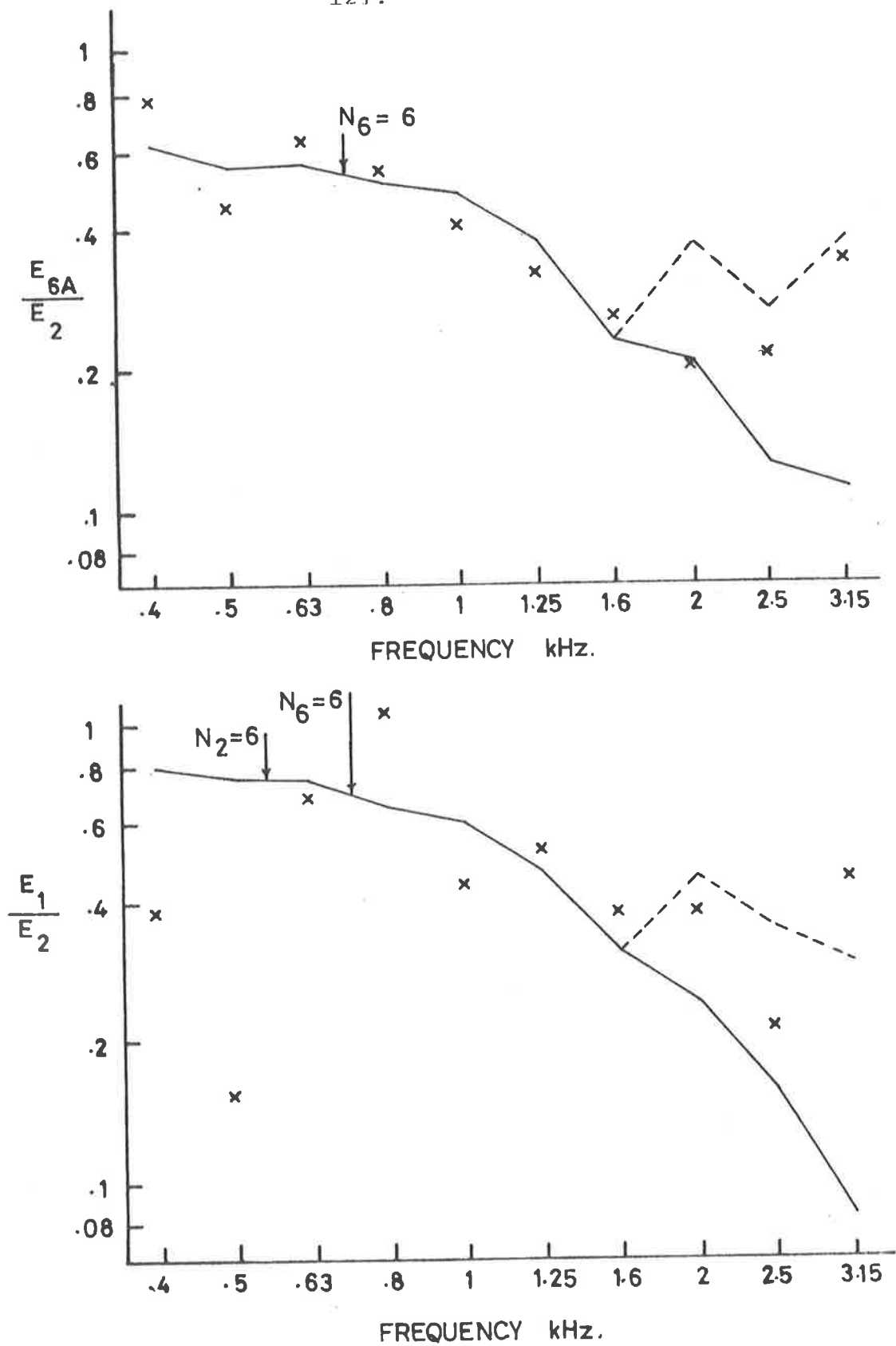


FIG. 5-7. EXPERIMENTAL AND THEORETICAL ENERGY RATIOS FOR THE THREE ELEMENT STRUCTURE, COMPRISING PLATES 1, 2, 6A, - PLATE 2 DIRECTLY EXCITED: —, PREDICTED; ---, ADJUSTED $R_2 > 1$; x, EXPERIMENT.

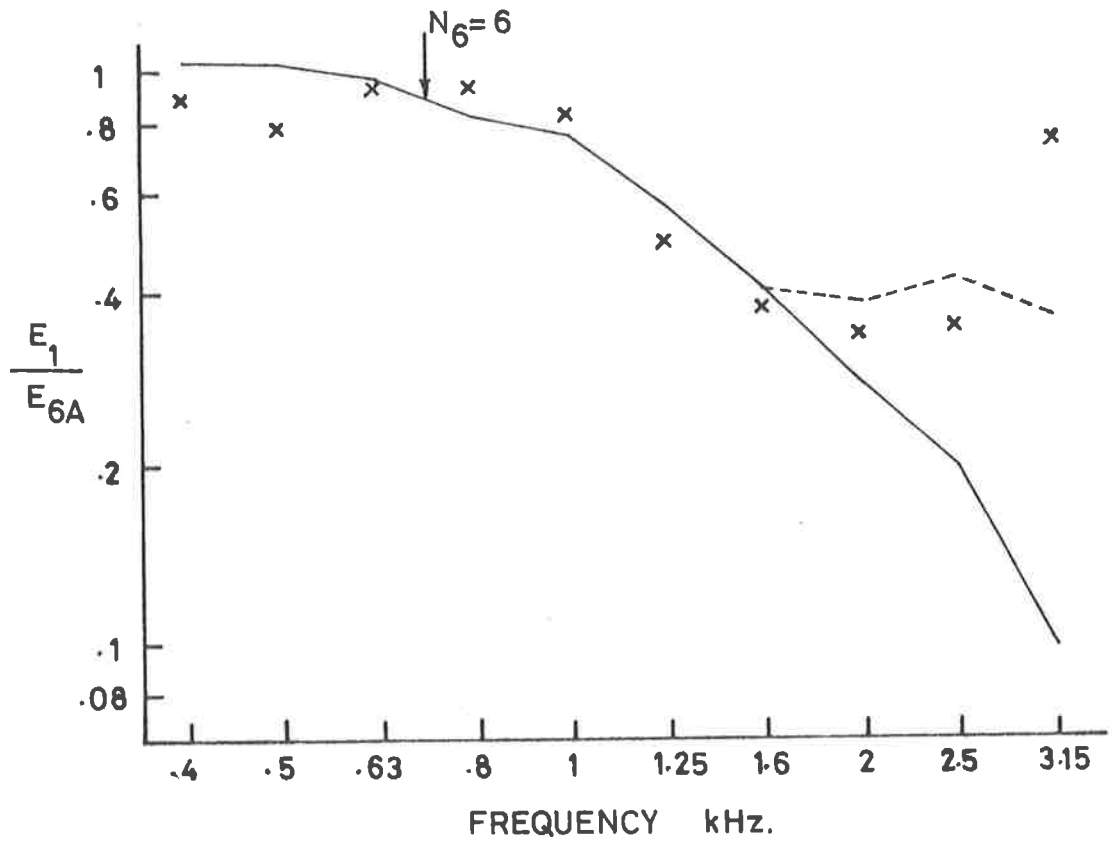
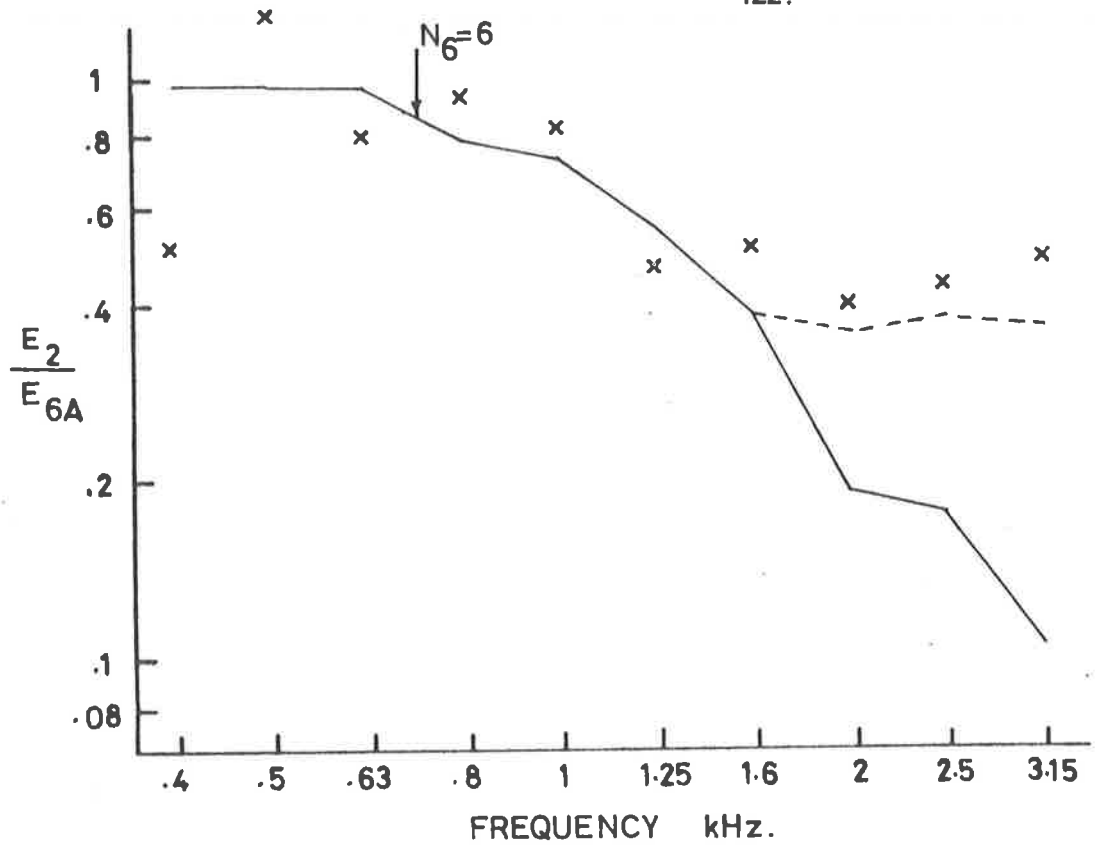


FIG. 5-8. EXPERIMENTAL AND THEORETICAL ENERGY RATIOS FOR THE THREE ELEMENT STRUCTURE, COMPRISING PLATES 1, 2, 6A, - PLATE 6 DIRECTLY EXCITED: —, PREDICTED; ---, ADJUSTED $R_2 > 1$; x, EXPERIMENT.

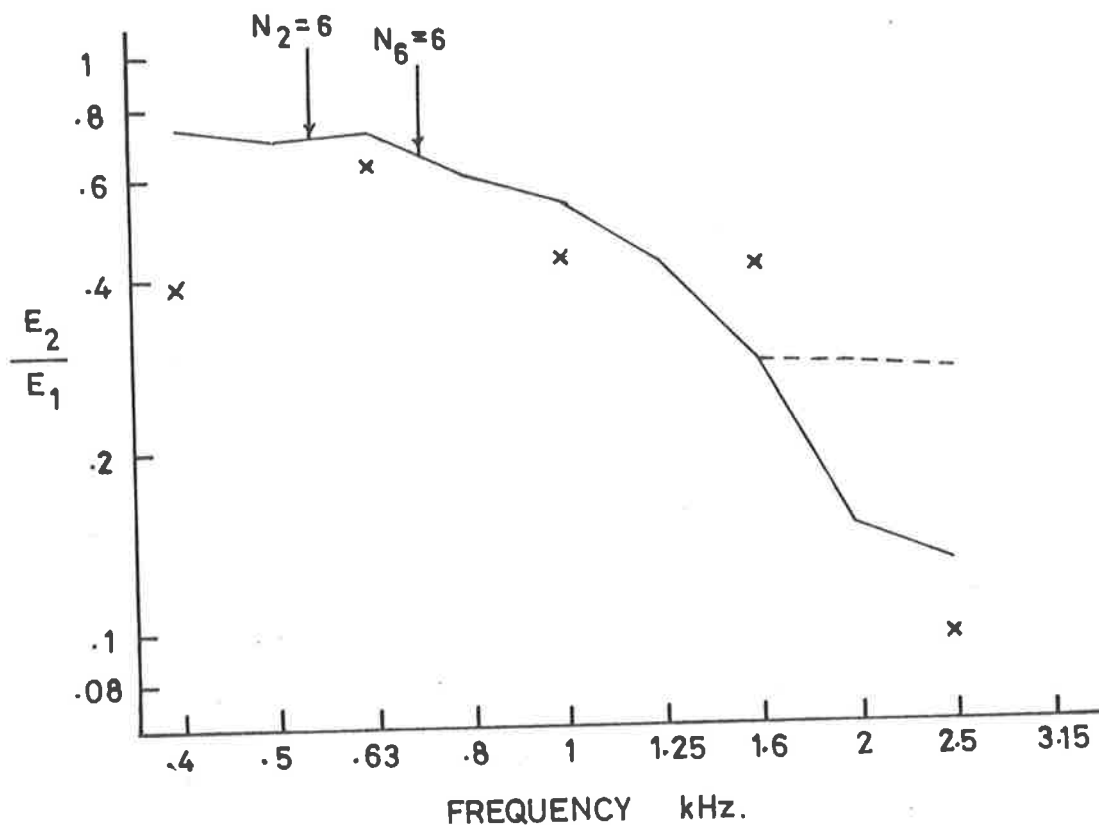
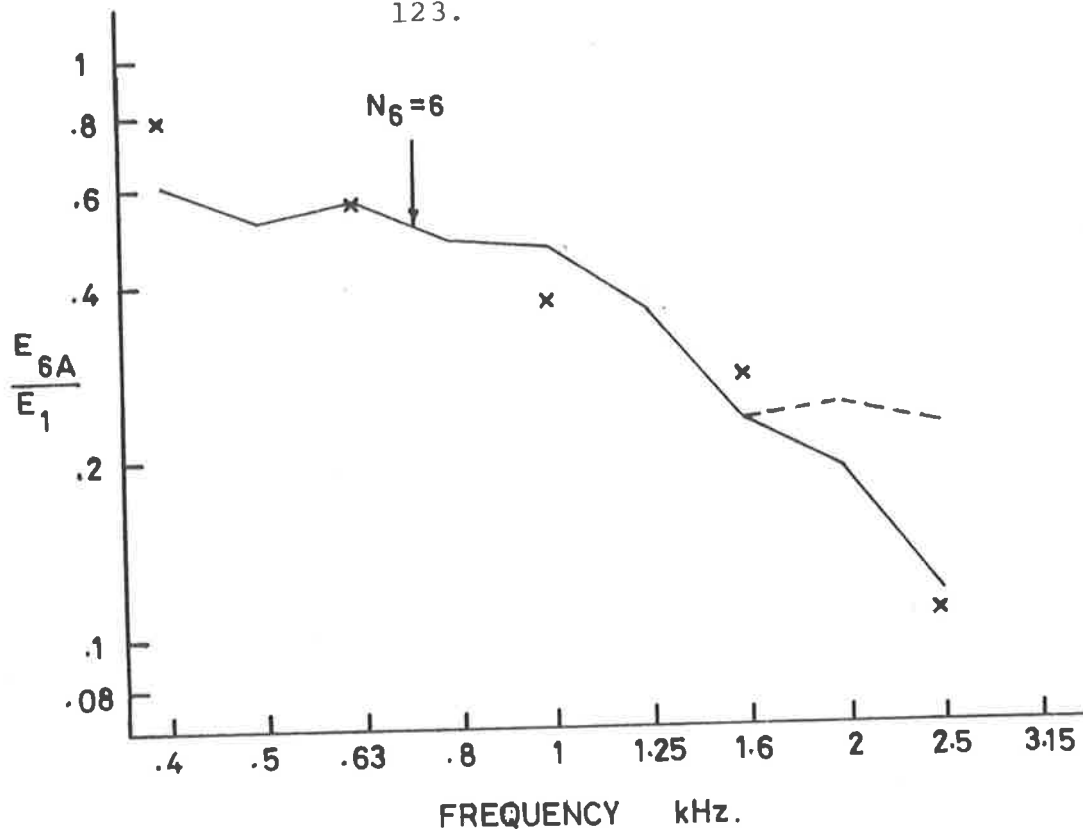


FIG. 5-9. EXPERIMENTAL AND THEORETICAL ENERGY RATIOS FOR THE THREE ELEMENT STRUCTURE, COMPRISING PLATES 1, 2, 6 A, - PLATE 1 DIRECTLY EXCITED: —, PREDICTED; - - - - , ADJUSTED $R_2 > 1$; x, EXPERIMENT.

Inspection of Figs. 5-7, 5-8 and 5-9 show that all the measured and predicted energy ratios are within $\pm 2\text{dB}$ between the two frequency limits determined by $N_2 = 6$ and $R_2 = 1$. In addition, the agreement for $N_2 < 6$ was also within $\pm 2\text{dB}$ in all cases except for two results; the energy ratio E_2/E_{6A} at 400Hz and E_1/E_2 at 500Hz. At frequencies above the upper bound (above 1600Hz) the measured energy ratios are generally in closer agreement with the adjusted predicted level for the tests where plates 6 and 2 were directly excited. However, when plate 1 was directly excited, the measured energy ratio was predicted more closely by the unadjusted theory.

(b) Plate 5A was added to the previous structure to form a four plate coupled structure where only two plates are coupled at any one join. The predicted and measured energy ratios E_1/E_2 , E_{5A}/E_2 and E_{6A}/E_2 , plate 2 being externally excited, are shown in Fig. 5-10. As there are three energy flow paths to each element, the question of which N and R values should determine the frequency bounds again arises. For each energy ratio considered, the N_{\min} lower frequency bound for the two elements involved is shown as well as the most restrictive lower bound of the four elements, determined by $N_{6A} = 6$ at approximately 700Hz. The upper frequency bound for the two elements involved is determined in each case by $R_2 = 1$, and $R_{5A} = 1$ determines the most restrictive upper frequency bound. The adjusted predicted energy ratios are shown for both $R_2 > 1$ and $R_{5A} > 1$ except for the E_{5A}/E_2 ratios where the $R_2 > 1$ adjustments are not required.

Inspection of Fig. 5-10 shows that for the three sets of results presented, the differences between the measured and the predicted energy ratios are within $\pm 2\text{dB}$ between all the bounds shown, although the lower bound for E_1/E_2 and E_{5A}/E_2 ($N_2 = 6$ at

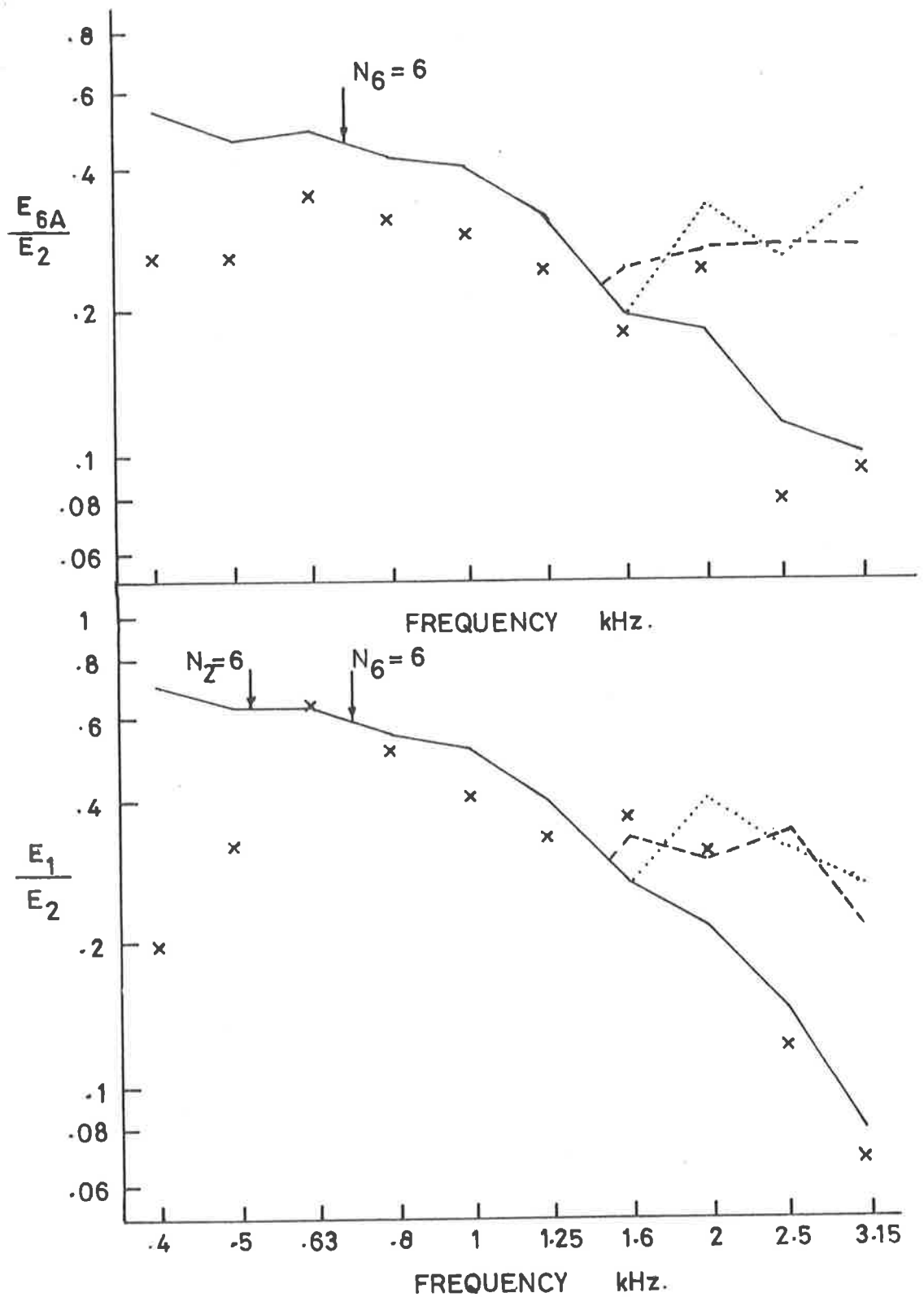


FIG. 5-10. EXPERIMENTAL AND THEORETICAL ENERGY RATIOS FOR A FOUR ELEMENT STRUCTURE 1, 2, 5A, 6A - PLATE 2 DIRECTLY EXCITED:—, PREDICTED; ---, ADJUSTED FOR $R_5 > 1$; ·····, ADJUSTED FOR $R_2 > 1$; x, EXPERIMENT.

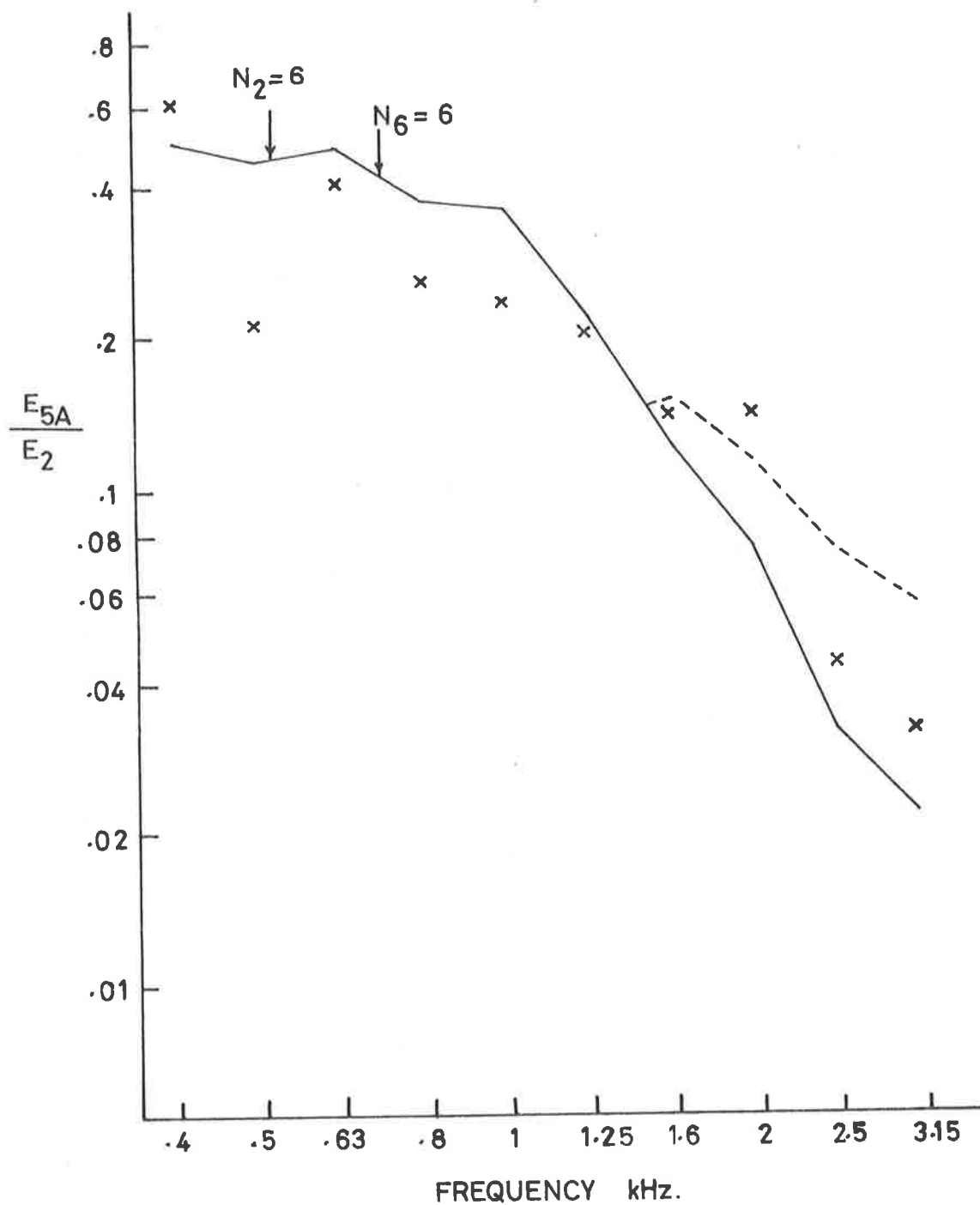


FIG. 5-10. EXPERIMENTAL AND THEORETICAL ENERGY RATIOS FOR A
 (cont'd) FOUR ELEMENT STRUCTURE 1, 2, 5A, 6A - PLATE 2
 DIRECTLY EXCITED: —, PREDICTED; ---, ADJUSTED
 FOR $R_5 > 1$; , ADJUSTED FOR $R_2 > 1$, x, EXPERIMENT.

approx. 550Hz) is close to the 500Hz result which shows a larger level difference of approximately 3dB in each case. The 2 sets of upper bounds are too close to each other to determine whether one should be used rather than another. For all three energy ratios, the measured results were closer to the prediction for $R_{\max} > 1$ than for the 'corrected' predicted energy ratio except in the 2000Hz band.

It is interesting to compare the predicted and measured energy ratio level differences for E_1/E_2 and E_{6A}/E_2 for both the three plate structure (Fig. 5-7) and the four plate structure (Fig. 5-10) at $R_{\max} > 1$. The adjusted prediction is more accurate for the three plate structure but the unadjusted energy ratios are closer to the measured energy ratios for the four plate coupled structure. None of the physical parameters of the plates have been altered; area, thickness, internal loss factors and coupling loss factors for elements 1, 2 and 6A are the same in each case. The only alteration is the changed boundary conditions of the plates 1 and 6A at the edges connected to plate 5A. This demonstrates that the adjustment to the predicted energy ratios for frequencies above $R_{\max} = 1$ must be regarded as a very approximate guide only.

The results shown in Figs. 5-7 to 5-10 show that the measured levels are within ± 2 dB of the predicted levels over the bounded frequency range and often within ± 2 dB of the adjusted predicted level where R_{\max} is greater than 1.0. Except for one result, (Fig. 5-8, E_1/E_{6A} at 3150Hz) the level difference was greater than ± 2 dB only where the measured level was less than (a) the adjusted predicted level for $R_{\max} > 1$, and (b) the predicted level for $N_{\min} < 6$.

5.3.2. Two, Three and Four Plate Joins

The structure comprising eight plates, described in Table 5-3 was excited by directly exciting plate 14. The measured energy ratios E_3/E_{14} , E_9/E_{14} and E_{12}/E_{14} are compared with the theoretical energy ratios, predicted as described in Section 5.1. The theoretically determined energy ratios and the measured energy ratios are presented in Fig. 5-11.

It is difficult to determine which elements should be used to define the upper and lower bounds which should be applied to the whole structure. It seems likely that there are some elements of the structure which would not cause the energy levels of other elements to alter greatly when their parameters are altered or the element is removed. Plate 3 is an example of this when considering the energy ratio E_9/E_{14} . It is probable that those elements which when altered, would cause a significant change in the energy levels of other elements, would be those in the most direct energy transmission paths. On this basis, the bounds shown in Fig. 5-11 are determined from the elements which appear to be in an important location in the structure. Also the most restrictive bounds are included, these being $N_3 = 6$ and $R_{4A} = 1$.

It would appear to be needlessly restrictive to use N_3 and R_{4A} to determine the bounds when considering E_9/E_{14} and E_{12}/E_{14} . However the difference between the adjusted predicted energy ratios for $R_{4A} > 1$ and $R_9 > 1$ are too close to each other to determine whether one element more than the other is controlling the response. Similarly, no conclusion can be made regarding which lower bound should be used. In nearly all lower frequency bands, the measured energy ratios are in good agreement with the predicted energy ratios well below the expected lower

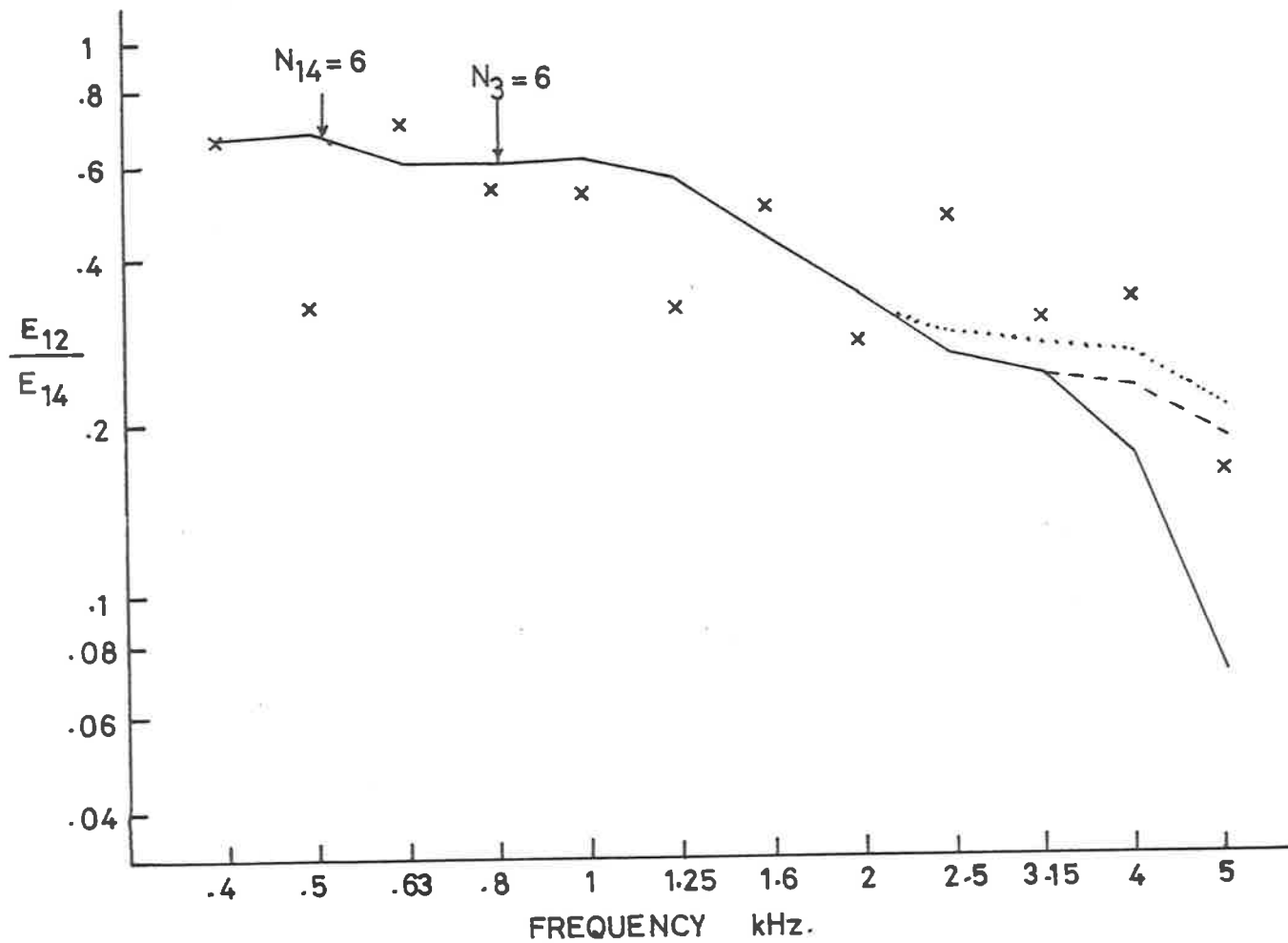


FIG. 5-11(a). EXPERIMENTAL AND THEORETICAL ENERGY RATIO FOR THE 8 PLATE STRUCTURE - PLATE 14 DIRECTLY EXCITED:
 ———, PREDICTED; - - - - , ADJUSTED FOR $R_g > 1$,
 , ADJUSTED FOR $R_{4A} > 1$; x , EXPERIMENT.

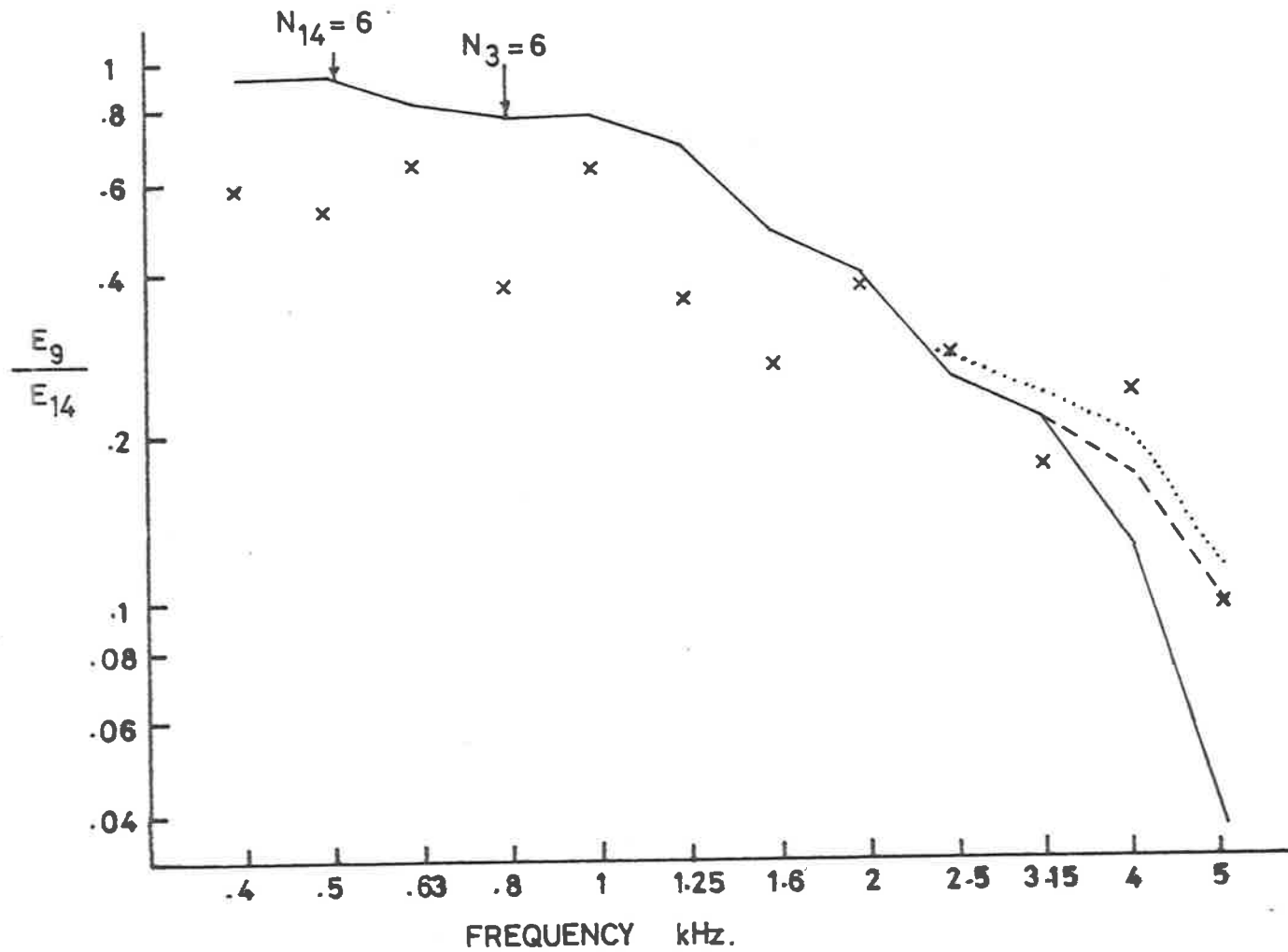


FIG. 5-11(b). EXPERIMENTAL AND THEORETICAL ENERGY RATIO FOR THE 8 PLATE STRUCTURE - PLATE 14 DIRECTLY EXCITED.
 —, PREDICTED; ---, ADJUSTED FOR $R_9 > 1$,
 , ADJUSTED FOR $R_{4A} > 1$; x , EXPERIMENT.

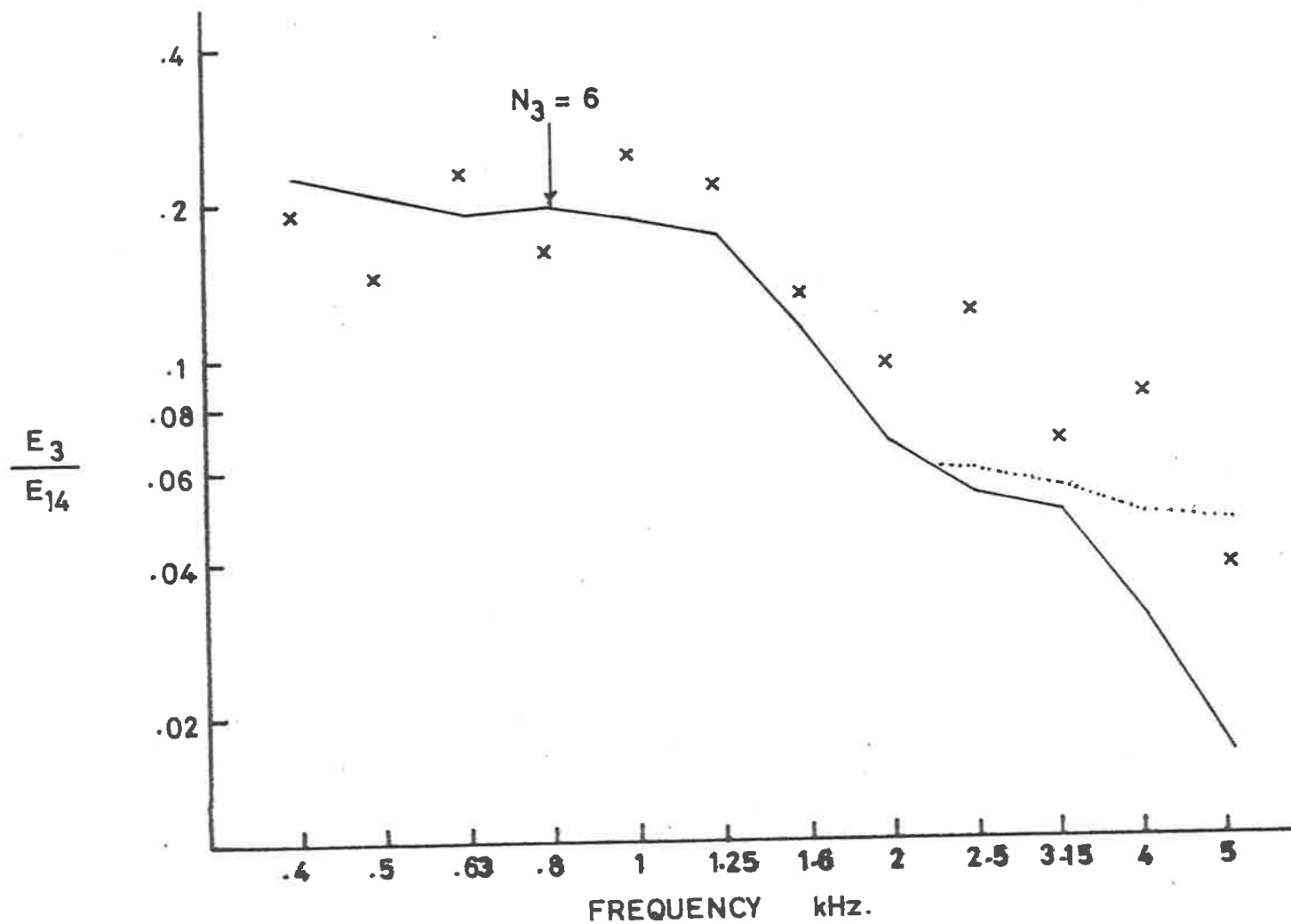


FIG. 5-11(c). EXPERIMENTAL AND THEORETICAL ENERGY RATIO FOR THE 8
 PLATE STRUCTURE - PLATE 14 DIRECTLY EXCITED.
 —, PREDICTED; - - - - , ADJUSTED FOR $R_9 > 1$,
 ······, ADJUSTED FOR $R_{4A} > 1$; x, EXPERIMENT.

frequency bounds determined by $N_{7A} = 6$ or $N_{14} = 6$. Again, where the measured and predicted energy ratios differed by more than 2dB, the measured ratios were less than the predicted ratios.

The lower than expected measured energy ratios E_9/E_{14} and E_{12}/E_{14} in the 1250Hz third octave band, well within all the

frequency bounds, demonstrates that the coupling loss factor prediction technique used in this work, although generally predicting the energy distribution satisfactorily

within the upper and lower frequency limitations, cannot be relied upon to give an accurate prediction in all cases. The poor agreement between predicted and measured energy ratio levels, discussed in 5.2.2 was also associated with plates 9 and 10 excited by a 1250Hz third octave band random signal. It should be noted, however, that even for these relatively poor results at 1250Hz, the predicted and measured energy ratio level differences are within 3dB. In many engineering applications, a prediction of energy distribution in a structure to this order of accuracy would be acceptable.

SECTION 6. CONCLUSIONS

A set of power balance equations written in a matrix form, Equation (3,9), enables the vibrational energy distribution in a connected structure to be evaluated, provided the coupling loss factors and internal loss factors are known. In order to apply this SEA technique to multi-plate structures, a simple means for calculating average coupling loss factors, for up to four plates at a single join, has been presented.

The coupling loss factor is related to an average transmission coefficient which can be calculated from an empirical equation. This equation very closely approximates the average transmission coefficients calculated using bending wave transmission theory and extensive computer integration procedures.

For an error in the predicted coupling loss factor of less than 2dB, the effect of longitudinal and transverse wave-fields, generated at the join need not be considered when $Q_{ab} < 0.018$, i.e. for steel $P_{ab} < 50\text{ms}^{-1}$. The wave transformation should be considered for $Q_{ab} > 0.036$. In the region between these limits, the bending wave solution can generally be used unless the structure contains two consecutive joins where the plate thickness ratios are greater than two to one. In such a structure, longitudinal and transverse wave generation should be considered when evaluating the coupling loss factors.

When considering thick structural elements or high frequencies, i.e. $Q_{ab} > 0.036$, the transformed longitudinal and transverse waves transport energy, some of which is transformed back to bending wave energy in subsequent plates. This additional bending wave energy can be allowed for in the matrix equation by using a 'corrected' bending wave to bending wave transmission coefficient to evaluate the required coupling loss

factor. Values for bending to bending, bending to longitudinal and bending to transverse wave average transmission coefficients for each of the joints are required to determine the 'corrected' bending to bending transmission coefficient. There does not appear to be any simple relationships enabling these coefficients to be determined, either by relating them to normal incident coefficients or to bending solution coefficients, hence empirically obtained charts relating the general solution transmission coefficients to the more easily evaluated bending solution coefficients, or time consuming computer evaluations, are still required.

The vibrational energy distribution in single joint structures of up to four plates with arbitrary coupling strength, can be predicted to an accuracy of $\pm 2\text{dB}$ with at least 90% confidence within the upper frequency bound ($R_{\text{max}} = 1$) and lower frequency bound ($N_{\text{min}} = 6$). The frequency range can be extended to R_{max} approximately equal to 5 with an adjustment to the predicted energy level for $1 \leq R_{\text{max}} \leq 5$. In the extended range, the energy levels can be expected to be within $\pm 2\text{dB}$ in the majority of measurements, with differences larger than 2dB generally such that the measured level is less than the predicted level. Agreement between predicted and measured energy levels in general multijoin structures can be expected, generally within $\pm 2\text{dB}$ and within 3dB over the extended frequency range.

It is more difficult to state which elements should be used to determine the upper and lower frequency bounds when considering a multijoin structure. It is thought probable that the N and R values of those elements in the major vibrational energy transmission paths would be those which determine the upper and lower frequency bounds for the structure, but further

experimental work is required to determine whether this is so.

Further experimental work is also required to investigate the validity of SEA for thick structures, that is with $Q_{ab} > 0.036$.^{*} For the structures where the bending, longitudinal and transverse waves are required to accurately predict structural energy distribution, it may be useful to produce charts or tables of the three average transmission coefficients τ_{BB} , τ_{BL} and τ_{BT} for various typical plate joins at specific frequencies. This would save a designer much computing time but is not warranted until the relevant experimental work has been carried out.

In conclusion it should be noted that SEA has been shown to be applicable to real structures with arbitrary coupling strengths, where the internal loss factor of each element in the structure was not only accurately determined, but was such that it would not alter significantly from the uncoupled state to the coupled state. However, for lightly damped metals, where radiation controls the measured internal loss factor, this is not so. In bolted, rivetted or spot welded structures additional losses, which need to be considered as part of the element internal loss factor, occur at the join, mainly due to air pumping. The estimation of the internal loss factors of elements in existing structures is difficult because of these variables. It would be useful for further research to be undertaken to investigate the dependence of the apparent internal loss factor of an element on the type of join and structure configuration. This could then be used to estimate the internal loss factors of elements in existing structures.

Provided the internal loss factors of the elements in a coupled plate structure are known, the vibrational energy

^{*}see postscript Page 14a.

distribution can be predicted within definable frequency limits, which depend upon the modal density and modal overlap characteristics of the elements involved, as well as the accuracy and the level of confidence required by the designer. The upper limit applies only to the coupling loss factor prediction method and is not necessarily a limitation of SEA.

APPENDIX A. ENERGY DECAY IN A TWO DIMENSIONAL FIELD

The procedure is analagous to that used to determine the energy decay in large rooms (Beranek, 1971(1)). The energy density of the field, D_p is due to all bending waves travelling in all directions with equal probability. The power lost at an edge ΔL where another plate is coupled is $D_p C_g \Delta L \tau / \pi$. This is completely analagous to the 3-D expression for power lost at a surface of a room. This energy loss is for one reflection. As the wave travels through the medium there are internal (and radiation) losses which can be represented by

$$D_p(x) = D_o e^{-mx} \quad (A,1)$$

where x is the distance travelled by the wave and m is a propagation loss factor. The amount of power reflected back into the plate at edge ΔL is $D_p C_g \Delta L r / \pi$ where

$$r = 1 - \tau \quad (A,2)$$

The same method as is used by Embleton (Beranek, 1971(1)) to achieve the reverberation time formulae for rooms, is applied. The time required for the total energy to undergo one reflection only is Δt and the energy density is

$$D_p(\Delta t) = D_o (r_1^{L_1/L_T} r_2^{L_2/L_T} \dots) e^{-md} \quad (A,3)$$

where d is the distance travelled by the waves in Δt , i.e.

$$\Delta t = d / C_g$$

where

$$d = \pi A_p / L_T$$

is the mean free path and C_g is the group velocity of the bending waves. L_T is the perimeter of the plate of area A_p . After time t , the energy density is

$$\begin{aligned} D_p(t) &= D_o (r_1^{L_1/L_T} r_2^{L_1/L_T} \dots) L_T C_g t / \pi A_p e^{-m C_g t} \\ &= D_o \exp \left[- \frac{C_g t}{\pi A_p} (-\sum L_i \ln r_i) - m C_g t \right] \end{aligned} \quad (A,4)$$

$$\text{Since } 10 \log e^x = 4.34x$$

$$10 \log (D_p(t)/D_o) = - \left[\frac{4.34 C_g}{\pi A_p} (-\sum L_i \ln r_i) t + m C_g t \right] \text{ dB} \quad (A,5)$$

The reverberation time T for a 60dB decay is then

$$T = \frac{60 \pi A_p}{4.34 C_g \left[-\sum L_i (1 - \tau_i) + \pi m A_p \right]} \quad (A,6)$$

Assuming there are no losses at the edges, i.e.

$$\tau_i = 0, \text{ then}$$

$$T = \frac{60}{4.34 C_g m} = \frac{4.4 \pi}{\omega \eta_1} \text{ sec.}$$

hence

$$m = \frac{\omega \eta_1}{C_g} \quad (\text{A}, 7)$$

For the case where there are no internal losses, $m = \eta_1 = 0$, and changing A_p to A_1

$$T = \frac{60 \pi A_1}{-4.34 C_g \sum L_i \ln(1-\tau_i)} = \frac{4.4 \pi}{\eta_{12}}$$

Since $C_g = 2C_b = 2\omega/k_1$, the coupling loss factor η_{12} can be written

$$\begin{aligned} \eta_{12} &= \frac{0.0505 \times 4\pi (-\sum L_i \ln(1-\tau_i))}{k_1 A_1} \\ &= \frac{2 (-\sum L_i \ln(1-\tau_i))}{\pi k_1 A_1} \end{aligned} \quad (\text{A}, 8)$$

For a plate with only one join of length L

$$\eta_{12} = \frac{2 L}{\pi A_1 k_1} (-\ln(1-\tau_{12})) \quad (\text{A}, 9)$$

which is equation (4,4) of the text. If τ_{12} is substituted for $-\ln(1-\tau_{12})$ in a similar way as α_{SAB} is substituted for $-\ln(1-\alpha)$ in room acoustics, (A,8) becomes

$$\eta_{12} = \frac{2}{\pi} \frac{\sum L_i (\tau_{12})}{k_1 A_1} \quad (A,10)$$

This is applicable where the join between two plates has 2 or more values of τ_{12} associated with it. This occurs when more than 2 plates are connected at a common join but the lengths of join for each are not equal. For example, (A,10) is required to evaluate the coupling loss factors at the junction of plates 4A, 7A, and 12 in the 8 plate test structure, described in Table 5-3. The length of join between plates 7A and 12 is $L_{7A 12} = 0.434\text{m}$. However, the joins connecting plate 4A to these two plates are less, $L_{4A 7A} = 0.360$ and $L_{4A 12} = 0.415$. Considering $\eta_{7A 12}$, $\tau_{7A 12}$ has one value along the length of the 3 plate join and a different value for the remaining length of $L_{7A 12}$. A similar approach is required to evaluate $\eta_{4A 12}$.

APPENDIX B. SOLUTION OF SIMULTANEOUS EQUATIONS TO OBTAIN
TRANSMITTED AND REFLECTED WAVE AMPLITUDES.

B1. BENDING WAVE FIELD ONLY

From the displacement equations (4,13) and (4,14) and the boundary condition that

$$w_i = 0 \text{ at } x_i = 0$$

then

$$0 = 1 + a_1 + a_1'$$

$$0 = a_n + a_n'$$

therefore

$$a_1' = -(1+a_1) \tag{B,1}$$

$$a_n' = -a_n \text{ for } n = 2, 3, 4 \tag{B,2}$$

Substituting (B,1) and (B,2) into (4,13) and (4,14) and differentiating with respect to x_i , the derivatives are

$$\left. \frac{\partial w_1}{\partial x_1} \right|_{x_1=0} = ik_1 \cos \alpha_1 + k_1 \sqrt{1 + \sin^2 \alpha_1} + a_1 (-ik_1 \cos \alpha_1 + k_1 \sqrt{1 + \sin^2 \alpha_1}) \tag{B,3}$$

$$\left. \frac{\partial w_n}{\partial x_n} \right|_{x_n=0} = a_n (-ik_n \cos \alpha_n + k_n \sqrt{1 + \sin^2 \alpha_n}) \tag{B,4}$$

$$\begin{aligned} \left. \frac{\partial^2 w_1}{\partial x_1^2} \right|_{x_1=0} &= a_1 \left(-k_1^2 \cos^2 \alpha_1 - k_1^2 (1 + \sin^2 \alpha_1) \right) - k_1^2 \cos^2 \alpha_1 - k_1^2 (1 + \sin^2 \alpha_1) \\ &= -2k_1^2 a_1 - 2k_1^2 \end{aligned} \tag{B,5}$$

$$\left. \frac{\partial^2 w_n}{\partial x_n^2} \right|_{x_n=0} = -2k_n^2 a_n \tag{B,6}$$

The second boundary condition that

$$\frac{\partial w_1}{\partial x_1} = \frac{\partial w_n}{\partial x_n} \text{ gives the three equations}$$

$$\begin{aligned} & k_1(i\cos\alpha_1 + \sqrt{1+\sin^2\alpha_1}) + a_1 k_1(\sqrt{1+\sin^2\alpha_1} - i\cos\alpha_1) \\ & = a_n k_n(\sqrt{1+\sin^2\alpha_n} - i\cos\alpha_n) \end{aligned} \quad (B,7)$$

Summing the bending moments about the join leads to

$$(1+a_1)D_1 k_1^2 + a_2 D_2 k_2^2 + a_3 D_3 k_3^2 + a_4 D_4 k_4^2 = 0 \quad (B,8)$$

To solve for a_2 , (B,7) is rearranged and the term B_1 substituted where

$$B_j = \sqrt{1+\sin^2\alpha_j} - i\cos\alpha_j \quad \text{for } j = 1, 2, 3, 4$$

$$B_1^* = \sqrt{1+\sin^2\alpha_1} + i\cos\alpha_1$$

$$a_3 = a_2 k_2 B_2 / k_3 B_3 \quad (B,9)$$

$$a_4 = a_2 k_2 B_2 / k_4 B_4 \quad (B,10)$$

$$a_1 = (a_2 k_2 B_2 - k_1 B_1^*) / k_1 B_1 \quad (B,11)$$

and

$$1+a_1 = (a_2 k_2 B_2 - 2ik_1 \cos\alpha_1) / k_1 B_1 \quad (B,12)$$

With these relationships appropriately substituted into (B,8) and rearranged,

$$a_2 = \frac{2iD_1 k_1^3 \cos \alpha_1 k_3 B_3 k_4 B_4}{k_1 k_2 k_3 k_4 \left[D_1 k_1 B_2 B_3 B_4 + D_2 k_2 B_1 B_3 B_4 + D_3 k_3 B_1 B_2 B_4 + D_4 k_4 B_1 B_2 B_3 \right]}$$

which reduces to

$$a_2 = \frac{2ik_1 \cos \alpha_1 B_3 B_4}{k_2 \left[B_2 B_3 B_4 + \frac{D_2 k_2 B_1 B_3 B_4}{D_1 k_1} + \frac{D_3 k_3 B_1 B_2 B_4}{D_1 k_1} + \frac{D_4 k_4 B_1 B_2 B_3}{D_1 k_1} \right]} \quad (\text{B,13})$$

Using the parameters

$$\chi_{ij} = k_j / k_i$$

$$\psi_{ij} = D_j k_j^2 / D_i k_i^2$$

(B,13) becomes

$$a_2 = \frac{2i \cos \alpha_1 B_3 B_4}{\chi_{12} \left[\sum_{j=1}^4 \frac{\psi_{1j} B_1 B_2 B_3 B_4}{\chi_{1j} B_j} \right]} \quad (\text{B,14})$$

a_3 can be found by following the same procedure as before and this leads to

$$a_3 = \frac{2i \cos \alpha_1 B_2 B_4}{\chi_{13} \left[\sum_{j=1}^4 \frac{\psi_{1j} B_1 B_2 B_3 B_4}{\chi_{1j} B_j} \right]} \quad (\text{B,15})$$

and similarly for a_4 .

The general form for $n = 2, 3$ or 4 can be written

$$a_n = \frac{2i \frac{\cos \alpha_1}{X_{1n}} \frac{B_2 B_3 B_4}{B_n}}{\left[\begin{array}{c} 4 \\ \Sigma \\ j=1 \end{array} \frac{\psi_{1j}}{X_{1j}} \frac{B_1 B_2 B_3 B_4}{B_j} \right]} \quad (B,16)$$

which is equivalent to equation (4,16).

Equation (B,14) is substituted into (B,11) and using (DEN) as a shorthand notation for the bracketed expression in the denominator of the last three equations

$$a_1 = \frac{2i \cos \alpha_1 B_2 B_3 B_4 - B_1^* (\text{DEN})}{B_1 (\text{DEN})} \quad (B,17)$$

This can be rearranged to give

$$\begin{aligned} a_1 &= \frac{-B_1 B_1^* \left(\frac{\psi_{12}}{X_{12}} B_3 B_4 + \frac{\psi_{13}}{X_{13}} B_2 B_4 + \frac{\psi_{14}}{X_{14}} B_2 B_3 \right) + B_2 B_3 B_4 (2i \cos \alpha_1 - B_1^*)}{B_1 (\text{DEN})} \\ &= \frac{-2 \left(\sum_{n=2}^4 \frac{\psi_{1n}}{X_{1n}} \frac{B_2 B_3 B_4}{B_n} \right) - B_1 B_2 B_3 B_4}{B_1 (\text{DEN})} \times \frac{B_1^*}{B_1^*} \\ &= \frac{\left(\sum_{n=2}^4 \frac{\psi_{1n}}{X_{1n}} \frac{B_1^* B_2 B_3 B_4}{B_n} \right) + B_2 B_3 B_4}{(\text{DEN})} \quad (B,18) \end{aligned}$$

which is equivalent to equation (4,15).

B2. BENDING, LONGITUDINAL AND TRANSVERSE WAVE FIELDS.

As $v_j = 0$ at $x_j = 0$ for $j = 1, 2, 3, 4$, Equation (4,48, g, h, i, j), amplitudes c_j and b_j can be related by

$$c_j \Big|_{x_j=0} = b_j \sin \beta_j / \cos \gamma_j \quad (\text{B,19})$$

With (B,19) substituted where applicable, and the terms common to all the displacement equations omitted, as discussed in Section 4.4, the displacement equations and their derivatives at $x_j = 0$ are:

$$u_j \Big|_{x_j=0} = (\cos \beta_j \cos \gamma_j + \sin \beta_j \sin \gamma_j) \frac{b_j}{\cos \gamma_j} \quad (\text{B,20})$$

$$\frac{\partial u_j}{\partial x_j} \Big|_{x_j=0} = -ib_j (p_j \cos^2 \beta_j + q_j \sin \beta_j \sin \gamma_j) \quad (\text{B,21})$$

for $j = 1, 2, 3, 4$.

$$w_1 \Big|_{x_1=0} = 1 + a_1 + a_1' \quad (\text{B,22})$$

$$\frac{\partial w_1}{\partial x_1} \Big|_{x_1=0} = ik_1 \cos \alpha_1 - ik_1 \cos \alpha_1 a_1 - k_1 \sqrt{(1 + \sin^2 \alpha_1)} a_1' \quad (\text{B,23})$$

$$\frac{\partial^2 w_1}{\partial x_1^2} \Big|_{x_1=0} = -k_1^2 \cos^2 \alpha_1 - k_1^2 \cos^2 \alpha_1 a_1 + k_1^2 (1 + \sin^2 \alpha_1) a_1' \quad (\text{B,24})$$

$$\frac{\partial^3 w_1}{\partial x_1^3} \Big|_{x_1=0} = -ik_1 \cos^3 \alpha_1 + ik_1^3 \cos^3 \alpha_1 a_1 - k_1^3 (1 + \sin^2 \alpha_1)^{1.5} a_1' \quad (\text{B,25})$$

and for $n = 2, 3, 4$

$$w_n \Big|_{x_n=0} = a_n + a_n' \quad (B,26)$$

$$\frac{\partial w_n}{\partial x_n} \Big|_{x_n=0} = -ik_n \cos \alpha_n a_n - k_n \sqrt{1 + \sin^2 \alpha_n} a_n' \quad (B,27)$$

$$\frac{\partial^2 w_n}{\partial x_n^2} \Big|_{x_n=0} = -k_n^2 \cos^2 \alpha_n a_n + k_n^2 (1 + \sin^2 \alpha_n) a_n' \quad (B,28)$$

$$\frac{\partial^3 w_n}{\partial x_n^3} \Big|_{x_n=0} = ik_n^3 \cos^3 \alpha_n a_n - k_n^3 (1 + \sin^2 \alpha_n)^{1.5} a_n' \quad (B,29)$$

Twelve linear equations are obtained by substituting the above relationships into the boundary equations (4,48). Considering continuity of linear displacement, (4,48a-f), using the previously defined parameters χ_{ij} and ψ_{ij} and introducing

$$H_j = \cos \beta_j \cos \gamma_j + \sin \beta_j \sin \gamma_j \quad (B,30)$$

the following are obtained.

$$\cos \gamma_3 H_1 b_1 + \cos \gamma_1 H_3 b_3 = 0 \quad (B,31a)$$

$$H_1 b_1 + \cos \gamma_1 (a_2 + a_2') = 0 \quad (B,31b)$$

$$-\cos \gamma_2 a_1 + \cos \gamma_2 a_1' - H_2 b_2 = -\cos \gamma_2 \quad (B,31c)$$

$$a_1 + a_1' + a_3 + a_3' = -1 \quad (\text{B, 31d})$$

$$H_1 b_1 - \cos \gamma_1 (a_4 + a_4') = 0 \quad (\text{B, 31e})$$

$$-\cos \gamma_4 a_1 + \cos \gamma_4 a_1' + H_4 b_4 = -\cos \gamma_4 \quad (\text{B, 31f})$$

Considering continuity of angular displacement (4, 48k, l, m),

$$-\cos \alpha_1 a_1 - \sqrt{(1 + \sin^2 \alpha_1)} a_1' + \chi_{1n} \cos \alpha_n + \chi_{1n} \sqrt{1 + \sin^2 \alpha_n} = -\cos \alpha_1 \quad (\text{B, 31k, l, m})$$

for $n = 2, 3, 4$

and summing bending moments (4, 48n),

$$\begin{aligned} -\cos^2 \alpha_1 a_1 + (1 + \sin^2 \alpha_1) a_1' + \sum_{n=2}^4 (-\psi_{1n} \cos^2 \alpha_n a_n + \psi_{1n} (1 + \sin^2 \alpha_n) a_n') \\ = \cos^2 \alpha_1 \quad (\text{B, 31n}) \end{aligned}$$

Summing forces in the two directions perpendicular to the y axis give the remaining two equations required.

$$\begin{aligned} i \cos^3 \alpha_1 a_1 - (1 + \sin^2 \alpha_1)^{1.5} a_1' - i F_{12} (\cos^2 \beta_2 + \frac{q_2}{p_2} \sin \beta_2 \sin \gamma_2) b_2 \\ - i \chi_{13} \psi_{13} \cos^3 \alpha_3 a_3 + \chi_{13} \psi_{13} (1 + \sin^2 \alpha_3)^{1.5} a_3' + i F_{14} (\cos^2 \beta_4 + \frac{q_4}{p_4} \sin \beta_4 \sin \gamma_4) b_4 \\ = i \cos^3 \alpha_1 \end{aligned}$$

$$\text{where } F_{1j} = E_j t_j p_j / D_1 k_1^3$$

$$\text{Since } q_j \sin \gamma_j = p_j \sin \beta_j$$

$$(\cos^2 \beta_j + \frac{q_j}{p_j} \sin \beta_j \sin \gamma_j) = 1$$

hence

$$\begin{aligned} & i \cos^3 \alpha_1 a_1 - (1 + \sin^2 \alpha_1)^{1.5} a_1' - i F_{12} b_2 - i \chi_{13} \psi_{13} \cos^3 \alpha_3 a_3 \\ & + \chi_{13} \psi_{13} (1 + \sin^2 \alpha_3)^{1.5} a_3' + i F_{14} b_4 = i \cos^3 \alpha_1 \end{aligned} \quad (\text{B31o})$$

Similarly

$$\begin{aligned} & i F_{11} b_1 + i \chi_{12} \psi_{12} \cos^3 \alpha_2 a_2 - \chi_{12} \psi_{12} (1 + \sin^2 \alpha_2)^{1.5} a_2' - i F_{13} b_3 \\ & - i \chi_{14} \psi_{14} \cos^3 \alpha_4 a_4 + \chi_{14} \psi_{14} (1 + \sin^2 \alpha_4)^{1.5} a_4' = 0 \end{aligned} \quad (\text{B, 31p})$$

These 12 linear equations can be solved simultaneously to obtain the wave amplitudes for any incident angle α_1 . To obtain the transmission coefficients, these equations must be solved for a large number of incident angles. The computing time required to solve the equations is reduced by eliminating the b_j terms leaving 8 simultaneous equations to be solved. The following relationships

$$\begin{aligned} b_1 &= -(a_2 + a_2') \cos \gamma_1 / H_1 \\ b_2 &= (1 + a_1 + a_1') \cos \gamma_2 / H_2 \\ b_3 &= -\cos \gamma_3 H_1 b_1 / \cos \gamma_1 H_3 \\ b_4 &= -\cos \gamma_4 H_2 b_2 / \cos \gamma_2 H_4 \end{aligned} \quad (\text{B, 32})$$

are substituted into the appropriate equations of (B,31).

At this point, the analysis, which has been completely general, is restricted by the assumption that the four plates are of the same material. The longitudinal wave speed is then the same for each element independent of its thickness, hence the subscript can be omitted from the H , $\cos\gamma$, $\sin\gamma$, p and q terms. Equations (B,32) become

$$b_1 = -(a_2 + a_2') \cos\gamma / H$$

$$b_2 = (1 + a_1 + a_1') \cos\gamma / H$$

(B,33)

$$b_3 = -b_1$$

$$b_4 = -b_2$$

The resulting 8 equations are presented in matrix form $Ax = B$ where

$$x = \begin{bmatrix} a_1 \\ a_1' \\ a_2 \\ a_2' \\ a_3 \\ a_3' \\ a_4 \\ a_4' \end{bmatrix}, \quad B = \begin{bmatrix} \cos^2 \alpha_1 \\ i H \cos^3 \alpha_1 + (F_{12} + F_{14}) \cos\gamma \\ 0 \\ -i \cos \alpha_1 / \chi_{12} \\ -1 \\ -i \cos \alpha_1 / \chi_{13} \\ 0 \\ -i \cos \alpha_1 / \chi_{14} \end{bmatrix}$$

A =

$$\begin{bmatrix}
 -\cos^2 \alpha_1 & 1 + \sin^2 \alpha_1 & -\psi_{12} \cos^2 \alpha_2 & \psi_{12} (1 + \sin^2 \alpha_2) & -\psi_{13} \cos^2 \alpha_3 & \psi_{13} (1 + \sin^2 \alpha_3) & -\psi_{14} \cos^2 \alpha_4 & \psi_{14} (1 + \sin^2 \alpha_4) \\
 \left[\begin{array}{l} i(H \cos^3 \alpha_1 - \\ (F_{12} + F_{14}) \cos \gamma) \end{array} \right] \left[\begin{array}{l} -\{H(1 + \sin^2 \alpha_1)^{1.5}\} \\ +i(F_{12} + F_{14}) \cos \gamma \end{array} \right] & 0 & 0 & 0 & -iX_{13} \psi_{13} H \cos^3 \alpha_3 & X_{13} \psi_{13} H (1 + \sin^2 \alpha_3)^{1.5} & 0 & 0 \\
 0 & 0 & i \left[\begin{array}{l} X_{12} \psi_{12} H \cos^3 \alpha_2 \\ -(F_{11} + F_{13}) \cos \gamma \end{array} \right] \left[\begin{array}{l} -[X_{12} \psi_{12} H (1 + \sin^2 \alpha_2)^{1.5}] \\ +i(F_{11} + F_{13}) \cos \gamma \end{array} \right] & 0 & 0 & 0 & -iX_{14} \psi_{14} H \cos^3 \alpha_4 & X_{14} \psi_{14} H (1 + \sin^2 \alpha_4)^{1.5} \\
 \frac{-i \cos \alpha_1}{X_{12}} & \frac{-(1 + \sin^2 \alpha_1)^{0.5}}{X_{12}} & i \cos \alpha_2 & (1 + \sin^2 \alpha_2)^{0.5} & 0 & 0 & 0 & 0 \\
 1 & 1 & 0 & 0 & 1 & 1 & 0 & 0 \\
 \frac{-i \cos \alpha_1}{X_{13}} & \frac{-(1 + \sin^2 \alpha_1)^{0.5}}{X_{13}} & 0 & 0 & i \cos \alpha_3 & (1 + \sin^2 \alpha_3)^{0.5} & 0 & 0 \\
 0 & 0 & 1 & 1 & 0 & 0 & 1 & 1 \\
 \frac{-i \cos \alpha_1}{X_{14}} & \frac{-(1 + \sin^2 \alpha_1)^{0.5}}{X_{14}} & 0 & 0 & 0 & 0 & i \cos \alpha_4 & (1 + \sin^2 \alpha_4)^{0.5}
 \end{bmatrix}$$

The $\sin\alpha_j$ and $\cos\alpha_j$ terms are transformed to expressions containing $\sin\alpha_1$. For any set of plates, $\sin\alpha_1 = s$ is the only variable.

A computer programme is used where the above equations are set into a Simpson's Rule integrating routine. The various transmission coefficients are calculated using the derived wave amplitudes. A listing of the programme used is given in Appendix C.

APPENDIX C. COMPUTER PROGRAMMES

C.1. COMPUTATION OF THE AVERAGE TRANSMISSION COEFFICIENT - BENDING WAVE SOLUTION

```

1      PROGRAM TRFC4(INPUT,OUTPUT,TAPE5=INPUT,TAPE6=OUTPUT)
C      CALCULATES TRANSMISSION FACTOR F(IJ) FOR UP TO 4 PLATES OF SAME
C      MATERIAL BUT DIFFERENT THICKNESSES----CONNECTED ALONG A COMMON
C      JOIN      JOIN ANGLE NOT IMPORTANT
5      C
C      LOSS FACTOR(IJ)=2LF(IJ)/(PI)A(I)K(I)
C      L IS LENGTH OF JOIN
C      K(I) IS WAVENUMBER IN PLATE I
C      A(I) IS AREA OF PLATE I
10     C
C      F(I,J) IS TRANSMISSION COEFFICIENT TOR(I,J)
C      -LN(1-TOR(I,J)) -LN- IS ALSO CALCULATED
C      -R- IS RATIO TOR AVERAGE/TOR NORMAL INCIDENCE
C      ANGLE FOR PLATES I AND J
15     C      TF12 BASED ON DIRECT SUBSTITUTION INTO POWER FLOW EQUATION
C      F12N IS F12 CALCULATED AT NORMAL INCIDENCE ONLY
C
C      THIS PROGRAM ONLY CALCS F(IJ) FOR I LESS THAN J
C      F(JI)=F(IJ)SQRT(T(J)/T(I))
20     C      EXTERNAL TCPW,DENZ,DNPW,RCFF
32    WRITE(6,1)
1     FORMAT(1H1,4X,24HTRANSMISSION COEFF TORIJ,50X,27HTF12 IS TRANSMISS
1     ION FACTOR,/)
1     WRITE(6,2)
25    2 FORMAT(4X,2HT1,3X,2HT2,3X,2HT3,3X,2HT4,8X,3HF12,11X,3HF13,11X,
1     13HF14,11X,3HF23,11X,3HF24,11X,3HF34,10X,4HTF12,10X,4HF12N)
C      PLATE THICKNESSES T1 T2 T3 T4 IN FIRST 4 FIELDS OF DATA CARD
C      5TH FIELD IS CONTROL 0 (LEAVE BLANK)---CONTINUE
C      -1.-----NEW PAGE
30    C      1.-----STOP AFTER THIS CARD
C      FOR 3PLATES T4=0
C      FOR 2 PLATES T4=0 AND T3=0

```



```

3 READ(5,6)T1,T2,T3,T4,S10
6 FORMAT(5F5.2)
  IF(T1)42,42,7
7 IF(T2)42,42,8
8 TR12=T2/T1
  IF(T3)40,34,34
34 IF(T4)40,35,35
35 TR13=T3/T1
  TR14=T4/T1
  IF(1.-TR12)9,10,10
9 Z12=1./SQRT(TR12)
  GOTO 11
10 Z12=1.
45 11 CALL SMPSN(TCPW,TR12,TR13,TR14,.0,Z12,0.0001,10,S11,SP12,N,IP12)
  A12=1.-SP12
  F12=-ALOG(A12)
  F13=.0
  F14=.0
  F23=.0
  F24=.0
  F34=.0
  R12=SP12/TCPW(.0,TR12,TR13,TR14)
55  R13=.0
  R14=.0
  R23=.0
  R24=.0
  R34=.0
  SP13=.0
60  SP14=.0
  SP23=.0
  SP24=.0
  SP34=.0
65  CALL SMPSN(RCFF,TR12,TR13,TR14,.0,1.0*0.0001,10,S11,SP11,N,IP11)
  CALL SMPSN(DEN2,TR12,TR13,TR14,.0,Z12,0.0001,10,S11,SP12,N,ID12)

```

```

70 CALL SMPSN(DNPW,TR12,TR13,TR14,.0,1.0,0.0001,10,S11,SD12,N,IS12)
   RS12=TR12*TR12
   RN12=3.1416*SP12/RS12
   RD12=3.1416/RS12-DN12-SD12
   FP12=RN12/RD12
   TRNM=TCPW(.0,TR12,TR13,TR14)
   AN12=1.-TRNM
75   F12N=-ALOG(AN12)
   IF(T3)40,12,13
12  IF(T4)40,30,44
13  TR21=T1/T2
   TR23=T3/T2
   TR24=T4/T2
80   IF(1.-TR13)14,15,15
14  Z13=1./SQRT(TR13)
   GOTO 16
15  Z13=1.
16  IF(1.-TR23)17,18,18
85 17  Z23=1./SQRT(TR23)
   GOTO 19
18  Z23=1.
19  CALL SMPSN(TCPW,TR13,TR12,TR14,.0,Z13,0.0001,10,S11,SP13,N,IP13)
   CALL SMPSN(TCPW,TR23,TR21,TR24,.0,Z23,0.0001,10,S11,SP23,N,IP23)
90   A13=1.-SP13
   F13=-ALOG(A13)
   A23=1.-SP23
   F23=-ALOG(A23)
   R13=SP13/TCPW(.0,TR13,TR14,TR12)
95   R23=SP23/TCPW(.0,TR23,TR21,TR24)
   IF(T4)40,30,20
20  TR34=T4/T3
   TR32=T2/T3
   TR31=T1/T3
100  IF(1.-TR14)21,22,22

```

```

21 Z14=1./SQRT(TR14)
   GOTO 23
22 Z14=1.
23 IF(1.-TR24)24,25,25
105 24 Z24=1./SQRT(TR24)
   GOTO 26
25 Z24=1.
26 IF(1.-TR34)27,28,28
110 27 Z34=1./SQRT(TR34)
   GOTO 29
28 Z34=1.
29 CALL SMPSN(TCPW,TR14,TR12,TR13,.0,Z14,0.0001,10,SI1,SP14,N,IP14)
   CALL SMPSN(TCPW,TR24,TR21,TR23,.0,Z24,0.0001,10,SI1,SP24,N,IP24)
   CALL SMPSN(TCPW,TR34,TR31,TR32,.0,Z34,0.0001,10,SI1,SP34,N,IP34)
115 A14=1.-SP14
   F14=-ALOG(A14)
   A24=1.-SP24
   F24=-ALOG(A24)
   A34=1.-SP34
120 F34=-ALOG(A34)
   R14=SP14/TCPW(.0,TR14,TR12,TR13)
   R24=SP24/TCPW(.0,TR24,TR21,TR23)
   R34=SP34/TCPW(.0,TR34,TR32,TR31)
125 30 SUMT=.0
   SUMT=SP11+SP12+SP13+SP14
   WRITE(6,4)SP12,SP13,SP14,SP23,SP24,SP34,TRNM
   4  FORMAT(22X,3HTOR,1X,6(E10.3,4X),10X,E14.3)
   WRITE(6,46)R12,R13,R14,R23,R24,R34
130 46  FORMAT(22X,1HR,3X,6(E10.3,4X))
   WRITE(6,31)T1,T2,T3,T4,F12,F13,F14,F23,F24,F34,FP12,F12N,SP11,
   1SUMT
31  FORMAT(2X,4F5.2,1X,2HLN,1X,7(E10.3,4X).E10.3/
   122X,6HTOR11=,E10.3,10X,8MSUM TOR=,E10.3//)
   IF(IP12)50,51,50

```

```

135      51 IF (IP13)50,52,50
      52 IF (IP14)50,53,50
      53 IF (IP23)50,54,50
      54 IF (IP24)50,55,50
      55 IF (IP34)50,56,50
140      56 IF (ST0)32,3,33
      50 WRITE (6,57) IP11,IP12,IP13,IP14,IP23,IP24,IP34
      57 FORMAT(2X,43HSIMPSON RULE CRITERIA NOT MET - ERROR CODES,2X,7I2)
      IF (ST0)32,3,33
      40 WRITE (6,41) T1,T2,T3,T4
145      41 FORMAT(2X,4F5.2,5X,31HDATA CARD ERROR   -VE THICKNESS,)
      IF (ST0)32,3,33
      42 WRITE (6,43) T1,T2,T3,T4
      43 FORMAT(2X,4F5.2,5X,35HDATA CARD ERROR   T1 OR T2 -VE OR 0,)
      IF (ST0)32,3,33
150      44 WRITE (6,45) T1,T2,T3,T4
      45 FORMAT(2X,4F5.2,5X,16HERROR   T3=0 T4≠0,)
      IF (ST0)32,3,33
      33 STOP
      END

```

```

1      SUBROUTINE SMPSN(F,W,Y,Z,A,B,DEL,IMAX,S11,S,N,IER)
C      BASED ON LIBRARY SIMPSON RULE ROUTINE FOR FUNCTION F(X)
C      THIS ROUTINE INTEGRATES FUNCTION F(X,W,Y,Z)
C      THE NUMBER OF ELEMENTS ARE DOUBLED EACH REPEAT UNTIL DESIRED
5      C      ACCURACY (DEL) IS MET OR MAX. NO. OF REPEATS (IMAX) IS MET
      S11=.0
      S=.0
      N=0
      RA=B-A

```

```

10      IF (BA) 19, 19, 20
19 IER=1
      RETURN
20 IF (DEL) 22, 22, 23
22 IER=2
      RETURN
15 23 IF (IMAX-1) 24, 24, 25
24 IER=3
      RETURN
25 X=BA/2.+A
      NHALF=1
      SUMK=F(X,W,Y,Z)*BA*2./3.
      S=SUMK+(F(A,W,Y,Z)+F(B,W,Y,Z))*BA/6.
      DO 28 I=2, IMAX
      SII=S
      S=(S-SUMK/2.)/2.
      NHALF=NHALF*2
      ANHALF=NHALF
      FRSTX=A+(BA/ANHALF)/2.
      SUMK=F(FRSTX,W,Y,Z)
30      XK=FRSTX
      KLAST=NHALF-1
      FINC=BA/ANHALF
      DO 26 K=1, KLAST
      XK=XK+FINC
35 26 SUMK=SUMK+F(XK,W,Y,Z)
      SUMK=SUMK*2.*BA/(3.*ANHALF)
      S=S+SUMK
      IF (ABS(S-SII)-ABS(DEL*S)) 29, 28, 28
40 28 CONTINUE
      IER=4
      COTO 30
29 IER=0
30 N=2*NHALF
      RETURN
45      END

```

```
1          C      FUNCTION TCPW(X,W,Y,Z)
                CALCULATES TRANSMISSION COEFFICIENT AT X=SIN(ALPHA 1)
                WMCO=(1.0-X*X*W)*(1.0-X*X)
                TCPW=W**2.5*SQRT(WMCO)*ASQ(X,W,Y,Z)
5          RETURN
          END
```

```
1          FUNCTION ASQ(X,W,Y,Z)
                COMPLEX SQ,SUSQ,A
                A=(0.,2.)*SQ(X,Y)*SQ(X,Z)/SUSQ(X,W,Y,Z)
                ASQ=REAL(A)**2+AIMAG(A)**2
5          RETURN
          END
```

```
1          FUNCTION SQ(X,W)
                COMPLEX SQ,SM,SP
                SQ=SP(X,W)-SM(X,W)
5          RETURN
          END
```

```
1      FUNCTION SP(X,W)
      COMPLEX SP
      SP=CMPLX(SQRT(1.+X*X*W),0.)
      RETURN
5      END
```

```
1      FUNCTION SM(X,W)
      COMPLEX SM
      WM2=1.-X*X*W
      WM=SQRT(ABS(WM2))
      SM=CMPLX(0.,WM)
      IF(WM2)1,2,2
1      SM=(0.,-1.)*SM
2      RETURN
      END
```

```
1      FUNCTION SUSQ(X,W,Y,Z)
      COMPLEX SUSQ,BMX,BMW,BMY,BMZ,A,B,C,D,SQ
      A=SQ(X,1.)
      B=SQ(X,W)
      C=SQ(X,Y)
      D=SQ(X,Z)
      BMX=B*C*D
      BMW=W**2.5*A*C*D
      BMY=Y**2.5*A*B*D
10     BMZ=Z**2.5*A*B*C
      SUSQ=BMX+BMW+BMY+BMZ
      RETURN
      END
```

```
1 C FUNCTION DEN2(X,W,Y,Z)
   ONE INTEGRAL EQUATION IN DENOMINATOR FOR POWER BALANCE APPROACH
   DEN2=SQRT(1.-X*X)*ASQ(X,W,Y,Z)*W
   RETURN
5 END
```

```
1 C FUNCTION DNPW(X,W,Y,Z)
   ONE INTEGRAL EQUATION IN DENOMINATOR FOR POWER BALANCE APPROACH
   RS=W*W
   WM=1.-X*X*W
   YM=1.-X*X*Y
   ZM=1.-X*X*Z
   IF(WM)1,2,2
1  WM=.0
2  IF(YM)3,4,4
3  YM=.0
4  IF(ZM)5,6,6
5  ZM=.0
6  SUMP=W**2.5*ASQ(X,W,Y,Z)*SQRT(WM)+Y**2.5*ASQ(X,Y,Z,W)*SQRT(YM)
   I+Z**2.5*ASQ(X,Z,W,Y)*SGRT(ZM)
15 DNPW=SUMP/RS
   RETURN
   END
```



```
1      C      FUNCTION RCFF(X,W,Y,Z)
          CALCULATES REFLECTION COEFFICIENT FOR PLATE 1 AT X=SIN(ALPHA 1)
          COMPLEX SUSQ,SSQP,A
          A=-SSQP(X,W,Y,Z)/SUSQ(X,W,Y,Z)
5      RCFF=REAL(A)**2+AIMAG(A)**2
          RETURN
          END
```

```
1      FUNCTION SSQP(X,W,Y,Z)
          COMPLEX SQ,SSQP,BMX,BMW,BMY,BMZ,APSQ,SP,SM,B,C,D
          R=SQ(X,W)
          C=SQ(X,Y)
5      D=SQ(X,Z)
          BMX=B*C*D
          APSQ=SP(X,1.)+SM(X,1.)
          BMW=W**2.5*C*D*APSQ
          BMY=Y**2.5*B*D*APSQ
10      BMZ=Z**2.5*B*C*APSQ
          SSQP=BMX+BMW+BMY+BMZ
          RETURN
          END
```

C.2. COMPUTATION OF THE AVERAGE TRANSMISSION COEFFICIENT - GENERAL SOLUTION

```

1      PROGRAM TFBLT(INPUT,OUTPUT,TAPE5=INPUT,TAPE6=OUTPUT)
      DIMENSION TD(4),T(4),TOR(4,3),TI1(4,3),WMT(4,3),TFC(4,3),DIFF(4,3)
      1,FSQ(4),TNM(4,3)
C      CALCULATES TRANSMISSION FACTOR F(IJ) FOR UP TO 4 PLATES OF SAME
C      MATERIAL BUT DIFFERENT THICKNESSES----CONNECTED ALONG A COMMON
5      JOIN --- BENDING, LONGT. AND TRANSVERSE WAVES CONSIDERED
C      LOSS FACTOR(1,J)=2LF(1,J)/(PI)A(1)K(1) ---FOR BENDING WAVES
C      L IS LENGTH OF JOIN
C      K(1) IS WAVENUMBER IN PLATE 1
10     A(1) IS AREA OF PLATE 1
C
C      F(I,J) IS TORBB TRANS. COEFF
C      OR TFCBB=-LN(1-TORBB) BUT BENDING WAVES FROM INCIDENT
C      LONGT. AND TRANSVERSE WAVES. TORRL AND TORBT MAY NEED TO BE
15     CONSIDERED AFTER THE FIRST JOIN OF A STRUCTURE.
C
17     WRITE(6,1)
1     FORMAT(1H1,5X,76HTRANSMISSION FACTORS - BENDING, LONGT. AND TRANSV
      ERSE WAVE FIELDS CONSIDERED,/)
C      CENTRE FREQUENCY IN FIRST DATA FIELD
20     4 PLATE THICKNESSES IN M.M. IN NEXT 4 FIELDS---T1 FIRST,T2,T3,T4.
C      AND PLATES 1 AND 3 OPPOSITE AND PERPENDICULAR TO 2 AND 4.
C      6TH FIELD IS CONTROL 0 (LEAVE BLANK)---CONTINUE
C      -1.-----NEW PAGE
C      1.-----STOP AFTER THIS CARD
25
C      T1 AND T2 MUST BE +VE
16     READ(5,10)F,(TD(I),I=1,4),STO
10     FORMAT(6F6.2)
      DO 22 I=1,4
22     T(I)=TD(I)/1000.
      RTF=SQRT(T(I)*F)
30     DO2 I=1,4
      2 FSQ(I)=(54.4*T(I)/T(1)/RTF)**2

```

```

11 WRITE(6,120)
120 FORMAT(4X,1HF,6X,2HT1,6X,2HT2,6X,2HT3,6X,2HT4,6X,3HFSQ,5X,3HTOR,
35 16X,2HBB,10X,2HBL,10X,2HBT,10X,3HTFC,6X,2HBB,10X,2HBL,10X,2HBT)
3 CALL SMSN2(T,F,.0,1.,.01,10,TNM,TI1,TOR,N,IER)
D04 I=1,4
D04 J=1,3
WMT(I,J)=1.-TOR(I,J)
40 4 TFC(I,J)=-ALOG(WMT(I,J))
IF(IER-4)8,5,8
5 D06 I=1,4
D06 J=1,3
6 DIFF(I,J)=TOR(I,J)-TI1(I,J)
45 WRITE(6,7)F,(TD(N),N=1,4),(FSQ(I),I,(TOR(I,J),J=1,3),I,(TFC(I,J),
1J=1,3),I=1,4),((TI1(I,J),J=1,3),I=1,4),((TNM(I,J),J=1,3),I=1,4)
7 FORMAT(2X,F5,2X,4(F5.2,3X),E10.3,2X,1H1,I1,3E12.3,6X,1H1,I1,3E12.3
1/3(41X,E10.3,2X,1H1,I1,3E12.3,6X,1H1,I1,3E12.3//)2X,
217HDEL NOT SATISFIED,40X,15HPREVIOUS VALUES,/4(55X,3E12.3//)2X,
50 328HTOR NORMAL INCIDENCE ONLY,/4(55X,3E12.3//)
GOTO 15
8 WRITE(6,9)F,(TD(N),N=1,4),(FSQ(I),I,(TOR(I,J),J=1,3),I,(TFC(I,J),
1J=1,3),I=1,4),((TNM(I,J),J=1,3),I=1,4)
9 FORMAT(2X,F5,2X,4(F5.2,3X),E10.3,2X,1H1,I1,3E12.3,6X,1H1,I1,3E12.3
1/3(41X,E10.3,2X,1H1,I1,3E12.3,6X,1H1,I1,3E12.3//)2X,
55 228HTOR NORMAL INCIDENCE ONLY,/4(55X,3E12.3//)
15 SUMT=.0
D088 N=1,4
D088 M=1,3
60 88 SUMT=SUMT+TOR(N,M)
WRITE(6,20)SUMT
20 FORMAT(2X,16HSUM OF TOR(I,J)=,E12.3//)
IF(ST0)17,16,18
18 STOP
65 END

```

```

1      SUBROUTINE SMSN2(T,F,AL,AH,DEL,IMAX,TNM,SII,S,N,IER)
C      THIS PROGRAM APPLIES SIMPSONS RULE TO A SET OF FUNCTIONS
C      INTEGRATED FROM AL TO AH.  ACCURACY IS SET BY DEL AND MAX. NUMBER
C      OF REPEATS IS SET BY IMAX.
5      THIS IS BASED ON A LIBRARY PROGRAM FOR A SINGLE VARIABLE FUNCTION
C      IN THIS PROGRAM THE INITIAL NUMBER OF ELEMENTS IS SET TO 128 TO
C      REDUCE COMPUTING.  MAX. OF 3 RUNS IS SET THEREFORE MAX. OF 512
C      ELEMENTS USED IN FINAL RUN.
      DIMENSION T(4),SII(4,3),S(4,3),SUMK(4,3),TBX(4),TLX(4),TTX(4),
10     ITBL(4),TLL(4),TTL(4),TBH(4),TLH(4),TTH(4),TCX(4,3),TNM(4,3),
      2TCAH(4,3),FSQ(4)
      DO2 I=1,4
      DO2 J=1,3
      SII(I,J)=.0
15     2 S(I,J)=.0
      BA=AH-AL
      IF(BA)19,19,20
19     IER=1
      RETURN
20     IF(DEL)22,22,23
22     IER=2
      RETURN
23     IF(IMAX-1)24,24,25
24     IER=3
25     RETURN
      X=BA/2.+AL
      NHALF=64
      CALL SOLVA(T,X,F,FSQ,TCX)
      CALL SOLVA(T,AL,F,FSQ,TNM)
      CALL SOLVA(T,AH,F,FSQ,TCAH)
30     DO3 I=1,4
      DO3 J=1,3
      SUMK(I,J)=TCX(I,J)*BA*2./3.
      3 S(I,J)=SUMK(I,J)+(TNM(I,J)+TCAH(I,J))*BA/6.

```

```

35      C      TEST RUN   IMAX=3
          IMAX=3
          D028 L=2, IMAX
          NHALF=NHALF*2
          ANHALF=NHALF
          FRSTX=AL+(BA/ANHALF)/2
40      CALL SOLVA(T,FRSTX,F,FSQ,TCX)
          D04 I=1,4
          D04 J=1,3
          S11(I,J)=S(I,J)
          S(I,J)=(S(I,J)-SUMK(I,J)/2.)/2.
45      4 SUMK(I,J)=TCX(I,J)
          XK=FRSTX
          KLAST=NHALF-1
          FINC=BA/ANHALF
          D026 K=1,KLAST
          XK=XK+FINC
          CALL SOLVA(T,XK,F,FSQ,TCX)
          D026 I=1,4
          D026 J=1,3
50      26 SUMK(I,J)=SUMK(I,J)+TCX(I,J)
          D05 I=1,4
          D05 J=1,3
          SUMK(I,J)=SUMK(I,J)*2.*BA/(3.*ANHALF)
          5 S(I,J)=S(I,J)+SUMK(I,J)
          D06 I=1,4
          D06 J=1,3
          IF(ABS(S(I,J)-S11(I,J))-ABS(DEL*S(I,J)))6,28,28
          6 CONTINUE
          GOTO 29
65      28 CONTINUE
          IER=4
          GOTO 30
          29 IER=0

```

```

70      30 N=2*NHALF
        RETURN
        END

1      SUBROUTINE SOLVA(T,S,FG,FSQ,TOR)
C      THIS SETS UP REQUIRED MATRIX FOR INCIDENT ANGLE ---S=SIN(ALPHA 1)
C      COMPLEX WAVE AMPLITUDES FROM MATRIX SOLUTION ARE USED TO CALCULATE
C      THE TRANSMISSION COEFFICIENTS FOR THE PARTICULAR VALUE OF S.
5      TORBB(1,N)=TOR(N,1) IN PROGRAM
C      TORBL(1,N)=TOR(N,2) IN PROGRAM
C      TORBT(1,N)=TOR(N,3) IN PROGRAM
C      DIMENSION A(8,8),B(8),X(16),CM2(4),CP2(4),EM(4),EP(4),EHM(4),
10     1CIP(4),CIM2(4),CIP2(4),CM(4),CP(4),PSM(4),PSP(4),T(4),TD(4),
2     2ASQ(4),BSQ(4),CSQ(4),TOR(4,3),EHP(4),F(4),CIM(4),SCR(2,8,40),TR(4)
3     3,AL(4),AT(4),FSQ(4)
        COMPLEX A,B,CCOM,H,COH,AL,AT,X1T4,X5T8,Q
        DO 70 N=1,4
        DO 70 M=1,3
15     70 TOR(N,M)=.0
        A(5,1)=(1.,0.)
        A(5,2)=(1.,0.)
        A(5,5)=(1.,0.)
        A(5,6)=(1.,0.)
20     A(7,3)=(1.,0.)
        A(7,4)=(1.,0.)
        A(7,7)=(1.,0.)
        A(7,8)=(1.,0.)
        B(5)=(-1.,0.)
        TF=T(1)*FG
25     RTF=SQRT(TF)

```

```

6 CB2=1.-S*S/(3.59E-04*TF)
  Z=ABS(CB2)
  CB=SQRT(Z)
30 109 SC=S/(3.20E-02*RTF)
      CC2=1.-S*S/(1.024E-03*TF)
      Z=ABS(CC2)
      CC=SQRT(Z)
35 111 SB=S/(1.90E-02*RTF)
      CCOM=CMPLX(CC,0.)
      HS=SB*SC
      HC=CB*CC
      H=CMPLX(HC+HS,0.)
      IF(CB2)9,2,2
40 9 H=CMPLX(HS,-HC)
     IF(CC2)4,2,2
4  H=CMPLX(HS-HC,0.)
   CCOM=CMPLX(0.,-CC)
2  COH=CCOM/H *(0.,-1.)
45 DO 3 N=1,4
    CM2(N)=1.-S*S*T(N)/T(1)
    Z=ABS(CM2(N))
    CM(N)=SQRT(Z)
50 113 CP2(N)=1.+S*S*T(N)/T(1)
     CIM2(N)=(1.-S*S)*T(N)/T(1)
     CIP2(N)=(1.+S*S)*T(N)/T(1)
     CP(N)=SQRT(CP2(N))
     CIM(N)=SQRT(CIM2(N))
     CIP(N)=SQRT(CIP2(N))
55 PSM(N)=CM2(N)*(T(N)/T(1))**2
    PSP(N)=CP2(N)*(T(N)/T(1))**2
    EM(N)=(CM(N)*SQRT(T(N)/T(1)))**3

```

```

EP(N)=(CP(N)*SQRT(T(N)/T(1)))**3
F(N)=54.4*T(N)/T(1)/RTF
60 3 FSQ(N)=F(N)*F(N)
A(1,1)=CMPLX(-CM2(1),0.)
A(1,2)=CMPLX(CP2(1),0.)
A(1,3)=CMPLX(-PSM(2),0.)
A(1,4)=CMPLX(PSP(2),0.)
65 A(1,5)=CMPLX(-PSM(3),0.)
A(1,6)=CMPLX(PSP(3),0.)
A(1,7)=CMPLX(-PSM(4),0.)
A(1,8)=CMPLX(PSP(4),0.)
70 A(2,1)=CMPLX(0.,EM(1))
A(2,2)=CMPLX(-EP(1),0.)
A(2,5)=CMPLX(0.,-EM(3))
A(2,6)=CMPLX(EP(3),0.)
A(3,3)=CMPLX(0.,EM(2))
A(3,4)=CMPLX(-EP(2),0.)
75 A(3,7)=CMPLX(0.,-EM(4))
A(3,8)=CMPLX(EP(4),0.)
A(4,1)=CMPLX(0.,-CIM(2))
A(4,2)=CMPLX(-CIP(2),0.)
A(4,3)=CMPLX(0.,CM(2))
80 A(4,4)=CMPLX(CP(2),0.)
A(6,1)=CMPLX(0.,-CIM(3))
A(6,2)=CMPLX(-CIP(3),0.)
A(6,5)=CMPLX(0.,CM(3))
A(6,6)=CMPLX(CP(3),0.)
85 A(8,1)=CMPLX(0.,-CIM(4))
A(8,2)=CMPLX(-CIP(4),0.)
A(8,7)=CMPLX(0.,CM(4))
A(8,8)=CMPLX(CP(4),0.)
90 B(1)=-A(1,1)
B(2)=CMPLX(0.,EM(1))
B(4)=A(4,1)
B(6)=A(6,1)

```



```

          B(8)=A(8,1)
          F24=F(2)+F(4)
95         F13=F(1)+F(3)
          IF(CM2(2))10,1,1
10        A(4,3)=A(4,3)*(0.,-1.)
          A(3,3)=A(3,3)*(0.,+1.)
          1 IF(CM2(3))12,13,13
100       12 A(6,5)=A(6,5)*(0.,-1.)
          A(2,5)=A(2,5)*(0.,+1.)
13        IF(CM2(4))14,5,5
14        A(8,7)=A(8,7)*(0.,-1.)
          A(3,7)=A(3,7)*(0.,+1.)
105       5 A(2,1)=A(2,1)-F24*COH
          A(2,2)=A(2,2)-F24*COH
          A(3,3)=A(3,3)-F13*COH
          A(3,4)=A(3,4)-F13*COH
          E(2)=B(2)+F24*COH
110       31 IF(T(3))20,15,16
          15 IF(T(4))20,17,18
          16 IF(T(4))20,19,7
          20 WRITE(6,33)
          33 FORMAT(2X,10HDATA ERROR)
115       DO 32 M=1,4
          DO 32 N=1,3
          32 TOR(M,N)=.0
          RETURN
C         -CLINIT- IS AN AVAILIABLE LIBRARY ROUTINE TO SOLVE COMPLEX MATRIX
120       C EQUATION AX=B THIS IS NOT REPRODUCED HERE.
          17 CALL CLINIT(A,B,X,4,1,DET,EX,CNR,SINGUL,8,SCR)
          L=2
          K=5
          GOTO 11
125       18 DO 63 J=5,6
          DO62 I=1,8

```

```

62 A(J,I)=A(J+2,I)
63 B(J)=B(J+2)
    D064 J=5,6
130    D064 I=1,6
64 A(I,J)=A(I,J+2)
    CALL CLINIT(A,B,X,06,1,DET,EX,CNR,SINGUL,08,SCR)
    K=13
    L=4
135    DO 68 I=9,12
    X(I+4)=X(I)
68 X(I)=.0

    GOTO 11
140 19 CALL CLINIT(A,B,X,06,1,DET,EX,CNR,SINGUL,08,SCR)
    K=9
    L=3
    GOTO 11
145 7 CALL CLINIT(A,B,X,8,1,DET,EX,CNR,SINGUL,08,SCR)
    K=13
    L=4
C   X(I) ARE THE PROPAGATING AND NON-PROPAGATING BENDING WAVE
C   AMPLITUDES.
C   FIND LONGT. AND TRANSVERSE WAVE AMPLITUDES FROM X(I)
150 11 D021 I=1,K,4
    J=(I+3)/4
21 ASQ(J)=X(I)*X(I)+X(I+1)*X(I+1)
    Q=CMPLX(X(3),X(4))
    X1T4=CMPLX(X(1),X(2))
155    X1T4=(1.,0.)+Q*X1T4
    Q=CMPLX(X(5),X(6))
    X5T8=CMPLX(X(7),X(8))
    X5T8=Q*X5T8
    AL(1)=-COH*X5T8
160    AT(1)=-SB*X5T8/H

```

```

AL(2)=COH*X1T4
AT(2)=SB*X1T4/H
IF(L-3)56,57,58
165 58 AL(4)=-AL(2)
AT(4)=-AT(2)
57 AL(3)=-AL(1)
AT(3)=-AT(1)
56 DO 60 J=1,L
BSQ(J)=REAL(AL(J))**2+AIMAG(AL(J))**2
170 60 CSQ(J)=REAL(AT(J))**2+AIMAG(AT(J))**2
IF(CIM(1))67,67,65
67 DO 66 N=1,L
DO 66 M=1,3
175 66 TOR(N,M)=.0
TOR(1,1)=1.0
GOTO 22
65 DO 22 N=1,L
IF(CM2(N))23,23,24
180 23 TOR(N,1)=.0
GOTO 28
24 TOR(N,1)=EM(N)*ASQ(N)/CM2(N)/CIM(1)
28 IF(CB2)25,25,26
25 TOR(N,2)=.0
GOTO 29
185 26 TOR(N,2)=F(N)*BSQ(N)*CB/CIM(1)/2.
29 IF(CC2)27,27,80
27 TOR(N,3)=.0
GOTO 22
80 TOR(N,3)=0.320*F(N)*CSQ(N)*CC/CIM(1)
190 22 CONTINUE
RETURN
END

```

C.3. COMPUTATION OF VIBRATIONAL ENERGY RATIOS OF A CONNECTED STRUCTURE.

```

1      PROGRAM ENCAL(INPUT,OUTPUT,TAPE5=INPUT,TAPE6=OUTPUT)
C      CALCULATES ENERGY RATIOS FOR CONNECTED STRUCTURES OF UP TO 10
C      ELEMENTS -----USING POWER FLOW EQUATIONS
C      LAST ELEMENT ONLY DIRECTLY DRIVEN ----ELEMENT (N)
5      DIMENSION CL(10,10),PL(9),A(10,10),CLF(10,10),PN(10)
11     READ(5,1)N,(PN(I),I=1,N)
1     FORMAT(12,10I3)
1     WRITE(6,14)(PN(I),I=1,N)
14    FORMAT(1H1,5X,19HPLATE ENERGY RATIOS//6X,10HPLATE NO.S,10I5//)
10   M=N-1
1     WRITE(6,2)(PN(I),I=1,M)
2     FORMAT(4X,1HF,8X,8(2HER,I2,10X),2HER,I1,/)
1     READ(5,3)((CL(I,J),J=1,10),I=1,N)
C     READ COUPLING LOSS FACTORS --- CALCULATED AT 1000HZ
15   C     1ST CARD CL 11,12,13,14,---ETC
C     NEXT CARD CL 21,22,23,24,---ETC
C     CONTINUE FOR N CARDS -- CL(I,I) DUMMY VALUES E.G. ZERO
C     ALL LOSSES ENTERED X1000.
3     FORMAT(10F7.3)
20   C     DATA CARD 1ST FIELD ---FREQUENCY
C           REMAINING FIELDS---INTERNAL LOSS FACTORS FOR PLATES 1 TO
C           N-1 IN ORDER. DRIVEN PLATE LOSS
C           FACTOR NOT REQUIRED
C     CONTROL--- F=20000. NEW SET OF DATA FOLLOWING
25   C     F G.T.20000 ---- STOP
4     READ(5,5)F,(PL(I),I=1,M)
5     FORMAT(F6,9F7.3)
1     IF(F-20000.)13,11,12
30  13 F=F/1000.
1     RF=SQRT(F)
1     DO 6 I=1,M
1     CL(I,I)=.0

```

```

SUMF=.0
DO 7 J=1,N
35 CLF(I,J)=-CL(I,J)/RF
7 SUMF=SUMF+CLF(I,J)
6 CLF(I,I)=- (SUMF-PL(I))
DO 9 I=1,M
40 9 CLF(N,I)=CL(N,I)/RF
DO 8 I=1,M
DO 8 J=1,N
8 A(I,J)=CLF(J,I)
CALL ASOL(A,M,1)
F=1000.*F
45 WRITE(6,10)F,(A(I,1),I=1,M)
10 FORMAT(2X/2X,F5,2X,9(E10.3,4X))
GOTO 4
12 STOP
END

```

```

1 SUBROUTINE ASOL(A,N,M)
C THIS IS A FAST MATRIX SOLVING ROUTINE WITH NO CHECKS
C USEFUL WHERE DET. OF A IS NOT NEAR ZERO.
C REFERENCE(HEMMERLE - 1967)
5 DIMENSION A(10,10)
L=N+M
DO 1 I=1,N
A(N+1,L)=1.0/A(1,1)
DO 2 J=2,L
10 2 A(N+1,J-1)=A(1,J)*A(N+1,L)
DO 3 J=2,N
DO 4 K=2,L
4 A(J-1,K-1)=A(J,K)-A(J,1)*A(N+1,K-1)
3 A(J-1,L)=-A(J,1)*A(N+1,L)
15 DO 1 J=1,L
1 A(N,J)=A(N+1,J)
RETURN
END

```

APPENDIX D. APPARATUS AND EXPERIMENTAL PROCEDURE

D.1. INTRODUCTION

In order to predict the energy distribution in a connected structure, using Equation (3,9), the internal loss factors of the individual elements are required, and these internal loss factors are obtained experimentally. Experimentally measured energy ratios are required to compare with the predicted energy ratios. That is, the experimental work involved the accurate measurement of uncoupled plate internal loss factors and the steady state energy levels of the plates comprising the test structure.

In this appendix, the apparatus required and experimental procedure used to measure the internal loss factors and plate energy ratios are described. In D.2, the structure support system and associated external drivers are described. The general instrumentation used and its calibration is discussed in D.3. Both steady state and decay methods of measuring the internal loss factors are described and discussed in D.4. The method of measuring the plate energy ratios is included in D.5, followed by a general discussion on the expected accuracy of the experimental results in D.6.

D.2. TEST STRUCTURE SUPPORT SYSTEM

D.2.1. Requirements

When measuring the loss factor of an element, it is important to reduce any losses via the support system to a degree where they are small compared with the measured loss.

In some early tests, the plates were supported by long piano wires from the ceiling. During the tests it was noticed that the strings were vibrating and accelerometer measurements showed that energy was being transferred into the ceiling. A support system which would block this energy flow was required.

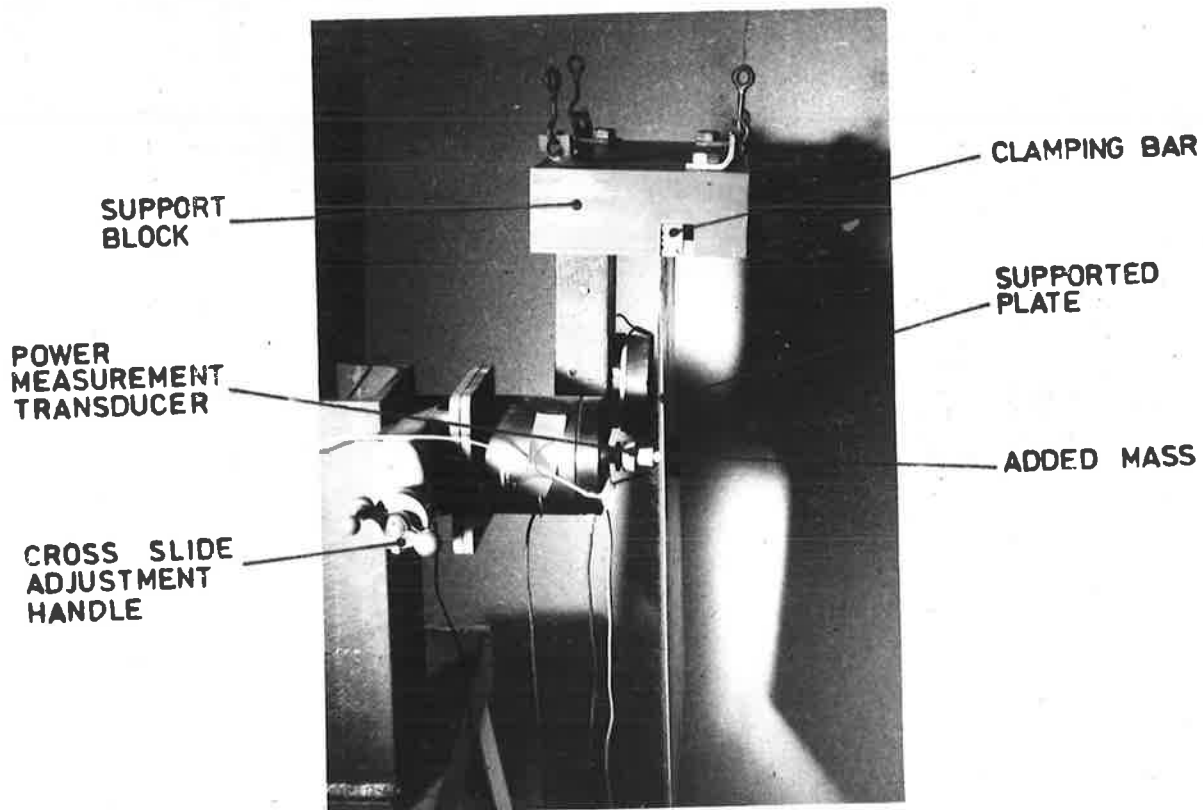


FIG. D-1 STEADY STATE MEASUREMENT OF THE PLATE INTERNAL LOSS FACTOR

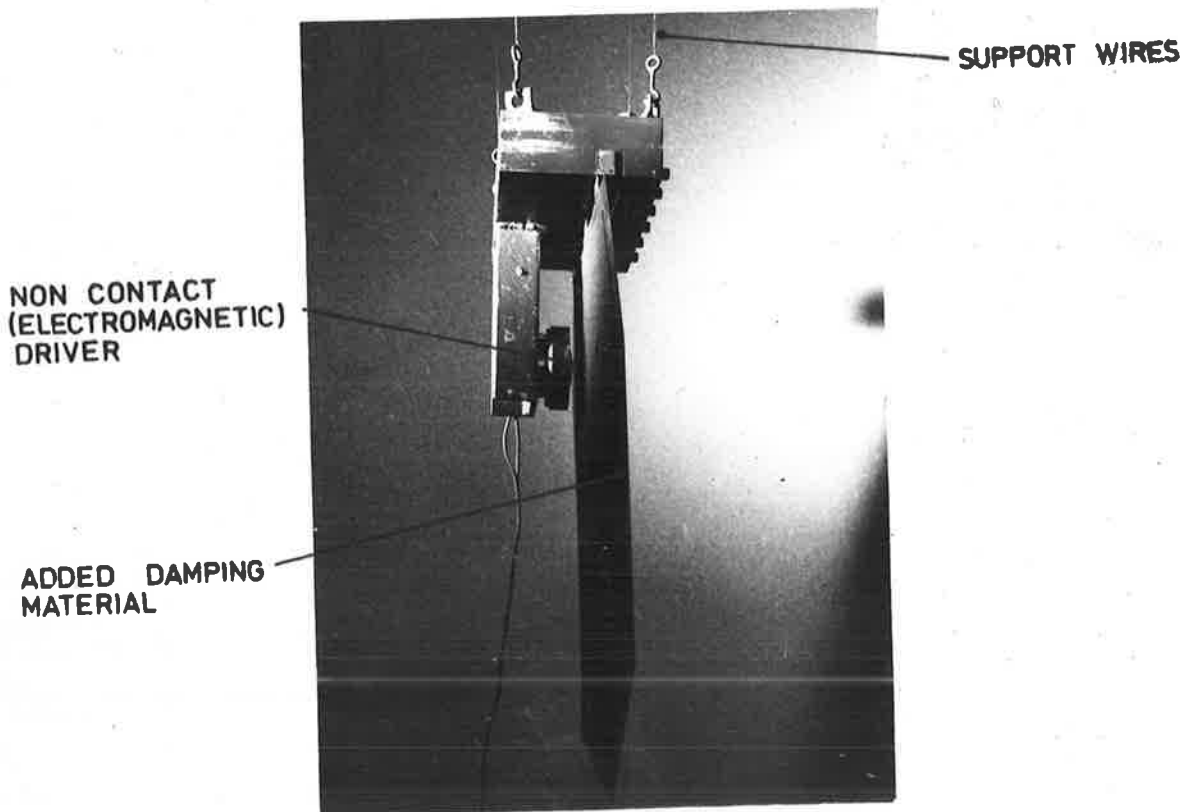


FIG. D-2 DECAY METHOD MEASUREMENT OF THE PLATE INTERNAL LOSS FACTOR

The other requirement was that the system should support the plate and the non contacting driver such that the distance between plate and driver was maintained during all tests.

D.2.2. Support Block

The support block is shown in the photographs Fig. D-1 and D-2. The plate to be supported was clamped firmly into a steel block, 250mm x 100mm x 50mm. The clamping was achieved by six high tensile set screws acting on a clamping bar, set into a milled slot in the block. The bar was grooved along the length of the clamping face so that the plate was gripped by an edge rather than a smooth surface. Each plate was cut so that it was held only at a maximum of three support points each approximately 20mm wide. The bar was clamped so that the bottom edge of the bar and the bottom surface of the block were flush. This ensured that no losses would occur from vibration or air pumping between the plate and a clamping surface overhang. The block was supported by four piano wires connected to an overhead beam.

The extreme impedance mismatch between the plate edge and the relatively massive block reduced energy losses to the support system. Accelerometers were placed on the support beam and no measurable outputs were obtained when the supported structure was excited.

D.2.3. Point Contact Driver Support

The steady state measurement of the internal loss factor required the measurement of input power to the plate whose loss factor was being measured. Although the mini shaker driver and transducer could have been mounted on the same plate support block, as was the electro magnetic driver, there would have been

required a provision for adjusting the position of the driver relative to the plate in at least two directions, and perhaps all three directions in space, to facilitate the lining up of the transducer and the mounting hole in the plate. (See description of the transducer in Appendix E.)

To avoid the complicated mounting requirements, the input power transducer and mini shaker were mounted on a cross slide which was rigidly connected to a free-standing frame.

The shaker was mounted such that its drive action was horizontal and the cross slide allowed horizontal adjustment in a direction perpendicular to the shaker movement. The four piano wires supporting the clamping block were able to be individually adjusted vertically. This not only enabled vertical position control of the plate relative to the input flow transducer but also allowed a fine degree of control of the orientation of the plate to the transducer. If the transducer was attached firmly to the plate when it was not normal to the plate, the bending moments exerted on the force transducer could cause false readings, which would indicate incorrect input power levels. The fine control on plate orientation allowed this problem to be reduced to a minimum.

D.3. INSTRUMENTATION AND ITS CALIBRATION

It will be seen later, in D.4 and D.5, that experimental individual plate internal loss factors and steady state plate energy levels can be determined from two types of measurements (a) acceleration levels at a number of different points on the plate i to obtain the mean square acceleration level $\langle a_i^2 \rangle$ and (b) the average power input, P_i into the directly driven plate i .

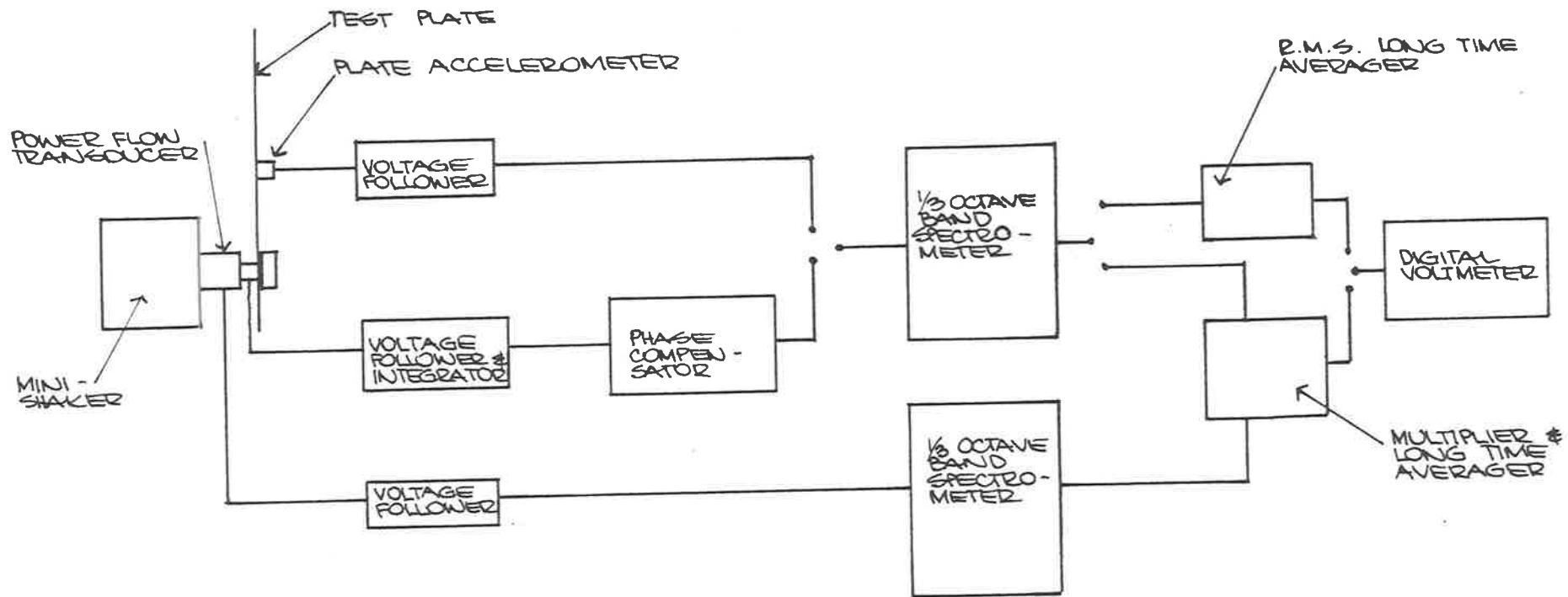


FIG. D-3. SCHEMATIC DIAGRAM - INSTRUMENTATION FOR THE MEASUREMENT OF STEADY STATE INTERNAL LOSS FACTOR.

D.3.1. Acceleration Measurement

The acceleration levels on the plates were measured using a Brüel and Kjaer accelerometer type 4344 in conjunction with a F.E.T. voltage follower and third octave band spectrometer. The band limited signal was averaged in a long time averaging circuit and the voltage output was displayed on a digital voltmeter. A schematic diagram of this circuit is included in Fig. D-3, where the point contact driver is shown. The same measurement method was used for electromagnetic (non-contact) excitation.

D.3.2. Input Power Measurement

The average input power was determined using the relationship

$$P_i = \frac{1}{T} \int_0^T f_{ci}(t) \cdot v_i(t) dt \quad (D,1)$$

where $f_{ci}(t)$ and $v_i(t)$ are the instantaneous values of the applied force and velocity at the point input to the directly driven plate i .

A transducer (Fig. D-4), described in Appendix E, was used to measure the force and acceleration simultaneously at the input point of the plate. The acceleration signal was integrated to give velocity, and the two signals were third octave band limited and then multiplied. (See Fig. D-3)

The multiplier incorporated an Analog Devices AD530J integrated circuit connected for use as a multiplier. The instantaneous output voltage was averaged to give the time averaged product of $f_c(t) \cdot v(t)$.

Phase compensation was used to offset any additional phase changes between the two instantaneous signals, introduced by the circuit.

D.3.3. Calibration

The third octave band spectrometer, multiplier and long-time averaging circuit each have gain and zero drift control. A pure tone (1000Hz - 3 Volts R.M.S.) was used as a reference signal for the gain setting of the averaging and multiplier circuits. The zero drift and gain controls were set before the calibration of the transducers and all settings were checked at least once every three hours during experimentation.

The method used to obtain the calibration constant for the power input measurement, P_c watts/volt, is included in the description of the power flow transducer in Appendix E.

A standard reference accelerometer was indirectly used to determine the calibration constant for the plate accelerometer. The accelerometer on the transducer was calibrated using the reference, mounted back to back, as described in Appendix E. The plate accelerometer response was then compared with the transducer accelerometer response by mounting them back to back. The plate accelerometer calibration constant $(PA)_c$ is then

$$(PA)_c = (TA)_c \frac{\langle A_{\text{power}} \rangle}{\langle A_{\text{plate}} \rangle} \text{metres/sec}^2/\text{volt}. \quad (D.2)$$

where $\langle A_{\text{power}} \rangle$ is the average voltage reading of the power flow transducer accelerometer and $\langle A_{\text{plate}} \rangle$ is the average voltage reading of the plate accelerometer measured simultaneously.

$(TA)_c$ is the calibration constant of the accelerometer on the power flow transducer.

In all cases, the excitation was third octave band limited and the measurement of each signal was through the same circuitry as that used in all experimental data recording.

A list of the calibration constants is given in Appendix E, table E-1.

D.3.4. Mass Loading

A mass loading factor (ML) was applied to the measured plate mean square acceleration levels to compensate for the reduced acceleration level measured due to the accelerometer mass loading the plate. This was determined from, (Beranek, 1971(3))

$$a_L/a_0 = z_p / (z_p + j\omega M_a)$$

where a_L is the measured plate acceleration level

a_0 is the unloaded plate acceleration level

M_a is the added mass

and z_p is the mechanical impedance of the test plate.

$$\begin{aligned} |(a_L/a_0)^2| &= |z_p^2| / \left[|z_p^2| + |\omega^2 m^2| \right] \\ &= 1 / 1 + |\omega m / z_p|^2 \end{aligned} \quad (D, 3)$$

hence (ML) = $1 + |\omega m / z_p|^2$

For steel plates,

$$\omega m / z_p = mf / 14.5t^2$$

Where m is accelerometer mass (kg.) and t is the plate thickness in mm.

The mass m was that of the accelerometer plus a typical amount of beeswax used to connect the accelerometer to the plate, and was 2.38gm.

D.4. INTERNAL LOSS FACTOR MEASUREMENT

D.4.1. Steady State Method

The internal loss factors of the uncoupled plates were determined from the measurements of input power and mean plate energy level during steady state excitation. From equation (4,63) where $dE_i/dt = 0$

$$\eta_i = P_i / \omega E_i \quad (D,4)$$

The steady state energy level for a plate of mass m is

$$E_i = m_i \langle a_i^2 \rangle / \omega^2 \quad (D,5)$$

where $\langle a_i^2 \rangle$ is the mean square acceleration level of plate i , hence the internal loss factor can be expressed as,

$$\eta_i = (\omega / m_i) (P_i / \langle a_i^2 \rangle) \quad (D,6)$$

Each test plate was supported from the clamping block and was directly driven by the mini shaker via the power input transducer, as shown in Fig. D-1. The force and velocity signals were multiplied and averaged to give a voltage V_p with the phase compensator set for the particular bandwidth being investigated.

$$P_i = V_p P_c \text{ watts} \quad (D,7)$$

The plate acceleration was measured in ten different locations over the plate surface to obtain the mean square acceleration voltage $\langle V_A^2 \rangle$ from which the mean plate energy can be determined

$$E_i = (ML)_i m_i \langle V_A^2 \rangle (PA)_c^2 / \omega^2 \quad (D,8)$$

and from equation (D,6)

$$\eta_i = \frac{\omega}{m_i (ML)_i} \frac{V_p^P c}{\langle V_A^2 \rangle (PA)_i^2} \quad (D,9)$$

The experimentally obtained internal loss factors for each plate are presented in Table 5-2.

D.4.2. Decay Methods

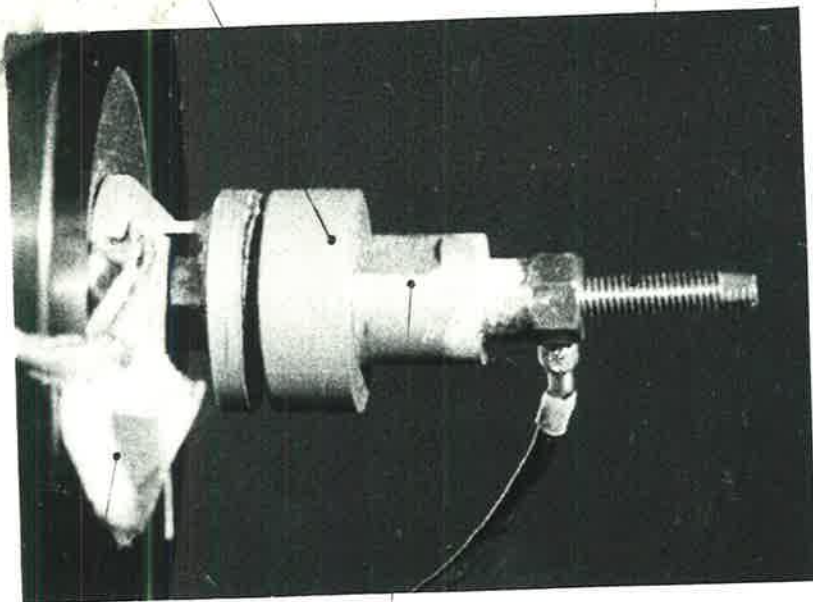
Energy decay tests were carried out on two plates to compare the internal loss factors measured using conventional decay methods with those obtained during steady state excitation.

The majority of results were obtained using a Brüel & Kjaer Reverberation Processor type 4422, which uses the Schroeder-Kuttroff double pulse method, and the remainder were measured using the standard pause method.

The longtime averaging RMS circuit consisted of a precision full wave rectification circuit with a variable response averaging circuit. The acceleration signal during the decay tests was fed into this circuit with an appropriate response time selected. An Analog Devices 755N logarithmic amplifier was used to convert the averaged RMS signal to a logarithmic output which was displayed on a storage cathode ray oscilloscope, (CRO). The decay slope was used, in conjunction with the CRO

FORCE TRANSDUCER
PROTECTIVE SHIELD

MOUNTING STUD



MINI-SHAKER
DRIVER

HEAD OF COMPRESSION BOLT

FIG. D-4. POWER FLOW TRANSDUCER.

ADDED DAMPING MATERIAL
-TO ALL PLATES-

PLATE
ACCELEROMETER

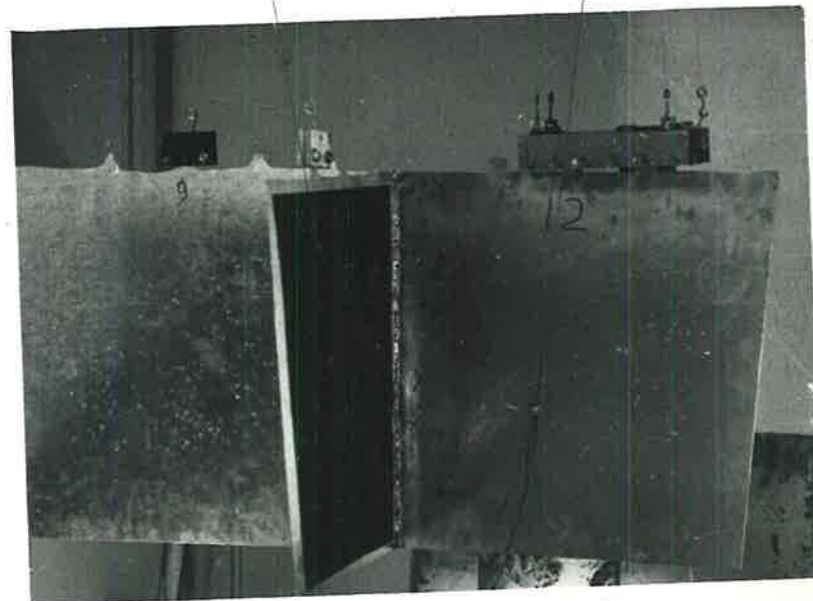


FIG. D-5. THREE PLATE STRUCTURE AND
SUPPORT SYSTEM.

voltage and sweep time settings, to obtain reverberation times, hence loss factors. The results of these measurements are discussed in Appendix E.

D.5. PLATE ENERGY RATIO MEASUREMENT

After individual plates had been welded to form a connected structure, it was supported from the clamping block such that the electromagnetic driver was able to directly excite the appropriate plate. Fig. D-5 shows a three plate single joint structure supported from the clamping block.

The plate energy ratios were determined using Equation (D,8), where the mean square accelerations were obtained from ten measurement locations over each plate for two coupled plate structures and eight points for three or more plate structures.

Since the same accelerometer was used to measure the plate acceleration level on all plates, the absolute acceleration levels were not required and the plate measured energy ratios are given by,

$$E_i/E_j = (m_i/m_j) (ML_i/ML_j) (\langle v_A^2 \rangle_i / \langle v_A^2 \rangle_j) \quad (D,10)$$

D.6. ACCURACY OF EXPERIMENTAL RESULTS

Although the voltage signals were measured through the instrumentation to an accuracy of $\pm 4\%$, the least accurate component being the multiplier with a specified error range of $\pm 2\%$, the accuracy of the internal loss factors, and energy level ratios, were determined by the accuracy of the measured mean energy levels of each plate. The mean energy level is proportional to

the mean square acceleration level, which is the mean of the square of a number of separate readings of the time averaged acceleration levels, measured at different locations on each plate. Since the plate time averaged response is not uniform over the plate, the accuracy of the determination of the mean square acceleration level, hence the mean plate energy level, is related to the number and locations of the measuring points.

The measuring points were randomly selected within small areas which were spread generally over the plate surface. Locations near plate edges, joins and driving points were avoided as much as possible to reduce any near-field effects.

The accuracy of the mean square values depends on the number of point readings used to obtain the mean square value. Tests were carried out on two plates at different frequencies to investigate the deviation of results about a 'true' mean. This 'true' mean square level was determined from a large number of point measurements. The 2 sigma points for different frequencies and different numbers of point measurements used to obtain a mean square value are shown in Fig. D-6. This indicates that the 95% confidence limits, applied to the mean square acceleration levels measured at different frequencies using 8 or 10 measurement locations, are less than $\pm 1.3\text{dB}$. At higher frequencies the 95% confidence limits decrease to $\pm 0.5\text{dB}$. These limits determine the overall accuracy of both internal loss factor and energy ratio results.

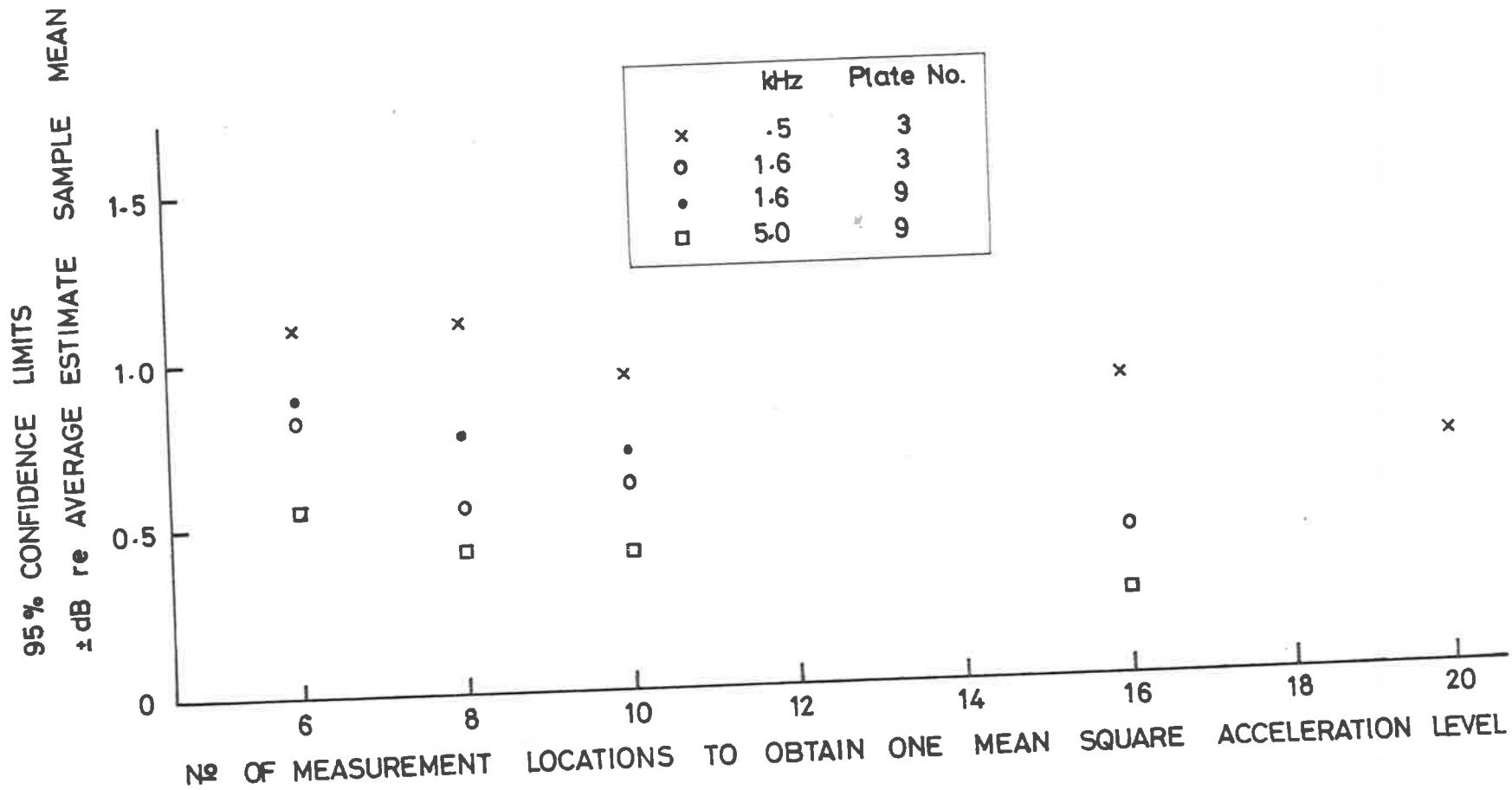


FIG. D-6. CONFIDENCE LIMITS FOR PLATE MEAN SQUARE ACCELERATION LEVELS AS A FUNCTION OF THE NUMBER OF MEASUREMENT LOCATIONS USED.

APPENDIX E. TRANSDUCERS AND INSTRUMENTATION FOR STEADY STATE
MEASUREMENT OF LOSS FACTOR

E.1. REQUIREMENTS

The average input power to the test plate can be measured by sensing the instantaneous force and velocity at the input point to the plate. The time average integral of their product is the input power.

$$P_i = \frac{1}{T} \int_0^T f_c(t) \cdot v(t) dt \quad (E,1)$$

It is essential that the phases of the two input signals be very carefully preserved prior to their introduction into the multiplier circuit in order to measure the correct input power, Fig. E-1, previously shown as Fig. D-3, shows the required circuitry and is repeated here for convenience.

E.2. TRANSDUCER CONSTRUCTION AND THEORY

The power flow transducer shown in Fig. E-2 consists of an annular piezo-electric crystal clamped between two brass bosses by a 3/16 inch U.N.F. brass bolt. A mica wafer separates the signal electrode from the grounded boss at one end and the other boss forms the shield. A B. & K. type 4344 accelerometer was bonded to the head of the compression bolt. The 3/16" thread of the compression bolt is compatible with the mini shaker driver. The body of the accelerometer and the brass bosses and bolt share a common ground in the signal circuit.

The signal from the accelerometer is integrated to give a velocity signal. The voltage from the clamped crystal is proportional to the axial strain, hence it is proportional to the axial force. The clamping bolt helps to protect the crystal from damage if accidental shear forces or bending moments are applied.

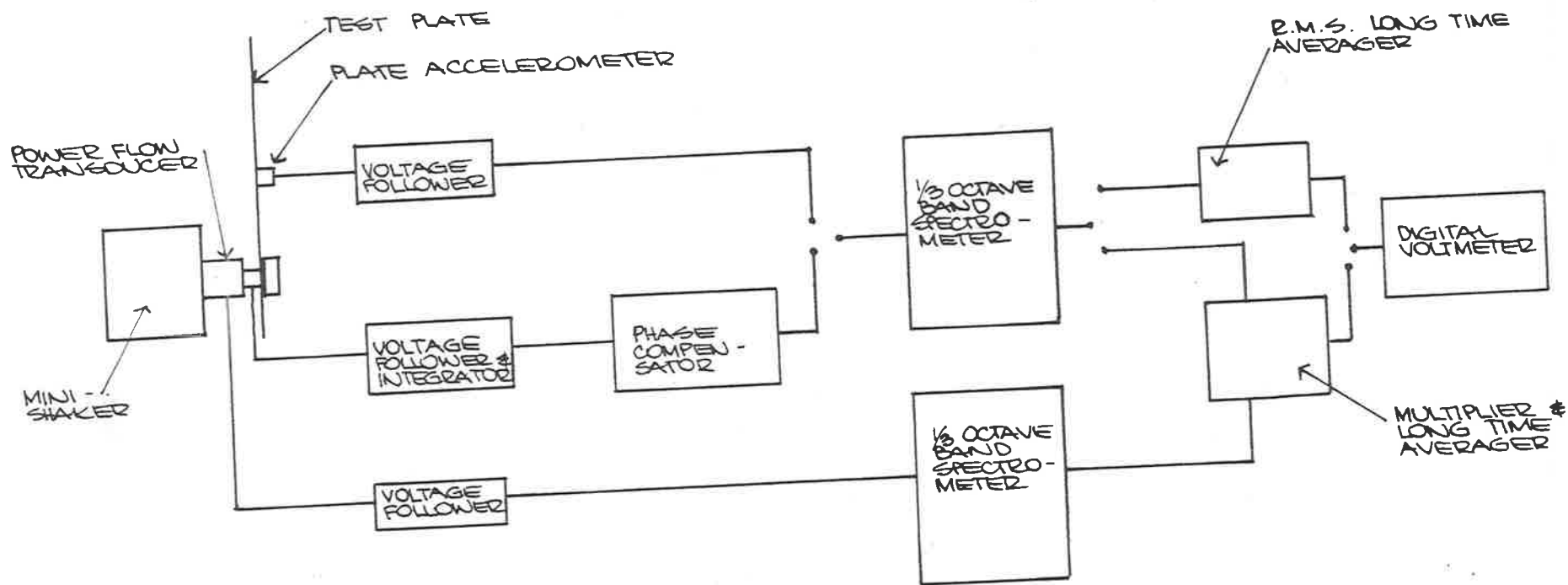


FIG. E-1. SCHEMATIC DIAGRAM - INSTRUMENTATION FOR THE MEASUREMENT OF STEADY STATE INTERNAL LOSS FACTOR.

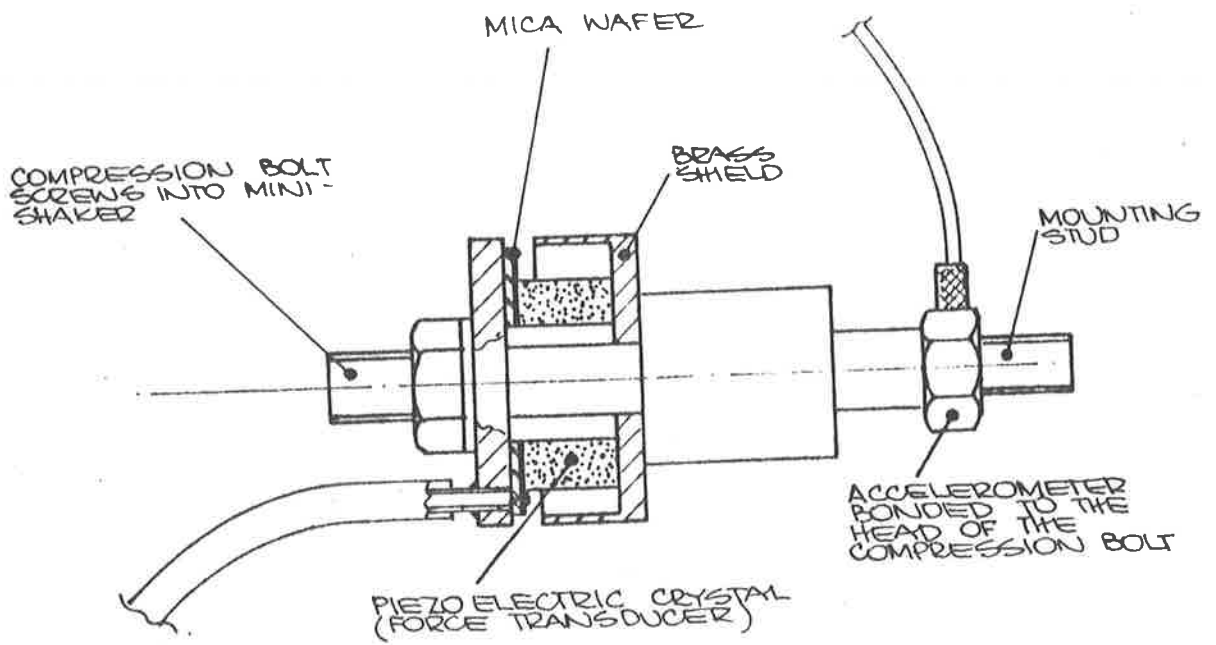


FIG. E-2. POWER FLOW TRANSDUCER - CONSTRUCTION.

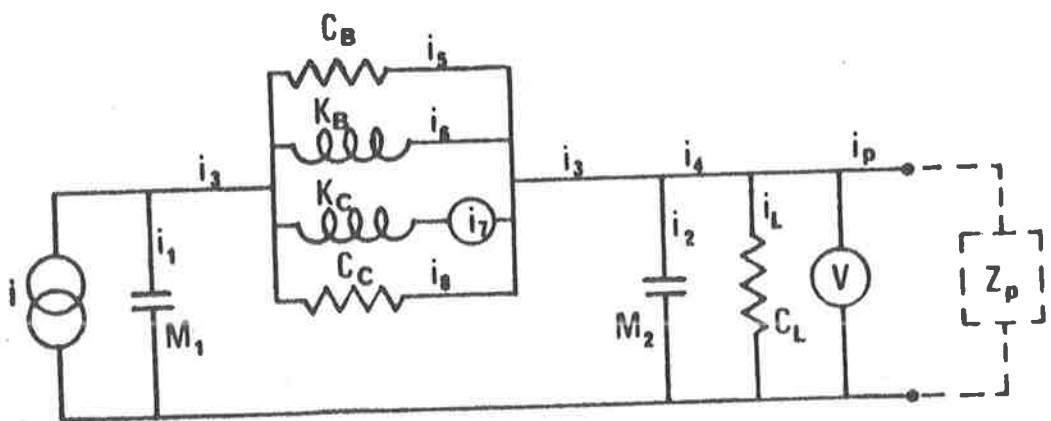


FIG. E-3. POWER FLOW TRANSDUCER - MOBILITY CIRCUIT.

The transducer is described by the mobility circuit shown in Fig. E-3. In this circuit M_1 is the dynamic mass of the shaker and metal on the shaker side of the force transducer, represented by a capacitance, as is M_2 , the mass on the plate side of the force transducer. The spring rates, K , of the compression bolt and of the piezo-electric crystal are represented by inductances. Real losses, C , the damping mechanisms, are represented by resistances, where C is proportional to $1/R$. In the circuit, the current, i , is analogous to force, f_c , and the voltage drop between two points is analogous to the relative velocity between those points, the velocity of the plate at the input point, v , is analogous to the voltage across Z_p , V . The real loss C_L represents any losses due to the accelerometer lead movement.

Referring to the mobility circuit, the power into the test plate is $\langle f_c \cdot v \rangle$ which is equivalent to $\langle i_p \cdot V \rangle$ in the mobility analogy. The use of the symbols $\langle \rangle$ will indicate the time average of the contained quantity.

$$\langle i_p \cdot V \rangle = \langle (i_3 - i_2 - i_L) \cdot V \rangle = \langle i_3 V \rangle - \langle i_2 \cdot V \rangle - \langle i_L \cdot V \rangle \quad (E,2)$$

Since the impedance M_2 is purely reactive, i_2 and V are in quadrature, hence $\langle i_2 \cdot V \rangle$ is zero, and therefore

$$\langle i_p \cdot V \rangle = \langle i_3 V \rangle - \langle i_L V \rangle \quad (E,3)$$

Both C_B and C_C are very large as both crystal and bolt have very low mechanical resistances, hence i_5 and i_8 are negligible, hence

$$i_3 = i_6 + i_7 \quad (E,4)$$

The ratio of i_6/i_7 is always the same, depending on relative moduli of elasticity and areas of the bolt and crystal, thus

$$i_3 = K_n i_7 \quad (E,5)$$

where K_n is a constant to be determined by calibration.

Hence

$$\langle i_p \cdot V \rangle = K_n \langle i_7 \cdot V \rangle - \langle i_L \cdot V \rangle \quad (E,6)$$

$\langle i_L \cdot V \rangle$ represents any work done on the accelerometer lead or any other energy loss from the plate side of the transducer. This could include any acoustic radiation from the piston-like vibrating bosses. These losses are small and were compensated for by the phase compensation circuit during calibration.

When the plate is not attached, the only net work done is attributable to these losses, $\langle i_p \cdot V \rangle = 0$

$$P_L = \langle i_L \cdot V \rangle = K_n \langle i_7 \cdot V \rangle \quad (E,7)$$

This power reading P_L , can be set to zero during calibration, hence after calibration

$$P_p = K_n \langle i_7 \cdot V \rangle \quad (E,8)$$

E.3. INSTRUMENTATION

The integrator was based on a B.&K. type 1606, where a high gain cathode follower was followed by a passive integration circuit. When the signal was integrated, it was phase shifted by approximately, but not exactly, 90 degrees. The amount of error varied with frequency. A slight phase difference also occurred between the two signals through the 1/3 octave band filters. This also varied from band to band.

The phase compensator shown in Fig. E-1, allowed the phase of one of the signals to be altered to compensate for the variations mentioned above and any unwanted energy losses at the transducer. This unity gain circuit was based on a previously published phase shifting network. (Baker, West and Hunter, 1973.) Some components were altered to suit this application, but it was basically the same circuit. A ten turn potentiometer with an attached counter allowed a specific phase shift to be set for each 1/3 octave band of interest.

E.4. CALIBRATION PROCEDURE

Calibration constants were required for the velocity and force signals.

These were both referenced to a standard test accelerometer which was mounted back to back with the transducer accelerometer.

The transducer accelerometer and reference accelerometer signals $\langle A_{\text{TRANS}} \rangle$ and $\langle A_{\text{REF}} \rangle$ were measured for each 1/3 octave band, using a long time averaging R.M.S. circuit and digital voltmeter. The force and velocity signals were measured in each band with the previously determined phase compensator setting. The signal monitored was the squared signal from the

multiplier, i.e. $\langle V_f^2 \rangle$ and $\langle V^2 \rangle$. All signals were measured at a particular amplifier setting of the spectrometers which had been previously calibrated using their internal reference signals.

The transducer accelerometer calibration constant was determined from

$$(TA)_c = (RA)_c \frac{\langle A_{ref} \rangle}{\langle A_{TRANS} \rangle} \text{metre/sec}^2/\text{volt}$$

where $(RA)_c$ is the known reference accelerometer calibration constant.

The velocity calibration constant

$$V_c = \frac{(TA)_c}{\omega} \frac{\langle A_{TRANS} \rangle}{\sqrt{\langle V^2 \rangle}} \text{metres/sec/volt.}$$

and the force calibration constant

$$F_c = M_c (TA)_c \frac{\langle A_{TRANS} \rangle}{\sqrt{\langle V_f^2 \rangle}} \text{newtons/volt}$$

were multiplied to obtain the power flow calibration constant

$$P_c = F_c V_c \text{ watts/volt}$$

Since the force and velocity signals were calibrated through the multiplier, then P_c was related to the multiplier output directly for specific amplifier settings on the spectrometers. The calibration constants are listed in Table E-1.

M_c was the calibration mass used. This comprised an added mass screwed onto the mounting stud plus an experimentally determined equivalent mass which is M_2 in the mobility circuit. M_2 was not just the mass of the boss, bolt head and accelerometer because the compression bolt connected the two bosses directly. The effect of this was unknown and hence M_2 was determined experimentally.

Various size masses were added to the transducer and the force and acceleration voltages measured in different bands and with different levels of excitation. Force/acceleration ratio was plotted against added mass, (Fig. E-4), and the line was extrapolated to the force/acceleration = 0 axis. The negative intercept indicates that the equivalent mass M_2 was approximately 11 grams.

E.5. TRANSDUCER-PLATE IMPEDANCE MATCHING

When the impedance mismatch between transducer and plate was great, the power measurement was small even with near maximum input force and velocity voltages to the multiplier. The fluctuations in the output due to the random nature of the exciting signal became significant compared with the average value. The only way to improve this was to increase the degree of matching between the plate and transducer impedances.

The point impedance into an infinite plate is purely resistive and a finite plate contains a reactive (stiffness determined) component as well. The transducer/driver impedance is determined almost entirely by its mass.

The initial attempt to match the impedances was to make the driver/transducer look like the plate. The transducer mass was reduced to a minimum and the driver was made to resemble a

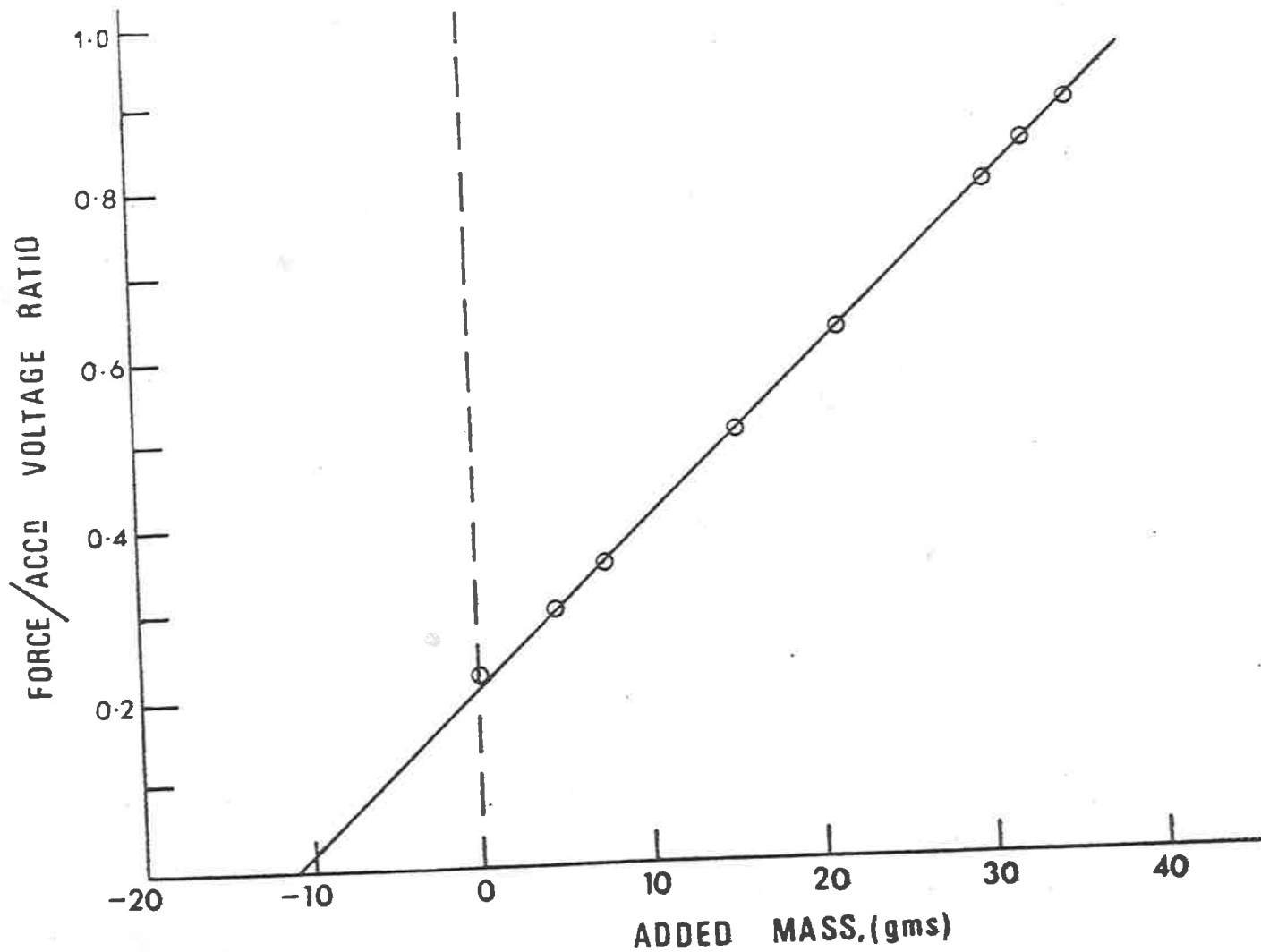


FIG. E-4. POWER TRANSDUCER FORCE/ACCELERATION VOLTAGE RATIO AS A FUNCTION OF DRIVEN MASS - TO DETERMINE EQUIVALENT MASS M_2 .

multimodal plate. The mini shaker excited a small stiff plate which had rolled mesh attached to its edges. This then gave a response similar to a large multimodal plate. The transducer was attached to the small plate (driver) and to the test plate, that is, a multimodal plate driven by a multimodal plate. Two serious problems were encountered with this approach which caused its abandonment. The two problems were that the dynamic effect of the accelerometer lead was increased since the total mass was small, and the response of the unloaded transducer was poor due to small but significant transverse accelerations introduced by the bending movement of the driving plate. The force and acceleration signals should remain in phase and the ratio between them should be constant during a sine sweep when the load was purely massive. This was not achieved when the transducer was plate-mounted, although it was achieved when the transducer was driven directly by the mini shaker.

A more successful second attempt involved the addition of a mass at the driving point of the plate so that locally, the driven plate impedance looked more like the mass-controlled transducer impedance.

The masses on each side of the force transducer were made approximately equal, that is, the dynamic mass of the driver and driver side boss, M_1 , was approximately equal to M_2 plus the added mass. This mass was then used as the added mass during the force calibration procedure. As the mass of the transducer was now large, the effect of the lead was reduced significantly.

The average power factor increased from typically 0.05 to 0.20 with some readings up to 0.5. Although this was not perfect matching, it was sufficient to reduce the fluctuations to a maximum of approximately two percent of the power input measurements.

E.6. TRANSDUCER TESTING

The direct calibration of force and acceleration, and hence velocity, transducers, allowed the power calibration constant P_c to be determined. A direct determination of this constant would have been better but this did not seem feasible because of the very small power levels involved.

A comparison between plate internal loss factors seemed the only way of testing the transducer, but this was not good since the rationale for developing the transducer was that the steady state determination may measure loss factors which control in the steady state but are not readily measured using the decay methods. However, steady state internal loss factors were measured using the procedure outlined in Appendix D. One of the damped plates was used to obtain decay measured loss factors. These loss factors are presented in Fig. E-5 (Swift & Bies, 1975).

The difference of about 2dB over the large range of results eliminates any errors due to additional losses, e.g. at the plate/transducer join, otherwise the linear differences should be the same at all frequencies, which is clearly not the case.

The similar overall pattern indicated that the transducer was measuring loss factors. The two possible conclusions are that the steady state measurement does show a larger loss factor which controls in the steady state situation, or that there was a calibration error.

The calibrations were checked and another plate tested using the Schroeder-Kuttruff reverberation processor. During these decay tests, some repeatable initial decay slopes (about 1dB) were noticed. These were increased to a measurable size, by adjusting the CRO voltage gain and sweep rate; the initial slope was then measured to obtain the loss factor. These results

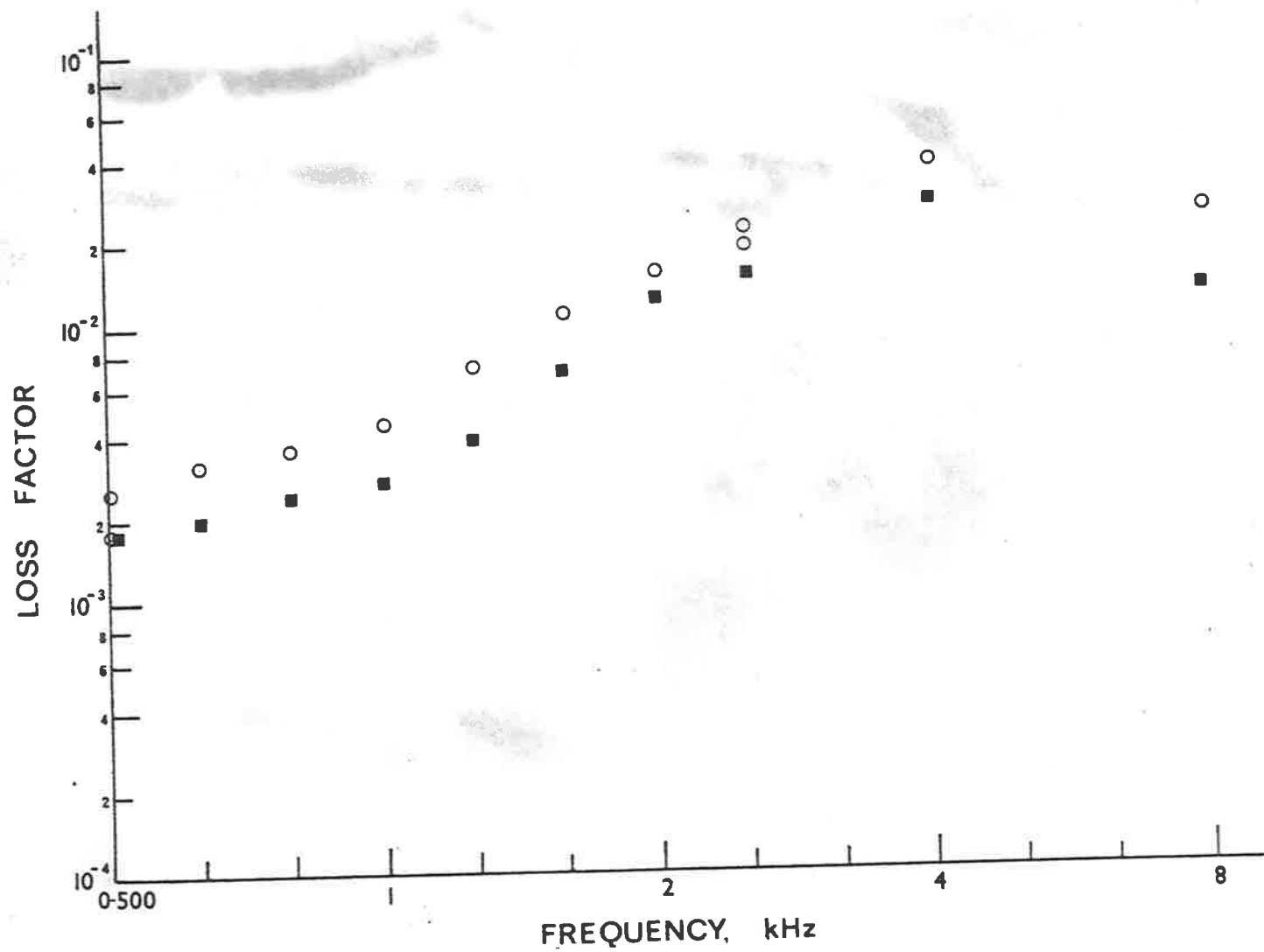


FIG. E-5. DAMPED PLATE - INTERNAL LOSS FACTOR; O , STEADY STATE MEASUREMENT; ■ , ENERGY DECAY MEASUREMENT.

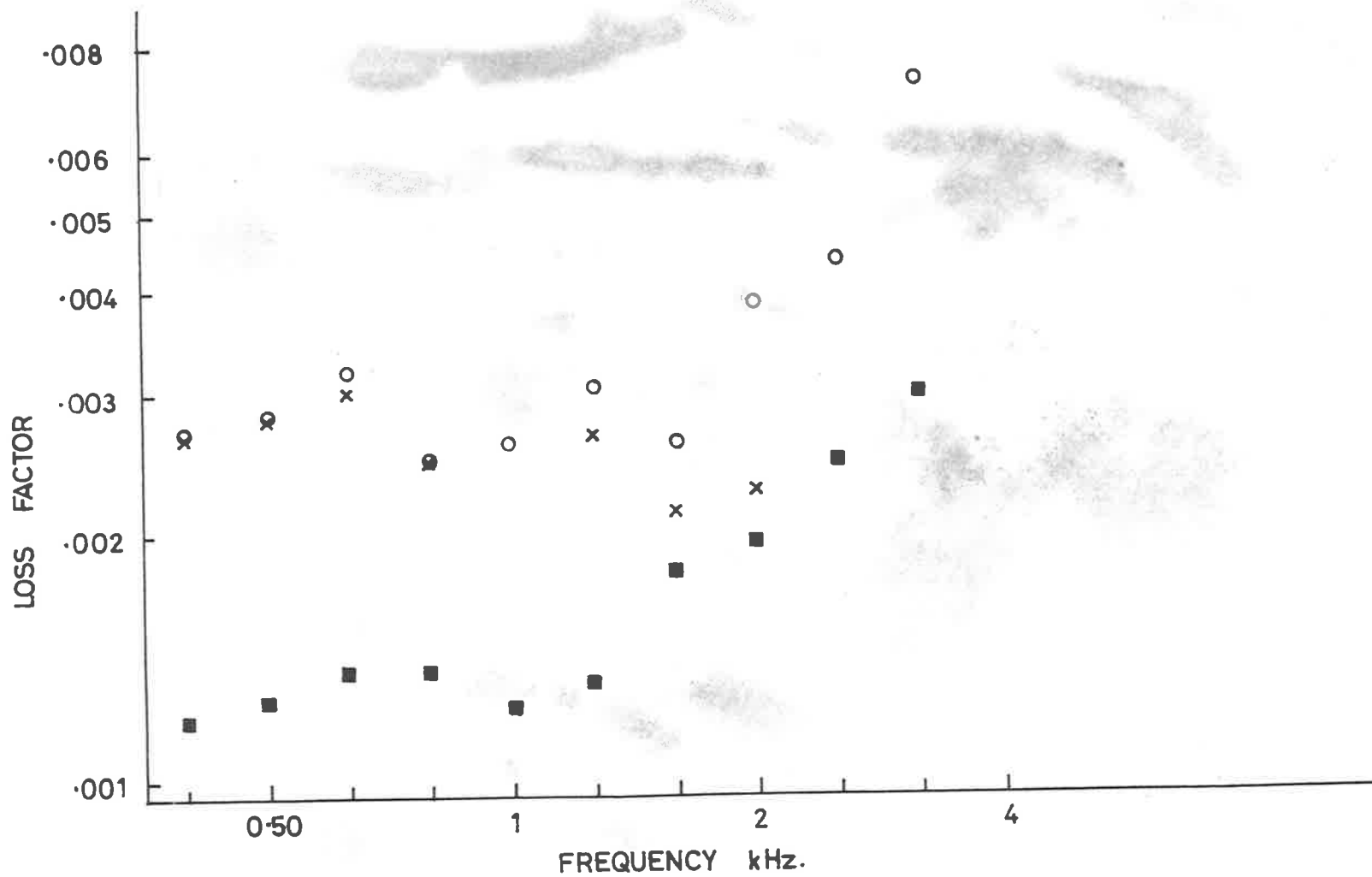


FIG. E-6. DAMPED PLATE INTERNAL LOSS FACTORS; ○, STEADY STATE MEASUREMENT; ■, ENERGY DECAY MEASUREMENT; FIRST 6dB; x, ENERGY DECAY MEASUREMENT FIRST 1 OR 2dB.

are presented in Fig. E-6 where the agreement between the short 1 or 2dB decay results and the steady state measurements is good in a number of third octave bands.

The agreement between these initial decay slope measured loss factors and the steady state measured loss factors, combined with the fact that the rechecked calibration constants agreed with those originally used, indicates that the steady state method is measuring the plate internal loss factor which controls the steady state response.

TABLE E-1. CALIBRATION CONSTANTS

Acceleration and Velocity Amplifier gain setting - 60dB
 Force Amplifier gain setting - 100dB

Frequency Hz	Plate Accelerometer (PA) $\frac{m/s^2}{\text{volt}}$	Velocity V_c $\frac{m/s}{\text{volt}}$	Force F_c N/volt	Power P_c watts/volt
400	3.67	.521	.183	.0951
500	:	:	.198	.103
630			.215	.112
800			.206	.107
1000			.202	.105
1250			.210	.109
1600		.521	.203	.106
2000		.524	.212	.111
2500		.540	.210	.113
3150		.552	.227	.125
4000		.584	.231	.135
5000		.625	.253	.158
6300		.712	.289	.205
8000		.968	.416	.403
10000	3.67	.835	.514	.429

REFERENCES

- Baker, M., West, M., and Hunter, R.D. 1973 A low cost phase shifting network and some possible acoustic applications. Technical Note - Applied Acoustics, 6
- Beranek, L.L. (Editor) 1971 Noise and Vibration Control McGraw-Hill Book Co.
(1) Chapter 9
(2) Chapter 11
(3) Chapter 3
- Bhattacharya, M.C. 1970 The transmission and radiation of acousto-vibrational energy. Ph.D. Thesis - Univ. of Liverpool.
- Bhattacharya, M.C. 1971 Propagation of sound energy by vibration transmission via structural junctions. J. Sound Vib. 18 (2)
- Budsin, S.V. and Nikiforov, A.S. 1964 Wave transmission through assorted plate joints. Soviet Physics - Acoustics 9
- Chintsun Hwang, W.S.P. 1973 Investigation of vibrational energy transfer in connected structures. N.A.S.A. CR-124456 Northrop Corp. NOR 73-105
- Crandall, S.H. and Lotz, R. 1971 On the coupling loss factor in statistical energy analysis. J. Acoust. Soc. Am. 49 (1)
- Cremer, L., Heckl, M., and Ungar, E.E. 1973 Structure Borne Sound Springer, Verlag, New York.
(1) Section V.2
(2) Section V.6
- Crocker, M.J. and Price, A.J. 1969 Sound transmission using statistical energy analysis. J. Sound Vib. 9 (3)
- Eichler, E. 1965 Thermal circuit approach to vibration coupled systems and the noise reduction of a rectangular box. J. Acoust. Soc. Am. 37 (6)
- Fahy, F.J. 1970 Energy flow between oscillators: Special case of point excitation. J. Sound Vib. 11 (4)
- Fahy, F.J. 1974 Statistical energy analysis - A critical review. The Shock & Vibration Digest 6 (7)
- Gibbs, B.M. and Gilford, C.L.S. 1976 The use of power flow methods for the assessment of sound transmission in building structures. J. Sound Vib. 49 (2)

- Hart, F.D. and Shah, K.C. 1971 Compendium of modal densities of structures.
N.A.S.A. CR-1773
- Heckl, M. 1962 Measurements of absorption coefficients on plates.
J. Acoust. Soc. Am. 34 (6)
- Hemmerle, W.J. 1967 Statistical Computations on a Digital Computer.
Blaisdale.
- Kayser, K.W. and Bogdanoff, J.L. 1975 A new method for predicting response in complex linear systems.
J. Sound Vib. 38 (3)
- Kihlman, T. 1967 Transmission of structure borne sound in buildings.
National Swedish Institute for Building Research - Stockholm - Report 9/67
- Kihlman, T. 1970 Sound transmission in building structures of concrete.
J. Sound Vib. 11 (4)
- Kuttroff, H. and Jusofie, M.J. 1967/8 Nachhallmessungen nach dem Verfahren der intergrierten Impulsentunt.
Letters, Acustica 19
- Lotz, R. and Crandall, S.H. 1973 Prediction and measurement of the proportionality constant in statistical energy analysis of structures.
J. Acoust. Soc. Am. 54 (2)
- Lyon, R.H. and Maidanik, G. 1962 Power flow between linearly coupled oscillators.
J. Acoust. Soc. Am. 34 (5)
- Lyon, R.H. and Eichler, E. 1964 Random vibration of connected structures.
J. Acoust. Soc. Am. 36 (7)
- Lyon, R.H. and Scharton, T.D. 1965 Vibrational energy transmission in a three element structure.
J. Acoust. Soc. Am. 38 (2)
- Lyon, R.H. 1975 Statistical Energy Analysis of Dynamical Systems: Theory and Applications.
MIT Press, Cambridge, Massachusetts.
(1) Chapter 2.
(2) Chapter 14.
- Maidanik, G. 1962 Response of ribbed panels.
J. Acoust. Soc. Am. 34 (5)

- Newland, D.E. 1966 Calculation of power flow between coupled oscillators. J. Sound Vib. 3 (3)
- Scharton, T.D. and Lyon, R.H. 1968 Power flow and energy sharing in random vibration. J. Acoust. Soc. Am. 43 (6)
- Schroeder, M.R. 1965 New method of measuring reverberation time. J. Acoust. Soc. Am. 37
- Swift, P.B. and Bies, D.A. 1975 Steady State measurements of Loss Factor. Paper N.1 90th Acoust. Soc. Am. Meeting, San Francisco. Calif.
- Ungar, E.E. and Carbonell, J. 1966 On panel vibration due to structural joints. A.I.A.A. Journal 4 (8)
- Ungar, E.E. and Scharton, T.D. 1967 Analysis of vibration distribution in complex structures. Shock and Vibration Bulletin 36 (5)
- Ungar, E.E. and Koronaios, N. 1968 Vibration distributions in multi-panel structures. Comparison of measurements with S.E.A. predictions. Shock and Vibration Bulletin 37 (2)
- Wöhle, W. and Elmallawany, A. 1975 Generalised model of the application of statistical energy analysis for the sound propagation in a complicated structure. J. Sound Vib. 40 (2)

REVIEWER'S COMMENTS AND AUTHOR'S REPLIES

(Supplement to PhD thesis "Vibrational Energy Transmission in Connected Structure" by P.B. Swfit)

Page No.	Paragraph	Line No.	Reviewer's Comments	Author's Reply
2nd page of Summary	Last	7	"these bounds" - basis for these "bounds" is rather ephemeral-- should use better established analysis (Ref. 1).*	These comments are mainly related to the lower bound and references are made to Prof. Lyon's book "Theory and Applications of Statistical Energy Analysis". In retrospect, the author agrees that it would have been more informative to use the product $N_i N_j$, rather than N_i , to investigate the lower bound, however, the references relating to this, (and to specific minimum values for the minimum number of modes-- Reviewer's reference 4), had not been sighted by the author as Prof. Lyon's book was not available when the data was processed or when the major part of the thesis was written.
3	1	13,14	"basic limiting no. of modes" no--required basic limiting number of interacting modes:, see later discussion.	
3	1	15	"broad band analysis" - no, see Ref. 2.	
3	1	19	"limits are not well defined", perhaps, but are better defined than the thesis assumes--see Ref. 1.	
6	1	1	discussion of bounds is misleading since it is based on mistaken ideas about the limits	
10	3		"no values for the minimum number of modes, etc".See Ref. 4	
96			Eq. (5.1) The lower bound should be determined from the effective number of interacting modes	
9			Weak coupling discussion is misleading. Ref. 3, the weak coupling assumption is not used to get Eq. (3,2)	
14	1		discussion of weak coupling - same comments as before	

* The Reviewer's references are listed on the last page of this attachment.

Page No.	Paragraph	Line No.	Reviewer's Comments	Author's Reply
11	1		<p>The condition on modal overlap stated here is not correct. In simple terms, the reverberant field should dominate the direct field. The direct field is formed by modal coherence, and, therefore, too much modal coherence is a limit to SEA applicability. An estimate of this limit is when $k d \eta < 2$ where $k = 2 \pi / \lambda$, $d =$ mean free path, $\eta =$ loss factor</p> $\eta < \frac{2}{k_b d} ; \omega \eta n_i < \frac{2 c_b n_i}{d} = \frac{1}{\pi} k_b P = \frac{P}{\lambda_b}$ <p>Thus, the "modal overlap should be smaller than the ratio of the plate edge length to a bending wavelength, not unity.</p>	<p>The development of $R_i = \frac{\omega \eta n_i}{2 \pi} < 1$ in the text is based on published works as referenced in the text. Prof. Lyon suggests that these works, or the interpretations of these works, are incorrect and that there is no upper bound.</p> <p>The author accepts this in so far as Crocker & Price (1969) obtained good results using SEA with $R_i \gg 1$; in fact the agreement was poor at $R_i < 3$, however, it is interesting to note that as Prof. Lyon suggests,</p> $R_i < P / 2 \pi \lambda_b$ <p>implies that there is an upper limit, although not at $R_i = 1$. This area needs further investigation.</p>
20	3		<p>The Lyon-Scharton paper assumes statistical independence of modes, not specifically lack of modal overlap.</p>	
97			<p>Eq. (5.2) This limitation has already been discussed.</p>	
13	1	15	<p>"reciprocity relation" is better described as a "consistency relationship".</p>	<p>This relationship is often referred to as reciprocity - see P122 of Prof. Lyon's reference.</p>

Page No.	Paragraph	Line No.	Reviewer's Comments	Author's Reply
24,25			<p>At this point, the proper role of a "box" in figure (3.1) should be noted: i.e., it is a collection of similar modes, not a structural element. If one continues to associate an SEA "box" with a subsystem, then equipartition between all mode (wave) types in that subsystem has been assumed.</p>	<p>The review in page 8 states the assumptions used in looking at a connected structure from the SEA view point.</p>
27			<p>Eqs. 4.8 and 4.9. These relations assume a lack of diffusion in the vibration field which is inconsistent with the SEA model. These relations are surely useful in some calculations but not in an SEA calculation in which it is assumed that the power incident on an edge of the structure can be related to reverberant vibration levels.</p>	<p>The same (travelling wave) model is used to determine both τ_{ij} and TF_{ij} relationships; τ_{ij} from its definition and TF_{ij} directly from substitution into the power flow equations. The closeness of the two results (fig. 4.3) show that there is little difference between them, τ_{ij} being used because of shorter computation time.</p>
39,40			<p>This discussion should point out that the parameter properly related to τ_{ij} is τ_{jj}. The TF factor is deficient for reasons pointed out above. The $-\ln(1-\tau_{ij})$ factor related to decay, not the steady state situation for which SEA is developed. (Of course, a decay rate experiment can determine $-\ln(1-\tau)$ from which τ can be found).</p>	

Page No.	Paragraph	Line No.	Reviewer's Comments	Author's Reply
43,44			<p>The use of $\tau(0)$ to determine τ assumes that there is no special construction at a join that would lead to coincidence effects at finite α -- this should be pointed out.</p>	<p>The use of $\tau(0)$ with factors M and T is purely an empirically derived mathematical convenience to allow an easier procedure for calculating τ. There are no join-type restrictions which should not also apply if τ was determined using the longer method, i.e.</p> $\tau = \int_0^1 \tau(s) ds \quad \dots \text{eq (4.23)}$
50 ff			<p>This discussion has an inconsistency. Only bending to longitudinal and transverse motion is included. However, if the plates were large enough so that there are resonant modes of this kind, why are such modes not included in the energy storage? Transverse and longitudinal modes and not the modal overlap may be the key to the higher transmission found in the data at high frequencies.</p>	<p>Generally, the experimental plates used would have their lowest longitudinal mode at 5 or 6 kHz, where-as most of the results showed greater transmitted energy from that predicted starting at 2 kHz and few results were taken at greater than 4 kHz. However, the point raised by Prof. Lyon is worth further investigation.</p>
99 ff			<p>Section 5.2 The increasing ratio of $E_{\text{expt}}/E_{\text{theo}}$ as frequency increases indicated that there is some mechanism not accounted for by the theory (the SEA model) and not a limitation of SEA as such (See Ref. 5)</p>	

Page No.	Paragraph	Line No.	Reviewer's Comments	Author's Reply
62			<p>It appears that while F^2 is a ratio of the square of longitudinal to bending wave impedance, the parameter Q is related to average modal separations. Aside from a constant, it is of the order of $n_i n_j / n_{l,b}^2$ where n_l is the modal density of longitudinal waves. Since</p> $n_{i,b} \approx n_{j,b} = 0.1$ <p>a value of $P \leq 50$ means $Q \leq 0.02$ or $n_l \leq 0.002$. The restriction of P amounts, therefore, to requiring that the modal density of the system for bending waves is about 50 times that for longitudinal waves. The correspondence of this condition with $f = 2$ kHz is consistent with the lowest longitudinal modes occurring in this frequency range.</p>	<p>The values of P and Q are based on mathematical predictions derived from considering travelling wave interaction at a join; the derivation does not consider resonant modes at any stage. It is interesting, that considering the modal densities of the different wave fields could lead to similar restrictions.</p>
68 ff			<p>In an SEA context, this discussion would be better placed by considering when longitudinal and transverse modes of structural elements might have to be considered as additional SEA boxes.</p>	<p>This is not necessary as the transverse and longitudinal waves are not considered to be resonant but are forced by the incident waves.</p>

Page No.	Paragraph	Line No.	Reviewer's Comments	Author's Reply
77	4		The concern about point drive relates back to the relation between the energy contained in direct vs. reverberant fields. I don't see the problem here if the dissipation is primarily in the reverberant field.	Fahy (1970) suggests that there is a problem. Experimental results also showed that there is a problem (P.79 Fig. 4.14). Further work carried out in the Mechanical Engineering Department, University of Adelaide after the completion of this thesis, has shown that generally, the energy ratios obtained when point-driving at one point differed from the energy ratios obtained using non-contact excitation.
78	15		The force from the non-contact excitation is also applied over a small area, and modal coherence is not eliminated.	
85	2		From preceeding discussion, I doubt that this concern is justified.	

REFERENCES

1. R. Lyon. "Theory and Applications of Statistical Energy Analysis", MIT Press, 1976, Section 4.2.
2. Ref. 1, p. 88.
3. Ref. 1, Section 3.2.
4. Ref. 1, pp. 138-140.
5. Ref. 1, p. 6, paragraph 3.